INVESTIGATIONS OF A ROTATIONAL MAGNETORHEOLOGICAL HONING PROCESS FOR IMPROVED PRODUCTIVITY OF NANO-FINISHED INTERNAL SURFACE OF CYLINDRICAL WORKPIECES

A thesis submitted in fulfilment of the requirement for the award of the degree of

DOCTOR OF PHILOSOPHY

IN

MECHANICAL ENGINEERING

Submitted by

SUNIL KUMAR PASWAN

Roll No. 901608006

Under the supervision of

Dr. ANANT KUMAR SINGH

Associate Professor, MED

Department of Mechanical Engineering,

Thapar Institute of Engineering and Technology, Patiala-147004, India

(Deemed to be University)

July, 2021

CONTENTS

CERTIFICATE

I, Sunil Kumar Paswan, Roll No. 901608006, hereby declared that the thesis entitled **"Investigations of a Rotational Magnetorheological Honing Process for Improved Productivity of Nano-finished Internal Surface of Cylindrical Workpieces"** submitted to the Department of Mechanical Engineering at Thapar Institute of Engineering and Technology, Patiala, Punjab (India) is an authenticated record of my own research work for the award of the degree "Doctor of Philosophy" under the supervision of **Dr. Anant Kumar Singh.** This report has not been submitted to any other institute for the award of any other degree.

09-07-2021

Sunil Kumar Paswan

Roll No. 901608006

Place: Patiala

Dated: 09-07-2021

This is to certify that above declaration made by the student is correct to the best of my knowledge.

Verified By:

09-07-2021

Dr. Anant Kumar Singh
(Supervisor)
Associate Professor
Department of Mechanical Engineering
Thapar Institute of Engineering and Technology, Patiala- 147001 (Punjab)
India

ACKNOWLEDGEMENT

First and the foremost, I wish to thank my supervisor **Dr. Anant Kumar Singh** for his valuable support and guidance. I am sincerely gratitude to him for judging my potential and providing me an interesting topic according to my capability. I am thankful for his positive suggestions, and meticulous guidance that helped me to improve my talent to write scientific research papers and carry out the new research. His patience and motivation enhanced me up to achieve my goal. I feel really honoured to have worked under his mentorship throughout my entire PhD work.

I thank the doctoral committee members **Dr. T.P. Singh** (Chairman, Board of Studies), **Dr. Ashish Singla**, **Dr. Sachin Singh** and **Dr. R.K. Gupta** for the feedback and reviews that were given on my research proposal and progress monitoring presentations. Their guidance was beneficial for me to improve my research work. I am also thankful to **Dr. Tarun Nanda** and **Dr. Gagandeep Bhardwaj**, our PhD coordinators for their approachability and keeping me informed with all the relevant communication throughout E-mails.

I am gratefully admitting the economic support given by the Science and Engineering Research Board (Department of Science and Technology), New Delhi, India (Project no. EMR/2015/000330). I am thankful to my father who has always supported and consistently motivated for this research. I am thankful to my elder brothers, sisters, and sisters-in-law for their love and great support for me. I am especially thankful to my elder brother Jitendra Kumar for his great emotional support throughout my entire research work. I am also very thankful to my younger sister Nitu for her act of elderly to me and motivating me a lot during this period. I am thankful for my fiancé Khushboo Kumari who always kept me motivated. I am thankful to my best friends Kundal Kumar Rai, Chandan Kumar, and Shami Akhtar who have always motivated me. I was also encouraged by my research team members Dr. Manpreet Singh, Mr. Ankit Aggarwal, and Mr. Kunal Arora. I am also thankful to my friend Prakhar Jain and Vipin Sharma who motivated me throughout this research. From the core of my heart, I thank to my entire family members for their never-ending love, encouragement, and support.

I thank to "**Almighty God**" for giving me the strength and patience for successfully completing my goal.

09-07-2021

Sunil Kumar Paswan

ABSTRACT

Fine finishing of the internal surface of cylindrical components such as cylindrical molds and dies, hydraulic cylinders, power steering housing cylinders, industrial choke valves, cylindrical barrels for injection moulding, etc. is highly required to improve their operational functionality. The fine finished internal surface of cylindrical components also results in resistance to wear, corrosion, pitting, oxidation, and chemical damage. In industries, mostly traditional finishing processes like grinding or honing are used to finish the internal surface of the various cylindrical components because of their easy accessibility and low making cost. The traditional internal finishing processes use rigid hard bonded abrasives for finishing the internal surface of the cylindrical workpieces. The uncontrolled finishing forces applied by these hard bonded abrasives introduce various types of defects on the final finished surface such as residual stress, torn and folded metals, less surface finish, surface irregularities, micro-cracks, heat affected zone, reduction of strength, and reliability of the part, etc. Moreover, the traditional finishing processes can finish the surface upto a certain level because of the use of the rigid hard bonded abrasives tool and further to achieve a fine level of surface finishing without surface defects may not be possible. Therefore, there is a mandatory requirement of the advanced finishing processes to finish the internal surface of the cylindrical components after the traditional finishing processes for enhancing their operational life in various machines or systems. The finished surface using the advanced finishing processes has several benefits like close tolerance design, reduction in wear, friction losses and increase in product service life, etc.

To achieve efficient and defect-free finished internal surface of the cylindrical workpieces, recently a permanent magnet-based magnetorheological honing (MRH) process developed for finishing the internal surface of the cylindrical workpieces after various consecutive development in internal finishing techniques. This process is found advantageous for finishing the ferromagnetic as well as non-ferromagnetic variable diametric cylindrical workpieces. Also, this process finishes upto a nano-scale level of surface asperity with controlled finishing forces and without inducing any heating problem. The MRH tool was made rotating and reciprocating during the inside surface finishing of the stationary cylindrical workpieces. Further, with the resumption of all good qualities of the recently developed a permanent magnet-based MRH process and based on literature related to enhancement in relative speed of abrasive particles, a novel rotational magnetorheological honing (R-MRH) process has been developed in the present work for improved productivity

and performance. In this process, the workpiece cylinder is also made rotating in the opposite direction at the same time when the tool is made rotating and reciprocating for finishing the inside surface of the cylindrical workpieces. Due to the oppositely rotating workpiece cylinder, the relative motion of the active abrasive particles gets enhanced which results in improved finishing productivity and performance. For developing this process, first of all, the theoretical analysis has been performed. Through the theoretical analysis, the effect of the rotating motion of the workpiece cylinder on the motion of the active abrasive particles has been studied in-depth. Also, under theoretical study, a surface roughness model has been developed to predict the finishing with the given process parameters. From the theoretical study, it is found that considering the tool rotational of 400 rpm, tool reciprocation speed of 70 cm/min, and cylinder workpiece rotation of 40 rpm opposite to the tool rotation in the present proposed R-MRH process, theoretically 65 nm of final surface roughness is evaluated with 40 min of finishing time from the initial surface roughness of 330 nm. Whereas in the existing MRH process when the tool rotation and reciprocation speed are kept the same i.e., 400 rpm and 70 rpm respectively but the workpiece cylinder is kept stationary, the final surface roughness is calculated as 102 nm with 60 min of finishing time from the initial surface roughness of 330 nm. Hence, theoretically, the improvement in productivity due to the workpiece rotation in the existing MRH process is clearly observed.

Further, based on the result observed from the theoretical analysis, the present rotational magnetorheological honing (R-MRH) process is developed. The design requirement in developing the R-MRH process is to rotate the workpiece cylinder precisely in the same axis of rotation as the MRH tool rotates and reciprocates during the finishing operation. Therefore, to fulfill this need of the design requirement, suitable fixtures have been designed and fabricated for holding and rotating the different size of workpiece cylinders. Further, to confirm the improvement achieved in finishing performance and productivity as compared to the existing MRH process, an experimental study has been performed. From the experimental study, it is found that using the R-MRH process, the final surface roughness value of 50 nm is achieved in 40 min as compared to the 90 nm in 60 min which is achieved while using the existing permanent magnet-based MRH process for the same initial surface roughness value of 330 nm. This also further experimentally validates the significant improvement in finishing performance and productivity with the present R-MRH process.

Furthermore, to validate the present developed R-MRH process performance in fine finishing of the real time industrial cylindrical workpieces, the detailed experimentations have been performed and successfully demonstrated on the inner surface of the outer race of ball

bearing of EN-31 steel, cylindrical barrel of hydraulic cylinder, cylindrical mold for manufacturing the plastic bottle caps, and cast-iron cylindrical mold. So, the optimal parameters are predicted using the response surface methodology to achieve the maximum finishing performance in terms of percentage reduction in surface roughness value on the ferromagnetic EN-31 steel material and on the above-mentioned real time industrial cylindrical workpieces. The results obtained from the different experimentations performed in the present work have been analyzed through the surface roughness measurements, scanning electron microscopy images, waviness, and circularity of the inside cylindrical profile of the workpieces. From the results obtained in this work, it has been observed that the present developed R-MRH process is found in good order for finishing the internal cylindrical surface of the various industrial components with improved productivity for improving their operational functionality. Also, the fine finished internal surface of the cylindrical molds can produce end products with a smooth surface and geometrically correct.

The R-MRH process is further improved in terms of the less expansive, less time, and labour-intensive by introducing an in-situ MR honing tool. Using the in-situ MR honing tool, the traditional honing as well as the R-MRH process can be performed on the internal surface of a cylindrical workpiece at a single setup. To confirm the feasibility of the in-situ honing tool for finishing the internal surface of the cylindrical workpiece through traditional honing as well as MR honing, preliminary experimentations have been performed. Using this tool, the internal cylindrical surface of the mild-steel workpiece has been finished first with the traditional honing and then the MR honing using the same in-situ tool on the same setup. The surface roughness value is achieved to 550 nm from the initial machined surface roughness value of 1510 nm with the traditional honing in 40 min and then 60 nm from the traditionally honed surface of roughness value of 550 nm with the present magnetorheological (MR) honing in 60 min. Hence, this result has experimentally demonstrated the ability of the newly designed in-situ MR honing tool to perform traditional honing as well as magnetorheological honing on a single setup which makes this tool more useful in industries for micro-finishing to fine finishing without changing the tool and finishing setup.

LIST OF FIGURES

LIST OF TABLES

LIST OF ABBREVIATIONS

AAPs	Active abrasive particles
AFF	Abrasive flow finishing
AFM	Abrasive flow machining
ANOVA	Analysis of variance
CAD	Computer aided design
CBN	Carbon boron nitride
CIPs	Carbonyl iron particles
CMAF	Chemically assisted magnetic abrasive finishing
CMM	Coordinate measuring machine
CNC	Computer numeric controller
EIPs	Electrolytic iron particles
FEA	Finite element analysis
FMAB	Flexible magnetic abrasive brush
MAF	Magnetic abrasive finishing
MAAFM	Magnetically assisted abrasive flow machining
MMCs	Metal matrix composites
MR	Magnetorheological
MRAFF	Magnetorheological abrasive flow finishing
MRF	Magnetorheological finishing
MRH	Magnetorheological honing
MRP	Magnetorheological polishing
MRR	Material removal rate
PLC	Programmable logic controller
R-AFF	Rotational abrasive flow finishing
R-MRAFF	Rotational magnetorheological abrasive flow finishing
R-MRH	Rotational magnetorheological honing
RSM	Response surface methodology
SEM	Scanning electron microscopy
SiC	Silicon carbide
SR	Surface roughness

LIST OF NOMENCLATURES

A_{mr}	Area of the MR polishing fluid lying in between a curved permanent and the cylindrical workpiece (m^2)
A_{prj}	Projected area by the indented part of an active abrasive particle on the workpiece surface (m^2)
Ar	Area of a cross section (m^2)
B'	Magnetic field in the working gap including the magnetic effect of the MR polishing fluid and the ferromagnetic workpiece cylinder (Wb/m^2)
B_r	Radial component of the magnetic field (Wb/m^2)
B_z	Axial component of the magnetic field (Wb/m^2)
D_s	Major diameter of the spline shaft (mm)
$B_\emptyset$	Azimuthal components of the magnetic field (Wb/m^2)
D_t	Translational distance of the rack (mm)
d	Depth of indentation (m)
d_a	Diameter of SiC abrasive particle (m)
d_i	Indentation diameter (m)
F_{axs}	Axial shear force (N)
F_{cen}	Centrifugal force applied by an active abrasive particle due to MRH-tool rotational motion (N)
F_{fr}	Frictional force (N)
F_{in}	Indentation force (N)
F_{int}	Magnetic interaction force (N)
F_{mn}	Normal magnetic force (N)
F_{mr_ax}	Axial shear force applied by an active abrasive particle during performing MR honing using in-situ honing tool (N)
F_{mr_cut}	Total cutting shear force applied by an abrasive particle while performing MR honing using in-situ honing tool (N)
F_{mr_n}	Magnetic normal force applied by an abrasive particle during performing MR honing using in-situ honing tool (N)
F_{mr_tn}	Tangential shear force applied by an active abrasive particle during performing MR honing using in-situ honing tool (N)
F_s	Total cutting shear force (N)
F_{tns}	Tangential shear force (N)
F_{tr_ax}	Axial shear force applied by an abrasive of honing stone of the in-situ honing tool on internal surface of the workpiece due to its reciprocating motion in traditional honing (N)
F_{tr_cut}	Total shear force applied by an abrasive of honing stone while performing the traditional honing (N)

F_{tr_n}	Normal force applied by an abrasive of the honing stone of in-situ honing tool on the internal surface of the workpiece due to its firm contact in traditional honing (N)
F_{tr_tn}	Tangential shear force applied by an abrasive of honing stone of in-situ honing tool while traditional honing (N)
F_{tw}	Tangential shear force due to the effect of the rotational motion of the cylindrical workpiece (N)
H_{BHN}	Brinell hardness number (BHN)
H_c	Height of permanent curved magnet (mm)
H_w	Height of the permanent curved magnet (mm)
H_r	Radial component of magnetic field intensity (A/m)
H_z	Axial component of the magnetic field strength (A/m)
$H_\emptyset$	Azimuthal component of magnetic field intensity (A/m)
H	Resultant magnitude of magnetic field intensity induced by the permanent curved magnet (A/m)
$\vec{J}$	Magnetic polarization (Wb-m)
j	Radius of the electrolytic iron particle (EIP) (m)
L	Length of helical path followed by an active abrasive particle (m)
L_{act}	Actual length covered by the abrasive particle (m)
l	Length of arc of the curved permanent magnet (mm)
l_a	Length of the base of roughness peak (m)
l_a	The length from which the material is removed by the active abrasive on the peak (m)
M	Magnetization of the magnetic field (A-m^2/kg)
M_{EIP}	Magnetization of electrolytic iron particles (EIPs) (A-m^2 /kg)
$\mathrm{M_{work}}$	Magnetisation of mild steel cylindrical workpiece (A-m^2/kg)
m	Mass of single electrolytic iron particle (kg)
m_{ab}	Mass of abrasive particle (kg)
N	Rotational speed of an active abrasive particle (rpm)
N_1	Rotational speed of the magnetorheological honing tool (RPM)
N_2	Rotational speed of the ferromagnetic cylindrical workpiece (RPM)
N_{ab}	Total number of active abrasive particle
N_{ah}	Number of active abrasive particles per helical path
n_{ab}	Total number of abrasive particles in the MR polishing fluid
P	Pitch of helical path (m)
P_n	Normal load acting on the internal surface of the cylindrical barrel of

	the hydraulic cylinder (N)
R	Outer radius of the permanent curved magnet (mm)
Ra	Centreline average roughness value (μm)
R_a^0	Initial surface roughness of the finishing surface (μm)
R_a^n	Average surface roughness in n^{th} stroke (μm)
R_a^{n-1}	Average surface roughness in $(n-1)^{th}$ stroke (μm)
r_0	Inner radius of the permanent curved magnet (mm)
r_1	Inner radius of mild steel cylindrical workpiece (mm)
T_s	Time period to complete one stroke by magnetorheological honing (MRH) tool (sec)
T_c	Time period to complete one finishing cycle by the MRH-tool (sec)
t	Thickness of permanent curved magnet (mm)
u_t	Tangential relative velocity of the active abrasive particles (cm/min)
v	Axial velocity (cm/min)
V_{re}	Volume fraction of electrolytic iron particles in the MR polishing fluid
V_{ra}	Volume fraction of SiC abrasive particles in MR polishing fluid
V_{sep}	Volume of single electrolytic iron particle (m^3)
V_{eip}	Total volume of electrolytic iron particles in the MR polishing fluid (m^3)
V_{abp}	Total volume of SiC abrasive particles in MR polishing fluid (m^3)
V_{sab}	Volume of single abrasive particle (m^3)
V_s	Volume of material removed by one active abrasive particle following the actual length of distance (m^3)
V_{ts}	Volume of material removed in one n^{th} stroke of finishing by total active abrasive particles (m^3)
V_{mr}	Volume of the MR polishing fluid in the working gap between the four curved magnets and inner surface of cylindrical workpiece (m^3)
Q	Collect coefficient
W	Distance amid the centres of two EIPs (m)
α	Helix angle (rad)
δ	Constant
θ	Half angle subtended at the centre of the abrasive particle by indented part of the abrasive particle (rad)
θ_s	Angular distance of the nut connected to the spline shaft (rad)
μ	Viscosity of the fluid (m^2/sec)
μ_0	Magnetic permeability of space (N/A^2)

μ_{sf}	Static friction coefficient
μ_l, μ_m, μ_n	Frictional interaction parameters of roughness peaks, valley and wear part respectively
μ_{MRP}	Relative permeability of MR polishing fluid
μ_{rwork}	Relative permeability of the mild steel cylindrical workpiece
τ	Shear stress of the viscous fluid (N/mm^2)
τ_0	Dynamic yield shear stress of the viscous fluid (N/mm^2)
τ_{axs}	Axial shear stress (N/mm^2)
τ_{tns}	Tangential shear stress (N/mm^2)
$\emptyset$	Angle made by permanent curved magnet at central axis of the magnet (rad)
$\emptyset_1$	Angle made by first lateral edge of the permanent curved magnet to the X-axis (rad)
$\emptyset_2$	Angle made by second lateral edge of the permanent curved magnet to the X-axis (rad)
χ_m	Mass of magnetic susceptibility (kg/m^3)
ω	Relative angular speed of an active abrasive particle (rad/min)

CHAPTER 1

INTRODUCTION

1.1 Introduction

Deviation of the surface along the normal direction from the ideal flat surface is defined as surface roughness. It is impossible to achieve zero height of the peaks and valleys on the surface, but it can be decreased. The process of reducing the roughness of any surface is known as the finishing of that surface. The aim of surface topography characterization is to reflect surface topography with parameters that can be used to monitor the manufacturing process and the functional performance of surfaces (Krolczyk *et* al., 2014). In the modern industries, the surface finishing is an extreme need of the components for improving their operational functionality, reliability, consistent performance, and prolonged service life, (Jain, 2008). Also, the fine finished surfaces of the industrial components add numerous of the crucial qualities such as dimensional precision, closer fits and tolerances, reduced power loss, friction, increased corrosion and wear resistance, etc. in the parts (Das *et* al., 2012; Jain *et* al., 2007). Categorically, the need of finished internal surface of the cylindrical components is very crucial for improving their precision fits, and functional improvement in modern industries. The examples of such industrial cylindrical components are hydraulic cylinders, hydraulic and pneumatic valves, aerodynamic bearings, precision machinery tools, medical device's components, cylindrical barrel in injection molding machines, engine cylinders, etc. (Martínez-Mateo *et* al., 2011; Quan *et* al., 2014). In the manufacturing industries, precise surface finishing of the products consumes 10% to 15% of the total cost of their manufacturing (Jain, 2008). The finishing expenses depend on the various aspect such as types of the material of components, level of finishing requirement, quantity of finishing, etc. The selection of an appropriate finishing process to finish a particular component for achieving the requirement at minimum cost is an important task. In this section of the present work, the finishing processes which are useful for finishing the internal cylindrical surface of the workpieces have been studied. The inner surface of the cylindrical workpieces is usually finished with the following traditional and advanced finishing processes.

1.2 Traditional finishing processes to finish the internal surface of cylindrical workpieces

In traditional finishing processes, materials are eradicated from the finishing surface of the workpieces by sharp-edged multipoint cutting tools with direct contact (McGeough, 1980).

The multipoint cutting edges are the rigidly bonded of the abrasives. Finishing with the traditional methods of surface finish causes the acting of uncontrolled finishing forces on the internal surface of the cylindrical workpieces. These uncontrolled finishing forces result in several surface defects on the finished surface of the workpieces. Finishing a component which has extraordinary material properties (high tensile strength, high heat resistance, high hardness, etc.), complex-shaped components, miniature features is a tedious task (Jain, 2008; Das *et* al., 2011). The cylindrical-shaped workpieces which require finished internal surface are used in a vast variety of application in the industries and individual's machinery equipment. The internal surface of the cylindrical workpieces is finished using various traditional finishing processes. Some of these important traditional finishing processes are discussed below.

1.2.1 Internal cylindrical grinding

Internal cylindrical grinding is a rigidly hard bonded abrasive based finishing process that grinds the inside surface of the cylindrical components. The internal cylindrical grinding method is mainly used to improve the operational condition of the internal cylindrical surface of the components (Daneshi *et* al., 2014). The cylindrical grinder is always smaller than the diameter of the holes which is being ground. For internal grinding of a cylindrical part, this component is fixed in the chuck and rotated in the opposite direction alongwith the rotating and reciprocating cylindrical grinder as shown in Fig. 1.1.

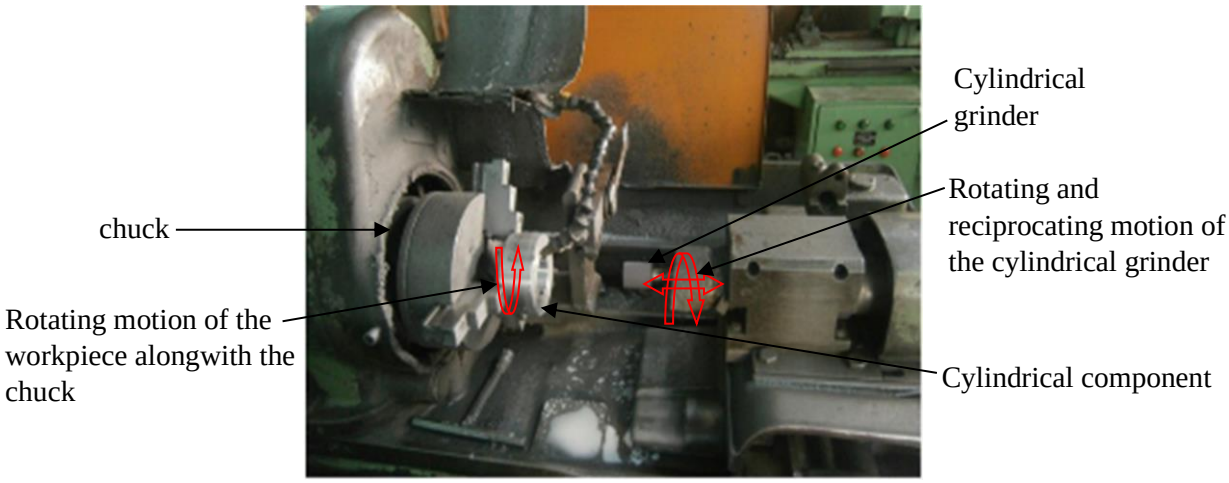

Fig. 1.1 Photograph of the experimental setup of the internal cylindrical grinding process (Jeevanantham *et* al., 2017).

The opposite rotational direction of the grinding wheel and the cylindrical component gives the reverse contact of the two surfaces resulting in the accomplishment of finishing action.

The surface finish obtained through cylindrical grinding on the cylindrical workpiece material steel (grade 90MnCrV8 with hardness 750 HV50) is ranging from 1.1 µm to 0.1 µm (Tawakoli *et* al., 2007). It can achieve out of roundness up to 1 µm (Tawakoli *et* al., 2007). However, the process has also some limitations. During the finishing operation, the grinding wheel makes a line contact for the substantial length of the cylindrical workpiece. This considerable line contact length results in an extensive rise in temperature which results in thermal damage. Also, it results in a change in mechanical properties of a workpiece due to continuous stresses and high temperature which leads to a thin martensitic layer on a workpiece and reduces material strength (Pan *et* al., 2017; Kumar *et* al., 2017). The cylindrical grinding plays a vital role in finishing the mechanical components of automotive industries (hydraulic cylinder, housing cylinder of power steering, brake master cylinder, engine valve, governor bushes, linkage lever governor, etc.), defense and aerospace industries (defense ammunition, bomb shell cartridge, auxiliary power unit, freezing cylinder, centrifugal separator, multi-cartridge filter housings, rocket motor casing, etc.), several kinds of molds for home appliances such as cookware, pressure cooker, cylindrical shaped tiffin box, etc.

1.2.2 Cylindrical lapping

Cylindrical lapping is a low normal pressure, two motions (rotating and axial), abrasive based finishing process. The material removal in this process is performed by abrasive particles mixed with fluid. The abrasive particles mixed fluid is rubbed between the lapping tool and the surface of workpieces. In this process, the removal of material takes place through abrasive mixed fluid rubbing between the lapping tool and the workpiece. The cylindrical lapping is used for lowering the out-of-roundness and surface roughness of the cylindrical holes of components (Alavijeh and Amirabadi, 2019). By employing the cylindrical lapping, the surface roughness is influenced greatly which further improves the service life and sincerely functioning of the component. Further, it also results in low friction and leakage. The experimental setup for the internal cylindrical lapping is shown in Fig. 1.2. There are many benefits of the lapping process, including highly dimensional and geometric precision, lowering the surface stress, reducing the surface roughness, etc. The minimum surface roughness achieved in this process is 64 nm from initial surface roughness of 1100 nm when the lapping tool was rotated at speed of 100 rpm. The internal diameter of the cylindrical workpiece (440c steel workpiece material) of 0.1 mm and its length is 20.82 mm (Alavijeh

and Amirabadi, 2019). This process is associated with the direct contact of rigid tool which results in several surface defects and finished upto limited range of surface finish.

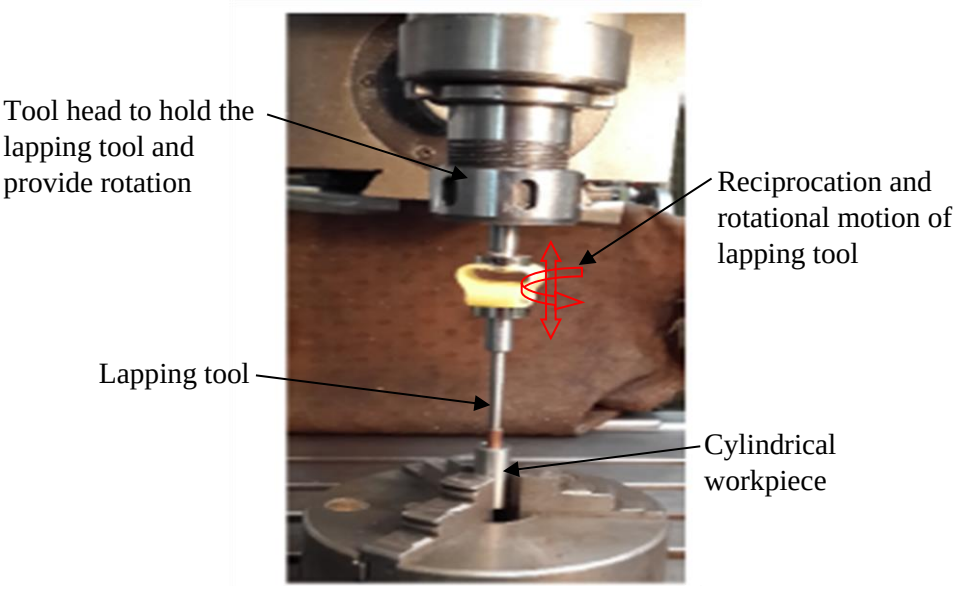

Fig.1.2 Experimental setup of the internal cylindrical lapping (Alavijeh and Amirabadi, 2019).

1.2.3 Jig grinding

Jig grinding is a finishing process that finishes the internal surface of the cylindrical as well as complicated-shaped holes to fulfill the requirement of the highest degree of accuracy. In this process, the jig grinder is used as a hard tool in which the position of table and spindle is made more accurate than the manual milling or lathe machine as shown in Fig. 1.3.

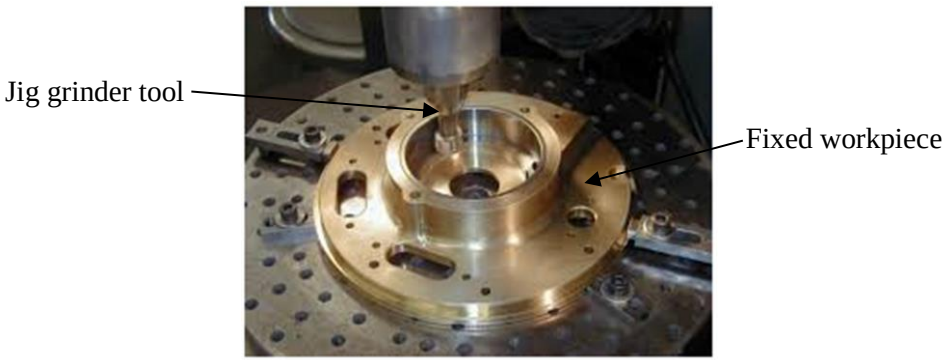

Fig. 1.3 Photograph of jig grinding operation (https://toolanddiemakings.blogspot.com/2016/12/jig-grinder.html?m=1).

Jig grinding machine uses automated control system to precisely control the motions of the grinder and tool holding spindle. Owing to which an operator assigns an incremental feed for

each reciprocating stroke between the successive feeds. The incremental feed distance and stroke count setting can be modified by a real-time operation. Therefore, such type of automation and control system make this process capable of providing the highest degree of accuracy and precision in finishing. Through this process, the accuracy in position and size can be achieved upto 2.5 µm (Sudheesh and Govindan, 2013). Therefore, process is highly used in the tool making industries for positional hole and pin die system. The applications of this process are to finish the components with very high-performance precision tools with blind hole type features. Also, this process is used in pneumatic valves, aerospace, automotive, electrical connector industrial components. The jig grinding machine is used to finish the internal surface of blind-hole type mold cavities. This machine uses coarse and fine abrasive bits respectively to finish the internal surface of the mold cavities. Due to the use of rigid abrasive bits and action of uncontrolled forces during finishing operation, the internal surface of blind hole type mold cavities results in some surface defects such as deep-seated groove, plowed material, and axial scratch (Bedi and Singh, 2018b).

1.2.4 Honing

Honing is a finishing process that can finish the internal surface of ferrous as well as non-ferrous cylindrical workpieces. In this process, honing tool performs simultaneously rotational and reciprocation motions inside the cylindrical workpieces. Due these motions of the honing tool, the cross-hatched lay pattern is formed which is used for retention of oil on the honed surface as shown in Fig. 1.4.

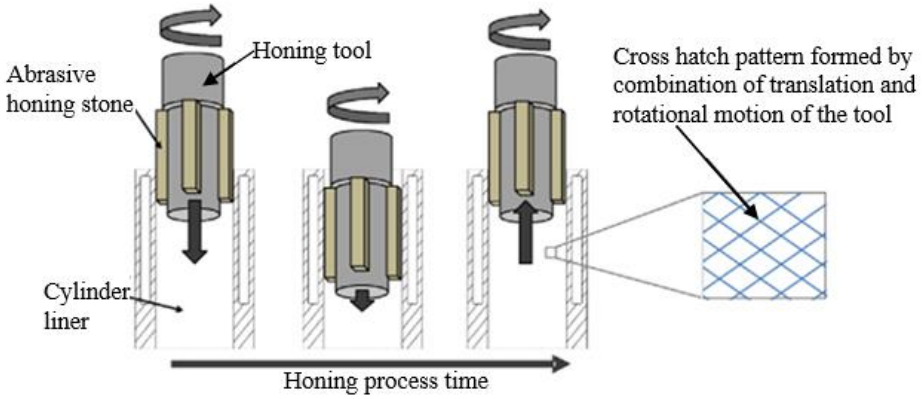

Fig. 1.4 Schematic of the honing process (Cabanettes *et* al., 2015).

The honing tool uses a honing stone to get a precisely finished surface on the internal cylindrical workpiece. The hone is made up of abrasive grits that are fastened with cement. The abrasive stone of hone is analogous to a grinding wheel, but the honing stone is more pulverulent so that it can adapt the form of the workpiece surface during abrasion (Tilger *et*

al., 2017). Alumina, silicon carbide (SiC), cubic boron nitride (CBN), and diamond are used for making a honing stone (Sabri *et* al., 2010).

In honing, contact of honing stone on the workpiece surface is relatively higher than in grinding. The higher contact of stone results in quick dissipation of heat generated during finishing (Hashimoto *et* al., 2016). Hence, lower thermal damage takes place due to low-temperature rise. As honing stones adapt the shape of the cylindrical workpiece surface, it continuously makes interaction with the cylindrical workpiece surface for a longer period of the finishing cycle with the light pressure due to honing stone. Therefore, the length of a chip obtained during finishing in this process is higher than the chip obtained in grinding (Jain, 2009). The speed of rotation, reciprocating, length of the honing stone, stroke, the position of the stroke and the pressure on honing stone are the parameters to take into consideration for performing honing on the internal cylindrical surface. The speed of honing stone in honing is relatively lower as compared to the grinding wheel in grinding (Sabri *et* al., 2011). But, still the material removal rate in honing is higher than in grinding. Because the higher contact of honing stone with workpiece surface abrades a higher material than material abraded in grinding process which is due to lower contact (line contact) of internal cylindrical grinding operation (Dimkovski *et* al., 2009). The honing operation typically removes upto 0.3 mm thickness of material (Grabon *et* al., 2010). Hydraulic and pneumatic cylinders, gun barrels, bearing liners, the bore of connecting rods, gear bore, etc. (Qin *et* al., 2016) are some essential industrial components in which honing plays a vital role in finishing. It also corrects the pre-operations inaccuracies like taper, out-of-roundness, waviness, axial distortion, undersize barrel, taper, boring marks, etc. The primary limitations of honing are it is not found useful for non-symmetrical or no-cylindrical workpieces. In addition, traditional honing can perform surface finishing to a certain extent of finishing, and after that finishing cannot be accomplished due to the rigid hard bonding nature of the abrasive tool. (Jain, 2009, Bedi and Singh, 2018).

1.3 Advanced finishing processes for the internal surface of cylindrical workpieces

The continuous development in materials science and their application have led to the need for nano-level surface finishing with excellent surface characteristics in various industries. To achieve these requirements using the traditional finishing processes is found a difficult task (Jain, 2008). Surface finishing on these newly evolved materials upto nano-level with high positional-accuracy, is a difficult task using the traditional finishing processes. Many times, the traditional finishing processes are found less effective to finish the products of various

shapes and sizes. Therefore, to get high precision, high accuracy over position and size, to enhance interchangeability of parts, to increase fatigue life, and to increase excellent quality, various types of advanced finishing processes have been developed (Jha and Jain, 2006a). All the advanced finishing processes which can finish the internal surface of cylindrical workpieces can be further categorized into two categories such as without and with external control over finishing forces. The advanced finishing processes without external control over finishing force are abrasive flow machining (AFM) (Loveless *et* al., 1994), rotational abrasive flow finishing (R-AFF) (Sankar *et* al., 2016). The advanced finishing processes with external control over the finishing forces are magnetic abrasive finishing (MAF) process (Heng *et* al., 2017; Mulik and Pandey, 2013), magnetorheological abrasive flow finishing (MRAFF) process (Jha and Jain, 2004), and rotational magnetorheological abrasive flow finishing (R-MRAFF) process (Das *et* al., 2010) whichs are mostly applicable for internal surface finishing of the non-ferromagnetic cylindrical workpieces. However, the electromagnet based magnetorheological honing (MRH) finishing process (Bedi and Singh, 2018a) and permanent magnet-based magnetorheological honing process (Grover and Singh, 2018) are the externally controlled (magnetic field assisted) internal surface finishing processes. These are applicable for finishing the internal surface of both ferromagnetic as well as non-magnetic cylindrical workpieces.

1.3.1 Abrasive flow machining (AFM)

AFM is the internal surface finishing process that is used to finish edges, deburr, and intricate surfaces with the use of the flow of abrasive-laden viscoelastic polymer (Rhoades, 1991). In AFM, two opposed piston extrude a viscoplastic polymer laden with abrasives to and fro through an obscure passage of workpiece as shown in Fig. 1.5. In this process, the abrasives interact where passage is restricted and their material removal takes place. The machining action in this process in comparison to the traditional internal cylindrical surface finishing processes is uniform and almost free from surface defects (Loveless *et* al., 1994). It helps to micro finish the materials ranging from soft materials like aluminum to hard materials like nickel alloys, ceramics, and carbides (Rhoades, 1991). This process is also found ideal for finishing the cylindrical dies and molds of automotive, aircraft, hydraulic components (Kumar and Hiremath, 2016). The consistency of material removal in this process allows precise sizing of miniature precision die passages (Kumar and Hiremath, 2016). This finishing process has a broad range of applicability from crucial aerospace and medical industrial components to higher production rates (Ibrahim *et* al., 2014). Using AFM, surface

roughness obtained as Ra 0.18 µm from 1.9 µm in five minutes cycle on multi-port aluminum extrusion die (Rhoades, 1991).

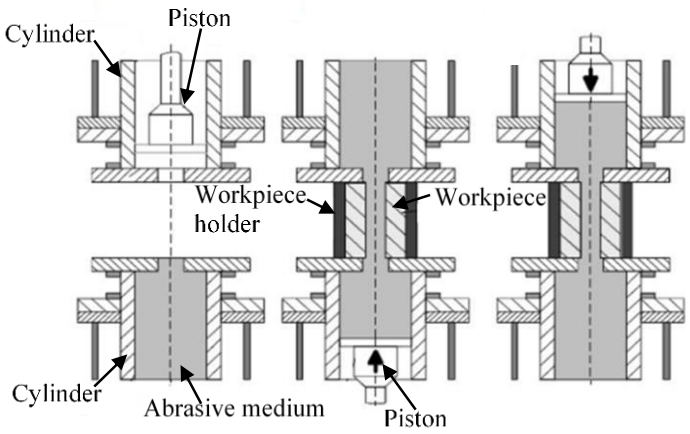

Fig. 1.5 Schematic diagram of finishing mechanism of the abrasive flow machining (Ibrahim *et* al., 2014).

With the use of this process in automotive industrial components, the performance of the high-speed type automotive engines is enhanced. It is also used in medical and turbine engine parts. In a turbine engine, the diffuser is finished through this process to improve the flow of air to the combustion chamber of the engine (Hashimoto *et* al., 2016). The main limitation associated with AFM is that, it is only applicable for the obscure passage of the cylindrical workpiece, this process is not suitable for the flat and open curved surface (Jain, 2008). The uncontrolled finishing forces applied by abrasive particles in this process induce several surface defects like pits, grooves, erosion marks on the internal surface of the workpieces.

1.3.2 Rotational abrasive flow finishing (R-AFF)

To achieve better surface finish, improvement in material removal rate (MRR), closer tolerances in abrasive flow finishing (AFF), the R-AFF process is developed. In this process, the cylindrical workpiece is rotated simultaneous to reciprocating motion of the finishing medium by the hydraulic actuators (Sankar *et* al., 2009) as shown in Fig. 1.6. The active abrasive particles perform the indeterministic motion due to the rotating motion of the workpiece cylinder at the same time when finishing medium is reciprocated (Sankar *et* al., 2009). Therefore, by incorporating the rotating motion of the workpiece cylinder in the previously established abrasive flow machining (AFM) method, enhancing the random motion of active abrasive particles is proven to be a crucial step for R-AFF development. This process has the same application as in abrasive flow machining (AFM). But the material

removal rate has enhanced due to the additional rotational motion of the workpiece in this process.

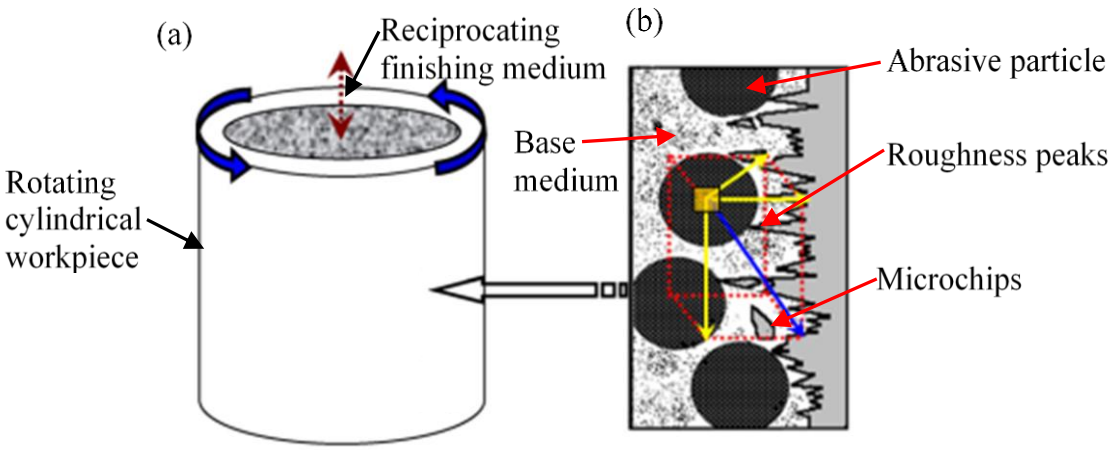

Fig. 1.6 (a) Schematic representation of finishing mechanism in R-AFF and (b) interaction of active abrasive particles with roughness peaks of cylindrical workpiece internal surface (Sankar *et* al., 2009)

1.3.3 Magnetic abrasive finishing (MAF)

MAF process is considered as the material removing process in the form of surface finishing in the existence of the magnetic flux density in the finishing region. This process is used to finish the surface of various shapes and sizes. To finish the inner surface of the tube-shaped workpiece, this process is used and known as the internal MAF process (Yamaguchi and Shinmura, 1999). Figure 1.7 shows a schematic of the internal MAF process with the stationary magnetic pole. Mixed powder of magnetic and abrasives particles is placed inside the tubular workpiece and are accumulated at the finishing area by the magnetic flux density, producing the finishing force on the inside surface of the cylindrical workpiece. The generator of the magnetic field can be an electromagnetic coil or a permanent magnet (Y. Wang and Hu, 2005). As the workpiece is made rotating at high rotational speed, the relative motion of magnetic abrasive particles taking place on the internal surface of the workpiece cylinder and abrades the material which results in the internal surface finishing of the workpiece cylinder. This process is found to achieve the surface finish upto 70 nm average surface roughness value on stainless steel (Yamaguchi and Shinmura, 1999). This process was mostly used for finishing the internal cylindrical surface of the hard materials like silicon nitride using a permanent magnet or electromagnetic (D. Wang *et* al., 2004).

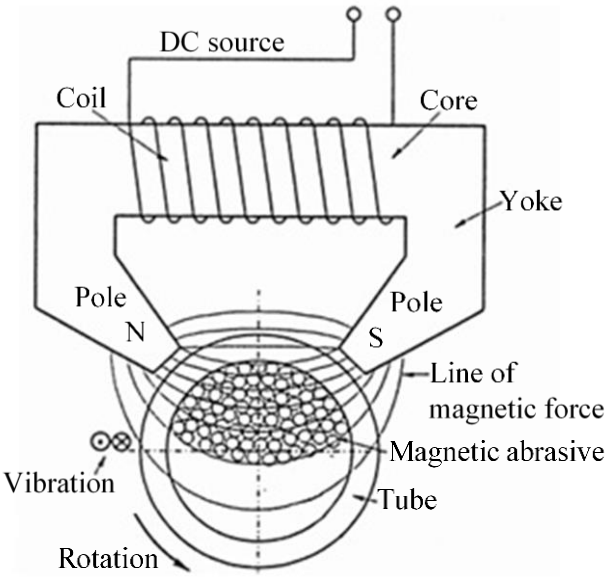

Fig. 1.7 Schematic of internal MAF process using stationary magnetic pole (Yamaguchi and Shinmura, 1999).

But, the MAF process has been used for effective finishing the internal surface of the non-ferromagnetic (SUS304) cylindrical tube in which FMAB performed the finishing (Yamaguchi *et* al., 2007). As in most of the literature on the MAF process, the source of the magnetic field is kept outside of the cylindrical workpieces. So, the MAF process has been found less effective for finishing the internal surface of the ferromagnetic cylindrical workpieces as relative motion of the FMAB over the ferromagnetic cylindrical workpiece surface may not be possible due to its stickiness. The FMAB formed by the dry powder of magnetic iron and abrasive particles under the influence of the magnetic field during the finishing process can produce scratches on the finished surface of soft workpiece materials (Heng *et* al., 2017). Also, a significant rise in temperature due to the dryness of the powder may cause thermal damage to the finishing surface (Yoon *et* al., 2014).

1.4 Magnetorheological polishing (MRP) fluid

Magnetorheological polishing (MRP) fluid is a magnetically keen smart fluid (Khatri *et* al., 2018). The MRP fluid is made by homogeneously mixing the magnetic iron and abrasives particles in the base fluid consisted of carrier medium like vegetable oil, mineral oil, paraffin oil, etc. and some surfactants or stabilizers such as grease, glycerol or oleic acid (Jain, 2009; Jha and Jain, 2004; Genc and Phule, 2002). In absence of the magnetic field, the MRP fluid acts like a Newtonian fluid. But, when it is kept under the existence of the magnetic field, this fluid acts like a non-Newtonian fluid (Sidpara *et* al., 2009). The MRP fluid follows the

Bingham plastic model according to which it behaves like a semi-solid when low stress is applied on the stiffened MRP fluid under existence of magnetic field. But, it flows like a viscous fluid when high stress is applied on the MRP fluid under magnetic field (Kamble and Kolekar, 2014). As the external magnetic field is applied to the MR polishing fluid, the magnetic particles of the polishing fluid produce dipoles. The particles with dissimilar poles get attracted and make chain structures of the magnetic iron particles as shown in Fig. 1.8. With the influence of the external magnetic field, the MRP fluid has a very rapid responses time with its responds in milliseconds (Sidpara *et* al., 2009).

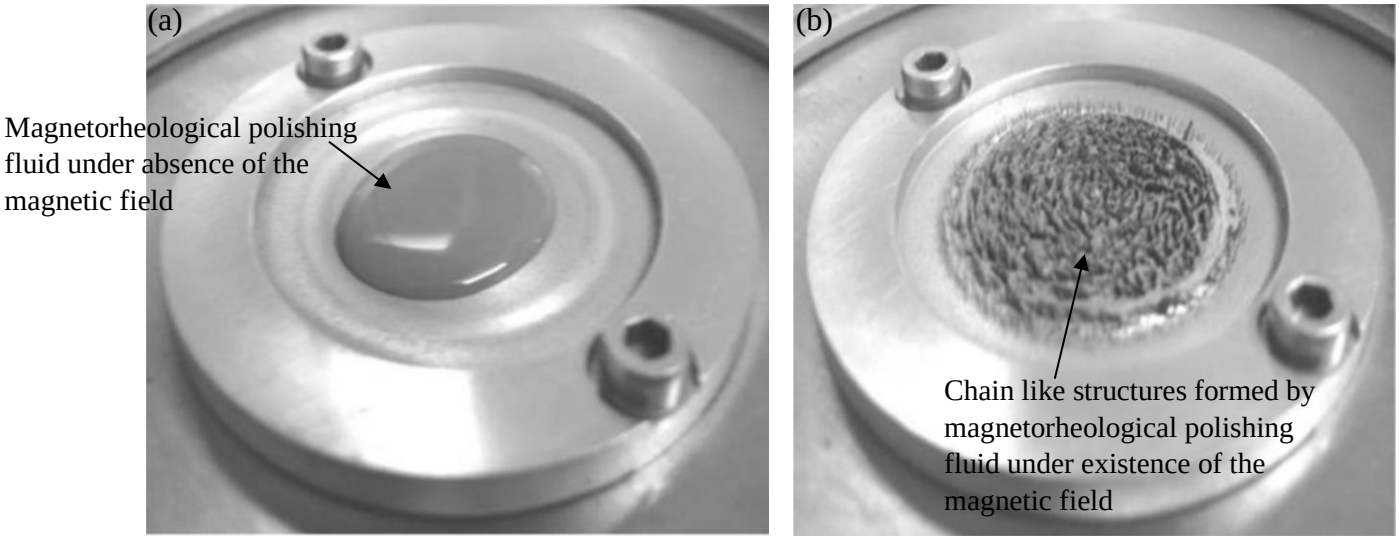

Fig. 1.8 Magnetorheological polishing fluid under (a) absence of the magnetic field, and (b) presence of the magnetic field (Sidpara *et* al., 2009).

1.4.1 Characteristics of the magnetorheological polishing (MRP) fluid

- MRP fluid is very quick responsive towards the magnetic field
- It has low viscosity under the absence of the magnetic field
- The MRP fluid shows great yield strength under influence of the magnetic field
- The oil as a base fluid of the MRP fluid makes it corrosive resistant
- Because the MRP fluid is thoroughly mixed, the particles contained in it have less lumps.

1.4.2 Constituents of the magnetorheological polishing fluid

The magnetorheological polishing (MRP) fluid performs a significant role in finishing operation when the magnetic field is applied into it. The MRP fluid is a suspension of magnetic iron particles and micron-sized abrasives in the base fluid (carrier medium i.e. oil or water, and surfactants or additives) (Niranjan and Jha, 2014). The various formulations of the

iron particles and abrasives based on their sizes are suspended and mixed homogeneously in the base fluid to produce the MRP fluid (Chen *et* al., 2016). The rheological nature of the MRP fluid is influenced by the its temperature change and chemical composition (Sidpara *et* al., 2009). The rheological properties of the MRP fluid differ with the variation in several formulations of the iron particles, abrasive particles, and base fluid under the different magnitude of the magnetic field. The detailed study about each constituent of the MRP fluid is given as follows.

1.4.2.1 Magnetic particles

The magnetic particles of the magnetorheological polishing fluid are the key components. These particles are the only responsible components of the polishing fluid for making the chain structures and gripping the abrasive particles under influence of the magnetic field. The gripped abrasive particles perform the finishing operation. This happens because of the rheological behavior of the magnetorheological polishing (MRP) fluid. Due to the magnetic field applied in the MR polishing fluid, the iron particles of the polishing fluid form dipole. So, each magnetic iron particle under the influence of an external magnetic field gets attracted towards the opposite pole of the nearby magnetic iron particle. Due to such activity performed by each magnetic iron particle of the MRP fluid in the influence of the magnetic field, a columnar structure or chain structure is formed. The strength of poles formed in the magnetic iron particles depends on the strength of the magnetic field. Therefore, as the distance of the MRP fluid from the magnetic field increases, the strength of the chain structures of the iron particles decreases (Jha and Jain, 2006), and accordingly it affects the finishing performance. The carbonyl iron particles (CIPs) and the electrolytic iron particles (EIPs) are the commonly used as the magnetic particles. The CIPs are very pure iron which are prepared of the pure iron pentacarbonyl. The shape of the CIPs is found spherical. The EIPs are formed by the electrolytic deposition of the metal from an aqueous solution in which a compatible electrolytic iron is produced. Also, this metal is laid on a cathode and can then be chipped away from the cathode and crushed into a fine powder. Unlike the CIPs, the shape of the EIPs is found as irregular.

1.4.2.2 Abrasive particles

The abrasive particles of the MRP fluid are non-magnetic hard particles that are gripped into the chain structure of the magnetic iron particles under the existence of the magnetic field. Due to their hardness and being firmly gripped into the stiff chains of the magnetic particles,

these abrasives cause the removal of material while finishing operation. The abrasives which contact the finishing surface of the workpieces while finishing operation are known as active abrasive particles. Since the abrasive particles face the peaks of the surface roughness for abrading them while finishing action, so the properties of the abrasives play a vital role for finishing operation. The properties of the abrasives which influence the finishing performance are shape, size, and hardness (Torrance, 2002). Some commonly used abrasive particles are silicon carbide (SiC), carbon boron nitride (CBN), alumina (Al_2O_3), etc.

1.4.2.3 Carrier fluid

In the MR polishing fluid, the carrier fluid is utilized to suspend the magnetic and abrasive particles in it. The carrier fluid must possess some vital characteristics for its better functioning in the MRP fluid which are the high boiling point, resistance to corrosion, low freezing point, and capable to add rheological behavior in the MR polishing fluid. Mostly carrier fluid is used as oil-based or water-based. The oil-based carrier fluid is found more effective against sedimentation as it has high viscosity (Sidpara *et* al., 2009). Some examples of the carrier fluid are vegetable oil, paraffin oil, water, mineral oil, etc.

1.4.2.4 Stabilizers/additives

To properly disperse the abrasive particles and magnetic iron particles in the carrier fluid for preparing the MR polishing fluid, the stabilizers are added (Sidpara *et* al., 2009). The AP3 grease or thixotropic additives are included in the MRP fluid for raising the stability of the particles. Also, some additives are urgently added to avoid the oxidation of suspended magnetic iron particles in the MR polishing fluid. The glycerol is added as a stabilizer in the MRP fluid for enhancing the suspension of the magnetic and abrasive particles in the polishing fluid (Sidpara and Jain, 2012).

1.5 Magnetorheological polishing (MRP) fluid-based internal finishing processes

The magnetorheological polishing fluid-based finishing processes are the magnetically controlled advanced finishing processes that use the MRP fluid as a finishing medium. The rheological behavior of the MRP fluid is altered according to the need by regulating the external magnetic field. This property of the MRP fluid enables the MR fluid-based finishing processes to finish a large variety of the workpieces from hard to soft material, from simple to complex intricate geometric shapes. Therefore, finishing processes have been developed for finishing the internal surface of the cylindrical workpieces. Some of MR fluid-based

finishing processes are only effective for internal finishing of non-ferromagnetic cylindrical workpieces, but some of the processes are suitable for both non-ferromagnetic and ferromagnetic cylindrical workpieces for internal finishing.

1.5.1 Advantages of using MRP fluid-based finishing processes for finishing of the internal surface of the cylindrical workpieces.

The advantages of using the MR polishing fluid-based finishing processes for the internal surface of the cylindrical workpieces are as follows.

- Capability to finish the workpiece surface upto nanometer-scale of centerline average roughness value.
- Capability to finish the workpiece of great variety from soft to hard material, ferromagnetic to non-magnetic material, and flat to intricate surfaces.
- Capable for precise process control, therefore, results in perfect and excellent finishing.
- There is the least chance for the damages caused by heat generation, grains deformation and stress residual because the base fluid of the MRP fluid acts a coolant during finishing operation.
- There is no wear of cutting tool takes place because of the processing of MRP fluid in the interval of a certain period of a finishing cycle.
- Controlled finishing forces are applied on the finishing surface of the workpieces by controlling the magnetic field during finishing operation.

1.5.2 Magnetorheological abrasive flow finishing (MRAFF)

To retain the adaptability of abrasive flow machining (AFM) process and simultaneously to possess determinism and controllability of magnetorheological finishing (MRF) process, an abrasive-laden MRP fluid based MRAFF is established (Jha and Jain, 2004). The rheological property (Saraswathamma *et* al., 2015) of magnetorheological polishing (MRP)fluid which is used as a finishing medium in the MRAFF is controlled by the external magnetic field. Therefore, the performance of MRAFF process depends on the externally applied magnetic field, the extrusion pressure from hydraulic cylinders, and the number of finishing cycles. The hydraulically powered setup is devised in which MRP fluid is extruded from both sides of the opposed cylinder. The north and south poles of the magnet are placed outside of the cylinder as shown in Fig. 1.9. The magnetic lines produced from the electromagnetic poles magnetizes the carbonyl iron powder (CIP) particles and stiffens the MR polishing fluid. The

MRP fluid is made from CIP particles, silicon carbide (SiC) abrasives which are suspended into the mixture of grease and mineral oil and are mixed properly.

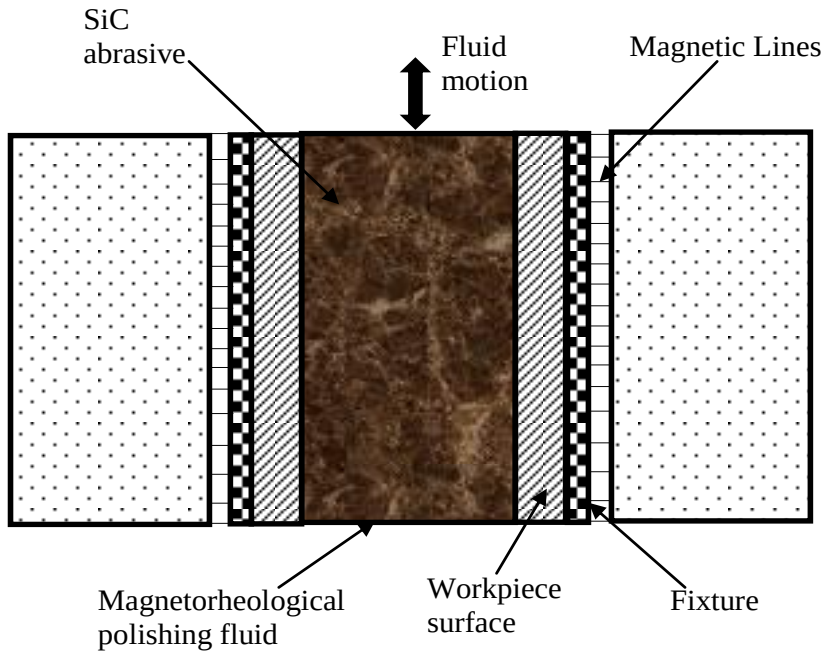

Fig. 1.9 Mechanism of MRAFF finishing action (Jha and Jain, 2006b).

The extrusion pressure acting on the MRP fluid is liable for material removal from the finishing surface of the workpiece. This results in cylindrical internal surface finishing. The best surface finish obtained in the MRAFF process was 0.09 µm surface roughness from 0.32 µm initial surface roughness in 200 finishing cycle. This result was achieved when MRP fluid was made of CIPs of diameter 18 µm and silicon carbide (SiC) particles of diameter 19 µm at magnetic field 0.531 T (Jha and Jain, 2006b).

1.5.3 Rotational magnetorheological abrasive flow finishing (R-MRAFF) process

A further improved finishing technique known as R-MRAFF (Das *et* al., 2010) has come into existence to finish the internal surface of the non-magnetic cylindrical workpieces with the improvement in the existing magnetorheological abrasive flow finishing (MRAFF) (Jha and Jain, 2004) process. In this process also, the magnetic poles are kept external to the cylindrical workpiece but these poles are made rotating when at the same time magnetorheological polishing fluid is reciprocated inside the cylindrical workpiece (Das *et* al., 2011). The motions of the polishing (MRP) fluid are intelligently controlled by the hydraulic unit associated with the setup (Fig. 1.10) to get the desired result regarding the surface finish. In this process, the MRP fluid is extruded through the inside surface of the

workpiece cylinder and provided reciprocating motion along with the axis of the tube by two opposed pistons in the workpiece cylinder by a hydraulic unit (Das *et* al., 2010). Simultaneously the magnetic poles are also given externally rotational motion. The rotational movement of the permanent magnetic poles surrounding the cylindrical workpiece fitments and the MRP fluid medium is also rotated. The surface finish obtained using this process is 16 nm in 1200 finishing cycles on cylindrical stainless-steel workpiece (Das *et* al., 2010). However, this process is found more effective to finish the internal surface of the non-ferromagnetic cylindrical workpieces such as stainless steel, high-speed steel, marine-grade steel, etc. and the least effective for the ferromagnetic cylindrical workpieces. This is because the magnetic field generator was kept outside the cylindrical workpiece/fixture. Due to which the magnetic field at the internal surface of the ferromagnetic workpiece cylinder is higher than in the MR polishing fluid. When ferromagnetic workpiece cylinder is finished, due to its magnetization effects all the magnetic particles of the MRP fluid get stuck on the finishing surface. Due to which the abrasive particles get resisted for performing the relative motion against ferromagnetic cylindrical workpiece surface and it results in inefficient finishing.

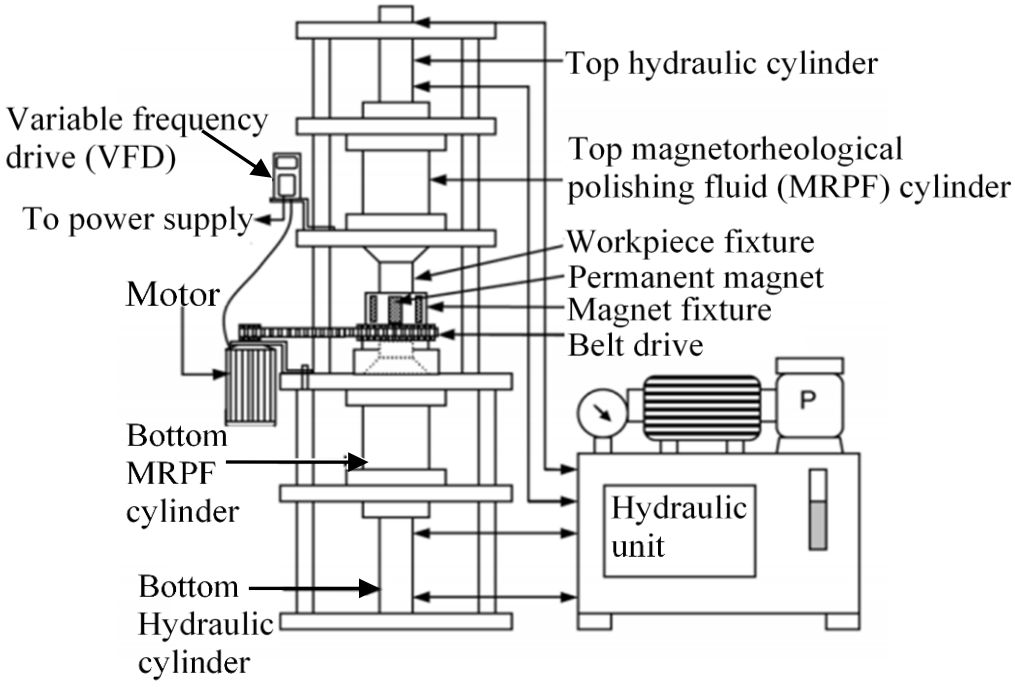

Fig. 1.10 Schematic diagram of experimental setup of R-MRAFF process (Das *et* al., 2010).

1.5.4 Magnetorheological honing (MRH) process for inner surface finishing of the ferromagnetic cylindrical workpieces

The MR polishing fluid-based process is developed to finish the inside surface of the ferromagnetic cylindrical workpieces. The scheme of the MRH experimental setup is shown in Fig. 1.11. In the existing MRAFF (Jha and Jain, 2004) and R-MRAFF (Das *et* al., 2010) processes, the MRP fluid is kept inside to cylinder and the magnetic poles are kept outside the cylindrical workpiece. Under presence of the magnetic field, the magnetic iron particles of the MRP fluid get magnetized and make a chain structure. The stiffness of the chain structure depends on the distance from the electromagnet. As the distance from the source of the magnetic field increases, the stiffness of chain structure decreases (Jha and Jain, 2006b). Therefore, in case of the ferromagnetic cylindrical workpiece, the MRP fluid gets stuck on the finishing surface and resists the relative motion of active abrasives over the inside surface of the cylindrical workpiece. To overcome this limitation, the MRH process has developed (Bedi and Singh, 2018a). In this process, an electromagnetic tool is made rotating and reciprocating inside the ferromagnetic cylindrical workpiece. Due to the inside location of the MRH tool, the strength of the magnetic field in the MRP fluid is higher than the inside finishing surface of the ferromagnetic cylindrical workpiece. The lower magnetic field at the finishing surface of the ferromagnetic workpiece enables the proper relative motion of active abrasive particles over it which results in the material removal causing in the form of nano-finishing. In this process, the surface finish is obtained as 83 nm in 90 minutes on the inside surface of the ferromagnetic mild steel) cylindrical workpiece from the initial surface roughness value 420 nm (Bedi and Singh, 2018a). The electromagnetic coils have been used to produce a sufficient magnetic field on the end surface of the electromagnetic MR honing tool. As continuous current is applied to the electromagnetic coils during the finishing operation, due to which coils get heated in just a few minutes. Therefore, the duration of a finishing cycle decreased in two consecutive finishing cycles. As a result, idle time increases, resulting in less productivity in the finishing process. Also, there were constraints on finishing the internal surface of the variable cylindrical workpieces with the same tool.

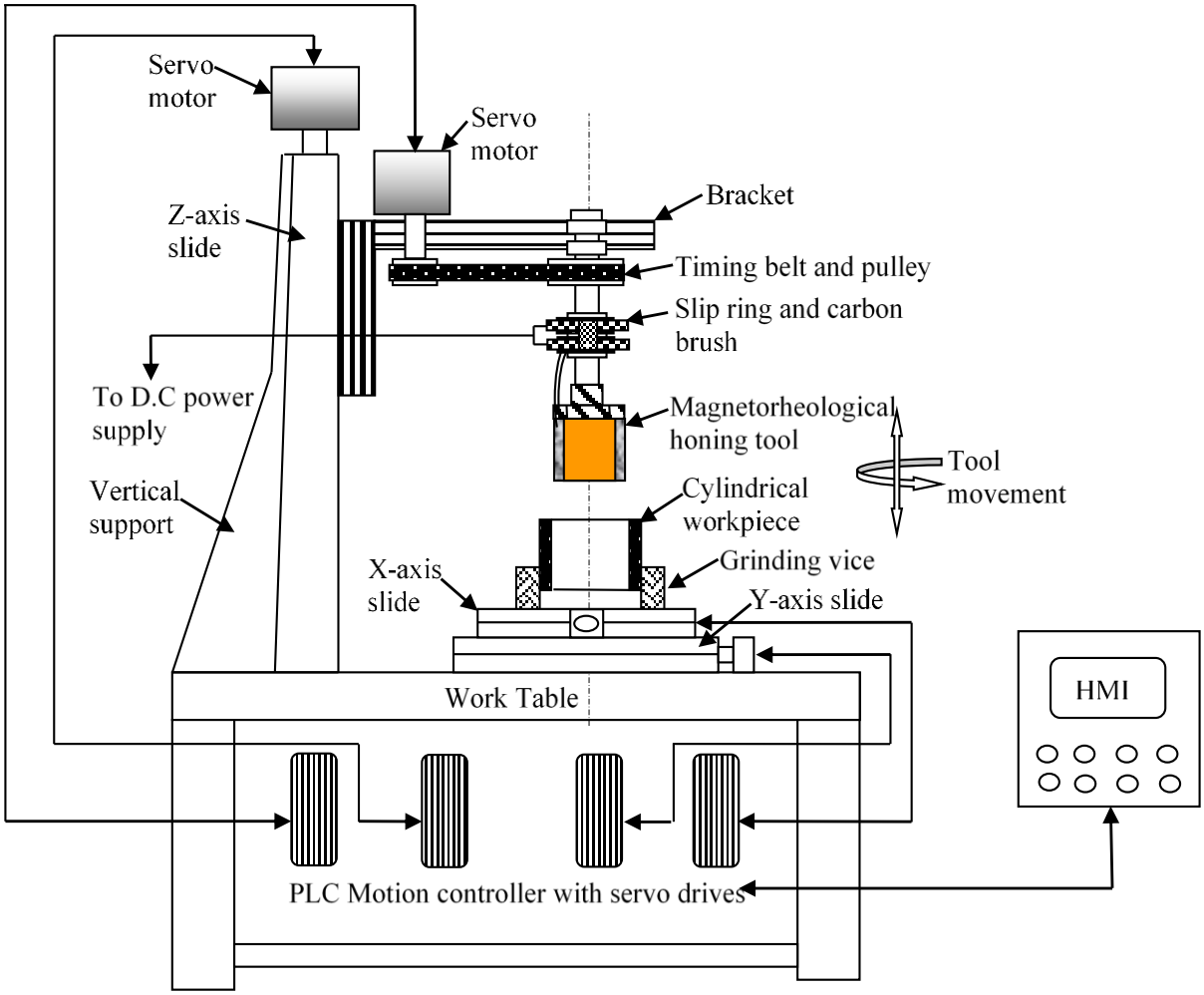

Fig. 1.11 Schematic representation of experimental setup of magnetorheological honing process for the inside surface of the ferromagnetic cylindrical workpiece (Bedi and Singh, 2018a).

1.5.5 Magnetorheological honing (MRH) process for internal surface finishing of variable diametric cylindrical workpieces

To overcome the limitations associated with the electromagnet based magnetorheological honing (MRH) process (Bedi and Singh, 2018a), a permanent magnet based magnetorheological honing process (Grover and Singh, 2018) is designed and developed for nano-finishing the internal surface of variable dimetric cylindrical workpieces as shown in Fig. 1.12. The MRH tool uses a permanent magnet as the magnetic field generator, and the distance of the magnet from the internal surface of the cylinder can be adjusted. This feature of the process therefore allows the various cylindrical workpieces of variable diametric sizes to be finished. In this finishing process, the surface roughness obtained on the internal surface of the ferromagnetic cylindrical workpiece is 88 nm in 60 minutes from the initial surface roughness value of 371 nm (Grover and Singh, 2018). With the assistance of servo motors, the permanent magnet-based MRH too is given rotating and reciprocating motion

simultaneously to perform the finishing action inside the fixed cylindrical workpiece. However, the finishing productivity of this process may be further improved with an increase in the relative motion of the active abrasive particles.

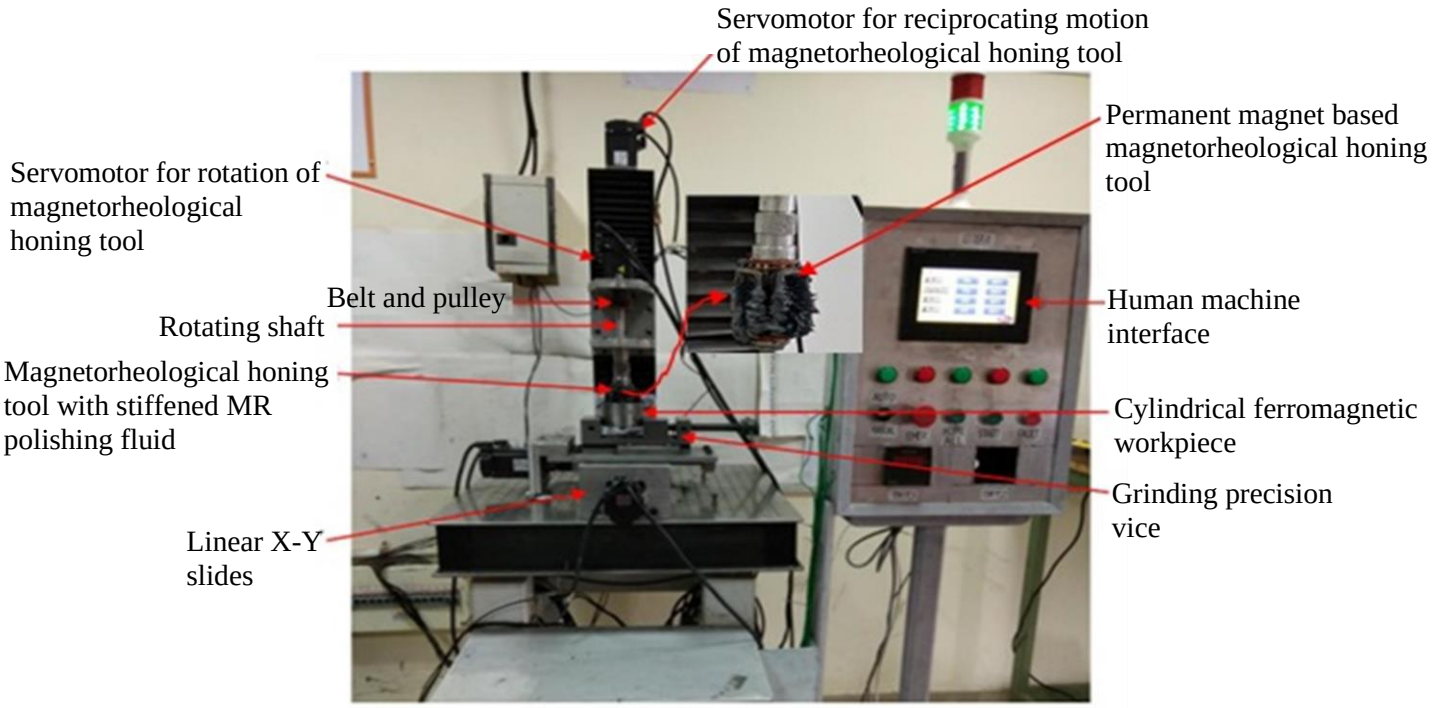

Fig. 1.12 Photograph of the experimental setup of the magnetorheological honing process for finishing the internal surface of variable diametric cylindrical workpieces (Grover and Singh, 2018).

1.5.6 Applications of various internal cylindrical parts in different industries

There is a great requirement of the finely finished components with the defect-free internal cylindrical surface to improve their functional performance. There are following some different types of industries where MR polishing fluid-based finishing processes can be used for effective internal surface finishing of the different cylindrical components.

- In defense industries various cylindrical components need a finely finished internal surface to improve the functional applicability, to make them corrosion-free, to make the related machinery less power-driven, reduce the noises while operating, etc. A few of these components used in the defense industry are a barrel of gun canon, cylinders, and valves of a defense vehicle engine, etc.
- The aerospace and automobile industries also need various cylindrical components with the finely finished internal surface for improving their functional performance, life cycle, to reduce the power loss by reducing friction on the internal surface of such

components. Some of the components used in the aerospace and automobile industries which need fine finished are hydraulic cylinders, hydraulic rack cylinder, power steering housing, cylinder liner, etc.

- Some cylindrical products which are produced by the casting method are found very critical to further finish using traditional finishing processes on their external surface because of their materials (plastic, glass, aluminum, fibers, and polyvinyl chloride). Therefore, for casting the components with highly finished external cylindrical surface, the mold's internal cylindrical surface must require fine finishing. The cylindrical molds which require fine-finished internal surface are centrifugal casting mold, cylindrical barrel for injection molding machine.
- In the optical industries, finishing the internal surface of the cylindrical optical products with the traditional finishing methods is a quite difficult task. Therefore, for MR polishing fluid-based finishing process can be a better alternative for finishing the internal surface of the optical industry. The components on which this process can be applied are optical lenses, funnels, tail, and headlights of cars, etc.

CHAPTER 2

LITERATURE REVIEW

The cylindrical components with uniform and the great integrity of the finished internal surface is a crucial aspect for improving operational functionality in manufacturing industries (Yamaguchi and Shinmura, 2000). Nowadays, nano-finishing the inner surface of the cylindrical workpieces is a major concern for many industries from different backgrounds. The advantages of nano-finishing in the components are dimensional accuracy, close fits and tolerances, enhancement in service-life of the tool, reduced wear, friction losses, etc. (Jha and Jain, 2008, Singh and Singh, 2019). The internal surface finishing with a higher accuracy and upto nano-scale is a tedious and time-intensive task (Gorana *et* al., 2004). The traditional finishing processes such as internal cylindrical grinding, jig grinding, and honing are commonly used to finish the internal surface of the cylindrical workpieces (Tawakoli *et* al., 2007; Sudheesh and Govindan, 2013; Sabri and Mansori, 2009). The cylindrical grinding uses grinding wheel that is bonded with hard abrasives. The grinding wheel is rotated inside the oppositely rotating workpiece cylinder for finishing its internal surface. Due to the rubbing action of the hard abrasive particles on the finishing surface of the workpiece, the materials get abraded and finishing action takes place. Similar action is performed in the jig grinding for precisely finishing the small holes. In this process, the tools and the workpieces are positioned accurately using automatically controlled system (Sudheesh and Govindan, 2013). In honing process, the tool is made rotating and reciprocating inside the workpiece cylinder. The honing tool is comprised of honing stones over its outside surface. The honing stones of the tool can be translated radially inward and outward depending on the required inner diameter of the workpiece cylinder to be finished. The honing stones are hard abrasives bonded stones which finishes the internal cylindrical surface. Traditional finishing processes utilize a rigid tool for finishing the internal surface of the cylindrical workpieces. Owing to which the tools of the traditional processes induce uncontrolled finishing forces in these processes. These uncontrolled forces generate various types of surface defects such as deep grooves, surface irregularity, cavities, grooves, residual stress, heat affected zone, torn and folded metals, and ploughed materials remained over the finished surface (Gupte *et* al., 2008; Jain, 2009). To achieve a good finishing and characteristics on the internal surface of the cylindrical components, several advanced finishing processes based on the magnetorheological polishing (MRP) fluid have been developed. The detailed literature on traditional and advanced finishing processes are explored in this chapter. Also, the limitations of the traditional finishing processes

in achieving fine-finished internal surface of the cylindrical components have been discussed in this chapter. In addition, it is explained the development of several advanced finishing processes, the material removal mechanism, and the theoretical analysis of some advanced finishing processes.

2.1 Literature related to the traditional finishing processes as applicable for finishing the internal surface of the cylindrical workpieces

The detailed literature review regarding traditional internal surface finishing processes is discussed as follows.

Tawakoli *et* al., (2007) developed a prototype internal cylindrical grinding machine. In this machine, two transmissible grinding wheels were placed on a spindle so that their axes of rotation are perpendicular to the rotational axis of the workpiece. The existing internal cylindrical grinding (Nadolny and Plichta, 2006) was concerned with a lot of undefined geometric cutting edges, large length of the tool for deep holes, less space in small holes causes poor supply for coolant. Due to these limitations in the traditional internal cylindrical grinding, it results in thermal damage, deflection of the tool, induced accuracy, and low material removal. Therefore, to overcome the issues related to the traditional internal grinding, this concept was introduced. In this concept, an internal cylindrical grinding unit was designed and developed using a 7 KW electromotor as spindle driver, flat belt for power transmission, and two grinding wheels for the left and right side of the unit. Abrasive grains used in the grinding wheel were of natural or synthetic material carbon boron nitride (CBN) with grain size of B126 and B252. The workpiece material considered for the experimentation was steel with grade 90MnCrV8. Its hardness was recorded as 750 Vickers hardness number. Using this newly developed unit, the improvement in surface roughness was achieved upto 0.1 µm and 0.2 µm by varying the infeed per grinding from 0.15 to 0.3 mm respectively. Despite these benefits of this internal cylindrical unit, it was only applicable for a cylindrical bore of a large diameter such as 100-110 mm.

Jeevanantham *et* al., (2017) studied the effect of the machining parameters on the material removal rate and surface roughness in the internal grinding process using the EN8 and EN31 steel. Using these two materials the experimentations were conducted. In this work, cutting force, cutting speed, and depth of cut are the machining parameters which were monitored to analyze the characteristics of outcome such as material removal rate (MRR), and surface roughness. For experimentation, the workpiece was fixed in the chuck of the lathe machine and the grinding wheel was held in the tailstock. The workpiece and the tool, both were made

rotating in the opposite direction to each other also the tool is made reciprocating simultaneously. From the results in the form of the relation between input parameters and output parameters, it was found that with an increase in depth of cut and cutting force from 0.13 to 0.2 mm and 44.33 to 114.1 N respectively, the surface roughness increases from 0.661 to 0.694 µm on the internal surface of EN8 steel cylindrical workpiece. However, on EN31 steel workpiece material with the same variation of the depth of cut and cutting force, the surface roughness increases from 0.628 to 0.682 µm. Hence, it was concluded that for achieving the good quality of surface finish on EN8 and EN31 steel, the depth of cut and cutting forces must be given as small as it could be possible for finishing action.

Hung *et* al., (2019) analyzed the effect of coolant parameters on the surface roughness in internal cylindrical grinding while finishing the annealed 9CrSi steel workpiece material. For this purpose, the concentration and flow rate of the coolant were investigated using central composited design and response surface methodology technique. With developed regression model, the effect of each parameter and their interaction effects were analyzed in this study. For this study, a MACHT-701 grinding machine equipped with a cylindrical grinding wheel was used. The optimum process parameters and their value used for the experimentation are tool depth of dressing cut at 0.15 mm, grinding wheel speed at 12 rpm, workpiece speed at 150 rpm, axial speed at 70 mm/min, and radial feed was considered at 0.0025 mm/double stroke. The minimum roughness surface roughness attained was 0.4102 µm from initial surface roughness 0.99 µm using the optimum parameters i.e., the concentration of coolant 3.907 % and the flow rate of 2.864 (ltr/min), respectively.

Sudheesh and Govindan (2013) performed comprehensive experimentation to evaluate the jig grinding process. Material removal rate and surface roughness were used to evaluate the finishing performance. The Taguchi L_9 orthogonal array technique is used to conduct the experimentation by selecting three parameters and three levels. The diamond abrasive with the vitrified bond is used in the grinding wheel. In each grinding experiment, the tool speed was varied as 48000, 51300, and 56200 rpm, and air was used as a coolant. For this experimentation, mild steel material is considered as the workpiece material. Through the experimental observation, it was found that 56200 rpm speed of grinding wheel, 50 mm/sec feed rate, and 0.03 mm depth of cut was the optimum value. At these optimum values of the parameters, the minimum surface roughness was achieved as 0.45 µm from initial surface roughness of 0.61 µm with 5 finishing set.

Lee and Malkin (1993) reported the basic investigation of the mechanics of the bore honing process. In this study, an experimental setup was established which was consisted of honing

machine instruments with spindle speed measuring sensors, expansion pressure, honing head displacement, and interfaced with a computer. The setup interfaced with computer was used for collecting the data and performing analysis. The honing machine used for experimentation in this work utilized an electric motor with configuration 3 to 6 V with 2.25 KW power. For reciprocating motion of the honing head during internal bore a hydraulic pump was used which was driven by the electric motor of power 2.25 KW. In this study, effects of normal force and grit size on the output parameters i.e., material removal rate, stone wear, honing ratio and surface roughness during honing of internal bore of cast iron with silicon carbide abrasive stone were investigated. From this study, the variation of surface roughness vs material removal rate with the variation of the grit sizes of the honing stones supplied by manufacturers (Mfr.) A, B, and C is shown in Fig. 2.1. As a result, the coarser grit stones produce rougher finishes. Clearly, the surface roughness requirement of the honing process imposes a limit on the grit size and removal rate which can be used.

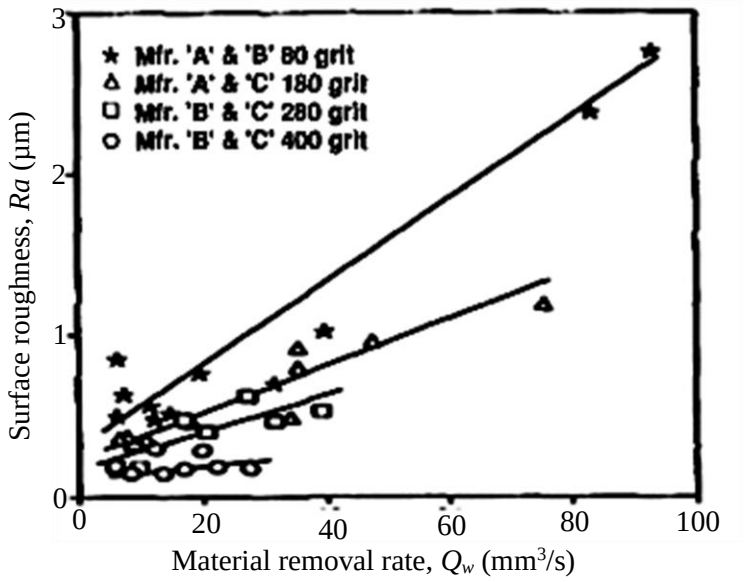

Fig. 2.1 Surface roughness versus material removal rate for grit sizes (Lee and Malkin, 1993).

Cabanettes *et* al., (2015) proposed a method to utilize a 3D confocal measuring instrument with automated positioning for measuring internal surface of the 600 motor blocks which were taken from production at different stages of the honing tool wear. This method was proved to be an improving action for performance of the liner system with accurate feedback of generated surface. To achieve the objective, there are six motor blocks with each having five-cylinder liners were examined with 20 topography per liner which makes a total 600 of 3D measurements. Beyond the 3D roughness measurement, honing texture information was also analyzed using the parameters. From this study, it was found that areal reduced summit height

(Spk), areal core roughness depth (Sk), and areal arithmetic mean summit curvature (Ssc) are the most important parameters linked with manufacturing characterization. The location on the internal surface of the bore where surface roughness measurement is performed did not influence the correlation between the roughness parameters and the honing tool wear. The relation between the measured parameter Sk on each cylinder and the honing tool wear is demonstrated in Fig. 2.2. From this figure, it was observed that Sk was influenced by the honing tool wear and cylinder's initial conditions. From the measured surface roughness values, it was observed that only a few parameters could trace the change in topography due to tool wear.

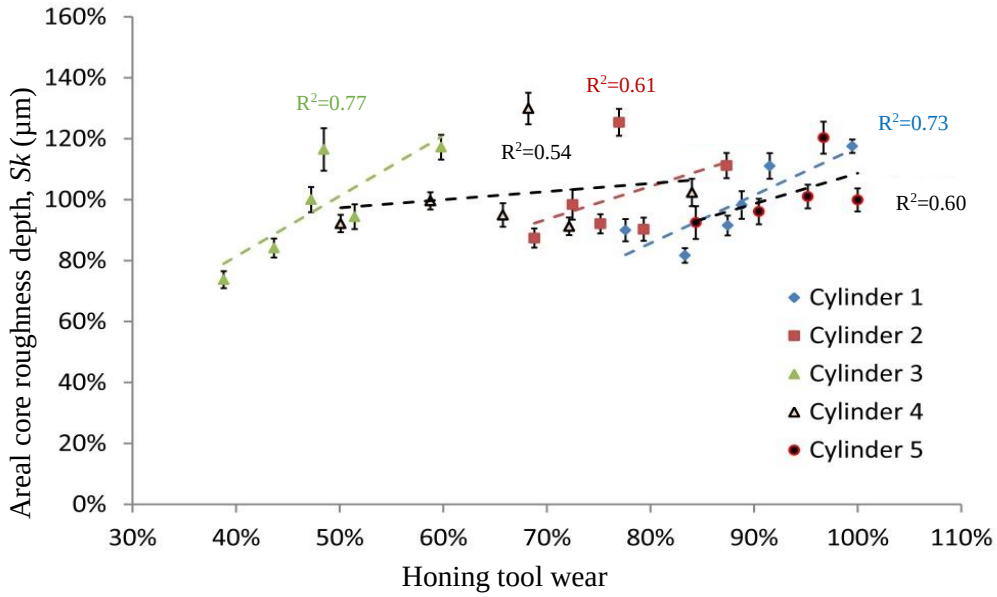

Fig. 2.2 The areal core roughness (*Sk*) increases with the honing tool specific to each cylinder (Cabanettes *et* al., 2015).

Sadizade *et* al., (2020) used a series of experiments and optimization desirability function approach to investigate the possibility of achieving the desired plateau surface in two steps of honing instead of three steps of honing to minimize machining time and increase productivity. For conducting this study, the initial surface roughness and honing angle for the plateau surface were considered as 0.75 µm and $30^{\circ} - 35^{\circ}$ respectively. The cast-iron cylinder blocks with a diameter of 99.86–99.88 mm and cylindricity tolerance of 0.015 mm were considered as the workpiece for this study. Rough honing and plateau honing were the two steps of the honing process to obtain the plateau surface. Both steps of the honing were performed at a single honing machine. For rough honing, the honing tool uses 8 honing sticks of the diamond abrasives whereas for plateau honing the same number of sticks of carbide materials were used. For optimization, five surface roughness parameters and a rough honing time were considered as output parameters in this study. From the optimized input parameters of this study, the

minimum surface roughness was achieved as 0.19 µm with 12.45 min of finishing time from the initial surface roughness of 2 µm. Therefore, the outcomes of this study disclosed that by replacing a three-step honing process with an optimized two-step process, the plateau surface can be achieved.

2.2 Superfinishing processes for the internal cylindrical surfaces without assistance of magnetic field

To achieve good surface properties in the various industrial cylindrical parts, several advanced finishing methods have been established that are based on the abrasive fluid finishing medium. The hydraulically powered extrusion pressure is used for providing the motions and finishing force to the abrasive particles of the fluid in such finishing processes. The literature reviews detailing the advanced finishing processes depending on the flexible abrasive based finishing medium and in which there is no external control on the finishing forces through the magnetic field are discussed below.

Gorana *et* al., (2006) performed a study to predict the surface roughness in the abrasive flow machining (AFM). In AFM, two vertically opposite cylinders extrude abrasive-laden viscoelastic putty back and forth in the passages formed between the workpiece and the machine tools. For various machining conditions of AFM, an analytical model is offered through which the surface roughness was simulated and predicted.

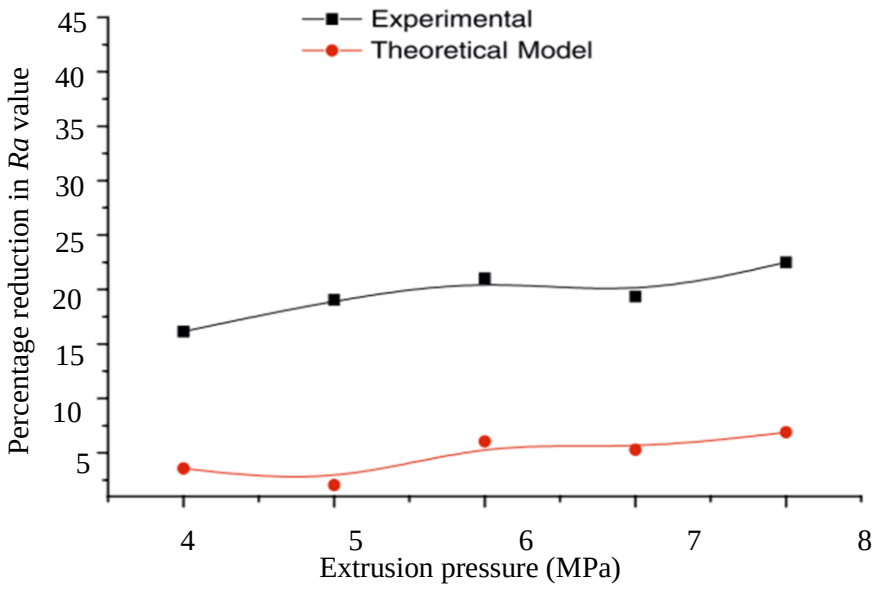

Fig. 2.3 Variation of percent reduction in surface roughness *Ra* values with extrusion pressure, when experimental conditions abrasive grain size=80, abrasive concentration=60% used (Gorana *et* al., 2006).

To describe the interaction between the abrasive grain and workpiece surface, the basic parameters of the AFM like, grain's size and concentration, active grain density, initial and final surface roughness are used. This study was conducted by systematically varying the parameters that are grain size, grain concentration, and extrusion pressure. The surface roughness model was developed assuming an asperity as an equilateral triangle. In the roughness model, the relation between the parameters and surface roughness was analyzed. For this study, the composition of the finishing medium was used silly putty and silicon carbide. To analyze the effect of the parameters predicted and the theoretical roughness, the experimentations were performed on the mild steel workpiece material. The trend of influences of extrusion pressure on theoretical roughness is found similar to the influence of the same parameter on experimental surface roughness. The error in the %age reduction in surface roughness of theoretical and experimental value is found approximately within the 10% with the variation of the extrusion pressure as shown in Fig. 2.3. From the outcomes of this study, it was also observed that with an increase in extrusion pressure, the %age reduction in surface roughness increases. Although this research provided a strong theoretical estimation of the effect of parameters on surface roughness.

Sooraj and Radhakrishnan (2014) performed internal finishing of the cylindrical workpiece with elastic abrasives using the concept of the abrasive flow finishing process. In this work, elastic abrasives were made by mixing the abrasive grits in the polymer beads using chemical solvent at an appropriate temperature. Based on the requirement of experimentation, the size of abrasive grits was selected for making these elastic abrasives. The fine abrasives were effectively ingrained in the elastomeric polymeric bead to generate elastic abrasive particles of an average size of 3 mm. The reciprocation motion to the elastic abrasives was given inside the cylindrical workpiece with the pneumatic power to the two oppositely installed pistons to the workpiece. Based on the reciprocating motion of the elastic abrasive particles, the axial shear force, and the effect due to this force in terms of volume of material removed was theoretically analyzed in this work. The experimentation was conducted on a tubular shaped sleeve of hardened steel 440C-58HRC workpiece. Further, the surface roughness was analyzed theoretically using the design of experiments with response surface methodology (RSM). Using central composite design under the RSM technique, the effect of axial-pressure, abrasive grain-size, and longitudinal stroke velocity of elastic abrasives on the surface finish was studied. Using this process for 60 min, 20-30 nm surface roughness was achieved from the initial surface roughness of 158 nm.

Sushil *et* al., (2015) performed an experimental investigation and optimized the process parameters of the abrasive flow finishing process for finishing the workpiece material of aluminium (Al) alloy with silicon carbide (SiC) and its metal matrix composites (MMCs). In this work, the composite materials with a high percentage of SiC (e.g., 20–60 % SiC in Al/SiC composites) were finished using the abrasive flow finishing method. The Taguchi method was applied to analyze the consequences of the input parameters on material removal rate (MRR) and change in surface roughness (ΔRa). It was noticed that the extrusion pressure is the most substantial factor in respect to MRR and ΔRa. The MRR and ΔRa got increased with an increase in the number of finishing cycles and then decreased. This trend was observed because initially there were more peaks and valleys which were initially abraded rapidly. From this study, the optimum MRR achieved from the confirmatory experiments was found as 8.81×10^{-6} g/s, and the predicted value of MRR was found as 8.59×10^{-6} g/s. Therefore, the percentage error between experimental and predicted MRR was found as 2.49. Similarly, the change in surface roughness (ΔRa) was found in the range of 0.40 µm - .70 µm. In addition, the maximum reduction in surface roughness (ΔRa) achieved at optimum process parameters was 1.72 µm in the experiments. However, this value (ΔRa) found from the predicted surface roughness model was 1.63 µm. Therefore, the %age error in a reduction in surface roughness from experimental to the predicted value was found as 5.23.

Sankar *et* al., (2010) introduced the rotating abrasive flow finishing (R-AFF) process to improve the finishing performance and material removal rate (MRR) of the existing abrasive flow finishing (AFF) process. The complete tooling setup was made rotational to make workpiece rotating and the finishing medium was reciprocated with the use of hydraulic actuators. Due to the rotational motion of the workpiece the abrasives of the finishing medium performed indeterministic motion with enhanced net relative speed. In comparison to the AFF, the finishing medium's active abrasive particles had a higher relative speed and indeterministic motion, which improved the finishing performance and MRR. The finishing medium used in this work was a mixture of styrene 25 % and butadiene 75 % repeating monomers along the polymer chain. The theoretical study of the shear force and motion performed by the active abrasives on the finishing surface of the workpiece was also carried out in this work. The workpiece materials utilized for the preliminary experimentations performed in this work were aluminium (Al) alloy and its metal matrix composites (MMCs). In this work, a comparative experimental analysis between AFF and R-AFF was performed to validate the improvement in finishing performance and MRR. In comparison to the AFF process for finishing on Al

alloy/SiC (10 %) MMC work materials, the R-AFF process resulted in a 44 % better improvement in surface roughness and 80 % greater material removal.

Sankar *et* al., (2019) prepared different kinds of in-house abrasive finishing medium with the variation of polymer (silicon-based), abrasive particles, and rheological additives. Viscoelastic base carrier, stearate as additives, silicone oil, hydrocarbon oil, and naphthenic oil as plasticizers, and silicon carbide as abrasive particles were used for preparing the finishing abrasive medium. Further, the static and dynamic rheological characterization was performed on the abrasive medium to understand the flowability and deformability of this medium. Using a central composite rotatable design, the static and dynamic rheological experiments were planned and performed on the parallel plate rheometer (Anton Paar® MCR series). The results of characterizations based on the composition of the abrasive medium are investigated through the ANOVA from the experimental study. Also, to understand the effect of different %age compositions of the abrasive medium on finishing of Al alloy/SiC (10 %) MMC and Al alloy/SiC (15 %) MMC, the experimentations are performed on the rotational abrasive flow finishing (R-AFF) setup. The effects of %age compositions of each constituent of the abrasive medium on the change in the surface finish were studied. Further, the optimum composition of material of finishing medium for the best finishing performance was found as silicon polymer 48 % by wt., plasticizer 5 % by wt. and the abrasive particles 37% by wt. for the workpiece material Al alloy/SiC (10 %) MMC. For this material (Al alloy/SiC (10 %) MMC) using optimum composition of finishing medium, the maximum reduction in surface roughness was recorded as approximately 0.20 µm.

2.3 Superfinishing processes for the internal cylindrical surfaces with assistance of magnetic field

Yamaguchi and Shinmura (2000) proposed an inner surface finishing technique based on magnetic abrasive by rotating the magnetic pole. This technique was introduced because in the previous research it is found that the process incorporating one of the characteristic behaviors of the abrasive, the jumbling of the abrasive, results in aggressive contact of the abrasive against the inner surface, disturbing the smooth surface finish. Due to which the smooth surface finish was getting disturbed. In this process, the permanent magnets were kept outside of the tube and the mixed powder of magnetic and abrasive particles was rotated by rotating the permanent magnet to finish the internal surface of the workpiece tube. There are two types of magnetic poles (tapered pole and non-tapered pole) based on their shape are used in this work to analyze the effect of their shape on finishing parameters. Therefore, the effect of the both

shapes of pole's rotational speed on the surface finish and material removal was analyzed. For this analysis, the initial surface roughness of the workpiece was considered as 2 µm. Beyond 1200 rpm, the material removal and surface roughness of the tapered pole were significantly improved. The tapered pole induces a magnetic field of high strength due to its edge effect at a small region of the finishing surface of the workpiece. This strong magnetic field results in a harder flexible magnetic abrasive brush (FMAB) which results in higher material removal at a higher rotational speed. But, for the non-tapered pole, when the pole was rotated from 600 rpm to 1200 rpm the material removal remained approximately constant upto 2400 rpm and beyond this slightly increases. Also, the surface roughness decreases continuously with the rotation of the non-tapered pole from 1200 rpm to 3000 rpm. This is because the non-tapered pole exposes a flat surface toward the finishing surface of the workpiece which results in a uniform magnetic field. Hence the uniform magnetic field causes uniform finishing. SUS304 stainless steel is used as a workpiece tube, and the finishing medium consists of iron particles of 510 µm and magnetic abrasive of 80 µm. The minimum surface roughness attained in this process is reported as 0.2 µm with 5 min of finishing time with 3000 rpm of non-tapered pole at SUS304 stainless steel workpiece material.

Singh and Shan (2002) discussed the possible improvement in the surface finish performance and rate of material removal with the use of a magnetic field around the workpiece cylinder in the abrasive flow machining (AFM). In this work, a finishing setup had been developed for a combined process named as magnetically assisted abrasive flow machining (MAAFM), and the effects of the key parameters on the finishing performance were studied. The electromagnet is used as the source of the magnet. Nylon and a non-magnetic material were used to make the fixture such that maximum magnetic field could be achieved at the internal surface of the workpiece. In this work, the brown super emery powder was used as abrasive particles in finishing medium. The finishing medium powder had 40 % magnetic particles, 45 % Al_2O_3, and 15 % Si_2O_3. The regression model was developed using the response surface methodology to analyze the %age improvement in surface finish and material removal rate. The experimentations were performed on the cylindrical component of brass material. To test the adequacy of the models and to get the significant parameters, the analysis of variance was applied. Experimental results indicate that MAAFM improves the finishing performance significantly better than AFM. The material removal rate (MRR) on cylindrical workpiece of brass in both AFM and in MAAFM is higher as than MRR on the workpiece cylinder of aluminum. The surface finish in brass with MAAFM process was achieved upto 0.30 µm from initial surface roughness of 1 µm with total of 7 finishing cycles.

Yamaguchi and Shinmura (2004) studied the application of a magnetic field-assisted finishing process for the internal surface of a component of alumina ceramic. The experiments were conducted on this component to investigate the effects of volume of the lubricant, size of ferrous particles, the size of abrasive grains on the finishing characteristics. In this work, the cylindrical workpiece of alumina ceramic was attached to the chuck of the computer numerical control (CNC) machine's lathe and made rotating (at 1800 rpm) instead of pole rotation. The magnetic normal force was applied due to the magnetic field caused by the poles of the magnetic abrasive finishing (MAF) setup. In this work, the workpiece was given vibratory motion due to which the abrasive particles applied axial shear force along the length of the tube. The tangential shear is applied by active abrasive particles due to the rotational motion of the poles along with the tangential direction of the rotating abrasives. The diamond abrasive and ferrous particles were used as the finishing medium. Using this process, the change in surface roughness and material removal was observed as shown in Fig. 2.4. With an initial increase in the size of abrasives from the range of 0-1 µm to range 4-8 µm, the material removal increases. Then on further increasing the size of abrasive (8-12 µm) slight reduction in material removal was observed. However, for reduction trend in surface roughness as shown in Fig. 2.4, it is observed that initially with increasing the size of abrasive from 0-1 µm to range 4-8 µm the greater reduction in surface roughness is observed upto 5 min of finishing after then the similar reduction is observed for all sizes of abrasive after 10 min. This is because the number of sharp edges in the large-sized abrasive gets decreased which causes less material abrasion and found less capable for further improvement in surface finish.

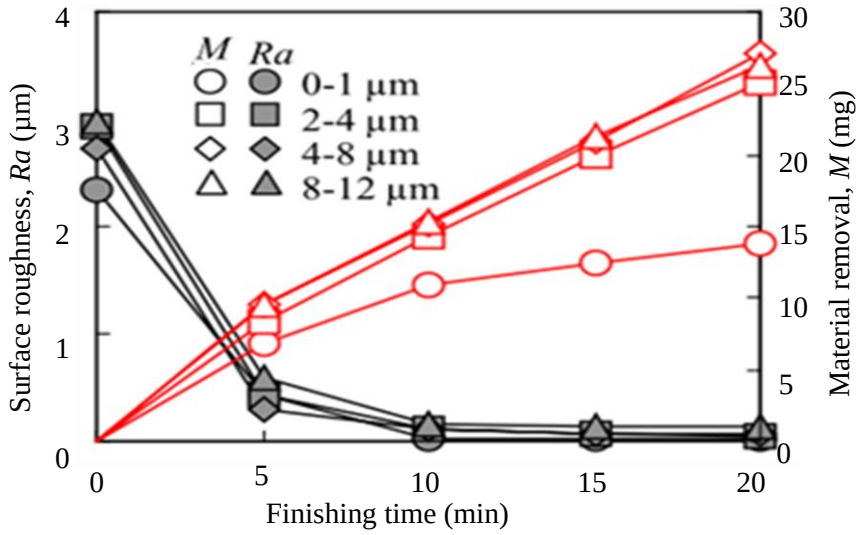

Fig. 2.4 Change in surface roughness and material removal with finishing time (Yamaguchi and Shinmura, 2004).

Wang *et* al., (2004) discussed the finishing characteristics of a magnetic field-based mechanochemical polishing process using a mixture of Cr_2O_3 abrasives and magnetic particles in case of wet finishing using distilled water which was introduced for internal finishing of Si_3N_4 fine ceramic tubes. This process is based on the chemical reaction between the Si_3N_4 and Cr_2O_3 and mechanically removal of the product of the chemical reaction through the high-speed rotation of the abrasive mixed medium inside the tube. To deal with the issues related to high heat generation and less finishing efficiency in the case of the dry finishing process with powder of Cr_2O_3 abrasive mixed with ferromagnetic iron particles, the wet finishing was conducted and examined finishing improvement. Magnetic poles made of Nd-Fe-B permanent magnets were placed outside of the Si_3N_4 tube and the polishing fluid was placed inside of the workpiece tube. The magnetic poles were rotated at 1800 rpm and vibrated at an amplitude of 5 mm for performing finishing operations. In this process, the surface roughness and material removal were changed in pattern as shown in Fig. 2.5. In this work, the maximum surface finish was achieved as 0.07µm from the initial surface roughness of 0.63 µm.

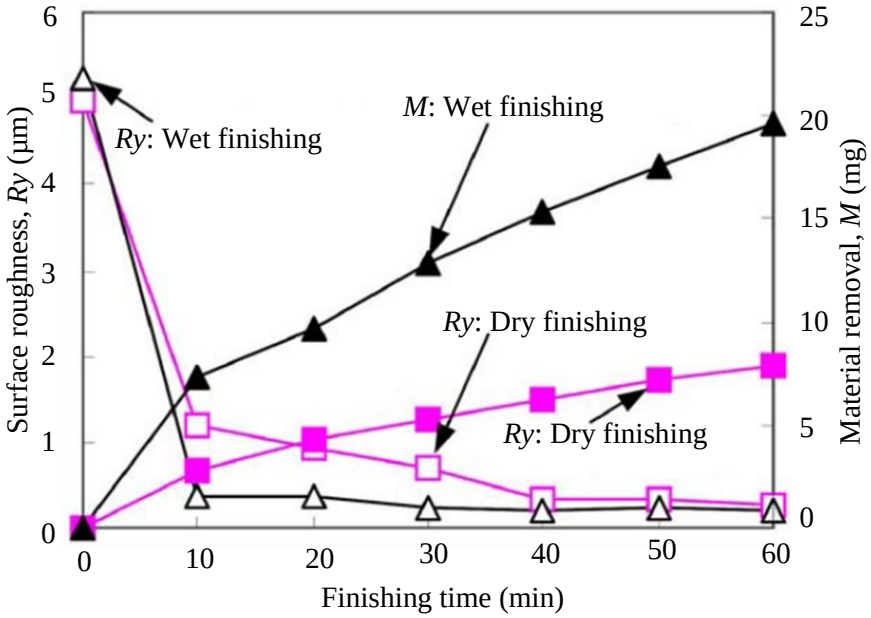

Fig. 2.5 Changes in material removal and surface roughness with finishing time (Wang *et* al., 2004).

Wang and Hu (2005) proposed a magnetic abrasive finishing (MAF) setup for the highly finished internal surface of the tubular components. The basic principle on which this work was developed is the magnetic abrasive particles placed inside the tube form flexible magnetic abrasive brush (FMAB) under influence of magnetic lines generated by the magnetic poles kept outside of the tube. Due to the magnetic field induced by the poles, the magnetic force was applied on the finishing surface for the application of pressure. However, with rotation and

vibration of the magnetic poles the shear forces were applied to remove the material in this work. This study was conducted on three types of workpiece materials such as Ly12 aluminum alloy, 316L stainless steel, and H62 brass. The objective of this work was to achieve the surface roughness of the inner surface upto 0.2 µm. To analyze its finishing capability and maximum material removal, there were four different experiments performed on 316L rolled tube for 4 min. The initial surface roughness was kept between 0.8 µm to 1.5 µm for performing the experimentations as shown in Fig. 2.6. So, it was obtained that with 4 min of finishing using this process, surface finish could be achieved to 0.1 µm. On further finishing after 4 min, the surface roughness did not decrease but uneven material removal took place which was not economical. The limitation with this work is observed as heating of finishing surface and mainly applicable for hard material. On soft materials, it can cause various issues with finishing operation such as thermal damages, scratch marks, less effective finishing, etc.

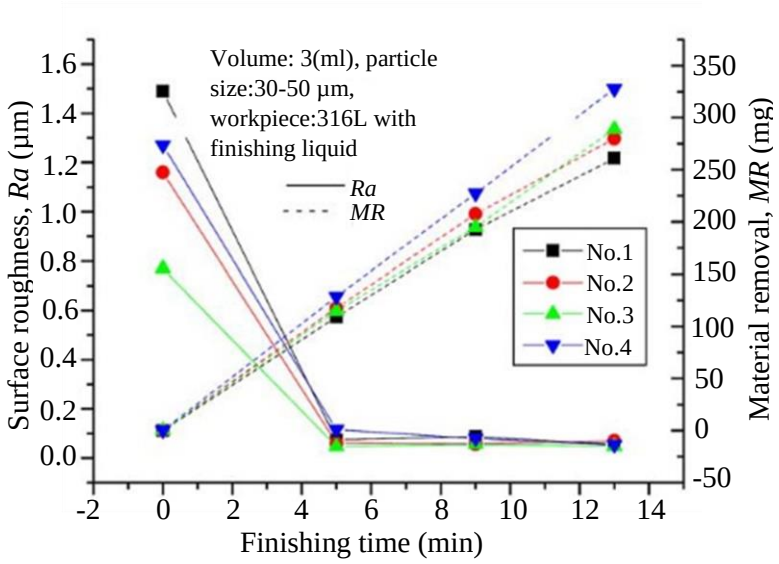

Fig. 2.6 Variation of surface roughness and material removal with finishing time (Wang and Hu, 2005).

Singh *et* al., (2020) improved the internal roundness of the Inconel 625 tube with the application of a chemically assisted magnetic abrasive finishing (CMAF) process. The CMAF process is generally used for finishing the hard alloys in which initially the workpiece's upper surface is conditioned with the chemical reaction using suitable etchants. Then the softened (etched) surface of the workpiece is applied magnetic-assisted abrasive finishing. In this work, the CMAF process was applied for internal finishing of Inconel 625 tube, and %age up-gradation in inner roundness was analyzed. The etched workpiece was attached with the chuck of the lathe machine and the magnets were attached with the aluminum fixture outside of the

workpiece tube (Ø25 mm × 150 mm × 2 mm). In this work, the mixture of ferric chloride and ethanol was used as chemical etchants, and a mixture of silicon carbide and electrolytic iron particles was used as abrasive magnetic particles for the magnetic assisted abrasive finishing process. The maximum %age improvement in the inner roundness was achieved upto 32 with a finishing time of 75 min at workpiece rotational speed of 180 RPM, 35 % of wt. of abrasives size of 60 µm, and 60 gm/ltr of chemical concentration. Improvement in the surface finish was analyzed through the improved texture of scanning electron microscopic images of the finished internal surface.

Jha and Jain (2004) developed a new precision finishing process termed as magnetorheological abrasive flow finishing (MRAFF) process for the complicated internal surface of the workpiece in which smart magnetorheological polishing (MRP) fluid was used as finishing medium. The rheological properties of the abrasive laden MRP fluid were controlled using the external magnetic field induced by the magnetic poles placed outside of the workpiece. This process resumed the versatility of abrasive flow machining (AFM) and introduced the determinism and controllability of rheological properties of MRP fluid of the magnetorheological finishing (MRF) process. The MRP fluid used in the process was comprised of carbonyl iron particles (CIPs) (20 % vol.) and silicon carbide (SiC) abrasives (20 % vol.) dispersed in the viscoplastic base fluid (60 % vol.) which is further made of grease (20 % by wt.) and paraffin oil (80 % by wt.).

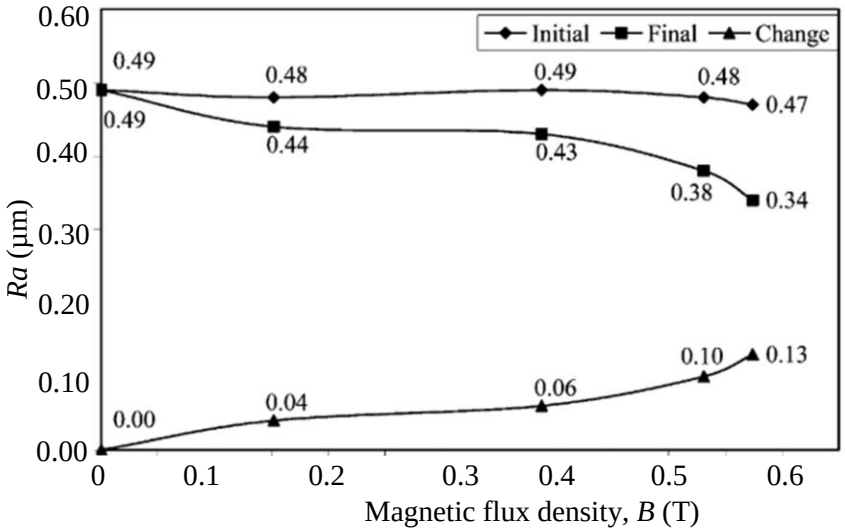

Fig. 2.7 Effect of magnetic field strength on *Ra* value (Jha and Jain 2004).

Due to the magnetic CIPs used in the MRP fluid, the change in rheological behavior under the existence of the external magnetic field was achieved. In this work, the magnets were placed outside of the stainless-steel workpiece cylinder. The MRP fluid was made in reciprocating

movement inside the workpiece with two hydraulic actuated pistons. Under existence of the magnetic field, the MRP fluid inside the workpiece gets stiffened and the abrasive of this fluid applied the magnetic force on the finishing surface of the workpiece. The reciprocation motion of the abrasives caused the action of axial shear force and performed finishing operation. As the magnetic poles were kept outside of the workpiece, the magnetic field at the finishing surface of the workpiece was higher than in the MRP fluid. So, when the ferromagnetic cylindrical workpiece is to be finished, the relative motion between abrasive particles and the finishing surface of the ferromagnetic cylindrical workpiece gets resisted and less finishing performance may be obtained. Therefore, this process was found limited to non-ferromagnetic cylindrical workpieces. As the finishing performance of this process relied on the rheological and viscous properties of the MRP fluid which was further dependent on the strength of the magnetic field, therefore, the effect of the magnetic field on the surface finish was studied and the result was reported graphically as shown in Fig. 2.7.

Jha and Jain (2006b) developed a surface roughness model for the magnetorheological abrasive flow finishing (MRAFF) (Jha and Jain 2004). For this study, the magnetic carbonyl iron particles (CIPs) and silicon carbide (SiC) abrasive particles were considered spherical in shape and uniform in their own sizes. The magnetic force exerted by active abrasive particles (AAPs) by magnetic CIPs in the presence of a magnetic field was found to be responsible for the indentation of AAPs in this study. As only reciprocation motion was given to the MRP fluid in this process, therefore, only axial shear force was found as the cause of material removal. The shear force was calculated by considering the MRP fluid as a Bingham plastic fluid. For developing the surface roughness model, it was assumed that in every stroke of finishing a roughness peak was cut upto the height equivalent to the depth of indentation of an AAP. The average value of the resultant peaks after each stroke gave the theoretical value of the average surface roughness. For validation of the developed surface roughness model, there were 6 experiments conducted by varying the size of magnetic and abrasive particles of the MRP fluid. With the developed surface roughness model, the %error obtained from the experimental surface roughness as -8.69 % to +11.76 %.

Kathiresan and Mohan (2018) applied the magnetorheological abrasive flow finishing (MRAFF) process to improve the surface finish quality of the internal surface of a workpiece of AISI stainless steel 316L upto the nano-level of surface finish. The optimum parameters of this process for finishing the AISI stainless steel 316L, response surface methodology (RSM) technique was applied. The effects of the process parameters on the final response in terms of surface roughness (SR) and material removal rate (MRR) were analyzed through the regression

model developed in this study under the prediction of optimum finishing parameters through the RSM technique. In this work, the electromagnet was used as the source of the magnet. Therefore, the finishing parameters and their optimized value obtained from this study were hydraulic pressure (38.72 bar), voltage (6.18 V), and the number of the cycle (118). The surface roughness and material removal rate were considered as the response of the study. Further using the analysis of effects of parameters the optimum process parameters were obtained. The best result of surface roughness and material removal rate in this work with the use of optimized finishing parameters were found as 53.10 nm and 1.817 mg/s, respectively.

Das *et* al., (2009) improved the performance of the magnetorheological abrasive flow finishing (MRAFF) by introducing a rotational motion to the source of magnetic field simultaneous to the reciprocation motion of the MRP fluid given by the hydraulic unit. This process was termed as rotational magnetorheological abrasive flow finishing (R-MRAFF) process. For developing the experimental setup, an additional feature is added to the existing MRAFF setup to rotate the magnets using pulley belt drive through AC motor. In this process, additional tangential force is applied on the internal surface of the workpiece resulting in improvement in surface finish as compared to the MRAFF process. The stainless steel, brass, and EN-8 materials are used as a workpiece for preliminary experimentations at different extrusion pressure to analyze the effect of these factors on surface roughness. Using this process, the maximum surface roughness reduction was attained upto 50 nm on the stainless steel from initial 270 nm with 600 finishing cycles whereas on the brass surface this value was attained upto 80 nm from the initial surface of 250 nm with the same number of finishing cycle. Hence, this result states the capability of this process in terms of surface finish improvement on hard materials. Since magnetic arrangement in this process was the same as that of magnetorheological abrasive flow finishing (MRAFF) (Jha and Jain 2004) process. Therefore, this process also carried the same limitation for finishing the ferromagnetic workpieces as MRAFF carried.

Das *et* al., (2010) conducted a study for analyzing the process parameters while internal finishing of the stainless-steel cylindrical workpiece. The experiments were conducted by intelligently controlling the reciprocation motion of the magnetorheological polishing (MRP) fluid as a finishing medium and rotational motion of the magnets. By such controlled motions, the mirror-like surface finish could be achieved in the range of nanometer scale. For investigation of optimum finishing parameters, the experiments were planned with the design of experiments, and response surface methodology was utilized to develop a regression model. Further, the effects of the finishing parameters on the developed model were analyzed in this work. The adequacy of the developed regression model in this study was analyzed with the

help of the analysis of variance (ANOVA) table. The optimum finishing parameters obtained for achieving the highest %age improvement in the surface finish (% ΔRa) were magnet rotational speed= 149 rpm, extrusion pressure= 40 bar, mesh size of abrasive particles= 153, and the number of finishing cycles= 1200. Utilizing the optimized finishing parameters, the best quality of surface finish achieved on the stainless-steel workpiece in this work was 16 nm.

Bedi and Singh (2018a) developed a new magnetorheological finishing process that was capable to finish the internal cylindrical surface of the ferromagnetic and non-ferromagnetic workpieces. In the existing MRP fluid-based finishing processes such as MRAFF and R-MRAFF, the source of magnet was kept outside of the workpiece cylinder. Due to which the magnetic field at the internal surface of the workpiece was higher than the magnetic field in the MRP fluid (Jha and Jain, 2004, Das *et* al., 2010). Considering the ferromagnetic workpiece cylinder for MRAFF and R-MRAFF process, the magnetostatic finite element analysis was performed in this study and the magnetic field distribution was obtained as shown in Fig. 2.8(a). As a higher magnetic field was observed at the inner surface of the ferromagnetic workpiece than the magnetic field in the MRP fluid, all the magnetic particles would get stuck onto the finishing surface of the workpiece. Therefore, the relative motion between abrasive particles and the finishing surface would get resisted and less finishing performance can be obtained. But, here in this process (Bedi and Singh, 2018a), the magnetic tool which was made up with the electromagnetic coil was moved inside of the ferromagnetic workpiece cylinder and rotated as well. Therefore, in this process, the magnetic field in the gap is higher than the magnetic field at the inner surface of the ferromagnetic workpiece as shown in Fig. 2.8(b). This trend of magnetic field distribution in the working gap allowed the easy relative motion of the active abrasive particles against the finishing surface and internal surface of the ferromagnetic workpieces was achieved. The final surface finish was achieved on the ferromagnetic (gray cast iron) workpiece upto 83 nm from initial surface roughness 368 nm in 90 min of surface finishing. As this process was using the fixed electromagnetic coils in a magnetic tool, therefore, this process is found only useful for the internal surface finishing of a fixed diametric cylindrical workpieces. Also, there was an issue of heating in its coil due to which a lot of time was getting wasted for cooling the coil in between two consecutive finishing cycles.

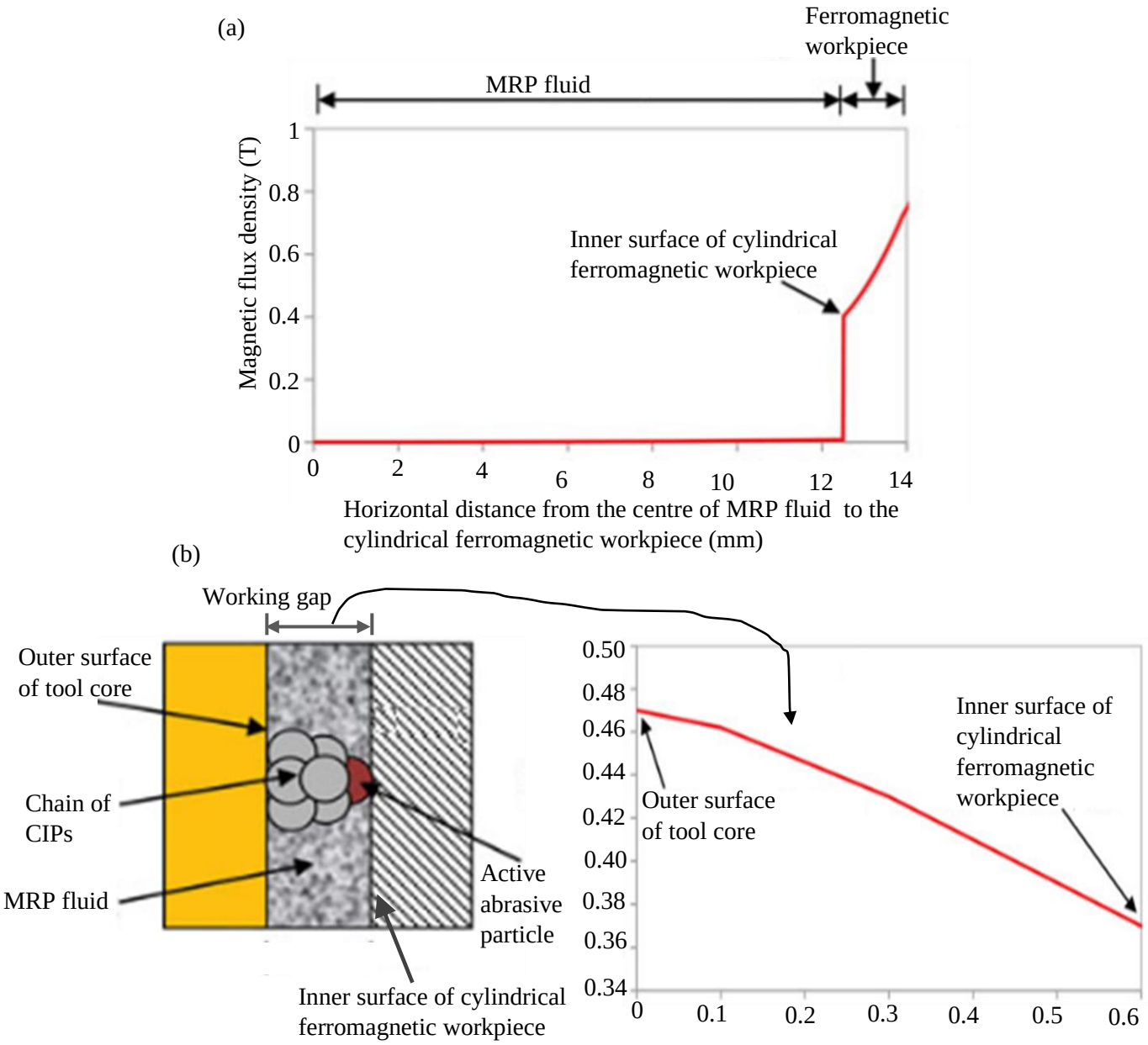

Fig. 2.8 Two-dimensional plot of distribution of magnetic flux density from magnetostatic finite element analysis (a) between the MRP fluid and surface of cylindrical ferromagnetic workpiece, and (b) between the MRP fluid and surface of cylindrical ferromagnetic workpiece (Bedi and Singh, 2018a).

Grover and Singh (2018a) developed an improved magnetorheological honing (MRH) process which was applicable for nano-finishing the internal surfaces of cylindrical workpieces with variable diameters. Since this process used the permanent magnet instead of the electromagnetic coil as a source of the magnetic field, this process is found free from the coil heating issue of the existing MRH process (Bedi and Singh, 2018a). Also, the MRH tool of this process was using such a mechanism through which the radial position of the permanent

magnets was adjusted by inward and outward motion. In this process, the mild steel material is used for the cylindrical workpiece. The magnetorheological polishing (MRP) fluid used in this work was composed of 20 % vol. of SiC abrasive particles with size 19 µm, 20 % vol. of carbonyl iron powder with size 18 µm, and base fluid with 60 % volumetric share. Also, in this work, magnetostatic finite element analysis (FEA) was performed to analyze the effect of the flat permanent magnet and a curved permanent magnet for finishing the internal surface of the ferromagnetic cylindrical workpieces. From this analysis, it was found that curved magnets induced a more uniform decrease in gradient of magnetic field in the working gap towards the finishing surface which results in uniform and efficient internal finishing of the ferromagnetic cylindrical workpieces. The maximum surface roughness was reduced upto 88 nm from 371 nm initial surface roughness with only 60 min of finishing time.

Grover and Singh (2018b) developed a theoretical model for evaluating the surface roughness for permanent magnet-based variable diametric cylindrical workpiece surface finishing magnetorheological honing (MRH) process. There were two types of motion were involved in this study which was rotation and reciprocation motion of the MRH tool inside the stationary workpiece cylinder. In this study, the size of the abrasive particles was assumed as tetrahedron which was relatively closer shape to the actual shape of the abrasive particles. For calculating the magnetic field induced by the permanent magnets used in the process, the Columbian approach was used. In this study, the abrasive particles were assumed as tetrahedron shaped. The length of the path followed by the active abrasive particles was also analyzed for evaluation of surface roughness. In this process, the workpiece cylinder is considered a mild steel ferromagnetic material. From the developed roughness model, the maximum percentage error between the experimental and theoretical surface roughness was found as 8.06 %. This value of %age error between theoretical and experimental surface roughness shows that the surface roughness model was in correct order to predict the surface finish quality. The overall change in surface roughness was recorded as 96 nm from 393 nm initial surface roughness in 720 numbers of finishing cycle. However, this study lacked the analysis of the role of tangential and axial shear forces in the finishing mechanism. Because literature related to internal surface finishing processes i.e., R-AFF and R-MRAFF suggests that there is a scope to improve the finishing performance and productivity of the MRH process due to increase in relative motion of the active abrasive particles.

2.4 Research gaps

From the literature survey, it has been observed that a lot of efforts have been made to develop the advanced finishing processes for the internal surface of the cylindrical workpieces. The

conventional internal grinding is used for the internal finishing of the cylindrical workpieces involved in solid-solid contact. Such type of contact during finishing results in the heat-affected zone, residual stress, deeper grooves, torn and folded metals, and less effective to finish upto nanometer range (Gupte *et* al., 2008; Jain, 2008).

The abrasive flow machining (AFM) process (Rhoades, 1991) and rotational abrasive flow finishing (R-AFF) process (Sankar *et* al., 2009) both are capable of finishing complex-shaped geometry and inaccessible area. But the non-magnetic behavior of the finishing medium makes this process least controllable. Therefore, the prediction of the results becomes tough and overall found inefficient for the intended function. Magnetic abrasive finishing (Wang and Hu, 2005; Yamaguchi and Shinmura, 1999) is capable to finish internal surfaces with controlled finishing forces but only applicable on hard and non-ferromagnetic materials. This is because in this process mixed dry powder of abrasives and magnetic particles are used as a finishing medium. Magnetorheological abrasive flow finishing (MRAFF) process (Jha and Jain, 2004) and Rotational magnetorheological abrasive flow finishing (R-MRAFF) process (Das *et* al., 2010) are better controllable and also able to finish the internal surface of the non-ferromagnetic cylindrical workpieces as stainless steel, high-speed steel, marine-grade steel, etc. However, as the magnetic field generator was kept outside the workpiece/fixture which resists the relative motion of an active abrasive particle against ferromagnetic cylindrical workpiece surface and results in inefficient finishing for the internal surface of the ferromagnetic cylindrical workpieces.

Magnetorheological fluid-based finishing process (Bedi and Singh, 2018a) was developed to finish the internal surface of ferromagnetic and non-ferromagnetic cylindrical workpieces. In this process, the tool used the electromagnetic coil to generate the magnetic field at its finishing end surface. Due to the use of electromagnetic coils the tool gets heated in a very few minutes. Therefore, the duration of a finishing cycle decreased in two consecutive finishing cycle. Thus, idle time also increased which resulted in less productivity. Also, there were constraints on the finishing of the internal surface of variable cylindrical workpieces. Further developed magnetorheological honing (MRH) process (Grover and Singh, 2018a) has taken care of the aforesaid limitations involved in existing MRP fluid based finishing processes. This was done by using the permanent magnet in the MRH tool and the mechanism of the tool was made in such a way that the magnets could be adjusted at the variable diametric position for finishing the internal surface of the variable cylindrical surfaces. In this process, the maximum change

in surface roughness was found as 76.28 % with 60 min of the finishing cycle (Grover and Singh, 2018a).

From the numbers of literature, it has been found that the relative motion of active abrasive particles w.r.t. the finishing surface of the workpiece has a better effect on the surface finish (Sankar *et* al., 2010; Das *et* al., 2010). In the magnetorheological honing (MRH) process, the MRH tool was reciprocated and rotated inside the stationary ferromagnetic cylindrical workpiece to finish the internal surface (Grover and Singh, 2018a). From the obtained results and finishing cycle duration, it was observed that the finishing productivity was likely to slow and needed to be improved. As a result, rotational motion of cylindrical workpieces has been incorporated into the MRH process at the same time as rotational and reciprocation movement of the MRH tool to improve the internal surface finishing perfromance and productivity. Hence, the following were found the important literature gaps as reported below.

- The finishing productivity and performance of the internal surface finishing of the cylindrical workpieces were seemed to be improved by increasing the relative motion of the active abrasive particles.

- Theoretical analysis for the tangential and axial shear forces, and surface roughness with the increased relative motion of the active particles due to the oppositely rotating cylindrical workpiece in the MR fluid based honing process was not reported to understand the mechanism of force acting and resulting in the surface finish.

- The effects of the increased relative speed of the active abrasive particles under effect of the oppositely rotating cylindrical workpiece on the parameters of the path followed by the active abrasives which further influences the finishing performance and productivity was not analysed in the existing MR fluid based honing processes.

- Most of the existing MR fluid-based internal finishing processes are lacking their validation for being applicable in finishing the various real-time industrial cylindrical workpiece.

- In the MR fluid-based processes, the micro-sized free abrasive particles find challenging to finish the surface with coarse surface roughness (machined surfaces). Therefore, for fine finishing of internal surface in all the existing internal MR fluid-based finishing processes, first of all, the initial surface is generated using the traditional finishing processes with the help of different finishing setups and the tools. In this way,

the involvement of the multiple tools and setups for fine finishing the internal surface of the cylindrical workpieces using existing MR fluid based honing process make them more time consuming and labor-intensive, and expansive.

In contrast with the aforesaid research gaps, there is a requirement of the theoretical study to analyze the effect of oppositely rotational motion of the cylindrical workpiece to the rotational motion of the magnetorheological honing (MRH) tool on the finishing performance and productivity of the existing MRH process. Also, formulation of the theoretical surface roughness model is required for easily validating the improvement achieved in the proposed process as compared to the existing MRH process. Then the proposed process is to be called rotational magnetorheological honing (R-MRH) and it is needed to be developed for internal surface finishing of the cylindrical workpieces with improved finishing performance and productivity. To validate the developed R-MRH process preliminary experiments are required. Also, the developed theoretical surface roughness is needed to be validated with the experimental surface roughness. The optimum process parameters for the developed R-MRH process are required for various industrial cylindrical workpieces of different materials such as EN-31, carbon iron alloy, cast iron, etc. Using the optimum process parameters, the improvement in the surface finish is required to be analyzed to further investigate the capability of the newly developed R-MRH process for improving the functionality of industrial cylindrical components. To further extend the applicability of the R-MRH process for finishing the internal surface of the large range of variable-sized cylindrical workpieces from the initial machined surface to the final MR finished surface without changing the tool and setup, an in-situ honing tool is needed to be developed. A preliminary experiment using the in-situ honing tool is required to be performed for confirming the applicability of the in-situ honing tool. Based on the research gaps as identified through the literature survey, the following research objectives are proposed as given below.

2.5 Research objectives

- Theoretical analysis in development of a new rotational magnetorheological honing process for improved productivity of nano-finished internal surface of cylindrical workpieces.
- Development of the rotational magnetorheological honing process for improved productivity of nano-finished internal cylindrical surfaces. Also, design and fabrication

of an in-situ honing tool which can finish the internal surface of the cylindrical workpieces in both methods traditional as well as the magnetorheological finishing.

- Preliminary experiments with the developed rotational magnetorheological honing process for validation of its performance in comparison with the existing magnetorheological honing process for finishing the internal surface of the ferromagnetic cylindrical workpieces.
- Analysis of the effects of different finishing parameters on the process response such as surface finish improvement using Response Surface Methodology (RSM) to optimize the developed rotational magnetorheological honing process for better performance.
- Performance validation of the developed rotational magnetorheological honing process for finishing the internal surface of the industrial cylindrical components.

2.6 Organization of the thesis chapters

The thesis is organized into the following chapters including the references.

Chapter 1 provides the introduction of the various traditional and advanced finishing processes with their applications for finishing the internal cylindrical surface of the workpieces. This chapter states the benefits of using advanced finishing processes with the controlled finishing forces with the involvement of the magnetic field as compared to the traditional finishing processes.

Chapter 2 represents the existing literature reviews associated with various traditional and advanced finishing processes applied for finishing the internal surface of the cylindrical workpieces. Also, based on the literature reviews, the requirement of the present work for fine finishing the internal surface of the various cylindrical workpieces with more effectiveness has been recognized. At the end of this chapter, the objectives of the present research work and organization of the thesis chapters have been included.

Chapter 3 reports the theoretical analysis in the development of the rotational magnetorheological honing process for improved finishing productivity performance of nano-finished internal surface of cylindrical workpieces.

Chapter 4 reports the development of the rotational magnetorheological honing process setup for the rotational magnetorheological honing process for improved productivity and finishing performance. Also, this chapter includes the design and fabrication of an in-situ honing tool that can perform finishing on the internal surface of the cylindrical workpieces through traditional honing as well as magnetorheological finishing.

Chapter 5 discusses the preliminary experiments with the developed rotational magnetorheological honing (R-MRH) process for validation of its performance in comparison with the existing magnetorheological honing process for finishing the internal surface of the ferromagnetic cylindrical workpiece. This chapter also briefly discusses the indigenous preparation of the finishing agent as magnetorheological (MR) polishing fluid. This chapter also reports the effects of finishing parameters on the process response such as surface finish improvement using the response surface methodology (RSM) conducted to obtain the optimum process parameters for better finishing on the internal surface of the cylindrical workpieces. Also, this chapter includes the experimentation using the in-situ magnetorheological honing tool for validating its feasibility for performing traditional as well as magnetorheological honing at a single setup.

Chapter 6 reports the fine-finishing of various typical and real-time industrial components using the rotational magnetorheological honing process with the optimized process parameters for their study of the maximum improvement in surface finish, surface texture, and geometric accuracy.

Chapter 7 gives the various conclusions and significant outcomes from the present research work and tells the scope for future work.

CHAPTER 3

THEORETICAL INVESTIGATION FOR DEVELOPMENT OF ROTATIONAL MAGNETORHEOLOGICAL HONING PROCESS FOR IMPROVING THE FINISHING PRODUCTIVITY AND PERFORMANCE

As stated under research gaps (chapter 2), the permanent magnet-based magnetorheological honing (MRH) process was developed by the authors (Grover and Singh, 2018a) for finishing the variable diametric internal surface of the ferromagnetic and non-ferromagnetic cylindrical workpieces. In the permanent magnet-based MRH process, the tool is rotated and reciprocated inside the stationary cylindrical workpiece which causes the relative motion of the active abrasive particles over its inside surface. The relative motion of the active abrasive particles tends to impart the shear force on the finishing surface. The shear force abrades the materials ploughed by the indented active abrasives from its vicinity. Therefore, based on the performance improvement achieved by enhancing the relative motion of abrasive particles in literature of rotational abrasive flow finishing (R-AFF) (Sankar, *et* al., 2010) and rotational magnetorheological abrasive flow finishing (R-MRAFF) (Das, *et* al., 2010), it is realized that the enhancement in relative motion of abrasive particles w.r.t. internal surface of the cylindrical workpiece in the existing permanent magnet-based MRH process (Grover and Singh, 2018a) may improve the finishing productivity and performance. Also, the theoretical study conducted for the permanent magnet-based MRH process (Grover and Singh, 2018b) lacks the analysis of the effects of the rotation of cylindrical workpiece along with the MRH-tool. The performance evaluation of that MRH process performed in every aspect while the cylindrical workpiece was kept stationary. Therefore, for further improvement in productivity of surface finished components, a new rotational magnetorheological honing (R-MRH) process is conceptualized where the workpiece cylinder is also made rotational instead of stationary as in the case of the existing MRH process (Grover and Singh, 2018a). Therefore, this new modification in the process is known as the R-MRH process. For analyzing the effect of parameters of the R-MRH process on the change in surface roughness and finishing rate, the theoretical study has been performed in this chapter. This theoretical study has been confirmed with the preliminary experiments conducted in the further chapter of this study where the cylindrical workpiece is made rotating in the opposite direction to the tool rotation and the tool is also made reciprocating at the same time. The present study also enlightens the shuffling mechanism of abrasive particles of the MRP fluid which is caused by the oppositely rotating

the cylindrical workpiece during R-MRH finishing operation. The shuffling of the abrasive particles leads to the continuous supply of sharp-edged abrasive particles during the finishing operation. Hence, the increased relative motion and continuous shuffling of abrasive particles improve productivity in fine-finishing of the inner surface of the cylindrical workpieces. The fine-finished inner surface of the industrial cylindrical components improves the features like appearance, resistance to abrasion which guards against wear, corrosion, and chemical damages of the surface. Therefore, the present proposed R-MRH process can perform fine-finishing on the internal cylindrical surface of the industrial parts such as hydraulic cylinders, molds, circular dies, hydraulic rack cylinder, and cylindrical barrel of the injection molding machine in less time as compared to existing MRH process.

3.1 Material removal mechanism in rotational magnetorheological honing (R-MRH) process

A rotational magnetorheological honing (R-MRH) process is a newly programmable logic controller (PLC) based magnetorheological finishing process which improves the finishing capability of the existing MRH process (Grover and Singh, 2018a). To improve the finishing productivity, the cylindrical workpiece is made rotational in present study whereas it was kept stationary in the existing MRH process (Grover and Singh, 2018a). Therefore, this process is named as R-MRH process in which the MRH tool is made rotational and reciprocation inside the oppositely rotating cylindrical workpiece as shown in Fig 3.1 (a). The MRH tool used in this process is made of four curved permanent magnets as a source of the magnetic field. The magnetorheological polishing (MRP) fluid is used as a finishing medium. The abrasive particles in the MRP fluid are used for finishing the surface of different workpiece materials. In the present R-MRH process, the abrasion action takes place by sliding the active abrasive particles along with the simultaneously rotating and reciprocating MRH tool over the inner surface of the rotating cylindrical workpiece in helical path. In this process, the workpiece cylinder is made to rotate in the opposite direction of the MRH tool's rotation. The surface finishing mechanism is caused by abrading the material through the penetrated active abrasives into the surface roughness and detaching the materials from the vicinity of the penetrated active abrasives (Jain *et* al., 1999). The electrolytic iron particles (EIPs) get magnetized when MRP fluid is applied over the permanent magnet of the magnetorheological honing (MRH) tool. The magnetized EIPs apply magnetic force on the abrasive particles.

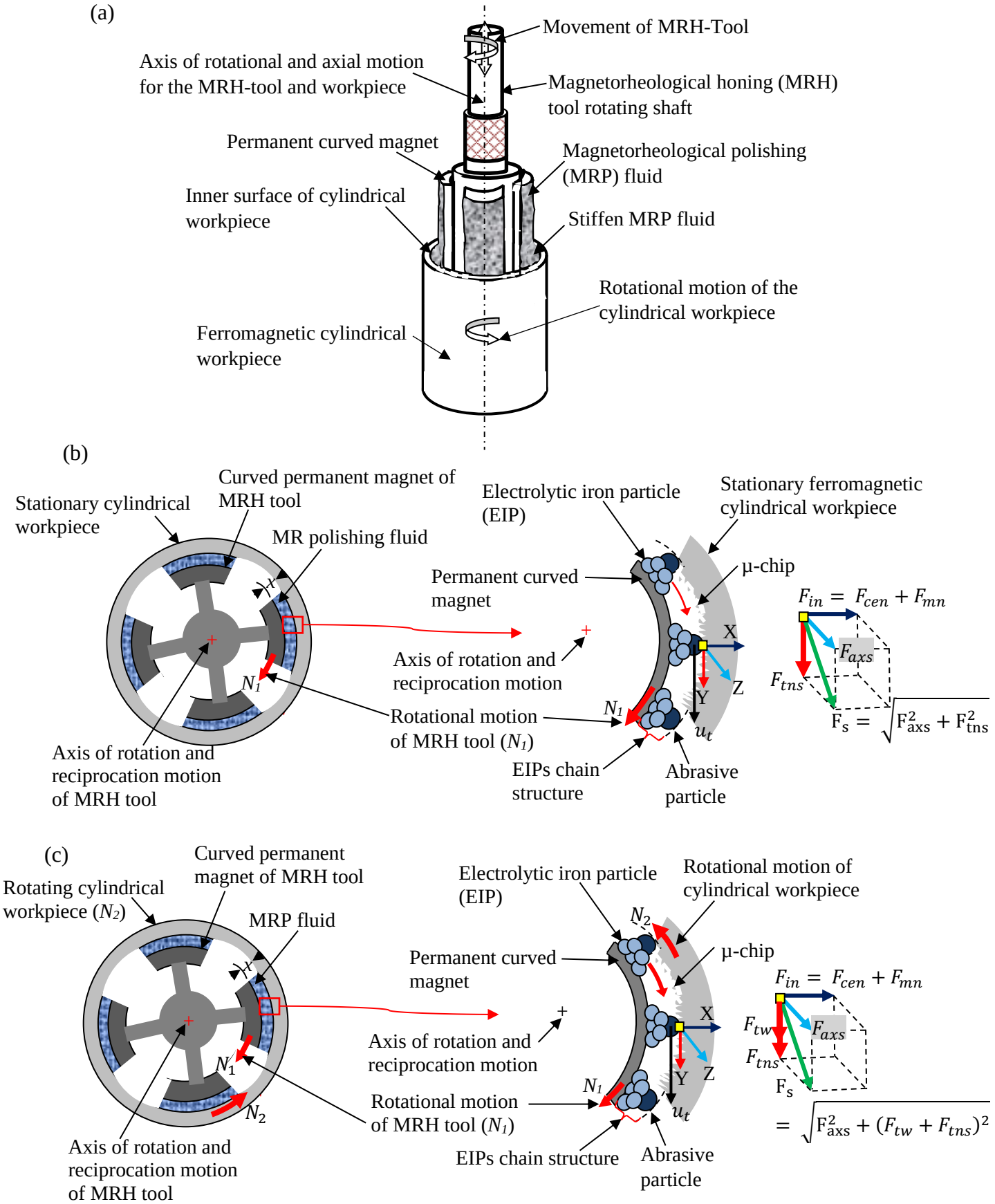

Fig. 3.1 Schematic representation of (a) rotational magnetorheological honing (R-MRH) process, (b) the forces acting in the existing magnetorheological honing process where workpiece cylinder is kept stationary (Grover and Singh, 2018a) and (c) the present proposed R-MRH process where workpiece cylinder is kept rotational.

Due to constricted space in the working gap between the end surface of the permanent magnet of the MRH tool and the inner surface of the cylindrical workpiece, the magnetic normal force (F_{mn}) is acted on the finishing surface. Also, due to the rotational speed of the active abrasive particles along with the MRH tool, the centrifugal force (F_{cen}) is applied in the normal direction to the internal finishing surface of the workpiece cylinder. Therefore, the forces (F_{mn} and F_{cen}) acting collinear and normal to the finishing internal surface of the cylindrical workpiece which results in the indentation of the abrasive particles over it as shown in Figs. 3.1 (b) and (c). So, combinedly these forces (F_{mn} and F_{cen}) acts like indentation force (F_{in}) in the hardness testing machine as an indent is made by the diamond indenter. The indentation leads to the micro-ploughing of the material around the indented abrasives mark. As the indented abrasives are made in simultaneous motion along with the axial and rotational directions over the inner surface of the rotating cylindrical workpiece, the micro-ploughed materials get abraded in the form of microchips. The continuous motion of the indented abrasives on the finishing surface of the cylindrical workpiece results in repetitive abrasion action on the materials which are micro-ploughed. The abrasive particles are stuck in the chain structure as formed by EIPs due to the magnetic field. The chain structure of EIPs with abrasive particles is stiffly stuck on the outer surface of the tool permanent magnet. Hence, the MRH-tool and the stiffly MRP fluid act as a unibody and the active abrasive particles move along with the movement of the MRH-tool. The active abrasive particles are made in contact with the inner surface of the workpiece cylinder when the MRH tool performs its movement inside the workpiece cylinder with the working gap. The relative rotating motion of the active abrasive particles of MRP fluid causes these particles to apply the tangential shear force as shown in Figs. 3.1(b) and (c). As in the existing MRH process (Grover and Singh, 2018a), the workpiece cylinder was kept stationary and the MRH tool was made rotational, the tangential shear force (F_{tns}) was applied on the peaks of the internal surface of the workpiece cylinder due to the tool rotation through the active abrasive particles as shown in Fig. 3.1(b). But in the present proposed R-MRH process, as the workpiece cylinder is also made rotational, so, the net tangential shear force gets combined shear effect due to the MRH tool rotation as well as workpiece cylinder's rotation in the form of ($F_{tns} + F_{tw}$) as shown in Fig. 3.1(c).

In the proposed work, the simultaneous rotational motions of the MRH-tool and cylindrical workpiece along with the reciprocation motion of the tool insist the active abrasive particles follow the helical path over the inner finishing surface of the cylindrical workpiece as shown in Fig. 3.2. Therefore, the rotational motion of the workpiece cylinder in the opposite direction

of the MRH-tool results in an increase in the relative speed of the active abrasive particles w.r.t. the inner surface of the workpiece cylinder.

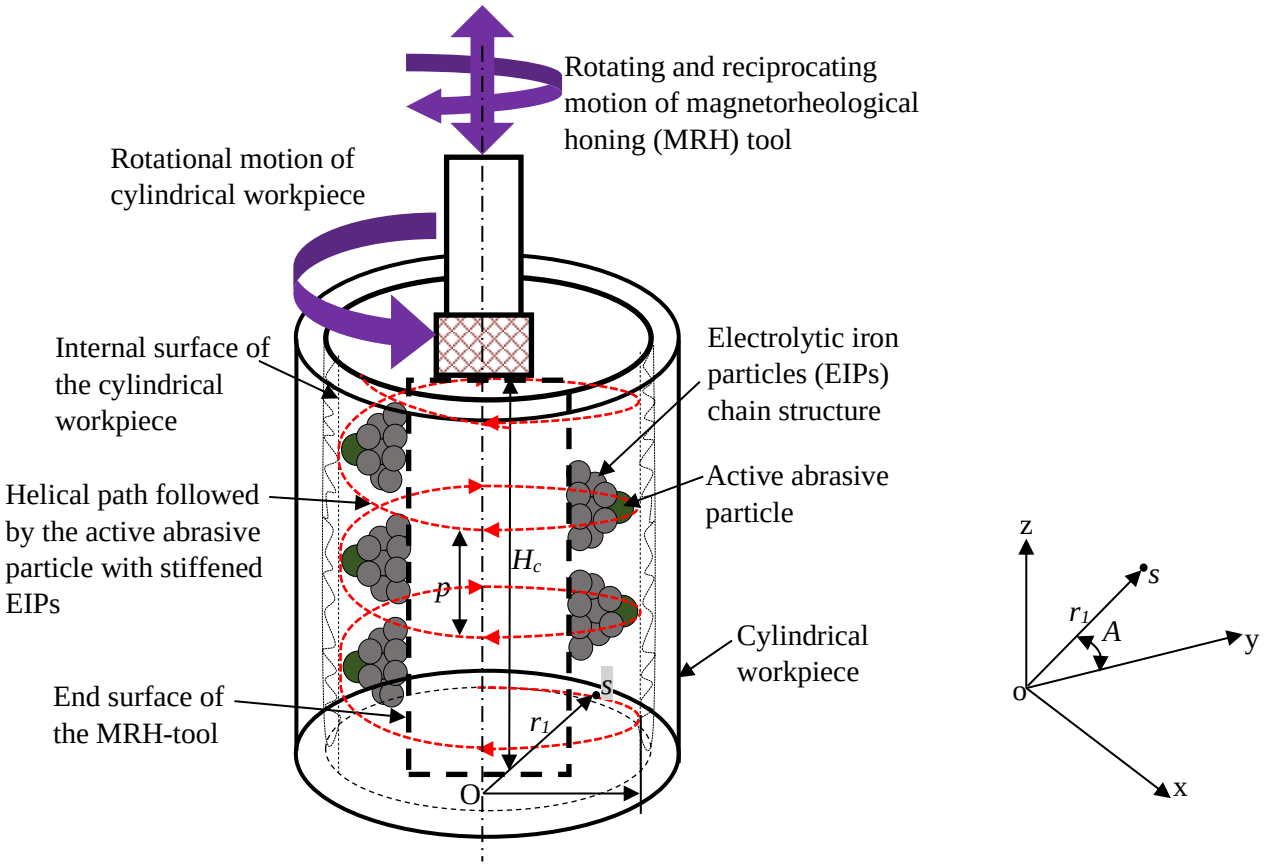

Fig. 3.2 The helical path followed by abrasive particles during rotational magnetorheological honing (R-MRH) process.

3.2 Analysis of the parameters related to the path followed by an active abrasive particle during R-MRH process

For investigating the helical path followed by an active abrasive particle in the present work, a coordinate system with origin O is considered as shown in Fig. 3.2. The origin of the coordinate is lying at the end point of the central axis of the helical path. Also, an arbitrary point s is considered on the helical path. Therefore, the parametric equation for the positional information of the point s is given as in Eq. (3.1).

$$x = r_1 \sin A, \;\; y = r_1 \cos A \;\; and \; z = z \tag{3.1}$$

where r_1 is the internal radius of the cylinder. The x, y, and z are the component of an arbitrary position vector on the helical path, $A = \omega T$ and ω is the angular speed of the particle following the helical path and T is the time period of performing the rotational motion. The helical path has some parameters based on which it can be defined such as the pitch of the helical path (p), helix angle (α), length of the helical path (L), etc. The pitch of the helical path (p) is defined

as the axial length travelled by the active abrasive particle with a rotation of 2π over the inner surface of the cylindrical workpiece. Mathematically it can be formulated as it is expressed in Eq. (3.2).

$$Pitch\ of\ helical\ path\ (p) = \frac{2\pi \times Axial\ speed\ of\ an\ active\ abrasive\ particle\ (v)}{Angular\ speed\ of\ the\ the\ active\ abrasive\ particle\ (\omega)} \quad (3.2)$$

The helix angle (α) is the angle made by an active abrasive particle on the helical path during the inner surface finishing of the cylindrical workpiece and it can be calculated by Eq. (3.3).

$$\alpha = tan^{-1}\left(\frac{30v}{\pi r_1 N}\right) \quad (3.3)$$

where N is the rotational speed of the active abrasive particles w.r.t. the internal surface of the cylindrical workpiece. From Eqs. (3.2) and (3.3), it can be observed that with increasing the rotational speed, the helix angle and pitch of helical path decreases. Decreasing of pitch means the number of turns of the helical path increases and become very close from one another which results in uniform material removal. The length of path (L) covered by the active abrasive particle along the helical path is calculated as in Eq. (3.4).

$$L = \frac{vT_s}{sin\,\alpha} \quad (3.4)$$

where T_s is the time taken to complete one stroke of finishing. Therefore, it is a half finishing cycle which can be calculated by the relationship as expressed in Eq. (3.5).

$$T_s = \frac{Height\ of\ workpiece\ cylinder\ (H_w)}{Axial\ velocity\ of\ the\ tool\ (v)}\ or\ \frac{Cycle\ time\ (T_c)}{2} \quad (3.5)$$

In the R-MRH process, the motion of an active abrasive particle plays an important role in the finishing process. As in this process the cylindrical workpiece is rotated in the opposite direction of the rotation motion of the MRH-tool simultaneously, the active abrasive particle rotating along with the MRH-tool experiences enhanced relative speed. Due to the concurrent axial and rotational motion performed by the active abrasive particle, the helical path over the inner finishing surface of the rotating cylindrical workpiece is covered by the active abrasive. The equations of parameters of the helical path with the rotational and reciprocation motion of abrasive particles have been formulated in the Eqs. (3.2) to (3.5).

Now Fig. 3.3 shows two types of conditions. In the first condition, the MRH-tool is rotated at N_1 rpm, and the workpiece cylinder is kept stationary as shown in Figs. 3.1(b) and 3.3(a). Whereas, in the second condition, the workpiece cylinder is also made rotational at N_2 rpm in the opposite direction to the tool rotating at N_1 rpm as shown in Figs. 3.1(c) and 3.3(b). In this condition, the relative rotational speed of the active abrasive particles gets summed up to $(N_1 + N_2)$ rpm. Eqs. (3.2) and (3.3) revealed that with an increase in the relative speed of the active abrasive particle, the pitch (P_r) and helix angle (α_r) of the helical path decreases. Also,

it is observed pitch length (P_r) and helix angle (α_r) of the helical path in R-MRH is less than the pitch length (P_s) and helix angle (α_s) in the existing MRH process where the cylindrical workpiece is kept stationary (Fig. 3.3(a)). This is because the relative rotational motion of the active abrasive is found in inverse relation with pitch length and helix angle (Eqs. 3.2 and 3.3).

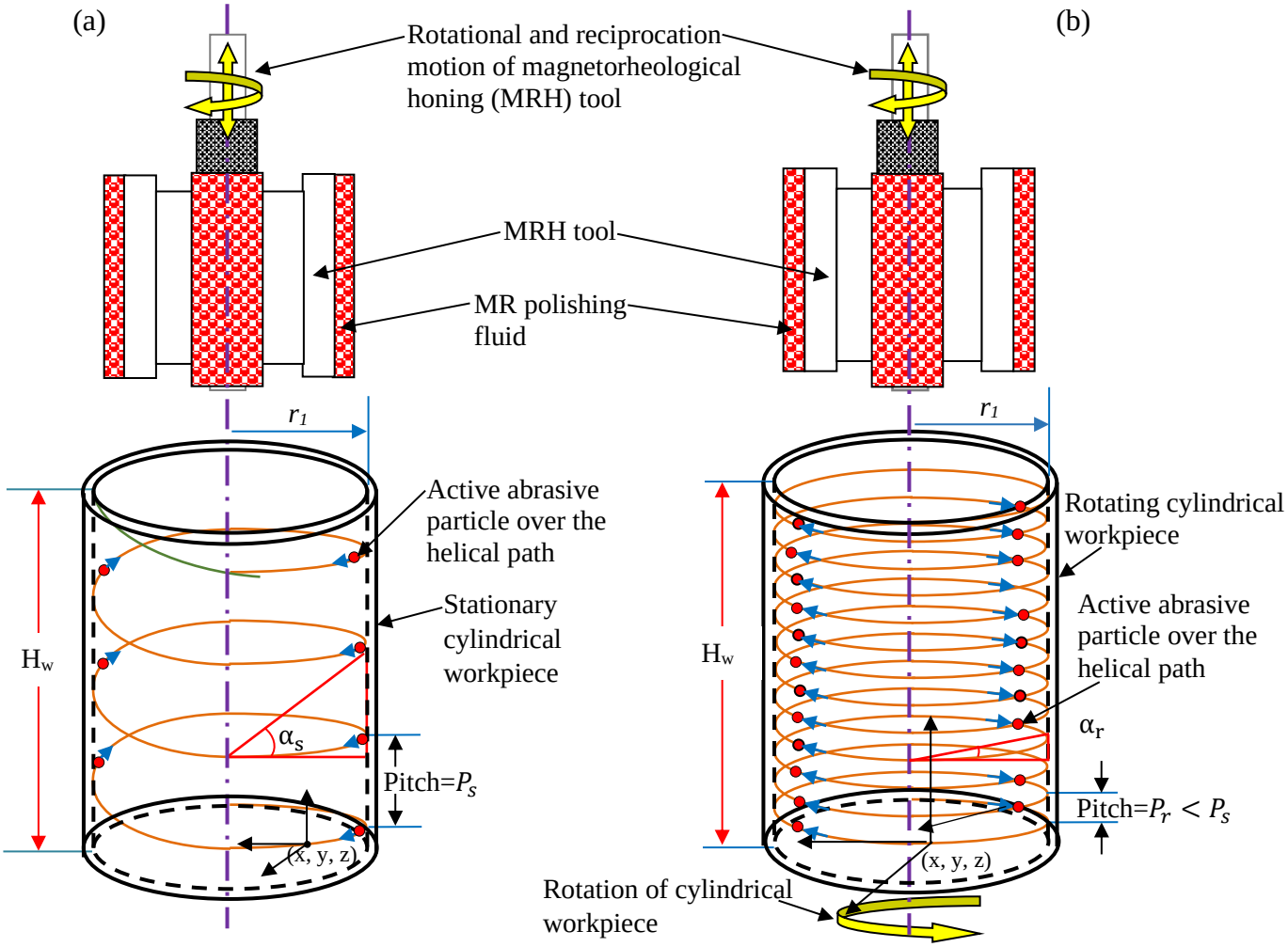

Fig. 3.3 Macroscopic view of the motion along the helical path of an active abrasive particle during the magnetorheological honing process when the cylindrical workpiece is kept (a) stationary and (b) rotational.

3.3 Analysis of the shear forces involved in the rotational magnetorheological honing (R-MRH) finishing process

For the indentation of the active abrasive particles (AAPs), the magnetic force is the only responsible force to indent them over the inner surface roughness of the cylindrical workpiece whereas shear forces are accountable for the abrasion of materials from the locality of the indented abrasive particles. The indented AAPs rotated and reciprocated simultaneously in the present rotational magnetorheological honing (R-MRH) process through the rotating and

reciprocating MRH-tool. Due to these motions, the active abrasive particle experiences the tangential shear force (F_{tns}) in the tangential direction of rotation of the active abrasive particle and the axial shear force (F_{axs}) acting along the axial direction as shown in Fig. 3.1. The resultant of these shear forces produces the total shear force (F_s) as given in Eq. (3.6). The total shear force abrades the material from the vicinity of the indented abrasive particles.

$$F_s = \sqrt{{F_{tns}}^2 + {F_{axs}}^2} \tag{3.6}$$

The repetitive action of the shear force on the roughness peaks causes the abrasion of the peaks as in the form of microchips (Mehra *et* al., 2018). This abrading of the materials in the form of microchips results in the fine-finishing of the internal surface of the cylindrical workpiece.

In the present rotational magnetorheological honing (R-MRH) process, the magnetorheological polishing (MRP) fluid used as a finishing medium, follows the Bingham plastic model. The shear forces in the tangential and axial direction of the MRH tool motions are calculated by assuming the MRP fluid as a Bingham plastic fluid. Therefore, the tangential shear force (F_{tns}) exerted by an active abrasive particle on the internal surface of the cylindrical workpiece can be obtained by using Eq. (3.7).

$$F_{tns} = A_{pr}\tau_{tns} \tag{3.7}$$

where A_{pr} is the projected area by the indented part of an active abrasive particle on the internal surface of the workpiece cylinder and τ_{tns} is the shear stress exerted by the indented abrasive particle due to its motion with the stiffened MRP fluid. The MRP fluid used as a finishing medium which acts like a Bingham plastic fluid. As per the Bingham plastic model, the Bingham plastic fluid acts like a stiff body at lesser stress whereas it acts like a viscous fluid at higher stress. Therefore, the viscoplastic fluid becomes stiff up to certain critical shear stress (yield shear stress), and beyond the yield stress, it works like a viscous fluid. Therefore, the generalized form of the Bingham plastic model is formulated as given in Eq. (3.8) (Sidpara *et* al., 2009).

$$\tau = \tau_0 + \mu \frac{du_t}{dr} \tag{3.8}$$

where τ is the shear stress applied by the fluid, τ_0 is the yield shear stress of a viscous fluid due to the magnetic field. The MRP fluid shows the yield stress under the influence of the magnetic field, μ specifies the viscosity of the fluid (Singh *et* al., 2013b), u_t is the tangential relative velocity of the active abrasive particle (Fig. 3.1), and $\frac{du_t}{dr}$ signifies shear rate. The tangential relative velocity (u_t) of the active abrasive particle over the internal cylindrical surface of the workpiece is calculated from Eq. (3.9).

$$u_t = \omega \times r_1 \quad (3.9)$$

where ω is the relative angular speed of the active abrasive particle over the internal finishing surface cylindrical workpiece and r_1 is the internal radius of the mild steel cylindrical workpiece over which the active abrasive particle is making interaction. As in the present rotational magnetorheological honing process, the cylindrical workpiece is rotated in the opposite direction of the rotational motion of the magnetorheological honing (MRH) tool, so the relative rotational speed of the active abrasive particle is the sum of the rotational speed of the MRH-tool (N_1) and the cylindrical workpiece (N_2). The tangential relative velocity (u_t) of an abrasive particle on the rotating cylindrical inner surface is calculated by using Eq. (3.10).

$$u_t = \frac{2\pi(N_1+N_2)}{60} \times r_1 \quad (3.10)$$

In Eq. (3.10), $(N_1 + N_2)$ is the net relative speed of an active abrasive particle due to the combined effect of the rotational speed of the MRH-tool and the workpiece cylinder respectively. Therefore, the tangential shear stress (τ_{tns}) acting over the rotating internal cylindrical surface rotating is calculated by substituting the Eq. (3.10) in the Eq. (3.8) and is given as in Eq. (3.11).

$$\tau_{tns} = \tau_0 + \frac{\pi\mu r_1}{30}\left\{\frac{d(N_1)}{dr} + \frac{d(N_2)}{dr}\right\} \quad (3.11)$$

The tangential shear force (F_{tns}) exerted by an active abrasive particle on the rotating internal surface of the cylindrical workpiece in the R-MRH process is the multiple of the area projected by an indented abrasive particle on the finishing surface and the shear stress applied by the abrasive particle. Therefore, the tangential force (F_{tns}) is formulated by using Eq. (3.7) and Eq. (3.11) and found as in Eq. (3.12).

$$F_{tns} = \frac{\pi}{4} d_i^2 \times \left[\tau_0 + \frac{\pi\mu r_1}{30}\left\{\frac{d(N_1)}{dr} + \frac{d(N_2)}{dr}\right\}\right] \quad (3.12)$$

Eq. (3.11) reveals that by introducing the rotational motion of cylindrical workpiece (N_2) in the existing magnetorheological honing (MRH) process when the workpiece cylinder was kept stationary, the shear stress applied by the abrasive on the finishing surface of the cylindrical workpiece gets enhanced. The enhanced shear stress (τ_{tns}) can exert on the internal cylindrical surface of the workpiece in the present developed R-MRH process. This causes the indented abrasive particle to pull out the materials at a higher rate. Thus, due to the enhancement in shear stress, the abrasion of materials on roughness peaks gets enhanced and the surface gets better finishing with a higher productivity.

Simultaneously, the reciprocation motion is also performed by the MRH tool. Therefore, the indented active abrasive particle also applies the axial shear stress (τ_{axs}) on the workpiece

surface in the direction of axial motion. The reciprocation velocity of the MRH-tool (v) is kept constant while finishing the inner surface of the rotating workpiece cylinder. The axial shear stress (τ_{axs}) on the inner surface of the workpiece cylinder during the reciprocation motion of the MRH-tool is calculated by Eq. (3.13).

$$\tau_{axs} = \tau_0 + \mu \frac{dv}{dr} \tag{3.13}$$

where $\frac{dv}{dr}$ is the shear rate along the axial direction of the MRH-tool motion. In the expression of shear rate along the axial direction $\frac{dv}{dr}$, dr is the working gap. The axial shear force (F_{axs}) acted upon the inner surface of the cylindrical workpiece by the active abrasive particle along its axial direction is calculated by Eq. (3.14).

$$F_{axs} = (\tau_0 + \mu \frac{dv}{dr}) A_{pr} \tag{3.14}$$

Due to the active abrasives particle's simultaneous rotational and reciprocation motion, two shear forces, tangential and axial, act on the finishing surface (Fig. 3.1). Therefore, the resultant cutting shear force (F_s) applied by an active abrasive on the inner surface of the rotating workpiece cylinder is calculated with the Eq. (3.15) by using the Eq. (3.12) and Eq. (3.14) in Eq. (3.6).

$$F_s = \sqrt{\left[\frac{\pi}{4} d_i^2 \times \left\{\tau_0 + \frac{\pi \mu r_1}{30}\left(\frac{d(N_1)}{dr} + \frac{d(N_2)}{dr}\right)\right\}\right]^2 + \left\{\frac{\pi}{4} d_i^2 \times (\tau_0 + \mu \frac{dv}{dr})\right\}^2} \tag{3.15}$$

The rotational motion of the cylindrical workpiece causes to increase in the relative rotational speed of an active abrasive particle on the internal cylindrical surface of the workpiece. Due to the increase in the rotational speed of the active abrasive particle on the finishing surface of the workpiece cylinder the rate of shear increases and it results in increased shear stress. The increased shear stress increases the resultant cutting shear force (F_s) in the present R-MRH process. In the current R-MRH process, the higher value of the resultant cutting shear force results in a higher abrasion rate while finishing the internal surface roughness of cylindrical workpieces.

3.4 Analysis of surface roughness in rotational magnetorheological honing (R-MRH) process

In the present study, four curved permanent magnets (NdFeB) are used as a source of the magnetic field generator. All the four permanent magnets are made of the same in shape, size, material, and field generating capacity. These magnets are used in the present magnetorheological honing (MRH) tool about an axis which is also the axis of rotation and reciprocation in the finishing process. Therefore, this arrangement of the magnets makes them symmetrical. Thus, calculation of the magnetic field density for a single magnet of the MRH

tool is applicable for the rest of the magnets used in this tool. For developing the mathematical model of the surface roughness in the present R-MRH process, the following assumptions are taken into account to simplify the analysis.

- The actual abrasive particles are irregular in shape and size. But, in order to simplify the calculations involved in analysis of the surface finish mechanism in R-MRH process and based on the existing literature of theoretical investigation of finishing mechanism in MR fluid-based finishing processes (Jha and Jain, 2006; Chen *et* al., 2015), all the particulate matters of the MRP fluid are assumed to be uniform in shape (spherical).
- The sizes are taken as average diameter of the abrasive particles 19 μm and average diameter of electrolytic iron particles (EIPs) 18 μm and assumed that these particles are suspended uniformly in the base fluid medium.
- The losses and leakage of the magnetic field are not taken into consideration during force calculation due to magnetic flux density.
- The normal magnetic force (F_{mn}) acting on the finishing surface through the active abrasive particle is solely responsible for its indentation. Whereas, the shear forces (F_{tns} and F_{axs}) are accountable for the abrasion of materials from the vicinity of the indented abrasive particles.
- The interference of magnetic flux density due to four magnets used in the MRH tool, and the ferromagnetic cylindrical workpiece has not been taken into consideration.

In this work, as the MRP fluid is placed on the outer end surface of the permanent curved magnets, the magnetic electrolytic iron particles (EIPs) present in the polishing fluid gets aligned along the magnetic lines of the magnetic flux density induced by the magnets. In the influence of the magnetic flux density, each magnetic EIP tries to stick on the surface of the magnet. Due to this behaviour of the magnetic EIPs, the non-magnetic abrasive particles get pushed away from the surface of the permanent magnets. Therefore, the force which insists abrasive particles to get away from the end surface of permanent magnet is known as magnetic force. The curved magnet used in this tool where the magnetic lines are emerging radially outward. The constrained space between the MRH-tool surface and the internal surface of the ferromagnetic workpiece cylinder results in experience the normal force on the internal surface of the workpiece cylinder. Thus, this normal magnetic force (F_{mn}) insists the abrasive particles to indent into the finishing surface of the workpiece cylinder. As the MRH-tool with stiff MRP fluid is reciprocated and rotated inside the rotating cylindrical workpiece, the indented abrasive

particles of the stiffened MRP fluid start applying the axial (F_{axs}) and tangential shear (F_{tns}) forces on the finishing surface of the cylindrical workpiece.

3.4.1 Modelling of magnetic flux density induced by the permanent curved magnet

In the present work, the specification of the permanent curved NdFeB magnet is shown in Fig. 3.4. The shape of the magnet is found as a part of the ring magnet in which magnetic polarization takes place in the radial direction. The outer radius (R) of the magnet is 28.3 mm, thickness (t) of the magnet is 7 mm, arc length (l) of 23.2 mm and the height of the curved (H_c) magnet is 60 mm. According to the geometry, as shown in Fig. 3.4, it is a tile permanent magnetic which magnetizes radially as per the Colombian model (Ravaud *et* al., 2008). The inner radius (r_0) of the magnet is 21.3 mm. As the arc length and outer radius of the magnet are given then its angular length is calculated as $\emptyset_2 - \emptyset_1 = \emptyset$ rad from the relation $l = R\emptyset$. The coordinate system for the calculation of the magnetic flux density induced by a magnet is established as shown in Fig. 3.4. As the magnet is a piece of cylindrical ring magnet in which radius, height, and angular length are given in Table 3.1. Therefore, the cylindrical coordinate system is considered for the evaluation of the magnetic flux density induced by the magnet. The polarization of the magnet ($\vec{J}$) is considered radially outward as shown in Fig. 3.4. The magnetic field induced by the permanent curved magnet is the resultant of the components of the magnetic field along each axis considered in the coordinate system. These three components of the magnetic field are radial component (B_r), axial components (B_z), and azimuthal components ($B_\emptyset$). Therefore, to calculate the magnetic flux density, separately magnetic strength of the curved magnet along each axis is calculated and finally resultant is calculated vectorially.

Considering an elementary volume of the permanent curved magnet at point Q positioned at $\vec{r}$ from the origin the magnetic field at any arbitrary point P in space is evaluated. The magnetic field strength due to the elementary volume of the magnet is calculated as dH_r, dH_z and $dH_\emptyset$ in the corresponding component of the cylindrical coordinate system. On integrating the magnetic field strength due to the elementary volume of the magnet for the complete volume of the magnet as shown in Fig. 3.4, the magnetic field strength due to complete volume of the permanent curved magnet in radial, axial, and azimuthal components are obtained as given in Eq**s**. (3.16), (3.18), and (3.20).

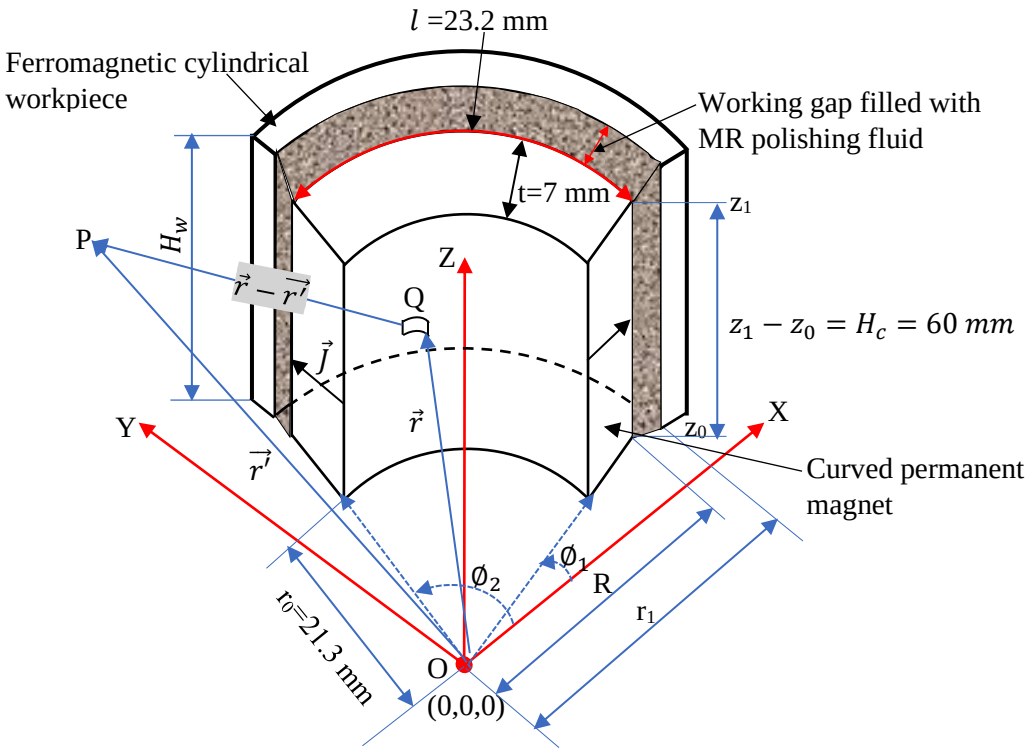

Fig. 3.4 Dimensional specification of the curved permanent magnet used in the magnetorheological honing (MRH) tool.

The radial component, $H_r(r,\emptyset,z)$ of the magnetic field strength of the curved permanent magnet is calculated from the Eq. (3.16) which is derived based on the Amperian model of the radially magnetized arc-shaped permanent magnet (R. Ravaud and G. Lemarquand, 2009).

$$H_r(r,\emptyset,z) = \frac{J}{4\pi\mu_0}\int_{z_0}^{z_1}\int_{r_0}^{r_1}\frac{r\sin(\emptyset-\emptyset_1)}{\left|\vec{r}-\overrightarrow{r'}(\emptyset_0,\ \tilde{z})\right|^3}d\tilde{r}d\tilde{z} - \frac{J}{4\pi\mu_0}\int_{z_0}^{z_1}\int_{r_0}^{r_1}\frac{r\sin(\emptyset-\emptyset_2)}{\left|\vec{r}-\overrightarrow{r'}(\emptyset_1,\ \tilde{z})\right|^3}d\tilde{r}d\tilde{z} +$$

$$\frac{J}{4\pi\mu_0}\int_{r_0}^{r_1}\int_{\emptyset_0}^{\emptyset_1}\frac{(z-z_1)\cos(\emptyset-\tilde{\emptyset})}{\left|\vec{r}-\overrightarrow{r'}(\tilde{\emptyset},z_1)\right|^3}d\tilde{r}d\tilde{z} - \frac{J}{4\pi\mu_0}\int_{r_0}^{r_1}\int_{\emptyset_0}^{\emptyset_1}\frac{(z-z_0)\cos(\emptyset-\tilde{\emptyset})}{\left|\vec{r}-\overrightarrow{r'}(\tilde{\emptyset},z_0)\right|^3}d\tilde{r}d\tilde{z} \qquad (3.16)$$

where

$$\frac{1}{\left|\vec{r}-\overrightarrow{r'}(a,\ b)\right|} = \frac{1}{\sqrt{r^2+r'^2-2rr'\cos(\emptyset-a)+(z-b)^2}} \qquad (3.17)$$

Similarly, for axial component of the magnetic field strength $H_z(r,\emptyset,z)$ is determined using the same method of integration and is given in Eq. (3.18).

$$\mathrm{H}_z\ (\mathrm{r},\emptyset,\mathrm{z}) = \frac{J}{4\pi\mu_0}\sum_{i=0}^{1}(-1)^i\left(\int_{r_0}^{r_1}\int_{\emptyset_1}^{\emptyset_2}\frac{r\tilde{r}\cos(\emptyset-\tilde{\emptyset})}{\left|\tilde{r}-\widetilde{r'}(\emptyset,\ z_i)\right|^3}\right)d\tilde{r}d\tilde{\emptyset} -$$

$$\frac{J}{4\pi\mu_0}\sum_{i=1}^{2}(-1)^i\left(\int_{r_0}^{r_1}\int_{\emptyset_1}^{\emptyset_2}\frac{\tilde{r}^2}{\left|\tilde{r}-\widetilde{r'}(\emptyset_i,\ z)\right|^3}\right)d\tilde{r}d\tilde{\emptyset} \qquad (3.18)$$

where

$$\frac{1}{\left|\vec{r}-\vec{r'}(a,\ c)\right|}=\frac{1}{\sqrt{r^2+\tilde{r}^2-2r\tilde{r}\,cos(\emptyset-a)+(z-c)^2}} \tag{3.19}$$

Now, the azimuthal component $H_{\emptyset}(r,\emptyset,z)$ of magnetic field induced by the curved permanent magnet is calculated using same method of integration. Therefore, by using the same amperian model, the azimuthal component's expression is given in Eq. (3.20).

$$H_{\emptyset}(r,\emptyset,z)=\frac{J}{4\pi\mu_0}\sum_{i=0}^{1}(-1)^i\left(\int_{r_0}^{r_1}\int_{\emptyset_1}^{\emptyset_2}\frac{(z-\tilde{z})\,sin(\emptyset-\tilde{\emptyset})}{\left|\tilde{r}-\widetilde{r'}_i(\tilde{r},\ \tilde{\emptyset})\right|^3}\right)\tilde{r}d\tilde{r}d\tilde{\emptyset}+$$

$$\frac{J}{4\pi\mu_0}\sum_{i=0}^{1}(-1)^i\left(\int_{r_0}^{r_1}\int_{z_0}^{z_1}\frac{r-\tilde{r}\,cos(\emptyset-\tilde{\emptyset})}{\left|\tilde{r}-\widetilde{r_i'}(\emptyset,\ \tilde{z})\right|^3}\right)d\tilde{r}d\tilde{z} \tag{3.20}$$

where

$$\frac{1}{|\tilde{r}-\tilde{r'}_i(\tilde{r},\ \emptyset)|}=\frac{1}{\sqrt{r^2+\tilde{r}^2-2r\tilde{r}\cos(\emptyset-\emptyset_i)+(\tilde{r}-r_1)^2}} \tag{3.21}$$

$$\frac{1}{|\tilde{r}-\tilde{r'}(\emptyset,\ \tilde{z})|}==\frac{1}{\sqrt{r^2+\tilde{r}^2-2r\tilde{r}\cos(\emptyset-\emptyset_1)+(z-z_i)^2}} \tag{3.22}$$

To calculate the numerical values of the radial, axial, and azimuthal components of the magnetic field strength, the dimensional parameters, and material properties are used from Table 3.1. In Eq. (3.16), Eq. (3.18), and Eq. (3.20), J represents magnetic polarization of the curved permanent magnet (NdFeB). The value of the magnetic polarisation for the NdFeB is considered as 1.519 T (Rodewald *et* al., 2002). The magnitude of magnetic field intensity (H) induced by the permanent curved magnet is the resultant of its vectorial components (radial, axial, and azimuthal components). Therefore, the magnetic field intensity and its vectorial components are related as in Eq. (3.23).

$$H=\sqrt{{H_r}^2+H_z^2+H_{\phi}^2} \tag{3.23}$$

where H_r is the radial component of magnetic field intensity, H_z is the axial component of the magnetic field intensity, and $H_{\emptyset}$ is the azimuthal component of the magnetic field intensity. The magnetic flux density (B) at any arbitrary point P is calculated from the magnetic field intensity of Eq. (3.23) and it can be calculated as given in Eq. (3.24). The magnetic field at point P is due to the sole effect of the permanent curved magnet and the point P is considered in the free space.

$$B=\mu_0 H \tag{3.24}$$

where μ_0 is magnetic permeability in free space and its value is given in Table 3.1.

Table 3.1 Dimensional specifications of the curved permanent magnets and related parameters.

Abbreviation	Parameters	value
H_c	Height of curved permanent magnet	60 mm
J	The magnetic polarization of the permanent magnet	1.519 Tesla
R	The outer radius of the permanent curved magnet	28.3
r_0	Internal radius of the permanent curved magnet	21.3 mm
r_1	Inner radius of the mild steel cylindrical workpiece (mm)	30 mm
Z_0	The distance of the first edge from the origin along the z-axis	0 mm
Z_1	The distance of the second edge from origin along the z-axis	60 mm
μ_0	The magnetic permeability in free space	$4\pi\times10^{-7}$ H/m
$\emptyset_1$	The angular position of one end of the curved magnet	0.1305π
$\emptyset_2$	The angular position of second end of the curved magnet	0.3915π

But in the present work, the point of interest (P) is to be considered in between the outer surface of the curved permanent magnet of the magnetorheological honing (MRH) tool and the internal surface of the ferromagnetic cylindrical workpiece. The gap between the outer surface of the curved permanent magnet and the internal cylindrical surface is filled up with the magnetorheological polishing (MRP) fluid. The magnetic field in the working gap is obtained by the magnetic field intensity (H) induced by the permanent radial magnet, the magnetization of the electrolytic iron particles (EIPs) as present in the MRP fluid, and the magnetization of the ferromagnetic cylindrical workpiece. Therefore, the magnetic flux density (B') at any point in the working gap is calculated from Eq. (3.25).

$$B' = \mu_0 H + \mu_0 \mu_{MRP} M_{EIP} + \mu_0 \mu_{rwork} M_{work} \tag{3.25}$$

where μ_{MRP} is the relative permeability of MRP fluid which value is taken as 5 (Sirwal & Singh, 2018), M_{EIP} is the magnetization of electrolytic iron particles (EIPs). In the MRP fluid, only EIPs is the constituent which can get magnetized. Therefore, the magnetizability of the MRP fluid is solely dependent on the magnetization of the EIPs. Due to this, the magnetization of MRP fluid is considered the same as the magnetization of EIPs. The relative permeability of the mild steel cylindrical workpiece (μ_{rwork}) is taken as 600. The magnetization of EIPs and mild steel cylindrical workpiece is calculated from the magnetization versus magnetic field (M-B) curves as shown in Fig. 3.5 (a) and (b) respectively. The magnetic flux density at an arbitrary point between the curved permanent magnet and the inner surface of the mild steel workpiece cylinder is determined and reported in Table 3.2. Using the magnetization of EIPs and mild steel (ferromagnetic) workpiece cylinder from Fig. 3.5 then magnetic force (F_{mn}) is evaluated.

(a)

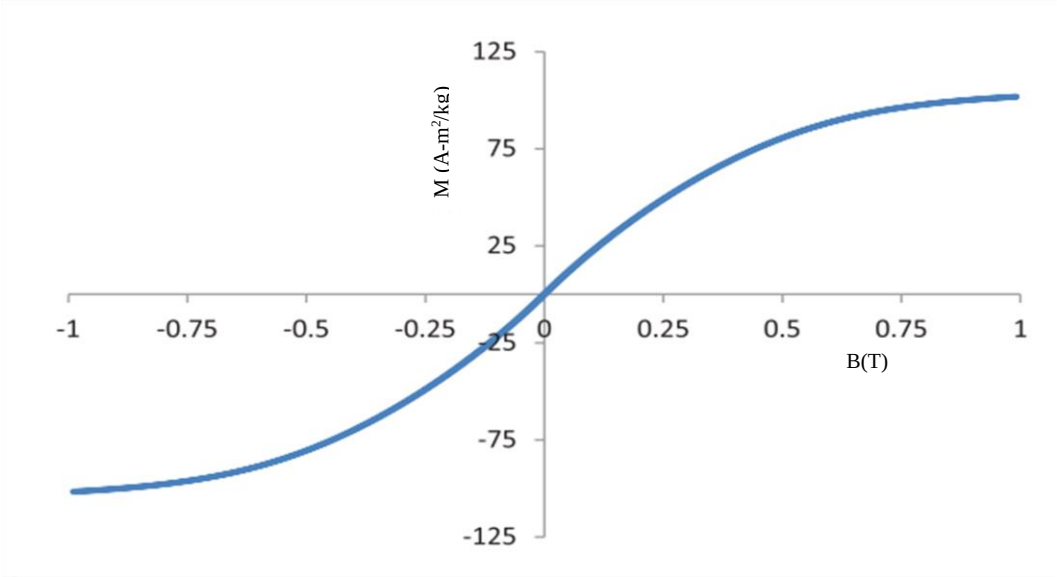

(b)

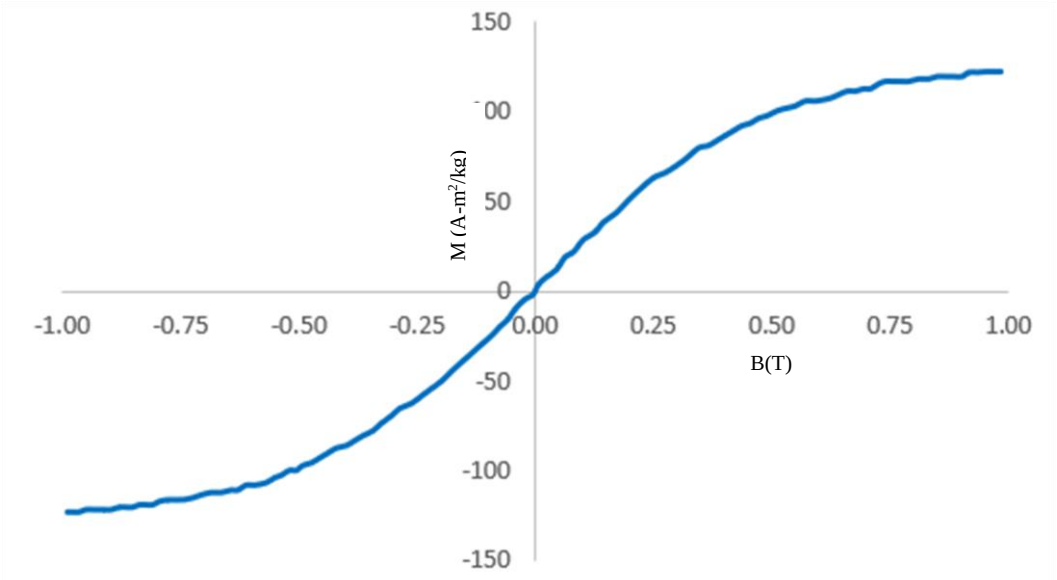

Fig. 3.5 M-B curve of (a) electrolytic iron particles and (b) ferromagnetic mild steel material.

3.4.2 Indentation force required for finishing action in R-MRH process

In the current rotational magnetorheological honing (R-MRH) process, magnetic force (F_{mn}) acting in the working gap is calculated as given in Eq. (3.26).

$$F_{mn} = \frac{m\chi_m B\prime(x)\frac{dB\prime(x)}{dr}}{\mu_0} \tag{3.26}$$

where m is the mass of an electrolytic iron particle which is calculated using the density of the iron particle (EIP) that is found within the range of 1.5-2.2 g/cm^3 (Pinchuk *et* al., 2019). χ_m is

the mass susceptibility of the magnetic iron particle. It can be calculated from Eq. (3.27) and with the help of the M-B curve for EIPs as shown in Fig. 3.5(a).

$$\chi_m = \frac{M}{H} = \frac{\mu_0 M}{B'} \tag{3.27}$$

Table 3.2 reports the experimental and theoretical values of the magnetic field. It is seen that the variation of magnetic field in the working gap shows the negative slope while moving from the end surface of the MRH-tool to the internal surface of the cylindrical workpiece. The magnetic electrolytic iron particles (EIPs) are attracted towards the higher magnetic field on the MRH-tool with a greater attractive force. Whereas, lower magnetic field on the inner ferromagnetic (mild steel) cylindrical workpiece surface results in a weaker attractive force getting experienced by magnetic EIPs. The weaker attractive force experiences by the magnetic EIPs towards the mild steel workpiece surface allows the active abrasive particles to perform relative motion w.r.t. workpiece surface which is extremely required for the MR finishing action.

Table 3.2 Theoretical and experimental values of the magnetic flux density in the working gap.

Distance from the centre axis of the magnet towards the inner surface of the cylindrical mild steel workpiece in the working gap (x) (m)	Theoretically calculated magnetic flux density (T) using Eq. (3.25)	Experimentally obtained magnetic flux density (T) using gaussmeter
0.0283	0.3114	0.321
0.02864	0.3044	0.312
0.02898	0.2974	0.306
0.02934	0.2900	0.290
0.02966	0.2834	0.279
0.03	0.2765	0.262

The term $B'(x)$ is the magnetic flux density at the distance x from the centre of the curved permanent magnet in the working gap with the effect of the curved permanent magnet, EIPs and the mild steel workpiece. It is obtained from the theoretically calculated magnetic flux density (Eq. 3.25, Table 3.2) which follows the trend with R^2 value 0.994 as given in Eq. (3.28).

$$B'(x) = -20.555x + 0.8931 \tag{3.28}$$

Therefore, $\frac{dB'(x)}{dr}$ is the positional magnetic field gradient from the end surface of the curved magnetic tool to the inner surface of the mild steel cylindrical workpiece. It is calculated by differentiating the Eq. (3.28), which is given as in Eq. (3.29).

$$\frac{dB'(x)}{dr} = -20.555 \tag{3.29}$$

Using calculated values from Eqs. (3.27), (3.28), and (3.29) in Eq. (3.26), the magnetic force is calculated at a different location of the particle in the working gap and reported in Table 3.3. The active abrasive particle can experience the force on the cylindrical inner surface through the magnetic effects of electrolytic iron particles in the working gap.

Table 3.3 Magnetic forces by an electrolytic iron particle in the working gap between the MRH-tool and workpiece cylinder.

Distance from the centre axis of the magnet towards the inner surface of the cylindrical mild steel workpiece in the working gap (x) (m)	Theoretically calculated magnetic flux density (T) Eq. (3.28)	Mass susceptibility of electrolytic iron particle (χ_m) (m^3/kg) Eq. (3.27) $\times 10^{-4}$	Magnetic normal force (F_{mn}) in working gap (N) Eq. (3.26) $\times 10^{-8}$
0.0283	0.3114	4.45647	5.44804
0.02864	0.3044	4.46626	5.33747
0.02898	0.2974	4.47595	5.22624
0.02934	0.2900	4.4861	5.10777
0.02966	0.2834	4.49507	5.00191
0.03	0.2765	4.50438	4.88868

Also, when the MRH tool is made rotating, the active abrasive particles of the MRP fluid stiffly retained over the rotating tool experience centrifugal forces (F_{cen}) in the outward direction of its rotational direction. F_{cen} applied by an abrasive particle on the finishing surface of the cylindrical workpiece when the MRH tool rotates at N_1 rpm is calculated using the Eq. (3.30).

$$F_{cen} = m_{ab}\left(\frac{2\pi N_1}{60}\right)^2 r_1 \tag{3.30}$$

where m_{ab} is the mass of an active abrasive particle. It is calculated using the volume of a single abrasive particles and its density. So, the active abrasive particles stuck in the EIPs chain structures on the rotating MRH tool apply magnetically as well as centrifugal force normal to the internal finishing surface of the workpiece whose summation cause in the indentation force. Therefore, the indentation force (F_{in}) is taken as the average of the magnetic forces calculated at different point in the working gap. Thus, the indentation force (F_{in}) is calculated by adding the average of the magnetic normal forces (F_{mn}) in the working gap and the calculated value of F_{cen}. The F_{cen} is calculated using the value of the involving parameters (m_{ab}, N_1 and r_1) to further obtain F_{in}. Therefore, F_{cen} applied by an active abrasive particle assuming MRH tool's

rotation speed at 400 rpm is calculated as 6.0639×10^{-10} N. Hence, indentation force ($F_{in} = F_{mn} + F_{cen}$ is calculated as 5.2290×10^{-8} N.

3.4.3 Analysis of material removal rate

The abrasive particle indents on the inner surface of the cylindrical workpiece due to the magnetic normal force is shown in Fig. 3.6(a) and it follows the helical path due to the rotation, and reciprocation motions of the MRH-tool as shown in Fig. 3.6(b). For evaluation of the material removal made by a single active abrasive particle, firstly the area of the indented abrasive particle perpendicular to the helical path is calculated as it is shown in Fig. 3.6(c). The second step is to multiply the area of the indented part of the indented abrasive particle with the total length of the helical path as calculated from Eq. (3.4). In Fig. 3.6(c), d_a is the diameter of the abrasive grain and, d_i is the diameter of the projected indented abrasive particle on the finishing surface and d is the depth of indentation. Therefore, to calculate the area of the indented part of an active abrasive particle MPN, firstly the depth of indentation and then the diameter of indentation is calculated. The abrasive particle can indent into the finishing surface if the indentation force (F_{in}) is greater than the reaction force (hardness value) of the workpiece material. Similarly, the material can be detached from the vicinity of micro-ploughed by the abrasive particle, if the shear stress acting on the workpiece surface through the abrasive particle is greater than the reaction shear force. The depth of indentation (d) and indentation diameter (d_i) can be calculated from the Eqs. (3.31) and (3.32).

$$d = \frac{d_a}{2} - \frac{1}{2}\sqrt{d_a^2 - d_i^2} \tag{3.31}$$

where the diameter of indentation (d_i) can be calculated from the Eq. (3.31) which is given in Eq. 3.32.

$$d_i = \sqrt{d_a^2 - (d_a - \frac{2\times10^{-6}\times F_{in}}{9.8\pi H_{BHN} d_a})^2} \tag{3.32}$$

The hardness number of the mild steel cylindrical workpiece is H_{BHN}, and its value is taken as 206. F_{in} is the indentation force which is taken as the average of the magnetic normal force calculated in the working gap. Therefore, using F_{in}, the indentation diameter (d_i) is calculated from Eq. (3.32). Further, the depth of indented active abrasive particle (d) is calculated from the Eq. (3.31) using the value of d_i calculated from Eq. (3.32). The cross-sectional area of the indented part (MPN) (A_{prj}) due to the indented active abrasive particle shown in Fig. 3.6(c) can be calculated by Eq. (3.33) using its geometry.

$$A_{prj} = Ar(MPN) = Ar(MPNO) - Ar\ (OMN) \tag{3.33}$$

where Ar stands for the area of section. Considering ΔMQO, the half angle (θ) subtended by the indented abrasive particle is calculated by the Eq. (3.34).

$$\theta = \tan^{-1}\left\{\frac{(d_i)}{2(\frac{d_a}{2}-d)}\right\} \tag{3.34}$$

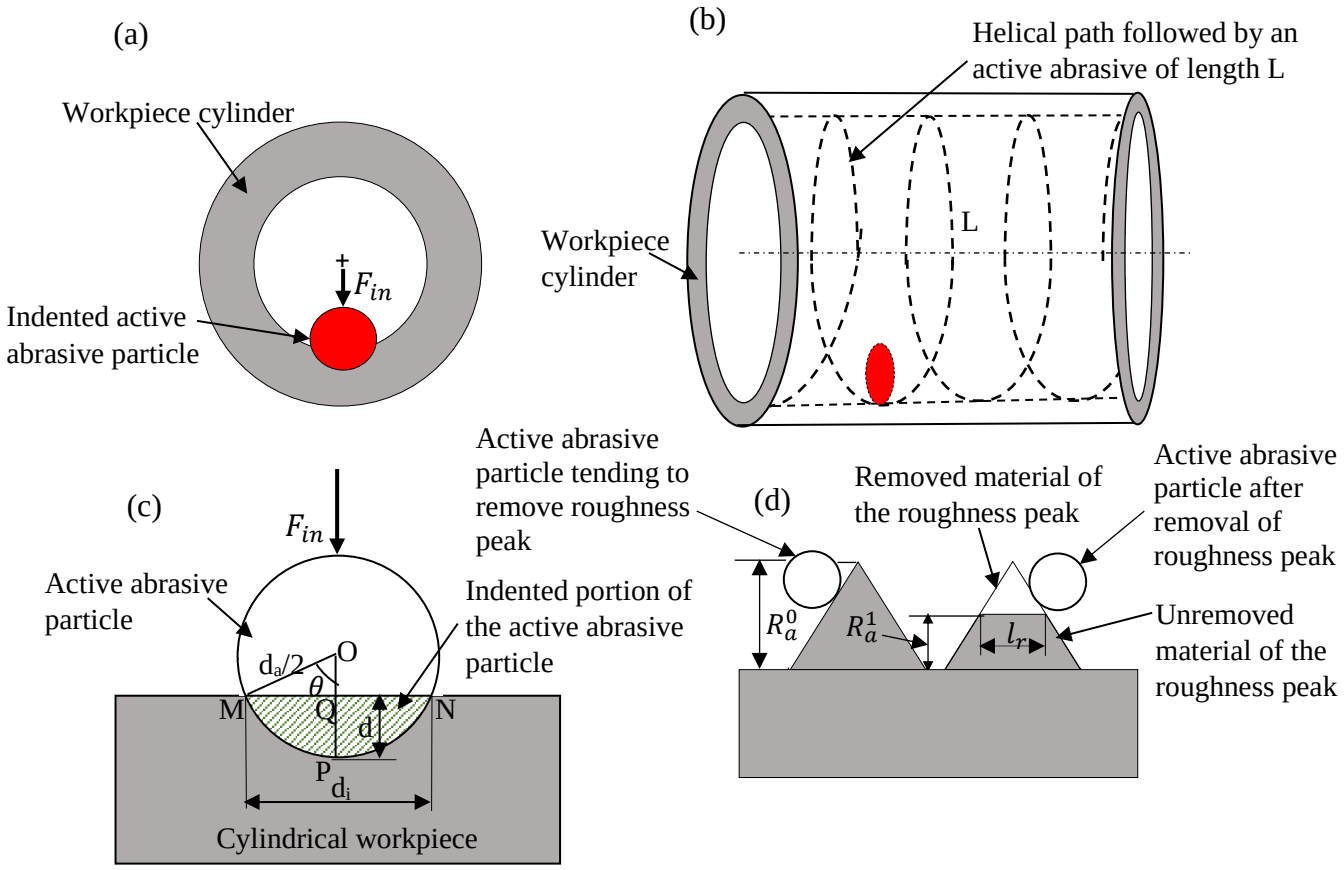

Fig. 3.6 Schematic representation of (a) an indented active abrasive on the inner cylindrical surface, (b) a helical path followed by the active abrasive particle, (c) geometry of the indented part of the active abrasive particle and (d) roughness peak geometry during material removed by the active abrasive particle.

The full angle 2θ subtended at the centre of the abrasive particle by indented part of the abrasive particle. The area of the sector MPNO is calculated with the Eq. (3.35) which is given as follow.

$$Ar(MPNO) = \frac{d_a^2 \times 2\theta}{2\times 4} \tag{3.35}$$

The area of OMN is calculated by the Eq. (3.36).

$$Ar\,(OMN) = 2Ar\,(MQO) = \frac{1}{2}(\frac{d_a}{2} - d) \times (d_i) \tag{3.36}$$

On substituting the value of 2θ, d_i and d in Eqs. (3.35) and (3.36), and then the outcomes from

these two equations are substituted in Eq. (3.33) which gives the area of part MPN. As the cross-section area of indented abrasive particle follows the helical path over the inside surface of the cylindrical workpiece, it can be interpreted that in following the helical path, the material is removed equal to the area of the indented cross-section multiplied by the total length of the helical path. Therefore, the material removed by one abrasive particle while following the helical path in nth stroke is given as in Eq. (3.37).

$$V_s = A_{prj} \times L_{act} \tag{3.37}$$

where V_s is the volume of material removed in nth stroke by one abrasive particle, L_{act} is the actual length of the helical path followed by an abrasive particle in one stroke. To calculate the actual length on which the active abrasive particle directly gets interacted, Fig. 3.6(d) is considered. Figure 3.6(d) shows that how an abrasive particle cuts a roughness peak. If the peak base dimension is of l_a, the length from which the material is removed by the active abrasive on the peak is l_r. Then it can be said that out of l_a length on the base of the roughness peaks, the active abrasive can contact only l_r. Then, for overall L length of the helical path on the internal surface of the cylindrical workpiece, the actual contact length is given by Eq. (3.38). As the complete height of the profile of Fig. 3.6(d) shows initial roughness peak as R_a^0, then after one stroke of material removal it is remains R_a^1. Then for the single stroke, the actual length of the interaction of abrasive particle can be obtained in Eq. (3.38) (Jain *et* al., 1999).

$$L_{act} = \frac{l_r}{l_a} \times L = (1 - \frac{R_a^n}{R_a^0}) \times L \tag{3.38}$$

Therefore, the volume of material removed from the inner surface of the cylindrical workpiece for a single helical path by an active abrasive particle in nth stroke is calculated as in Eq. (3.39).

$$V_s = \left(A_{prj}\right)L_{act} = A_{prj}(1 - \frac{R_a^n}{R_a^0}) \times L \tag{3.39}$$

Eq. (3.39) indicates that a higher helical length followed by a single abrasive particle it can remove a higher amount of material from the finishing surface. Also, from Eq. (3.4), it has been seen that the length of the helical path is in inverse relation with the sinusoidal function of the helix angle (α). Therefore, as the helix angle increases, the length of the helical path decreases and when the helix angle decreases due to the rotational motion of the cylindrical workpiece, the length of the helical path increases. This results in an improvement in the volume of material removal by the active abrasive particle. The increased volume of material removal indicates a higher rate of material abrasion which confirms the enhancement in productivity of

this R-MRH process.

In the present work, the workpiece is also rotated in the opposite direction to the rotational motion of the MRH-tool. Due to the rotational motion of the workpiece cylinder, all abrasive particles get shuffled continuously. The number of active abrasive particles with the fresh edge is enhanced. It is assumed that on the inner surface of the cylindrical workpiece in front of the four permanent curved magnets only abrasive particles are present. Therefore, the total number of active abrasive particles (N_{ab}) are calculated from Eq. (3.40) which are responsible for the removal of material.

$$N_{ab} = \frac{4(\emptyset_2 - \emptyset_1)2\pi r_1 \times L}{360 \times \pi (d_a)^2} \tag{3.40}$$

Therefore, the volume of material removed in a n^{th} stroke of finishing (V_{ts}) can be calculated by using the Eqs. (3.39) and (3.40), in the form of Eq. (3.41).

$$V_{ts} = \mathrm{N}_{ab} \times V_s \tag{3.41}$$

3.4.4 Model of change in surface roughness value

On further solving the Eq. (3.41) by substituting the related terms, the volume of workpiece material removed in nth stroke (V_{ts}) is found as in Eq. (3.42).

$$V_{ts} = \frac{4(\emptyset_2 - \emptyset_1)2\pi r_1 \times L}{360 \times \pi (d_a)^2} \times (A_{prj})(1 - \frac{R_a^n}{R_a^0}) \times L \tag{3.42}$$

As per the continuity equation, the summation of all the indented grooves forms the volume of material which is equivalent to the material removal from the finishing workpiece surface. Material removed in nth stroke is equal to the multiplication of actual interacting length, the inner circumferential length of the workpiece, and the total height of material removed. It is formulated as in Eq. (3.43).

$$V_{ts} = (1 - \frac{R_a^n}{R_a^0}) \times L \times 2\pi r_1 \times (R_a^{n-1} - R_a^n) \tag{3.43}$$

On substituting the value of V_{ts} from Eq. (3.42) in Eq. (3.43), and on further solving the surface roughness model for nth stroke of finishing cycle is obtained as in Eq. (3.44).

$$R_a{}^n = R_a^{n-1} - \left(\frac{4 \times (\emptyset_2 - \emptyset_1) A_{prj} \times v \times T_c}{360 \times \pi \times {d_a}^2 \sin \alpha}\right) \tag{3.44}$$

Thus, the developed surface roughness model clearly shows that in the present magnetorheological finishing process performed with MRH tool, the size of the magnet, projected area of the indented active abrasive particles (A_{prj}), reciprocating speed of the active

abrasive particle (v), and the finishing time (T_c) affect directly to the surface finishing performance. As the value of these parameters increases, more reduction in surface roughness takes place which results in better surface finish. In this roughness model, the helix angle (α) is related in direct relation. As α relies upon rotating and reciprocating speeds of the active abrasive particle which is related indirectly and directly (Eq. 3.3) respectively, so, with increase in relative rotational speed of abrasive particle the value of α decreases. Therefore, when α decreases, the sinusoidal value decreases which results in more reduction in surface roughness. Hence, from the developed surface roughness it can be said that by enhancing the relative rotational speed of the active abrasive particle by adding the rotational motion to the workpiece cylinder the finishing performance of the R-MRH process enhances.

For numerically confirmation of the improvement in the present proposed R-MRH process as compared to the existing magnetorheological honing process (Grover and Singh, 2018a), theoretical calculation of those parameters which influence the surface roughness and productivity has been made and reported in Table 3.4. For calculation of the parameters, the rotational speed of the MRH tool (N_1) is taken as 400 rpm, reciprocation motion of the MRH tool (v) is taken as 70 cm/min, and workpiece rotational speed is considered as 40 rpm in the opposite direction to the MRH tool's rotation. The initial surface roughness considered for the theoretical analysis is 330 nm. Other important data which have been used for the calculation in this study are as the diameter of an EIP particle, $d_{eip} = 18 \times 10^{-6}\, m$, the mass of an EIP $m = 2.3989 \times 10^{-11}$ kg, the diameter of SiC abrasive particle, $d_a = 19 \times 10^{-6}$ m, mass of an abrasive particle, $m_{ab} = 1.152 \times 10^{-11}$ kg, etc. Using these values of the involving terms in the theoretical analysis, the calculation of the results through which the improvement in performance of the proposed R-MRH process has been analyzed.

From the theoretical calculation of the performance parameters involved in the R-MRH finishing process (Table 3.4), it can be easily observed that by introducing the rotational motion of the cylindrical workpiece in the MRH process, a significant change in each parameter is obtained. The pitch length and helix angle values get decreased in the rotational magnetorheological honing (R-MRH) process which means the active abrasive particles makes more numbers of turns while following the helical path on the internal surface of the rotating workpiece cylinder. The length of the helical path followed by active abrasive particles increases as the number of turns of the helical path increases, as confirmed by the calculated value for one stroke of the MRH tool while finishing. Due to the additional rotating motion of the MRH tool in the present R-MRH process as compared to the existing MRH process, the

tangential shear force gets enhanced which further results in an increase in the total shear force applied by the active abrasive particles while finishing operation takes place. This fact is confirmed with the theoretical numerical value of the tangential shear force and total shear force calculated in Table 3.4.

Table 3.4 Theoretical analysis of rotational magnetorheological honing (R-MRH) process with respect to the MRH process (cylindrical workpiece kept stationary).

Sr. No.	Parameters	Magnetorheological honing (MRH) process when workpiece cylinder is kept stationary (N_2=0) and only tool rotates at N_1=400 rpm and reciprocating speed $v = 70$ cm/min	Rotational-magnetorheological honing (R-MRH) process when workpiece cylinder rotates at N_2=40 rpm in opposite direction of tool rotation at N_1=400 rpm and reciprocating speed $v = 70$ cm/min
1	Pitch of the helical path, P (m) (Eq. 3.2)	0.00175	0.00159
2	Helix angle, α (deg.) (Eq. 3.3)	29.13	26.86
3	Length of the path covered by an active abrasive particle along the helical path, L (m) (Eq. 3.4)	0.143	0.154
4	Tangential shear force (F_{tns}) (N) (Eq. 3.12)	6.3808×10^{-7}	7.1023×10^{-7}
5	Total shear force, F_s (N) (Eq. 3.15)	6.3811×10^{-7} N	7.1025×10^{-7} N
6	The volume of material removed in a n^{th} stroke of finishing by one abrasive (V_{ts}) (m^3) (Eq. 3.42)	4.1085×10^{-13} m^3 for n=1	4.8025×10^{-13} m^3 for n=1
7	Surface roughness after nth stroke of finishing cycle ${R_a}^n$ (Eq. 3.44)	102 nm from the initial Ra value of 330 nm with 60 min	65 nm from the initial Ra value of 330 nm in 40 min

As all the parameters reported in Table 3.4 are linked with the extent of material removal and quality of finishing, the theoretical numerical value of the material removed in one stroke clearly states the improvement in productivity of the present R-MRH process. From the evaluation of the volume of material removed in case of rotational and stationary workpiece cylinder, it is observed that the material removed in one stroke of MRH tool movement from the inner surface oppositely rotational workpiece is higher than the material removed from the same surface of the stationary workpiece. Therefore, it can be said that the introduction of rotational motion of the workpiece cylinder in the existing MRH process results in enhanced finishing productivity as the theoretical material removal rate gets enhanced. Using this developed surface roughness model, the value of the surface roughness is calculated. Therefore, it is found that when the workpiece cylinder is kept stationary and the MRH tool is made rotating and reciprocating inside the workpiece cylinder and the theoretical surface finish could

be achieved upto 102 nm from the initial surface roughness value of 330 nm with 60 min of finishing cycle. However, the theoretical surface roughness value on the inside surface of the rotating cylindrical workpiece is calculated as 65 nm from the initial surface roughness value of 330 nm with 40 min of finishing time. Thus, from theoretical analysis, it is confirmed that the present proposed R-MRH process can be found more capable for improving the finishing productivity as well as performance as compared to the existing MRH process when the workpiece cylinder is kept stationary (Grover and Singh, 2018a).

3.5 Mechanism of active abrasive particles' shuffling under effect of rotational motion of the workpiece cylinder

The abrasive particles are stuck in the electrolytic iron particles (EIPs) chain structure under the magnetic field and perform the motion along with the MRH-tool over the inside surface of the rotating hollow cylindric workpiece. The oppositely rotating cylindric workpiece to the rotating direction of the MRH-tool encouraged for applying the resistance on the active abrasive particles. This resistance offered by the internal surface of the cylindric workpiece causes irregular shaped abrasive particles to perform the random motion. Due to the random motion of the abrasive particles during finishing operation, the shuffling of the active abrasive particles takes place (Ravi Sankar *et* al., 2010). The shuffling mechanism ensures the constant presence of the sharp-edged active abrasive particles at the finishing surface. To analyze the shuffling mechanism of the active abrasive particles, the schematic diagram is utilized as shown in Fig. 3.7. It is assumed that an EIPs chain structure with two abrasive particles 'A' and 'B' completes its helical track by keeping the abrasive particle 'A' as an active abrasive particle during finishing the inside surface of the static cylindric workpiece which is schematically shown in Fig. 3.7(a). The abrasive particle 'A' completes a helical path without any shuffle with another abrasive particle. Due to this, the active abrasive particle 'A' may get blunted due to continuously rubbing on the finishing surface and its abrading potential also gets reduced. This results in a lower finishing performance of the active abrasive particles in this process (when the hollow cylindric workpiece is static).

The shuffling mechanism of the active abrasive particles during the inside surface finishing of the rotating hollow cylindric workpiece is schematically explained with the help of Fig. 3.7(b). Let us consider, three random snaps of the MRP fluid chain structure during its motion over a helical path on the inside surface finishing of the rotating hollow cylindric workpiece. It is considered that the EIPs chain structure is involved in finishing action with four different abrasive particles 'A', 'B', 'C' and 'D' as schematically depicted in Fig. 3.7(b).

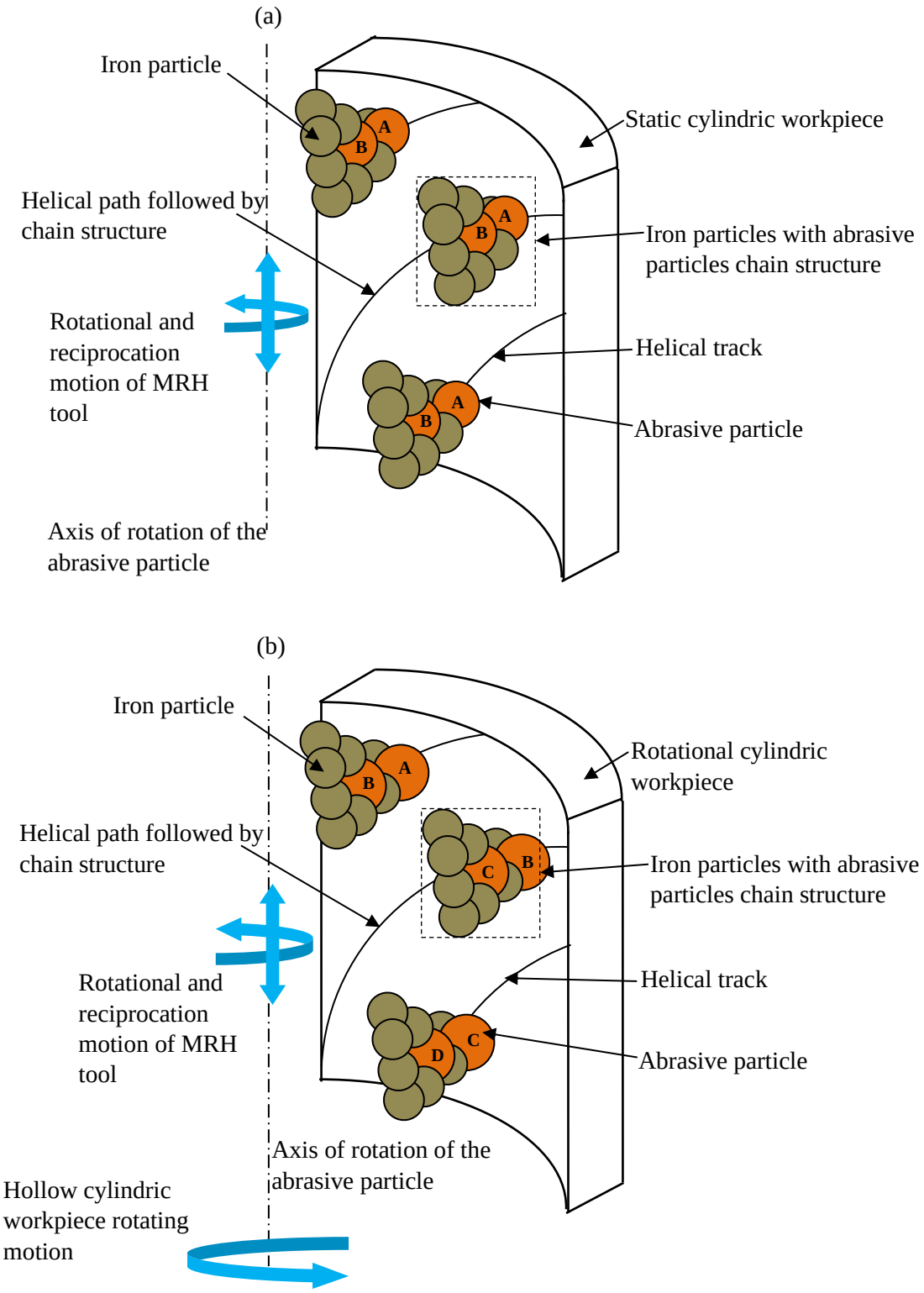

Fig. 3.7 Interaction mechanism of an active abrasive particles in the rotational magnetorheological honing process when (a) the hollow cylindric workpiece is stationary and (b) the hollow cylindric workpiece is rotating.

In the first snap on the helical path, the abrasive particle 'A' is acting as an active particle initially because it is in contact with the finishing surface. However, the abrasive particles B',

‘C’, and ‘D’ are not acting as active abrasives because these abrasive particles are not in contact with the finishing surface of the rotating hollow cylindric workpiece. In the second snap of the EIPs chain structure after its further movement on the helical path, the abrasive particle ‘B’ acts as an active abrasive particle whereas the rest of the other three abrasive particles are not in contact with the finishing surface of the workpiece. Similarly, at the end of completing the helical path (third snap of EIPs chain structure), the abrasive particle ‘C’ acts as an active abrasive particle. In this way, the shuffling of the active abrasive particles continuously takes place as the rotating motion is given to the cylindric workpiece. Therefore, the workpiece rotation is found useful not only for enhancing the forces acting on the finishing surface due to the elevated relative speed of the active abrasive but also it offers the shuffling of the sharp-edged active abrasive particles. This shuffling of the active abrasive particles causes the involvement of many sharp-edged abrasive particles on the inside surface finishing of the rotating cylindric workpiece. Therefore, consistent contact of numerous of sharp-edged active abrasive particles with the rotating workpiece finishing surface results in a better finishing performance of the R-MRH process (when the cylindric workpiece is rotated) as compared to the finishing the inside surface of the static workpiece. Thus, theoretically, it is confirmed that enhancement in the relative motion of the active abrasive particles due to the oppositely rotational motion of cylindrical workpiece to the MRH tool’s rotational direction in the present R-MRH process enhances the finishing productivity and performance. Also, the rotational motion of the cylindrical workpiece in the opposite direction to the MRH tool rotation contributes in an increasing the finishing productivity and performance by enhancing the shuffling of the active abrasive particles during the finishing operation.

3.6 Conclusions

From the theoretical analysis of the parameters involved in finishing the internal surface of the cylindrical workpiece with the proposed rotational magnetorheological honing (R-MRH) process for improving the finishing productivity of the existing magnetorheological honing process (when the workpiece cylinder is kept stationary), the following conclusions have been made.

- The pitch length and helix angle of the helical path gets decreased due to the inverse relationship with the relative speed of the active abrasive particles. Whereas, the length of the helical path traced by the active abrasive particles gets increased because it is in direct relation with the relative motion of the active abrasive particles. The decreased

pitch length and helix angle of the helical path, and increased length of the helical path over the finishing surface of the cylindrical workpiece caused to improve in uniform surface finishing performance with productivity as compared to the existing magnetorheological honing process.

- Significant improvement in the calculated shear force applied by an active abrasive particle on the internal finishing surface of the rotating workpiece cylinder w.r.t. the calculated shear force applied by the abrasive particle on the inside surface of the stationary cylindrical workpiece advocate the capability of the present R-MRH process for improved finishing productivity and performance.
- The negative slope of the theoretically calculated and experimentally measured magnetic field from the curved end surface of the MRH tool's magnet to the inner surface of the ferromagnetic workpiece cylinder ensured that the active abrasive particles of MRP fluid can perform relative motion over the inner surface of the ferromagnetic cylindrical workpiece as iron particles of the MRP fluid get attracted towards the higher magnetic field.
- The substantial enhancement in the calculated volume of material removed from the internal surface of the workpiece cylinder by an active abrasive particle in one stroke with rotational magnetorheological honing (R-MRH) process when the workpiece is made rotational with 40 rpm w.r.t. the volume of material removed when the workpiece cylinder is kept stationary revealed the finishing capability of the R-MRH process for improving the finishing productivity and performance as compared to the existing MRH process.
- The theoretical surface roughness value achieved in the R-MRH process upto 65 nm from initial surface roughness value of 330 nm in only 40 min of finishing time when the workpiece cylinder is kept rotating at 40 rpm is found better for saving 20 min of finishing time and 37 nm more reduction in surface roughness as compared to the MRH process when the workpiece cylinder is kept stationary. Therefore, it can be concluded that the R-MRH process shows the direct improvement in surface finishing productivity and performance with the extent of improvement in surface finish and reduction in finishing time.
- The rotational motion of the cylindrical workpiece causes the shuffling of the sharp-edged active abrasive particle due to which the abrasive particles with sharp edges remain continuously available while performing the finishing operation. Thus, in this

way while introducing the rotational motion of the workpiece, the productivity and performance of the R-MRH process gets significantly enhanced.

CHAPTER 4

DEVELOPMENT OF ROTATIONAL MAGNETORHEOLOGICAL HONING PROCESS AND DESIGN AND FABRICATION OF AN IN-SITU HONING TOOL

4.1 Development of rotational magnetorheological honing process

In chapter 3 of the present work, a theoretical study has been conducted to analyze the effects of the rotational motion of the cylindrical workpiece during magnetorheological honing (MRH) process on the finishing performance and productivity. From the theoretical analysis it has been found that while introducing the rotational motion to the cylindrical workpieces in the existing MRH process (Grover and Singh, 2018a), the surface roughness is reduced more significantly with lesser finishing time. Further, it has been observed that the volume of material removal in a single stroke of finishing by the active abrasive particles get increased. This is because of the involving parameters which positively influence the uniformity and finishing performance with the rotational motion of the workpiece cylinder. Therefore, based on the theoretical results achieved in the chapter 3, the rotational magnetorheological honing (R-MRH) process has been developed and discussed in this chapter. The R-MRH process is a magnetorheological polishing (MRP) fluid-based internal cylindrical surface finishing process in which unlike the MRH process (Grover and Singh, 2018a), the workpiece cylinder is also given rotational motion along with rotating and reciprocating motion of the MRH tool. The rotational direction of the workpiece cylinder and the MRH tool is kept opposite to each other in this process. The proposed R-MRH process improves the finishing productivity and performance by introducing the oppositely rotational motion of the cylindrical workpiece in the existing MRH process. Therefore, the development of the R-MRH setup needs a fixture that can hold and provide the rotational motion to the cylindrical workpiece at the same time when the MRH tool (Grover and Singh, 2018a) is made rotating and reciprocating inside workpiece cylinder. Hence, in this work, a fixture that can provide the rotational motion to the cylindrical motion is designed and fabricated.

Thus, with further advancement in the existing MRH process, the present R-MRH process setup is developed as shown in Fig. 4.1. The key components of the computer-controlled R-MRH setup are the base frame, breadboard, personal computer, multi-axes motion controller, servo-drives, servo motors, Z-slide, C-bracket, and fixture for rotating the workpiece cylinder. Further, the fixture of this R-MRH process setup contains two kinds of sub fixtures. The first is to hold and rotate the cylindrical workpiece, second is to mount the servo motor which can

provide the rotational motion to the workpiece cylinder. Also, the overall fixture of this setup consists of a servo motor, v-groove pulley, v-belt for power transmission, and two ball bearings. The computer aided design (CAD) model of the rotational magnetorheological honing (R-MRH) setup is shown in Fig. 4.1. The millimeter (mm) unit is used as a unit for dimensions throughout this chapter while generating CAD model of each part. Thus, in development of the present R-MRH process, fixtures to hold and rotate the workpiece cylinder and to mount the workpiece rotating servo motor are designed and fabricated.

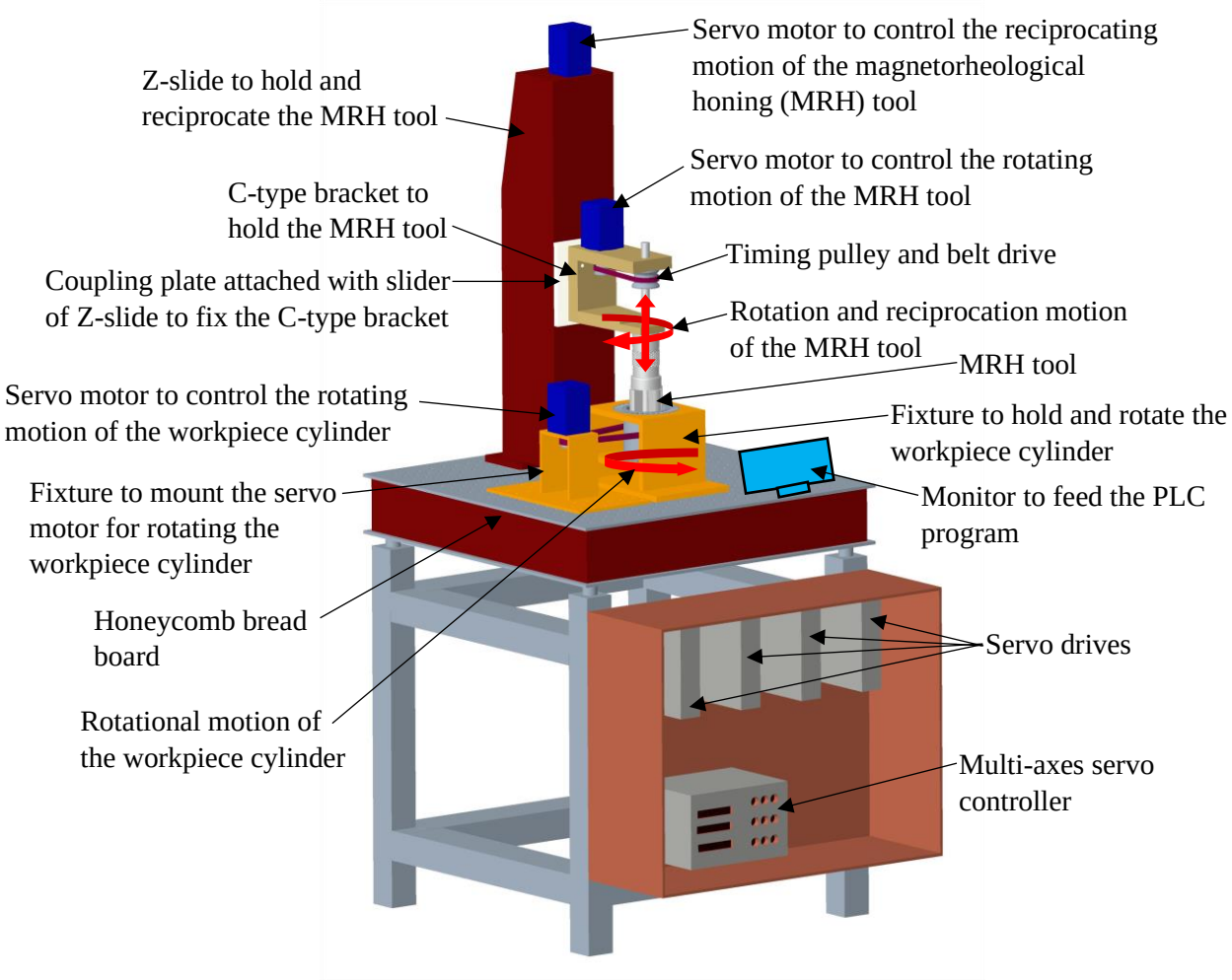

Fig. 4.1 Three-dimensional (3-D) computer-aided design (CAD) model of the rotational magnetorheological honing setup.

4.1.1 Design of fixture to hold and rotate the workpiece cylinder

Based on the operational requirement of the proposed finishing setup of the rotational magnetorheological honing (R-MRH) process, the fixture for holding and providing the rotational motion to the cylindrical workpiece is designed and fabricated. Figure 4.2 (a) shows the three-dimensional (3-D) computer aided design (CAD) model of this fixture. The necessity

of this fixture is that the workpiece cylinder should have very accurate and precisely rotational motion without much vibration and wobbling during its internal surface finishing with the rotational and reciprocation motions of the MRH tool.

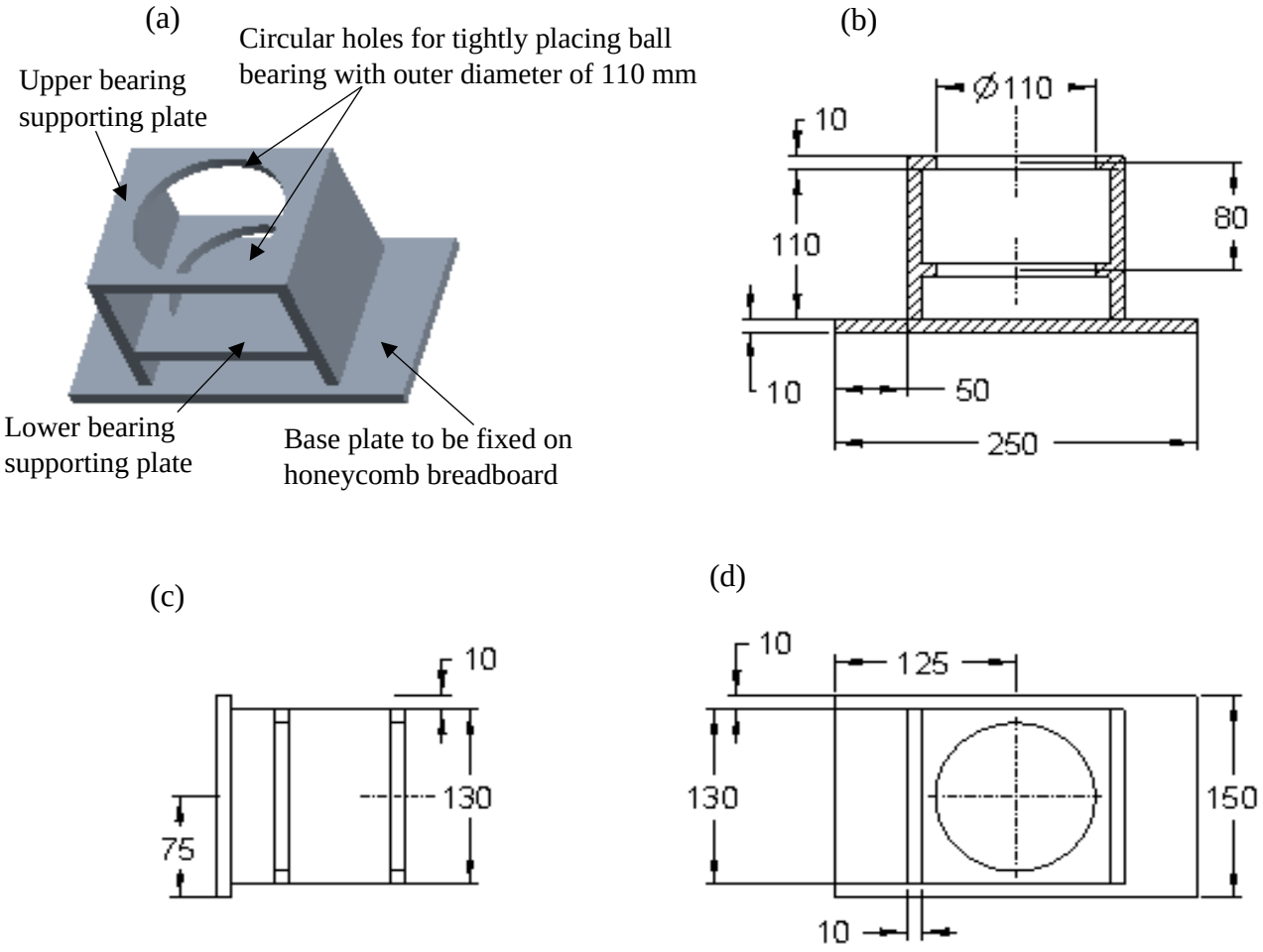

Fig. 4.2 (a) Three-dimensional CAD model, (b) sectional front view, (c) projected side view, and (d) projected top view of the fixture used for holding and rotating the cylindrical workpieces.

Therefore, the plates of thickness 10 mm of mild steel material are selected for its fabrication. Figures 4.2 (b), (c), and (d) demonstrate the sectional front view, projected side view, and projected top view of the CAD modelled fixture respectively for representing the dimensional specification of this part. In the upper and lower holes of this fixture, two ball bearings of dimensional specification as 110 mm of outer diameter and 75 mm of inner diameter are tightly fixed. The cylindrical workpiece with an outer peripheral diameter of 75 mm can be used in this designed fixture. This fixture is attached to the honeycomb breadboard (Fig.4.1) in such a way that the central axes of the workpiece cylinder fixed in the fixture and the magnetorheological honing (MRH) tool coincide.

4.1.2 Design of fixture to mount the servo motor for rotating the workpiece cylinder in the rotational magnetorheological honing setup

The fixture over which the servo motor is mounted for transmitting the power to rotate the cylindrical workpiece is made of a mild steel plate with thickness of 5 mm. The 3-D CAD model of this fixture is shown in Fig. 4.3 (a). Figures 4.3 (b), (c), and (d) demonstrate the dimensional specifications of this fixture through the section front view, projected side view and projected top view of the 3-D CAD model of the fixture for mounting the workpiece rotating servo motor respectively. Using these dimensional specifications (Fig. 4.3 (b), (c), and (d)), this fixture is fabricated. The material for the fixture mounting the servo motor is selected as mild steel. The plates of thickness 5 mm are used for fabrication of this tool. For mounting the servo motor on this fixture, there are four through holes of diameter 6 mm are provided on its support plate of the servo motor. On the breadboard, this fixture is fastened rigidly using a bolt in its side plates.

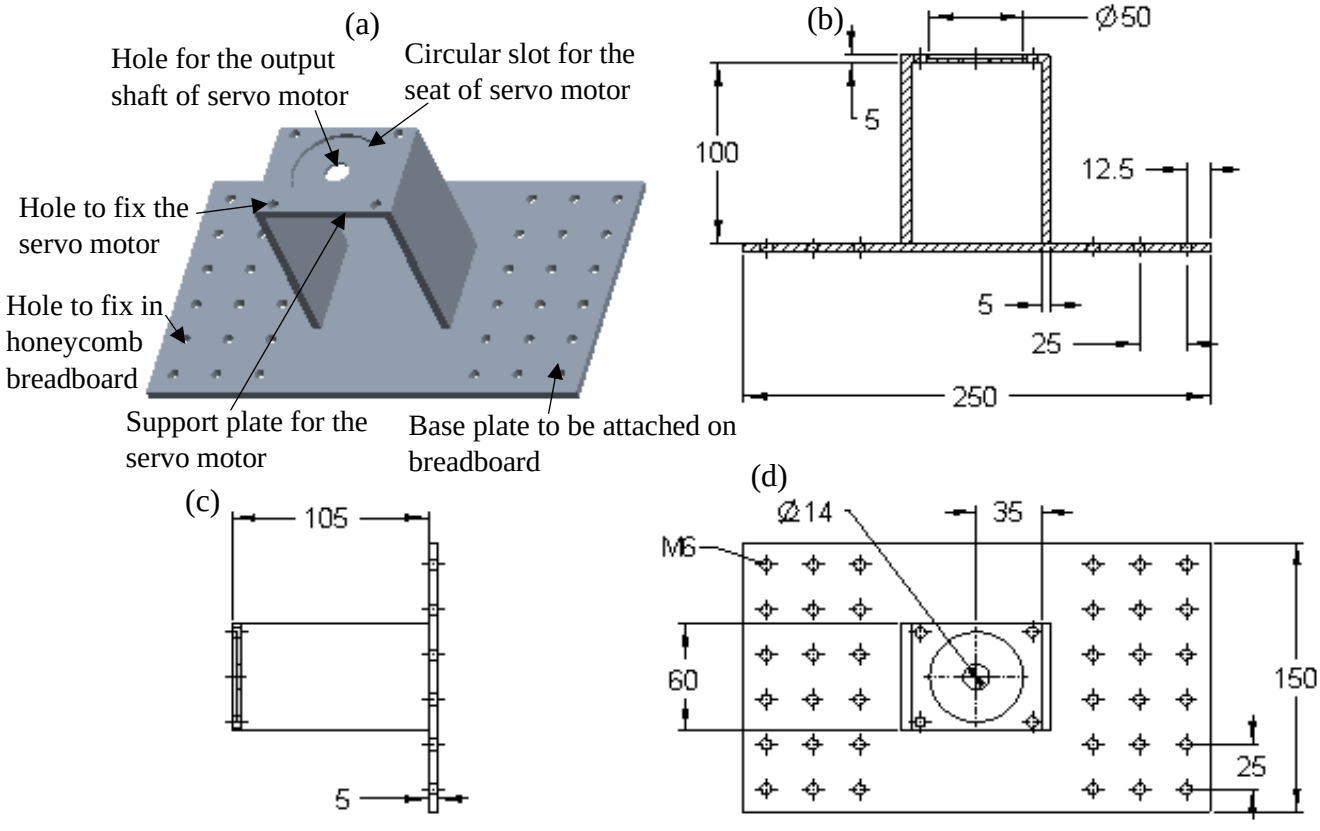

Fig. 4.3 (a) Three-dimensional CAD model, (b) sectional front view, (c) projected side view, and (d) projected top view of the fixture for mounting the workpiece rotating servo motor.

4.1.3 Fabrication of complete fixture for providing rotating the workpiece cylinder in the rotational magnetorheological honing (R-MRH) setup

The complete fixture for rotating the cylindrical workpiece is assembled as shown in Fig. 4.4(a). This fixture (Fig. 4.4) is made up of two sub-fixture which are the fixture to hold the workpiece cylinder and the fixture on which the workpiece rotating servo motor is mounted. Also, this fixture (Fig. 4.4) includes v-groove pulley, v-belt, and two flange ball bearings, etc. Using the fabricated components and with commercially available components, the fixture is assembled in the rotational magnetorheological honing setup as shown in Fig. 4.4 (b).

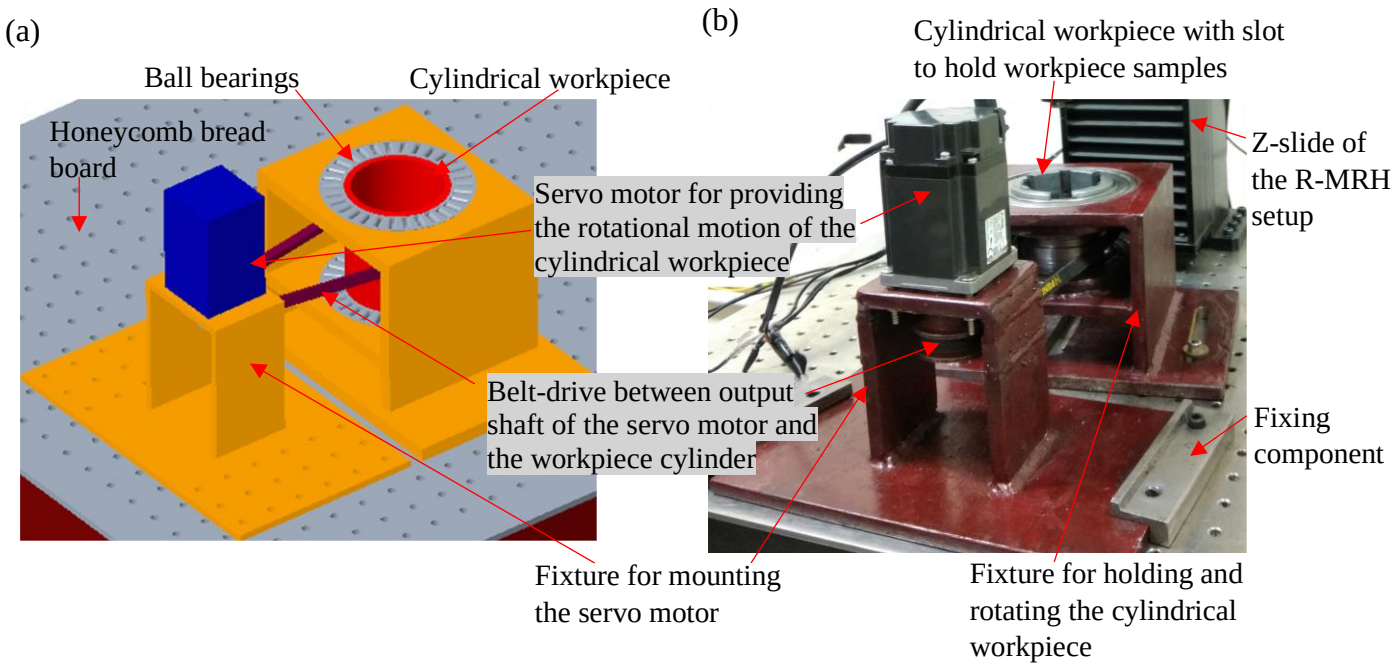

Fig. 4.4 (a) Three-dimensional CAD model of complete fixture and (b) photograph of the complete fabricated fixture used for holding and rotating the cylindrical workpieces during its inner surface finishing in the R-MRH process.

In this fixture, the cylindrical workpiece is fixed. To avoid the slipping of the v-belt over the external surface of the workpiece cylinder, a v-grove has been made on its peripheral surface. The fabricated fixture is fixed on the honey comb bread board with the M6 screw nut and fixing component. Using the designed fixture (Fig. 4.4), the rotational magnetorheological honing (R-MRH) process setup is developed as shown in Fig. 4.5. This R-MRH process setup with the fabricated fixture provides rotational motion to the cylindrical workpiece along with the rotating and reciprocating motion to the magnetorheological honing (MRH) tool. The MRH machine structure is made up of three servo motors to provide three types of motions during the finishing operation. The first servo-motor is mounted on Z-slide for performing the reciprocation motion of the MRH-tool. The second servo motor rotates the MRH-tool and the

third servo motor is used for rotating the cylindrical workpiece. All the machine components are mounted on a non-magnetic steel honeycomb breadboard. The programmable logic controller (PLC) is used to govern all the motions performed by the servo motors in the current developed R-MRH process. The two flange ball bearings used in this setup are attached in the workpiece rotating fixture's upper base plate and lower base plate. Both ends of the cylindrical workpiece are fitted inside the two ball bearings. Due to this proper fitment of bearings and workpiece cylinder in the fixture, the workpiece cylinder is rotated with zero deviation from the axis of rotation during the finishing operation.

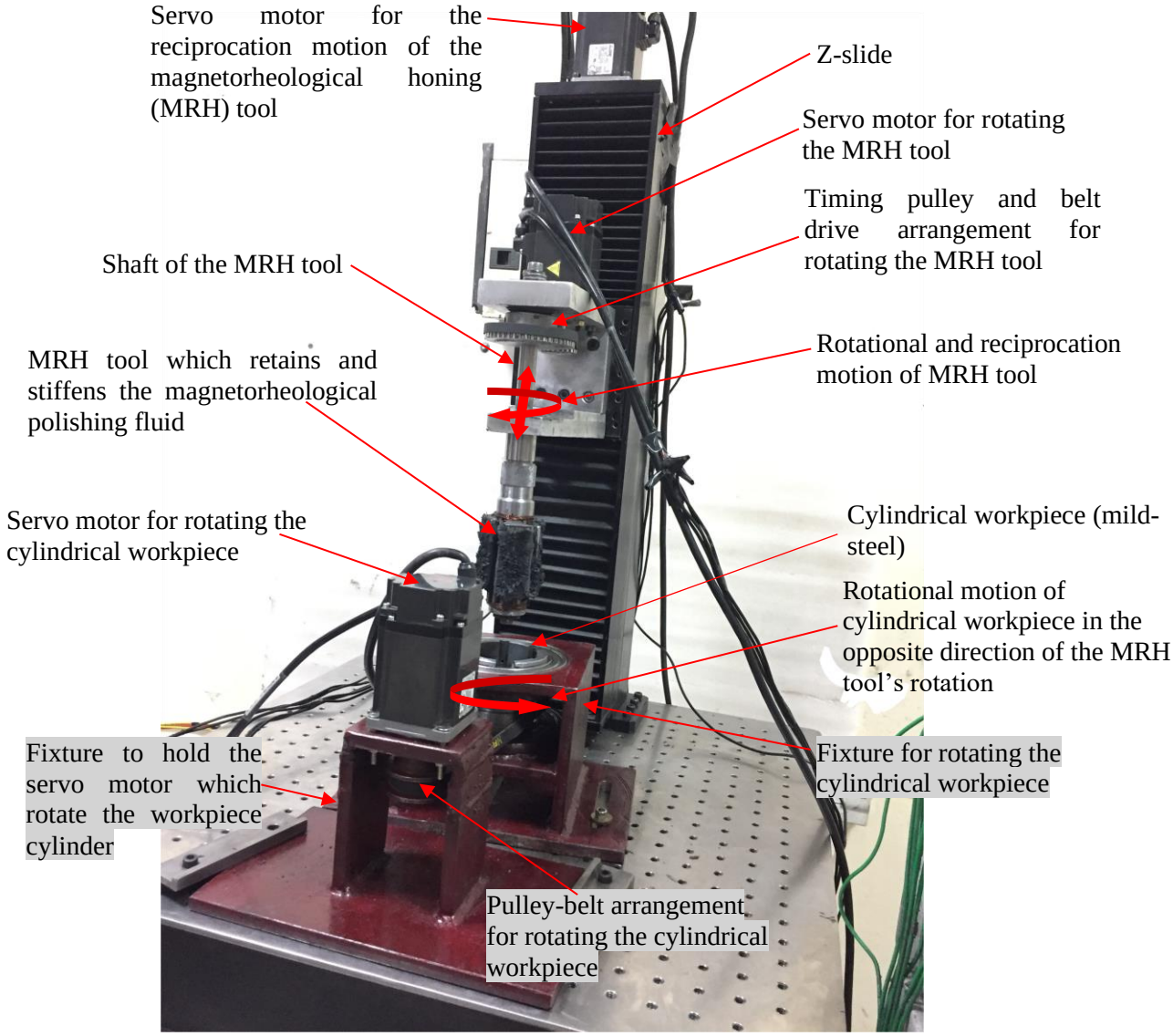

Fig. 4.5 Photograph of the rotational magnetorheological honing process with the fabricated fixture for rotating the workpiece cylinder.

The v-shaped pulley is mounted on the output shaft of the servo-motor and connected with the cylindrical workpiece through a v-belt drive for rotating the cylindrical workpiece. Therefore,

this fixture performs the rotational motion of the workpiece cylinder in the opposite direction of the MRH tool's rotation. Due to which the relative speed of the active abrasive particles of the magnetorheological polishing (MRP) fluid gets enhanced. The enhanced relative motion of the active abrasive particles enhances the tangential shear force applied by these abrasive particles. This results in enhancement of finishing performance and productivity for the internal surface of the cylindrical workpieces as discussed in chapter 3. The magnetorheological honing (MRH) tool is made up of four permanent NdFeB magnets strips on its outer surface and can move its outer magnetic surface (permanent magnet strips) radially inwards or outwards about the central axis of the finishing tool as per the need of the interior surface diameter of the cylindrical workpiece to be finished. The radial movement of the outer magnetic surface is provided to adjust the position of the permanent magnets before the start of the finishing. Then that position of the permanent magnets is locked after sustaining a proper working gap for MR polishing fluid while performing the finishing. Based on the improved capability of the present developed R-MRH process, this process can be found intensively useful in industries for fine finishing the internal surface of the cylindrical components.

4.1.4 Limitations of the initially developed fixture for providing the rotational motion to the different sizes of the cylindrical workpieces in the rotational magnetorheological honing process

The initial designed fixture uses the two ball bearings for holding the cylindrical workpiece and providing rotational motion very precisely. However, due to the fixed diameter of these two bearings, only the workpiece of fixed diameter is attached in this fixture, the initially designed fixture has some limitations which are given as follows.

- It is found only applicable for rotating the fixed diametric cylindrical workpieces.
- In the initially designed fixture, a v-groove on the outer peripheral surface of the cylindrical workpiece was necessarily to be made for power transmission from the servo motor to the workpiece through the v-belt drive. This indicates that the initial fixture was designed to more focus on precise motion for a limited diametric size of cylindrical workpieces and was less useful for variable diametric cylindrical workpiece.

The above-mentioned limitations in the initially developed fixture for providing rotational motion to the cylindrical workpieces while the R-MRH process may limit this setup for finishing the internal surface of the variety of the industrial cylindrical components. These limitations triggered the initially designed fixture of the R-MRH setup to be improved to

overcome the above-stated limitations so that the variable diameters of the cylindrical industrial components could be rotated during their MR finishing of the internal surface.

4.1.5 Design and fabrication of the improved fixture for rotating the variable diameter of the workpiece cylinders in rotational magnetorheological honing process

Considering constraint encountered in the initially fabricated fixture of the R-MRH process related to the size variability of the cylindrical workpieces, further an improved fixture is designed for holding and rotating the different sizes of the cylindrical workpieces in the R-MRH setup. This fixture includes one servo-motor, and an auto-centering three-jaw chuck that is connected to a coupling shaft. Also, two pillow block bearing, two v-groove pulleys, and a v-shaped belt drive are used in this fixture as shown in Fig. 4.6.

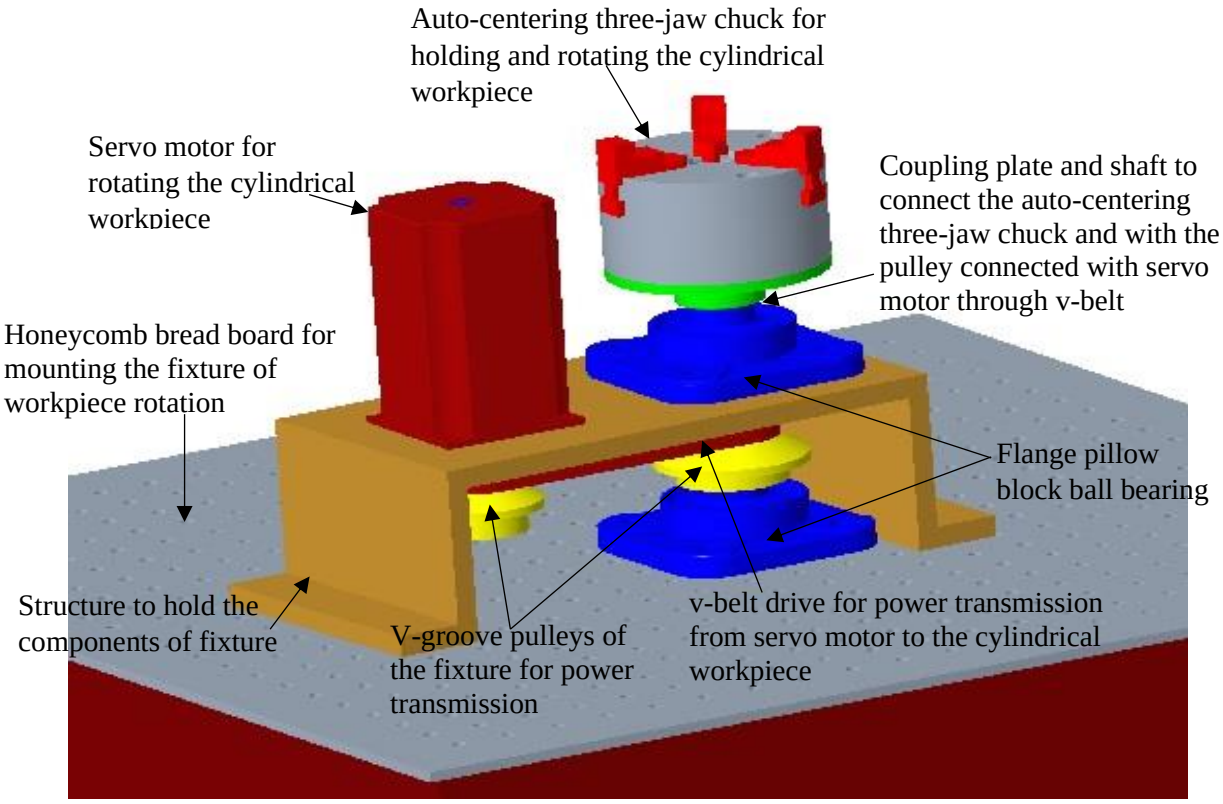

Fig. 4.6 Three-dimensional CAD model of the improved fixture for rotating the cylindrical workpieces of variable diameters.

This figure shows the 3-D view of the improved fixture lying on the honeycomb bread board. In the improved fixture, one pulley is attached to the coupling shaft and another pulley is mounted on the output shaft of the servo motor. In between two v-groove pulleys of the fixture, a v-belt drive is utilized for power transmission from the servo motor to the auto-centering three-jaw chuck through coupling shaft. The cylindrical workpiece is attached in the auto-

centering three-jaw chuck which can hold the cylindrical workpieces of the variable outer diameters upto 110 mm. The components which are not available commercially have been designed and fabricated. Whereas the components which are commercially available have been directly utilized in this fixture. Together, the fabricated and commercially available components make the complete fixture that holds and rotates the workpiece cylinders of variable diameters to accomplish the requirement of the rotational magnetorheological honing (R-MRH) process.

4.1.5.1 Design and fabrication of the improved fixture to mount the servo motor and three-jaw chuck to hold variable diametric cylindric workpieces in the rotational magnetorheological honing setup

For fabricating the improved fixture to hold and rotate the cylindrical workpieces of variable diameter, the component as shown in Fig. 4.7(a) (CAD model) is designed. This structure/fixture is made of mild steel and it holds the workpiece rotating servo motor at its one side. Whereas, at its other side, a three-jaw automatic chuck is mounted which tightly grips the cylindrical workpieces of variable diameters. Figure, 4.7 (a) shows the 3-D CAD model of this structure. This view shows the features such as hole for the coupling shaft attached with auto centering 3-jaw chuck, hole for the output shaft of the servo motor, and holes for attaching the flange pillow block bearings and servo motor over this fixture (Fig. 4.7). The detailed dimensional specification of this fixture part is provided for its fabrication through the three orthographic views i.e., front, side, and top views as shown in Figs. 4.7 (b), (c), and (d) respectively. Since, this component holds the cylindrical workpiece for its rotation, the accuracy in its level is ensured by the horizontal spirit gauge leveler while its fabrication. With the specified dimensions as shown in Fig. 4.7, this structure of the fixture is fabricated using the plates of mild steel of thickness 10 mm.

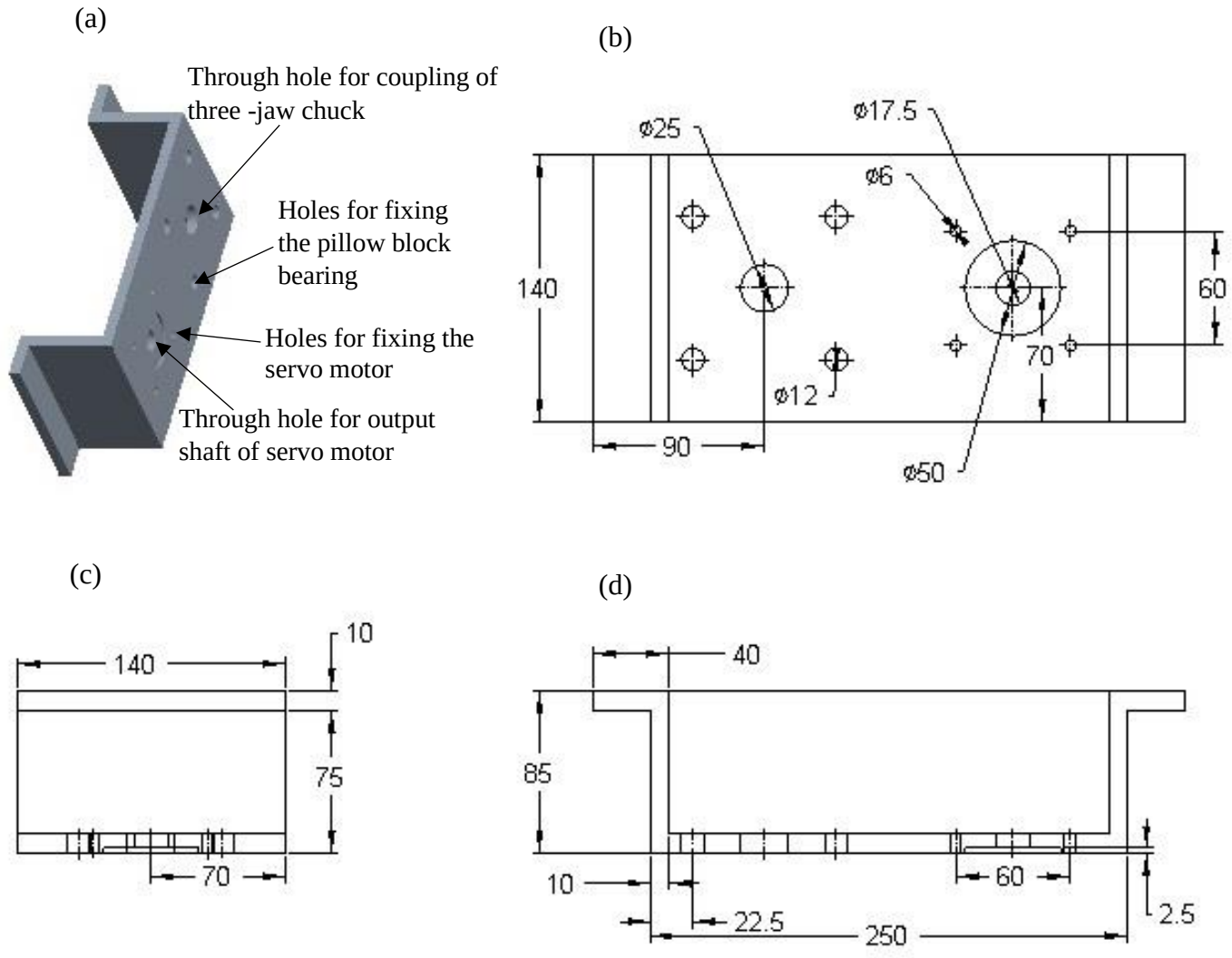

Fig. 4.7 (a) Three-dimensional view (b) front view (c) side view, and (d) top view of the computer aided design model of the fixture/structure.

4.1.5.2 Design and fabrication of coupling shaft to connect auto-centred three jaw chuck with the improved fixture for rotating the variable sizes of cylindrical workpieces

A coupling is designed and fabricated for connecting the auto-centred three-jaw chuck with the main body of the improved fixture. The shaft of this coupling is utilized for mounting the v-pulley which causes the rotational motion of the cylindrical workpiece through a v-belt drive connected from the pulley of the servo motor's output shaft. Figures 4.8 (a) and (b) demonstrate the top view and side of the 3D CAD model. All the dimensions shown in Fig. 4.8 are in mm. The 3-D CAD model and dimensional specification which has been used for the fabrication of the coupling are shown in Fig. 4.8. With the help of 3-D CAD model as shown in Fig. 4.8 (c), the shape of the coupling is observed while fabricating. The plate of the coupling with which the three-jaw chuck is connected has been made of the same diameter as the chuck. There are

three through holes made in the plate of coupling through which the three-jaw chuck is fixed over it.

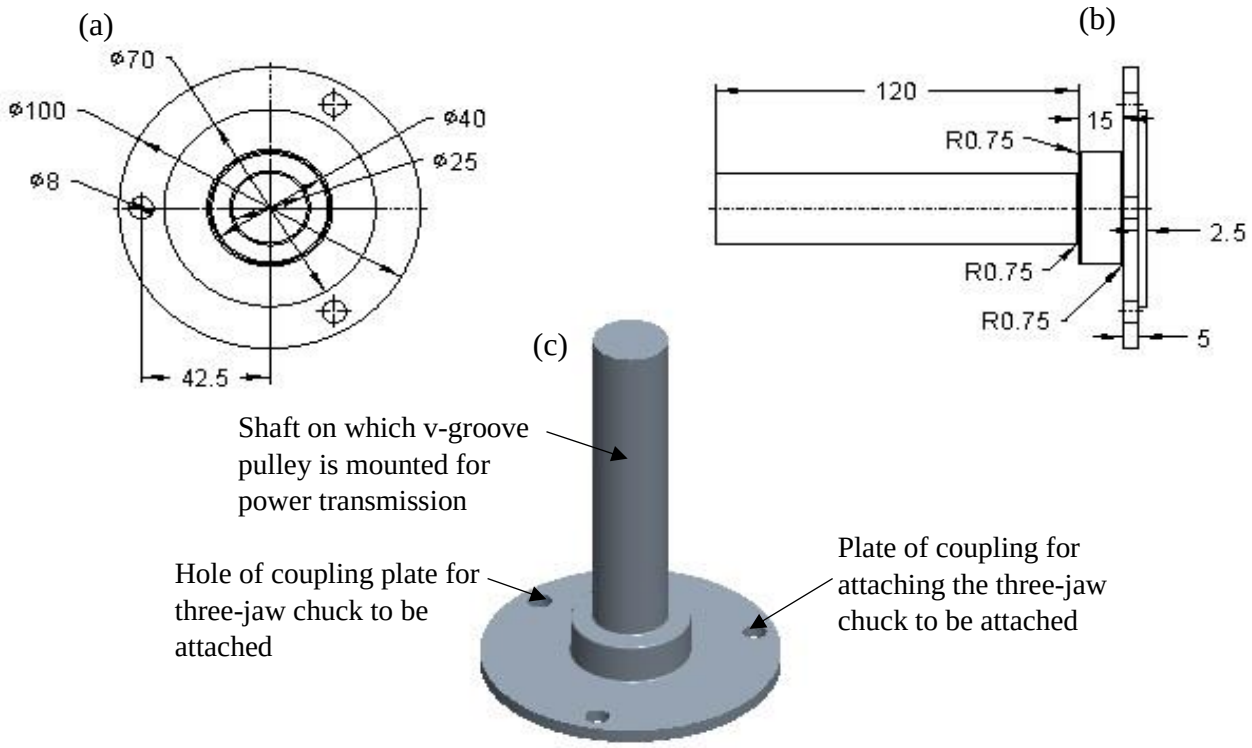

Fig. 4.8 (a) Top view (b) side view, and (c) 3-D CAD model of the coupling shaft for its fabrication.

Finally, the designed components of the improved fixture (Fig. 4.6) are fabricated and the commercially available components of the fixture are directly assembled. as shown in Fig. 4.9. The features (holes, height, width, etc.) assigned to the fabricated components of the improved fixture are primarily based on its requirement and then functionally matching the need of commercially purchased components to get assembled. The improved fixture is attached tightly on the honeycomb bread board with the M6 screw using an intermediate mean which acts like clamping washers as shown in Fig. 4.9. Therefore, utilizing the improved fixture after its fabrication, the rotational magnetorheological honing (R-MRH) setup is developed as shown in Fig. 4.10. This improved setup is used for fine finishing the internal surface of the variable sizes of the cylindrical workpieces. This improved fixture is fixed on the breadboard in such a way that axes of rotation of the cylindrical workpieces and MRH tool attached to the C-shaped bracket on the Z-slide of R-MRH setup are to be collinear. All the servo motors are wire-connected with the servo-drives which are further regulated through the programmable logic controller (PLC) by feeding the different desired motions. The different desired motions are fed in the PLC program through the computer's monitor interface. Based on the type of motions

and their values provided in the program, the motions of each servo motor are controlled through the servo drives.

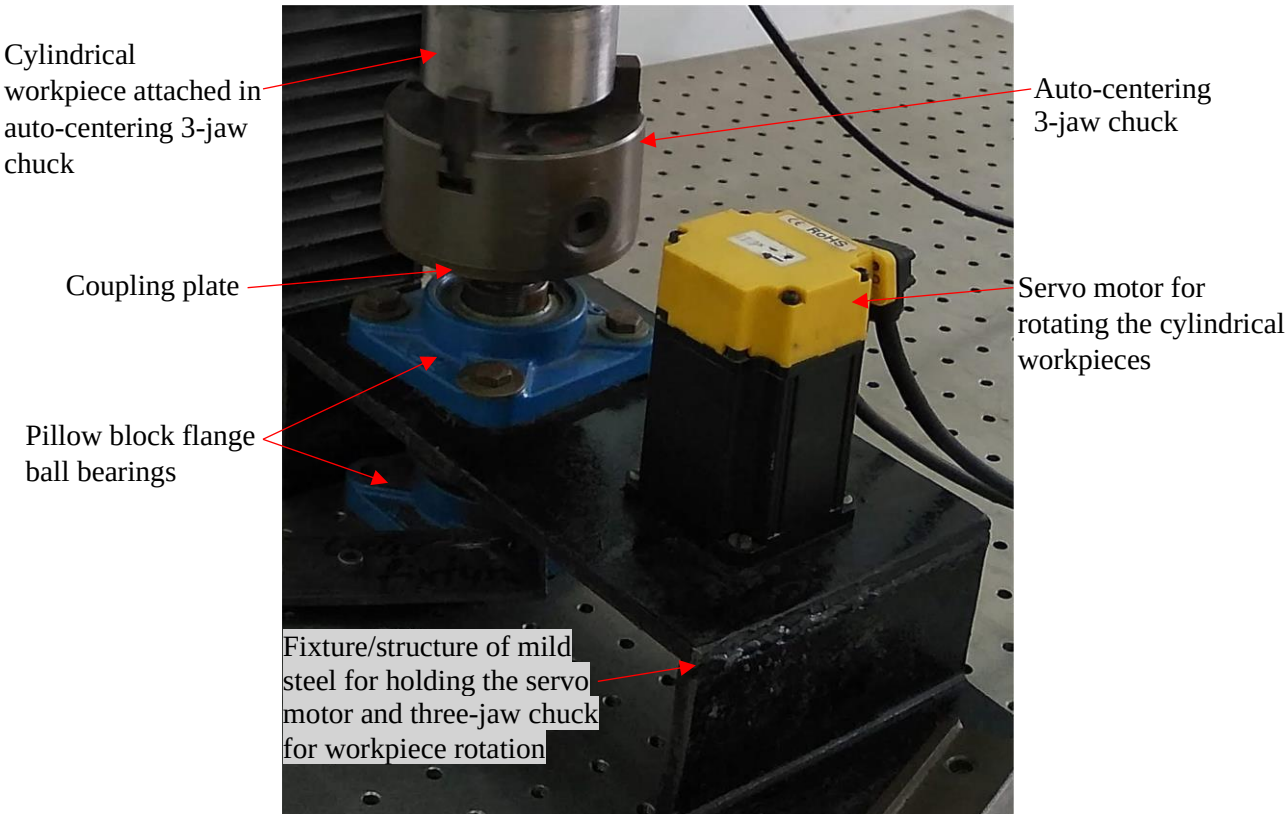

Fig. 4.9 Fabricated improved fixture for holding and rotating the cylindrical workpieces of variable diameter.

The honeycomb breadboard is placed on the frame structure which has four legs. Each leg of the frame structure is featured with a screw height adjustment mechanism through which the uniform level of the honeycomb breadboard is ensured to achieve uniformity in workpiece level. Therefore, the R-MRH setup along with the improved fixture allows itself to hold the cylindrical workpieces of variable diameters. Also, the MRH tool has the flexibility to finish the internal surface of the variable diametric cylindrical workpieces. Hence, the flexibility in the improved fixture and the MRH tool makes this improved setup very useful for finishing the internal surface of the variable diameters of numerous of industrial cylindrical products like hydraulic cylinders, moulds, circular dies, hydraulic rack cylinder and cylindrical barrel for injection moulding machine. Thus, the improved fixture is to enhanced the applicability of this R-MRH setup significantly.

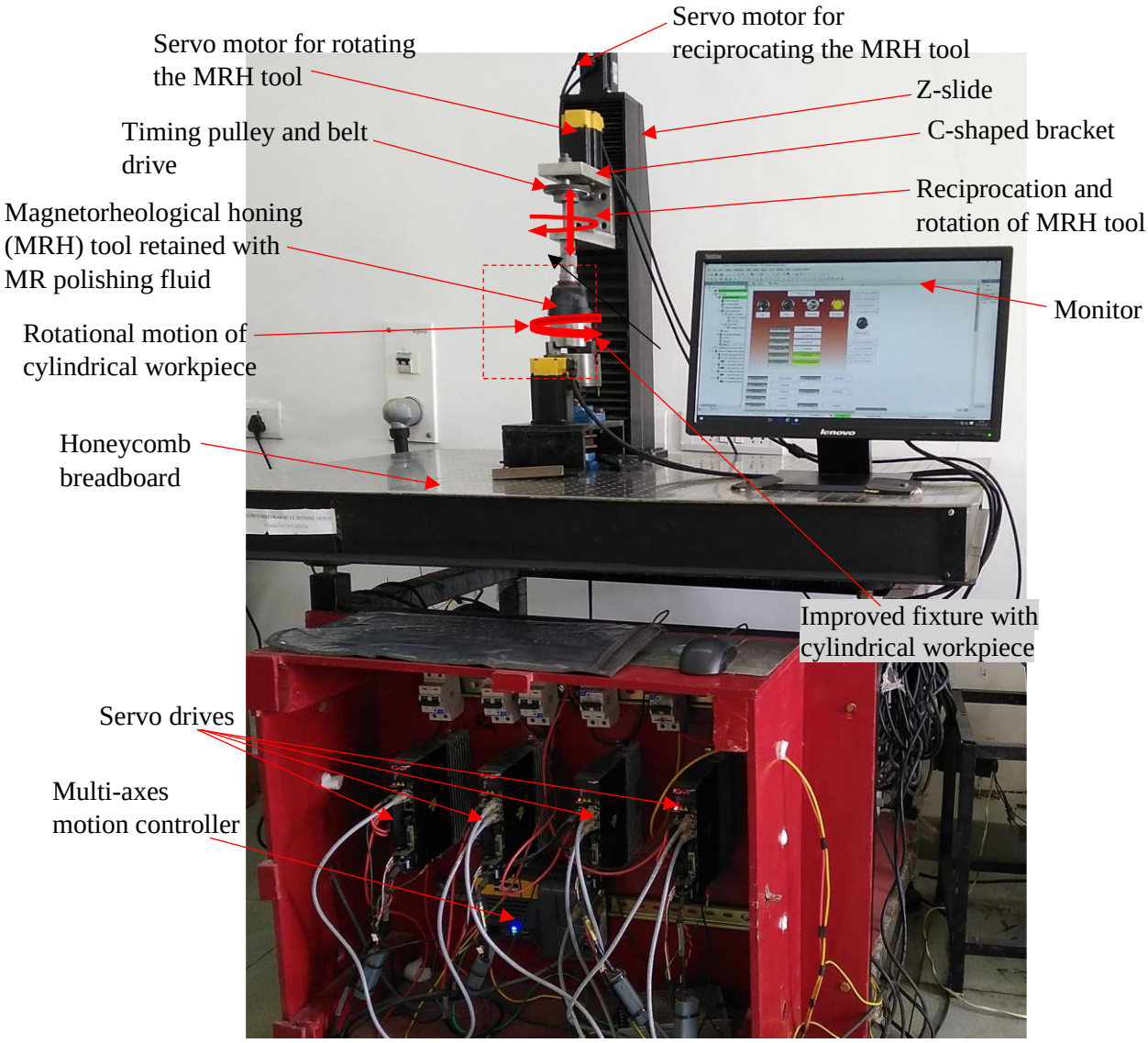

Fig. 4.10 The R-MRH setup along with the improved fixture for finishing the internal surface of the cylindrical workpieces of variable diameters.

4.1.6 Advantages of the developed rotational magnetorheological honing process

With the development of both types of the fixture to hold and provide the rotational motion to the cylindrical workpieces in the rotational magnetorheological honing (R-MRH) process, the following advantages have been drawn.

- The rotational motion of the cylindrical workpiece in the reverse direction of the magnetorheological honing (MRH) tool adds more shear force due to the enhancement in the relative speed of the active abrasives which may result in better surface finishing in lesser time than the existing MRH process (Grover and Singh, 2018a).
- The fixture with two ball bearings to hold the cylindrical workpiece gives precisely accurate rotational motion to the cylindrical motion.

- The fixture developed with the auto-centering three-jaw chuck enables the R-MRH setup to be applicable for finishing the internal surface of variable diametric industrial cylindrical components.
- Due to the improvement in the finishing capability of this process, it may be used in many important industrial applications. For example, nano-finishing of the hydraulic cylinders, hydraulic and pneumatic valves used in manufacturing machinery, aerodynamic bearings as highly essential for the precision machinery tools, high-speed machines and various medical devices.
- The improvement in relative rotational motion of the abrasive particles caused by the developed R-MRH process setup results in decrease in the pitch of helical path followed by the active abrasive particles as discussed in the chapter 3 (Eq. 3.2) which results in more efficiently uniform internal surface finishing as compared to the existing MRH finishing process (Grover and Singh, 2018a).

Thus, the present developed R-MRH process can be found more useful in fine finishing the internal surface of the cylindrical workpieces with the improved productivity.

4.2 Design and fabrication of an in-situ magnetorheological honing tool

The internal surface finishing of the cylindrical workpieces is mainly performed by traditional honing. When the same cylindrical workpiece surface needs to be further fine finished, it requires another advanced finishing tool and setup like magnetorheological polishing (MRP) fluid-based finishing process. Therefore, it is expensive and labor-intensive due to the use of separate tools and setups for traditional and fine-finishing on the same internal cylindrical workpiece surface. Also, the initial surface required for applying the rotational magnetorheological honing (R-MRH) process is either ground or honed surface after the traditional grinding or honing operation. So, the R-MRH process is further improved in terms of the less expansive, less time, and labor-intensive by introducing an in-situ MR honing tool. Using the in-situ MR honing tool, the traditional honing as well as the R-MRH process can be performed on the internal surface of a cylindrical workpiece at a single setup. Hence, the in-situ MR honing tool may have the ability to perform fine finishing from the initial machined surface using the traditional honing as well as MR finishing on a single finishing setup. To sort out the issues related to the involvement of the multiple tool and setup in MRP fluid-based finishing processes for the internal surface of the cylindrical workpiece, a new tool is required to perform the traditional honing and rotational magnetorheological honing (R-MRH) on the variable diametric cylindrical workpieces with a single tool at a single setup. So, to accomplish

this requirement, an in-situ R-MRH tool is developed. The proposed design of the in-situ MRH tool is shown in Fig. 4.11.

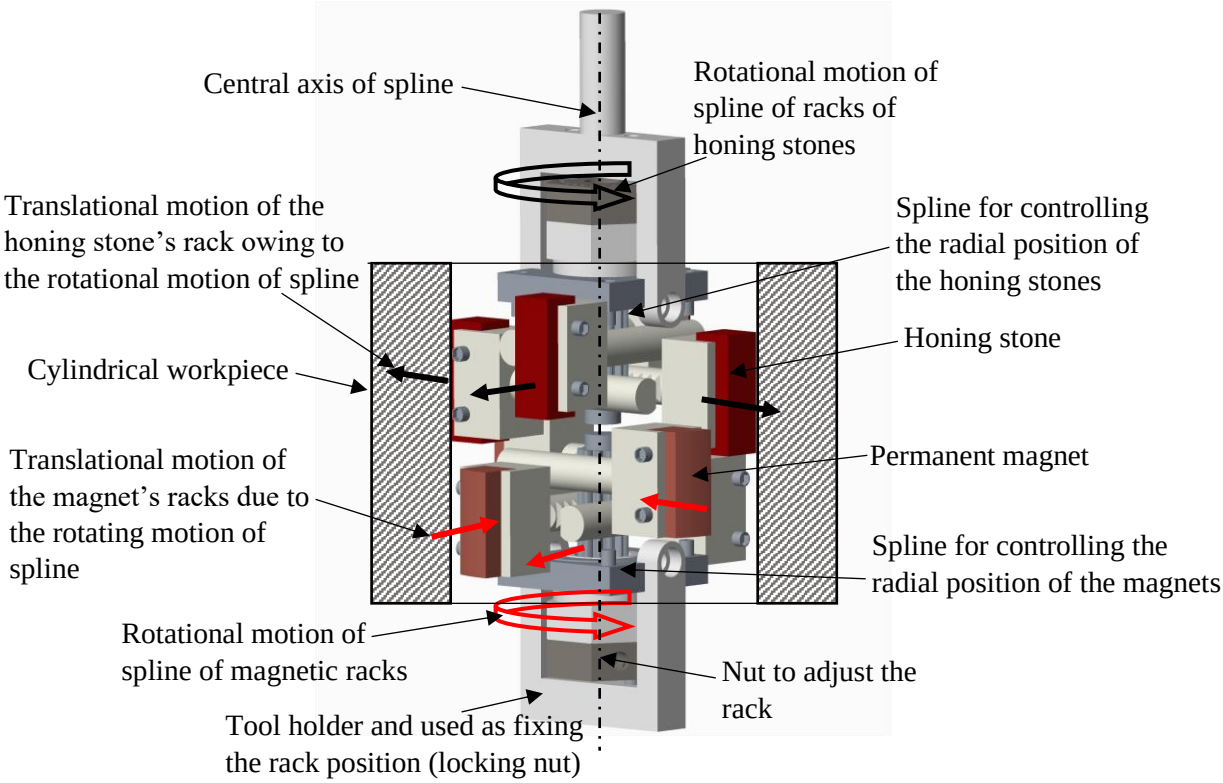

Fig. 4.11 Proposed design of in-situ magnetorheological honing (MRH) tool for initial surface generation using traditional honing and final fine finishing using the R-MRH with a same single tool.

This novel in-situ MRH tool improves the productivity of the operation with more efficiency for fine-finishing the interior surface of the cylindrical workpieces from the machined surface. This tool uses the spline rolling rack mechanism (Killop and Warren, 1976) to incorporate the requirement of the process. This tool uses two splines, and eight racks as seen in Fig. 4.11. Four racks hold the abrasive-bonded honing stones and the rest of the four racks hold the magnets. The racks which hold the permanent magnets are mounted at one spline, whereas, the racks holding the honing stones are mounted on another spline of this tool. Both splines are attached with two nuts separately. Through these nuts, the splines are rotated to adjust the position of the honing stones and magnets of the tool. The racks of the magnets and the honing stones are adjusted by rotating the spline shaft upto a certain diameter of the tool that is suitable for carrying out the finishing. As all racks are indexed with spline, so, the racks of this tool are at an offset distance (equals to the radius of base circle of the spline shaft) from the central axis of the spline.

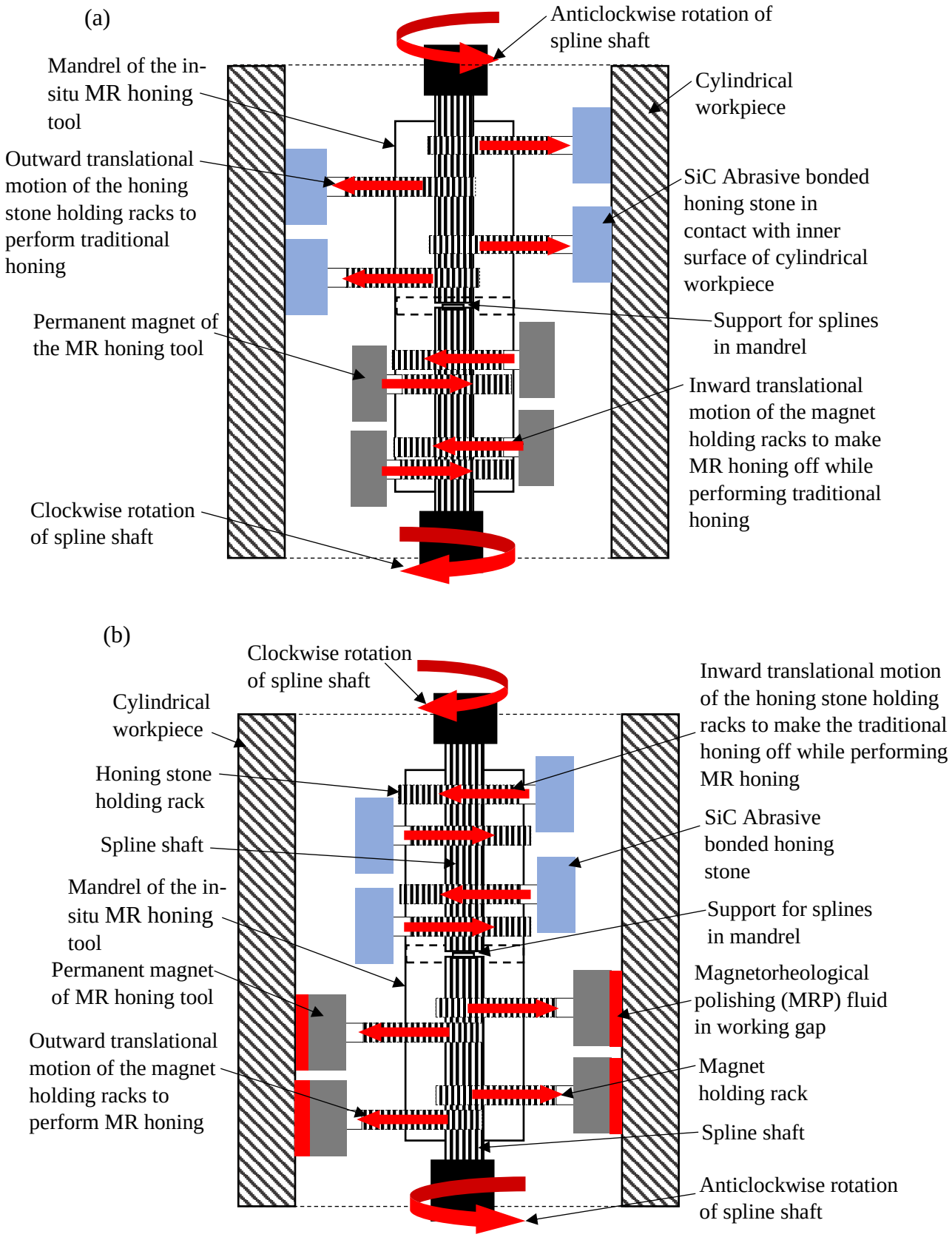

Fig. 4.12 Proposed in-situ magnetorheological honing (MRH) tool for (a) initial surface generation using conventional honing and (b) final fine finishing using R-MRH process.

The inside view of the mandrel of the in-situ magnetorheological honing (MRH) tool is shown in Fig. 4.11. This view reveals the arrangement of racks of honing stone and permanent magnets on the splines of the in-situ MRH tool inside the mandrel. With the rotation of the splines which are indexed to the racks, these racks perform translational motion in the outward direction. The nuts which are connected to the spline shafts and the lock nuts have several small holes as shown in Fig. 4.11 and 4.12. The racks which hold the magnets are translated inward by rotating the indexed spline in the counter direction of the rotating direction of the spline indexed with racks of honing stone. When the honing stones and magnets have achieved the desired diametric position, a pin is inserted in the corresponding holes of the nut attached to the spline and the lock nut at that position of the tool racks. Besides the tool holding shaft in the in-situ MRH tool, to avoid unlocking the racks, the screws are tightened upto the lower and upper nuts via the rack lock screw when operated. The honing stones and magnets are fastened in the rack by two lock screw nuts. The spline indexed to the honing stone rack is rotated anticlockwise so that the honing stones are firmly contacted to the inner surface of the cylindrical workpiece for the initial finishing as shown in Fig. 4.12(a). However, at the same time, the spline shaft of magnets is rotated clockwise for making it in an off state while traditional honing is performed as shown in Fig. 4.12(a). Similarly, while MRH process on the inner surface of the cylindrical workpiece with the engagement of the permanent magnets, the traditional honing process is made off with the inward motion of the honing stones as seen in Fig. 4.12(b). Therefore, the proposed in-situ MRH tool conducts both conventional and magnetorheological honing on the inner surface of the cylindrical workpieces. Due to the spline rolling rack mechanism utilized in this tool, it is found useful for a great diametric range i.e., 90 mm to 140 mm to finish the inside cylindrical surfaces. Therefore, the present developed tool's diametric range of applicability allows this tool to be commercially useful for finishing high diametric ranged components such as outer bearing raceways, spindle housings, vehicle bearing rings, cylindrical molds, etc. (Danobat, 2020). The proposed novel in-situ magnetorheological (MR) honing tool is designed and fabricated for fine-finishing the interior cylindrical workpieces surface. The in-situ MRH tool and its working mechanism are designed as depicted in Fig. 4.12.

The primary purpose of this tool is to finish the interior cylindrical surface of variable diametric workpieces by the traditional honing as well as the R-MRH process at a single setup which uses a single controller, fixture, and other assisting equipment. Thus, to achieve the purpose behind the development of this tool, the functions of both traditional and MRH are incorporated into a single tool known as the in-situ magnetorheological (MR) honing tool. Both splines of

this tool transfer the motion to the racks of honing stone and magnetic holding racks independently in a single housing. Therefore, the radial position of the honing stones and the permanent magnets are controlled independently using the upper nut and lower nut connected with the upper spline shaft and lower spline shaft respectively. Therefore, these features of the proposed tool make it capable to produce an initial finished surface through traditionally honing and further fine finishing on the traditionally initial generated internal surface of the cylindrical workpieces using the R-MRH process at a single finishing setup.

4.2.1 Magnetostatic simulation for distribution of the magnetic field induced by the permanent magnet of the in-situ magnetorheological (MR) honing tool

The magnetostatic analysis through the finite element analysis (FEA) is conducted to ensure the proper and effective operation of the in-situ MRH tool. This simulation gives the analysis of the distribution of the magnetic field from the curved surface of the NdFeB permanent magnet to the inside cylindrical workpiece's surface i.e., within the working-space. The radial curved shape of the magnet provides a more uniform working-space amid the magnetic curved surface of the in-situ MRH tool and the workpiece surface than any other shape of the magnet (Grover and Singh, 2018a). Due to this reason the end surface of the magnet used in this tool is kept curved. The in-situ MRH tool uses a spline rolling rack mechanism to change the diametric position of the magnets and honing stones with a broad range of variable diameters. Owing to the roller rack mechanism, the magnets of this tool is adjusted to a radially offset position. Therefore, to maintain a uniform gap between the permanent magnets of the tool and the internal surface of the tubular workpiece, the shape of the magnets of the present in-situ MRH tool is designed as a combination of the trapezoidal and the curved magnets (irregular). The working-space for the present analysis in finishing the inside surface of the cylindrical workpiece is assigned as 2 mm. The materials and their relative permeability assigned to each part of the in-situ MRH tool system are listed in Table 4.1. Using the Maxwell Ansoft V13 a magnetostatic module of ANSYS software, the magnetic field distribution induced by the four permanent magnets of this tool in the working gap is studied. For magnetostatic simulation, the CAD model generated in the 'PTC Creo Parametric 7.0.0.0' of the in-situ MRH tool system along with the MRP fluid and ferromagnetic (mild-steel) cylindrical workpiece is saved as IGES file format. The assignment of the materials along with the relative permeability for each component of the tool is made on the basis of the literature (Singh *et* al., 2013) and the available library in Maxwell Ansoft V13 listed in Table 4.1. The boundary conditions are defined before running the FEA simulation. Then, the magnetic field distribution was analyzed by introducing

the solution setup in it. Further, the numerous magnetostatic FEA simulations are performed by varying numbers of magnets, dimensions of the magnets, working materials of components of the tool, and their sizes for the final tool design.

Table 4.1 Material of the components of the in-situ magnetorheological (MR) honing tool system and their magnetic properties.

Component	Material	Relative permeability
Mandrel	Stainless steel	1.003
Magnet holding rack	Stainless steel	1.003
Spline shaft	Stainless steel	1.003
Permanent magnet	Neodymium (NdFeB)	1.099
Magnetorheological polishing (MRP) fluid	Mixture of electrolytic iron particles (EIPs), silicon carbide (SiC) abrasives, paraffin oil and AP3 grease	5
Ferromagnetic cylindrical workpiece	Mild steel	600

Based on results of the magnetic field distribution obtained in various magnetostatic FEA simulations performed, four permanent magnets are considered for the development of this tool.

4.2.1.1 Magnetic field distribution in the working-space with the new proposed in-situ tool

The magnetic field distribution in the working-space amid the end curved surface of the NdFeB permanent magnet of the tool and the inside surface of the cylindrical mild-steel workpiece is obtained from the FEA simulation as shown in Fig. 4.13. The variation of the magnetic field in the working-space between the curved end surface of the NdFeB magnetic tool and the internal surface of the mild steel cylindrical workpiece is depicted in Fig. 4.13(a). The trend of the magnetic field distribution in the working-space through FEA is found decreasing as shown in Fig. 4.13(b). A similar trend line of the magnetic field distribution is obtained through the experimental measurements using the gaussmeter in the working-space are demonstrated in Fig. 4.13(b). The magnetic field values obtained from the magnetostatic simulation (FEA) are found higher than the actual values (experimental measured) of the magnetic field. This is because magnetostatic FEA is performed in various ideal conditions with consideration of the ideal value of magnetic parameters available in Ansoft Maxwell software. The magnetic field obtained from the magnetostatic FEA simulation has been found to be useful in comparing the magnetic fields generated by various tool designs and deciding on the best design based on the practical requirements. Based on the values of the magnetic field and the trend line obtained in the magnetostatic FEA study, the present in-situ MRH tool is selected for the final design.

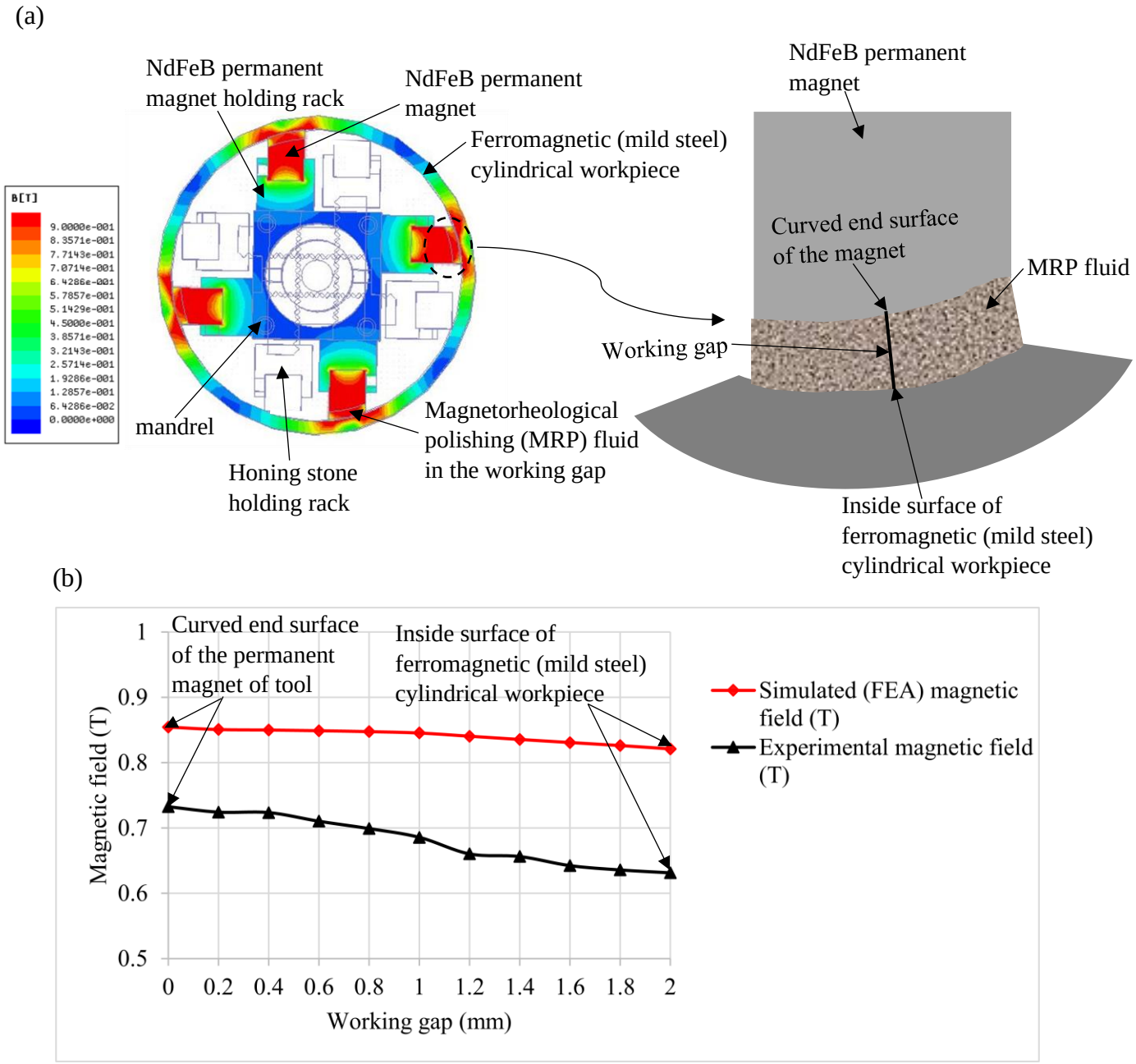

Fig. 4.13 (a) Finite element analysis (FEA) image of magnetic field distribution in the in-situ MRH tool along with the MRP fluid in the working gap and mild steel cylindrical workpiece, and (b) plot of magnetic field distribution in the working gap obtained from the FEA and experimentally measured.

The trend line of the magnetic field variation shows the negative gradient of the field in the working-space from the magnetic curved surface of the in-situ MRH tool to the inside surface of the mild-steel cylindric workpiece (Fig. 4.13b). This design of the in-situ MRH tool is considered for fabrication because the magnitude and negative gradient of the magnetic field distribution in the working-space ensures the performing of relative motions by the active

abrasive particles (AAPs) (Paswan et al., 2017). From Fig. 4.13(b), it is observed that magnetostatic FEA simulated and experimental measured magnetic field at the curved end surface of the magnet is approximately 0.85 T and 0.73 T respectively. Whereas the magnetostatic FEA simulated and experimentally measured magnetic field at the inside surface of the workpiece is 0.82 T and 0.63 T respectively which is sufficient values of the magnetic field for making the stiff chain structures of the MRP fluid (Grover and Singh, 2018a; Paswan *et* al., 2017) in MR finishing of the initial surface of the cylindrical workpieces. Thus, these analytical studies of magnetic field are found helpful in deciding the final design of the in-situ MRH tool for its fabrication.

4.2.1.2 Magnetic field distribution along curved surface of the tool's NdFeB permanent magnet

The uniform finishing is one of the prime objectives of the present design and development of the in-situ MRH tool. The uniformity in the surface finish depends on how the uniform normal force is applied while finishing the surface. In the magnetorheological polishing (MRP) fluid-based finishing processes, the normal force is dependent of the magnetic field (Singh *et* al., 2013). Hence, the induction of the uniform magnetic field from the magnet of the tool is necessarily required for abrasive particles to apply the uniform magnetic normal force. Therefore, to investigate the uniformity in the magnetic field generated by the NdFeB magnet on its curved surface, the magnetic field is analyzed through the magnetostatic analysis finite element method (FEA) and experimental measurement using gaussmeter as depicted in Fig. 4.14. The magnetic field distribution image on the curved end surface profile of the permanent magnet with the FEA magnetostatic simulation is shown in Fig. 4.14(a). Also, the distribution of the magnetic field through magnetostatic FEA and experimental measurement are plotted as depicted in Fig. 4.14(b). Due to the unequal length of the sides of the magnet (Figs. 4.13 and 4.14), there is a slight variation in magnetic field distribution on the curved surface of the permanent magnet is observed. The minimum magnetic field distribution is observed on both edges of the curved side of the magnet. The magnetic field at the edge of the start point of the curved magnet is found larger than the edge of the endpoint of the curved magnet. The magnetic field distribution tends to remain constant after its slight initial increment at each edge of the curved profile of the magnet. Thus, due to the uniform magnetic field distribution on the curved end surface of the NdFeB permanent magnets, the uniform magnetic force can act during the finishing operation which results in uniform finishing using the new designed in-situ MR honing tool.

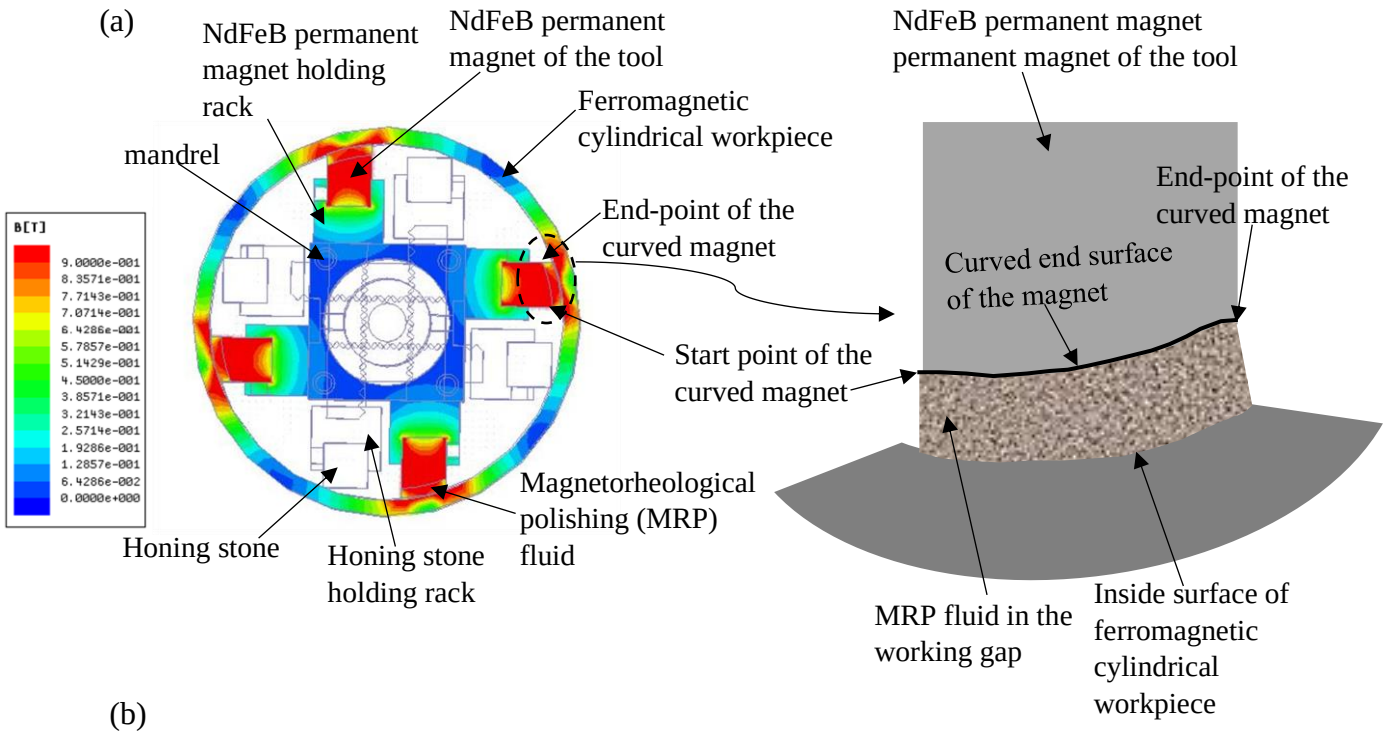

(b)

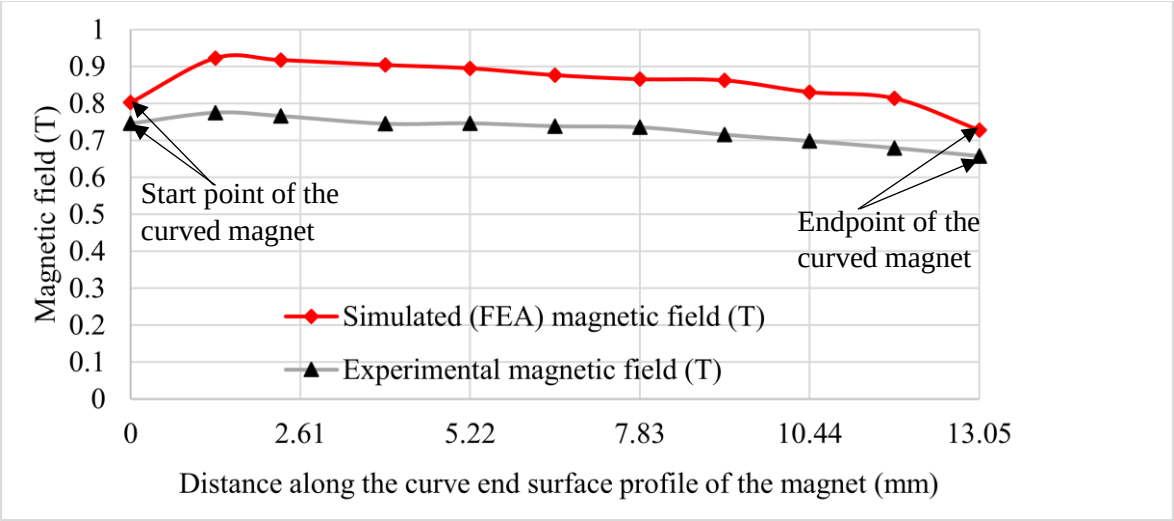

Fig. 4.14 (a) Finite element analysis image of magnetic field distribution on the curved end surface of the tool's permanent magnet and (b) plot of magnetic field distribution on the curved end surface of the tool's permanent magnets obtained from the analysis through FEA and experimental measurement.

4.2.1.3 Magnetic field distribution along the height of the curved end surface of the tool's permanent magnets

Uniform magnetic normal force enhances the uniformity in the finishing surface. Moreover, the normal force in the MR finishing processes is altered by the magnetic field distribution. Therefore, to ensure the uniform finishing of the surface along the height of the workpiece in

the present work, the analysis of the magnetic field generated by the permanent magnet along its height is performed. The analysis of the magnetic field is conducted through the FEA magnetostatic simulation and experimentally measured magnetic field at different points along the height of the magnet. Figure 4.15(a) shows the magnetic field distribution on the curved surface of the NdFeB permanent magnet along its height through the FEA magnetostatic simulation. As the permanent magnets are symmetrical about their cross-sectional mid-plane, therefore, the distribution of magnetic field induced by a magnet along the height over its end curved surface is found symmetrical. Fig. 4.15(b) reveals the trend of the magnetic field distribution along the height over the curved end surface of the NdFeB permanent magnets. On observing in FEA result (Fig. 4.15) from the bottom to upper end of the magnet, initially the magnetic field starts increasing from 0.77 T to 0.91 T and then decreases to 0.89 T. Further, it approaches the consistent distribution of magnetic field on the height and before reaching over the top end of the permanent magnets, the magnetic field again increases and decreases in similar way to the magnetic field distribution at lower end of the magnet. However, on most of the part of the magnets along its height, the distribution of the magnetic field remains constant. A similar trend is noticed in the experimentally measured magnetic field as shown in Fig. 4.15(b). Thus, it can be said that the magnets used in this tool are suitable for the uniform magnetic normal force which leads to the uniform fine magnetorheological finishing on the internal finishing of the cylindrical workpieces. From the complete study of magnetic field analysis, it is observed that the prime objective of the proposed in-situ MRH tool for fine-finishing of the internal cylindrical surface of the workpieces can be fulfilled. This is owing to the magnitude of the induced magnetic field (Fig. 4.15) is found sufficient to form the stiff magnetic iron-particles chain structure and perform the MR finishing action (Sidpara and Jain, 2013; Yadav and Singh, 2019). Also, the negative gradient of magnetic field distribution from the end curved surface of the in-situ MRH tool's NdFeB permanent magnet to the inside cylindrical workpiece surface ensures relative motion of the active abrasive particles (AAPs) w.r.t. the finishing surface which favours the fine-finishing capability of this tool. The almost uniform distribution of the magnetic field on the curved surface along the curved profile and the height of the tool's magnet dictates the application of uniform normal force over the finishing surface by the AAPs through magnetic electrolytic iron-particles (EIPs) chain-structure. Therefore, the uniform normal force applied by the AAPs consequences in the uniform finishing of the interior surface of the cylindrical workpieces.

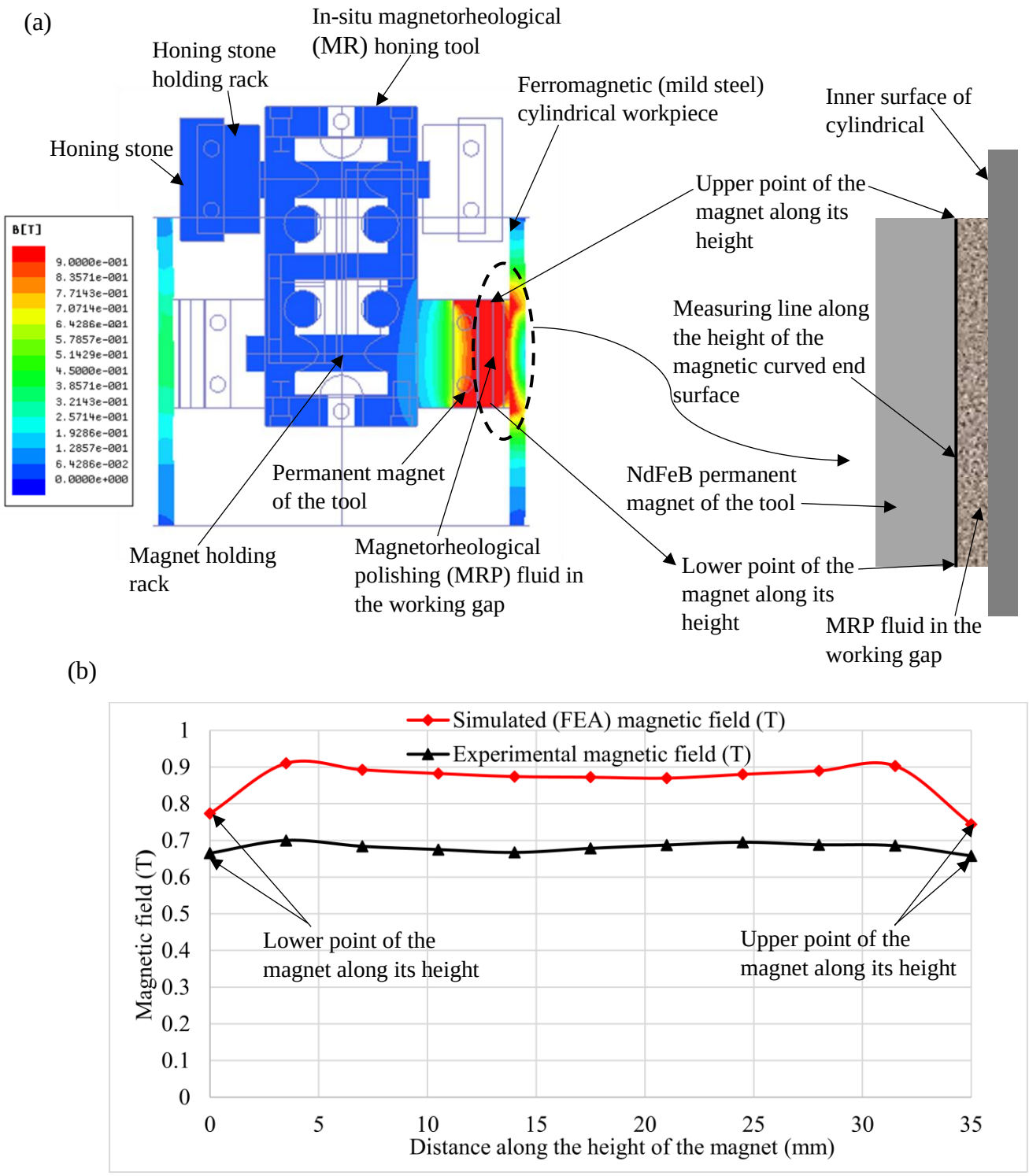

Fig. 4.15 (a) Finite element analysis (FEA) image of magnetic field distribution on the curved end surface along the height of the permanent magnet and (b) plot of magnetic field distribution on the curved end surface along the height of the tool's permanent magnet obtained from the FEA and experimentally measured.

4.2.1.4 Analysis of the magnetic lines flow in the in-situ magnetorheological (MR) honing tool in the presence of MRP-fluid and the mild-steel cylindrical workpiece

The materials selected for the magnetostatic FEA of the in-situ magnetorheological (MR) honing tool are already reported in Table 4.1. The materials of the tool play important role in the directions of the magnetic lines emerging from the magnets. As in the present developed in-situ MRH tool, all the materials of the tool's supporting parts are of stainless steel, so the orientation of the magnetic-lines emerging out from the magnets in this tool is shown in Fig. 4.16. It can be observed that all the magnetic-lines are emerging in the outward radial direction from the curved surface of the in-situ MRH tool's magnets. The sides of the magnet holding racks resist the magnetic lines to transmit from its face because of its non-ferromagnetic (stainless-steel) material.

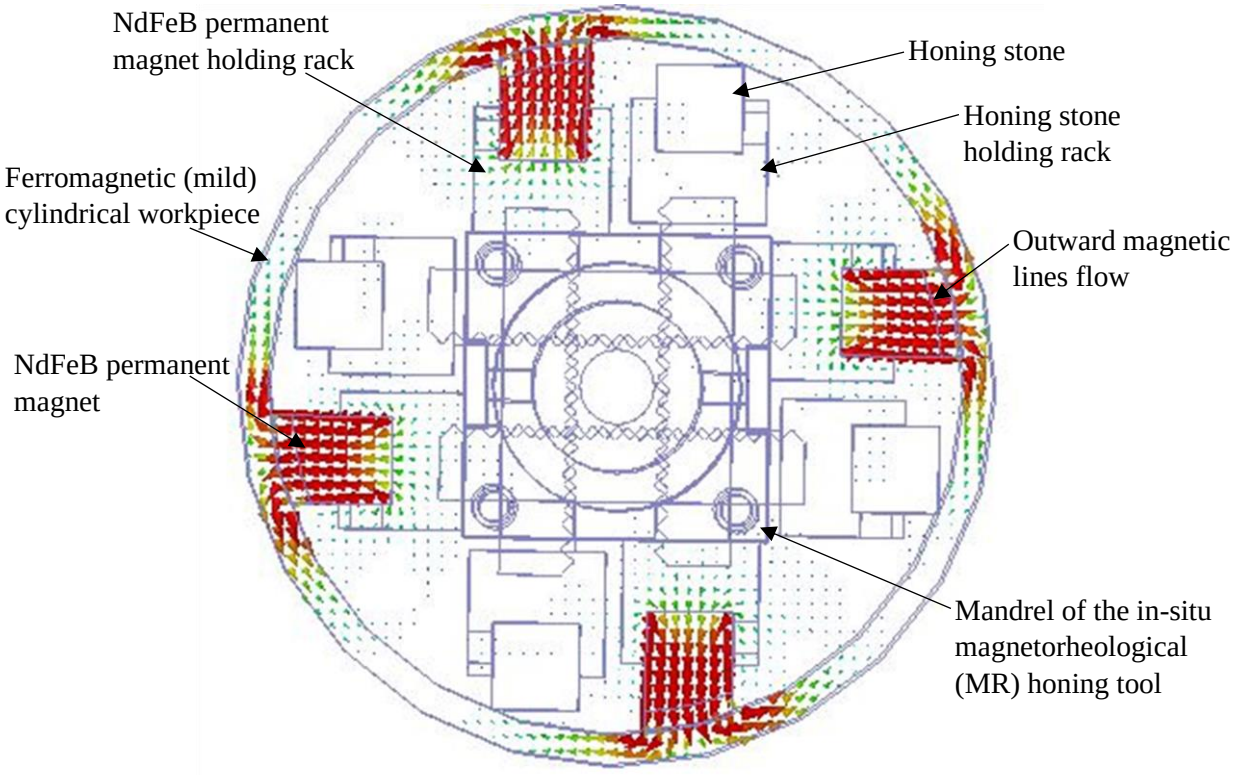

Fig. 4.16 Magnetic vector representation of the magnetic flow lines in the in-situ magnetorheological honing tool in the presence of MRP fluid and the ferromagnetic mild-steel cylindric workpiece.

Therefore, the whole magnetic lines are managed to emerge out from the curved face of the permanent magnets. The radially outward magnetic-lines from the curved end surface of the magnets cause the active abrasive particles to apply the normal magnetic forces on the inside surface of the cylindrical workpiece through the EIPs of the MRP fluid (Paswan et al., 2017). Therefore, these directions of the magnetic lines are found beneficial for applying the magnetic normal force on the inner finishing surface of the cylindrical workpiece which can result in a

better finishing action. Thus, the proposed design of the in-situ MRH tool can be found effective to perform MR finishing on the inner cylindrical surface after completing traditional honing on it.

4.2.2 Computer aided design (CAD) model of the components of the in-situ MRH tool

Based on the magnetostatic simulation results and the distribution of magnetic field analyzed in the working gap between the end curve surface of the magnet and inner surface of the workpiece cylinder, on the curved end surface of the permanent magnet, and along the height of the permanent magnet of the in-situ MRH tool, the proposed tool is accepted for the fabrication. Therefore, fabrication of each component of this tool needs the computer aided design (CAD) model for easy interpretation of the drawing and providing the dimensional specification.

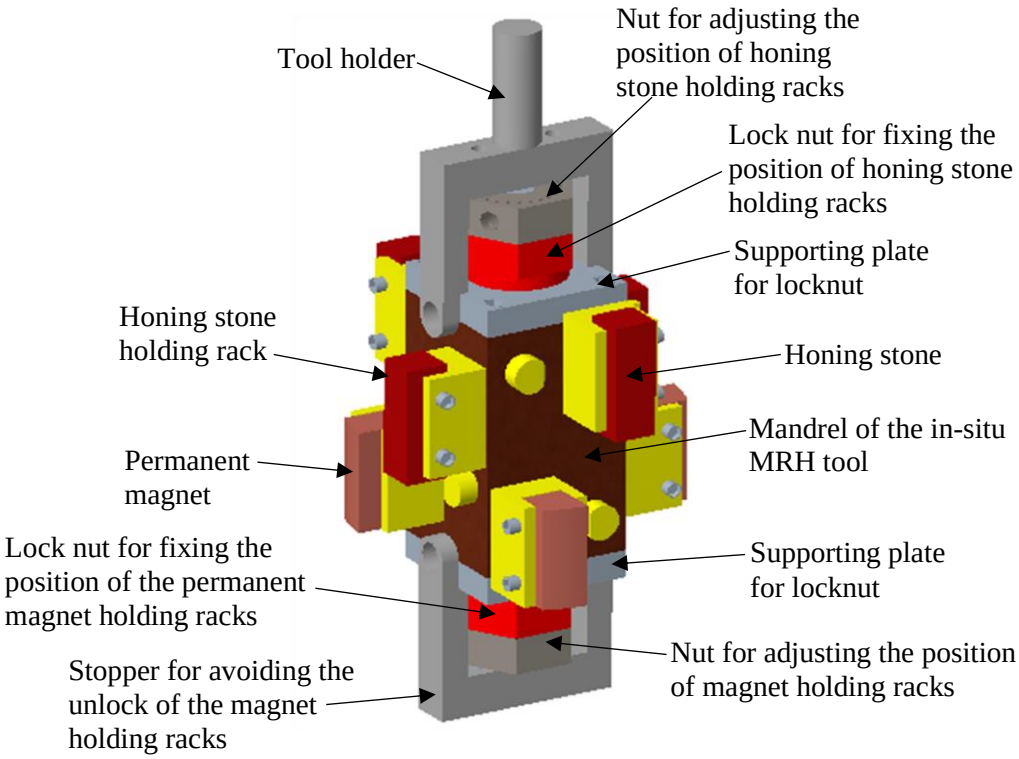

Fig. 4.17 Three-dimensional CAD model of the in-situ magnetorheological honing tool.

The 3-dimensional CAD model of the in-situ MRH tool is as shown in Fig. 4.17. While creating the CAD model of each component of the in-situ honing tool, all dimensions of have been taken in millimetre (mm). The components of the in-situ MRH tool such as splines shaft, racks for holding the honing stones and magnets, mandrel, locknut, supporting plate for locknut, nut for adjusting the position of the racks, stopper for avoiding the unlocking of rack position, and

tool holder, fine SiC grits bonded honing stone, trapezoidal shaped NdFeB permanent magnet with radial shape of end surface. The detailed design of these components of the in-situ MRH tool is given below.

4.2.2.1 Mandrel of the in-situ honing tool

The mandrel is one of the important components of this tool. This component provides support to every component of the in-situ honing tool. Externally it is a rectangular block in which a circular blind hole is made from both longitudinal sides as shown in a 3-D CAD model Fig. 4.18(a). In the blind circular hole of the mandrel spline shaft of the tool is placed with support of the locknut and supporting plate.

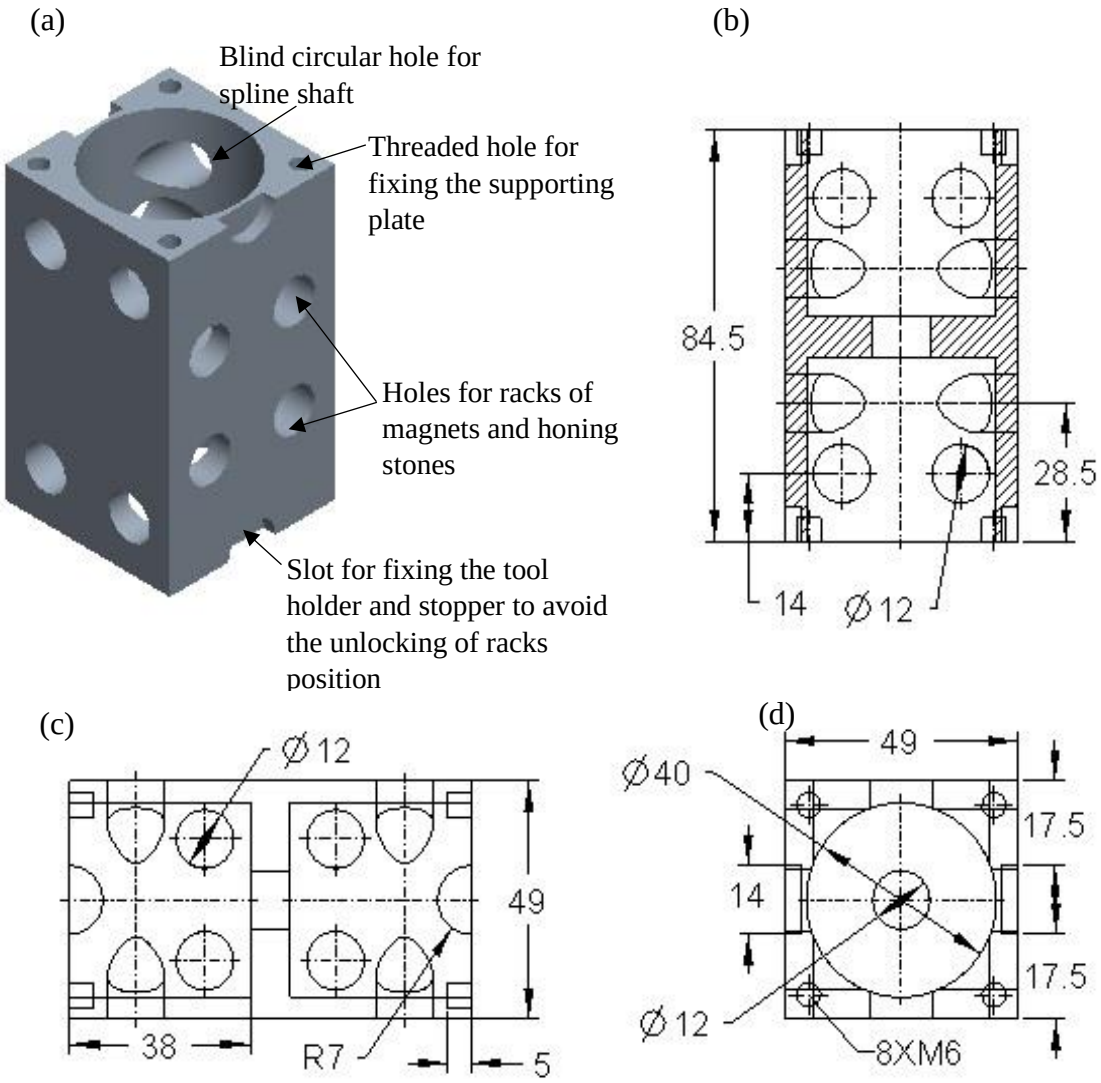

Fig. 4.18 (a) 3-D view, (b) sectional front view, (c) projected side view, and (d) projected top view of the CAD model of mandrel for its fabrication.

Through the holes on the the ractangular side faces, the racks are translated for adjusting the position of honing stones and magnet. For fabricating this mandrel, the dimensional specifications provided in Fig. 4.18 (b), (c) and (d) is utilized. Figure 4.18(b), (c) and (d) represents the front view, projected side, and top view of the 3-D CAD model of mandrel respectively (Fig. 4.18 (a)).

4.2.2.2 Spline shaft of the in-situ honing tool

The spline shaft is the drive shaft over which there are equally spaced ridges or teeth. These teeth mesh with the groove of the racks of the in-situ honing tool. By providing rotational motion to the spline shaft, the racks meshed with it performs the translation motion.

Table 4.2 Parameters used for CAD model of the spline shaft of the in-situ honing tool.

Parameters	Value	Parameter	Value
Module	1.25	No. of teeth	12
Pitch (mm)	3.93	Pressure angle (deg.)	30°
Pitch circle diameter (mm)	15	Base circle diameter (mm)	13

The CAD model of the spline shaft is created considering the compactness and objective of this tool. The dimensional specification of the spline shaft is explained by the orthographic views of spline shaft as shown in Fig. 4.19 (a) and (b). Figure 4.19 (c) shows the 3-D CAD model of the spline shaft through which gives an idea about the shape of this component while fabricating. Further, the basic parameters which are used for creating the teeth in the spline are as reported in Table 4.2. The circular slot in the spline shaft is given for attaching it with nut which adjusts the diametric position of the honing stones and the permanent magnet by rotating. Using the dimensional detail and parametric detail of teeth of the spline, it is fabricated on the high precision CNC machine.

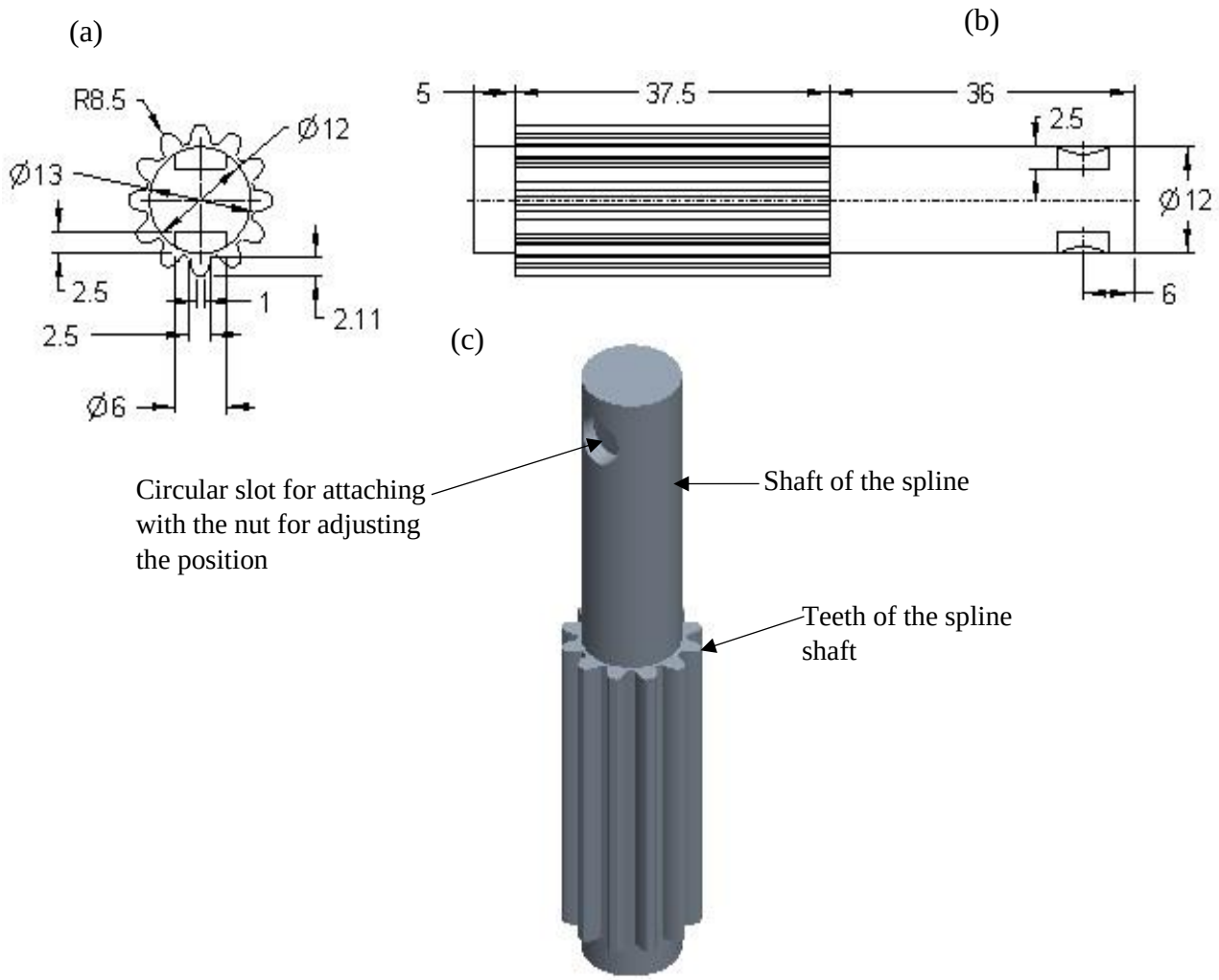

Fig. 4.19 (a) Top view, (b) side view, and (c) 3-D view of the CAD model of spline shaft for its fabrication.

4.2.2.3 Rack of the in-situ magnetorheological honing tool

The racks are used in the in-situ magnetorheological honing (MRH) tool for holding and translating the honing stones and the permanent magnets of this tool. This component is translated by rotating the nut attached with the spline shaft for adjusting the diametric position of the honing stones and permanent magnets for performing the finishing. The rack is featured with a rectangular wedge in which there is slot for holding a permanent magnet or a honing stone. In the shaft of the rack, the spline teeth mating threads have been crated with the help of the parametric Table 4.2. With the help of these threads of the rack, it is indexed with the spline shaft in the assembled in-situ honing tool. With the rotational motion of the nut attached with spline shaft, the rack is given translational motion. The rack is fabricated with the help of 3-D CAD model as shown in Fig. 4.20 (a) which gives an idea about the shape of this component. The exact dimensions of this components are obtained from the orthographic views i.e., top

view, side view and front view of its CAD model in Fig. 4.20 (b), (c) and (d) respectively for its fabrication.

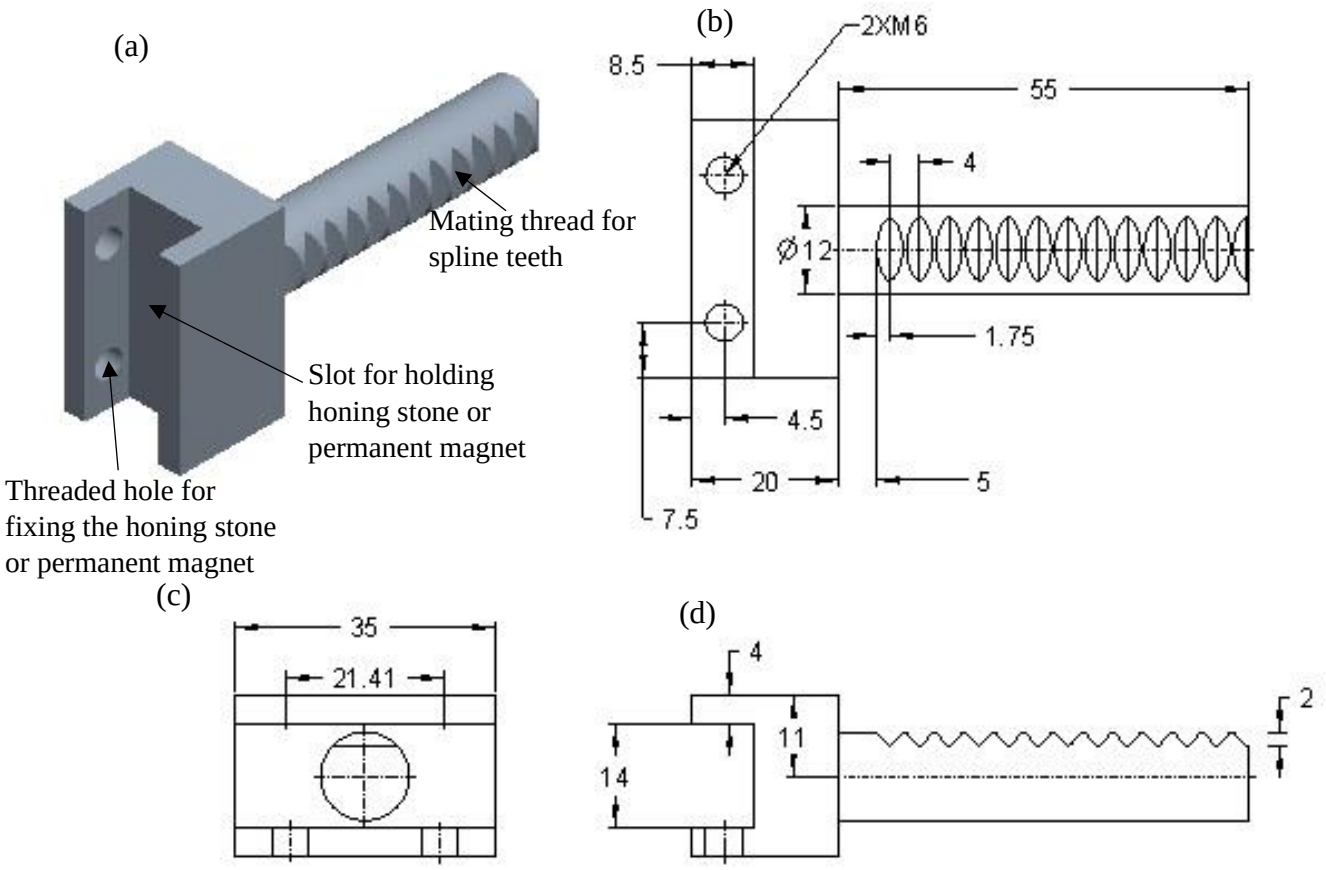

Fig. 4.20 (a) 3-D view, (b) top view, (c) side view, and (d) front view of the CAD model of a rack for holding and translating the honing stones and the permanent magnets of the in-situ MRH tool.

4.2.2.4 Supporting plate of lock nut of the in-situ honing tool

The supporting plate is used for fixing the locknut with the main body (mandrel) of the tool. The spline shaft is attached with the nut by crossing the locknut as shown in Fig. 4.21 which shows the sub-assembled 3-D CAD model of nut, locknut and supporting plate for locknut. The supporting plate attached with mandrel acts like a unibody in which the spline shaft can be rotated using nut and fixed in the locknut. The supporting plate is fabricated with the help of 3-D CAD model and its orthographic views as shown in Fig. 4.22. The dimensional specification and a 3-D CAD model of the cover plate is shown in Fig. 4.22. With the help of 4 holes made in the top face of the supporting plate, it is fixed with mandrel. Whereas two holes in its longitudinal face the locknut is made attached. The holding shaft of the spline is passed through the centre hole of the supporting plate as shown in Fig. 4.22 (a).

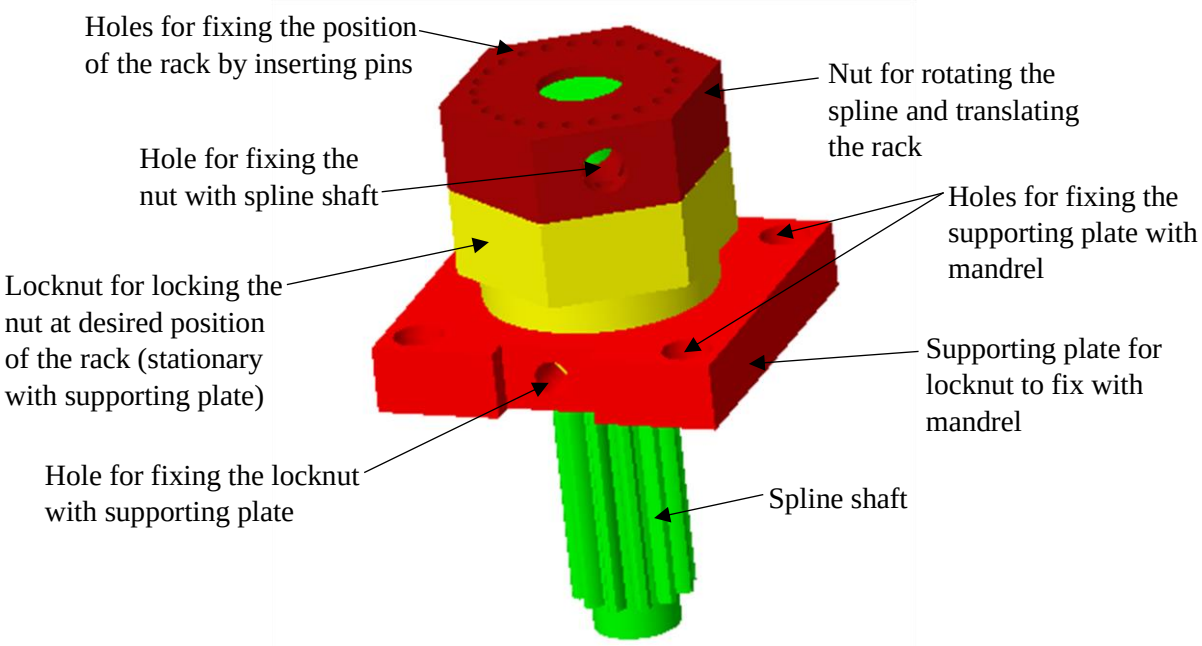

Fig. 4.21 3-D CAD model of the sub-assembled nut, locknut and supporting plate of the in-situ MRH tool.

Figures 4.22(b)-(d) show the detailed dimensional specification of the locknut supporting plate. Therefore, using the information related to the shape and dimensional specification of this plate from Fig. 4.22, the locknut supporting plate is fabricated.

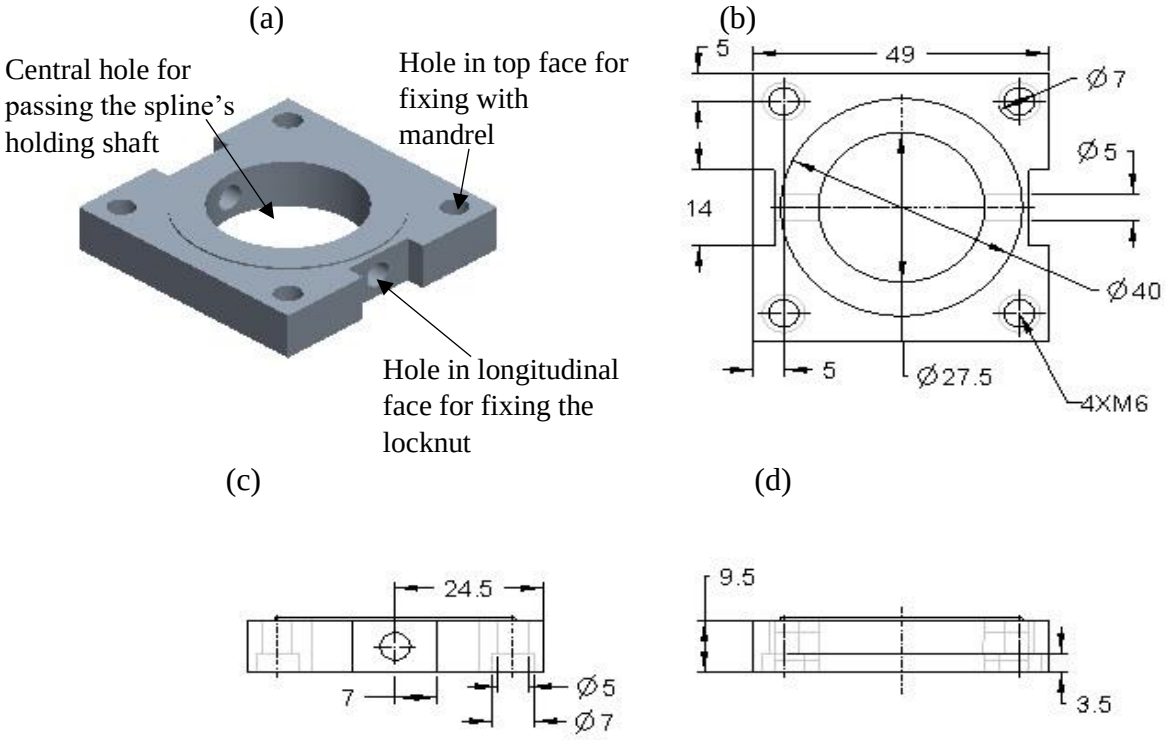

Fig. 4.22 (a) 3-D view, (b) top view, (c) side view, and (d) front view of the CAD model of locknut supporting plate of the in-situ MRH tool.

4.2.2.5 Locknut of the in-situ honing tool

The locknut of the in-situ MRH tool is a component which is used to lock the diametric position of the honing stones or magnet holding racks. This is fixed in the mandrel through supporting plate. This component has 25 small holes of diameter 2.5 mm in its top face as shown in Fig. 4.23 (a). These holes are used for locking the undesired rotation of the spline by inserting the pins in it crossing the nut of the tool. One side of the locknut is inserted into the supporting plate and fixed using a screw nut. On its other side, the nut attached with the spline is assembled. This component is fabricated based on the shape and dimensional detail as shown in Fig. 4.23. Figure 4.23(a) shows the 3-D CAD model of the locknut. Also, the top view, side view, and front view are shown in Fig. 4.23 (b), (c) and (d) respectively for providing the detailed dimensional information.

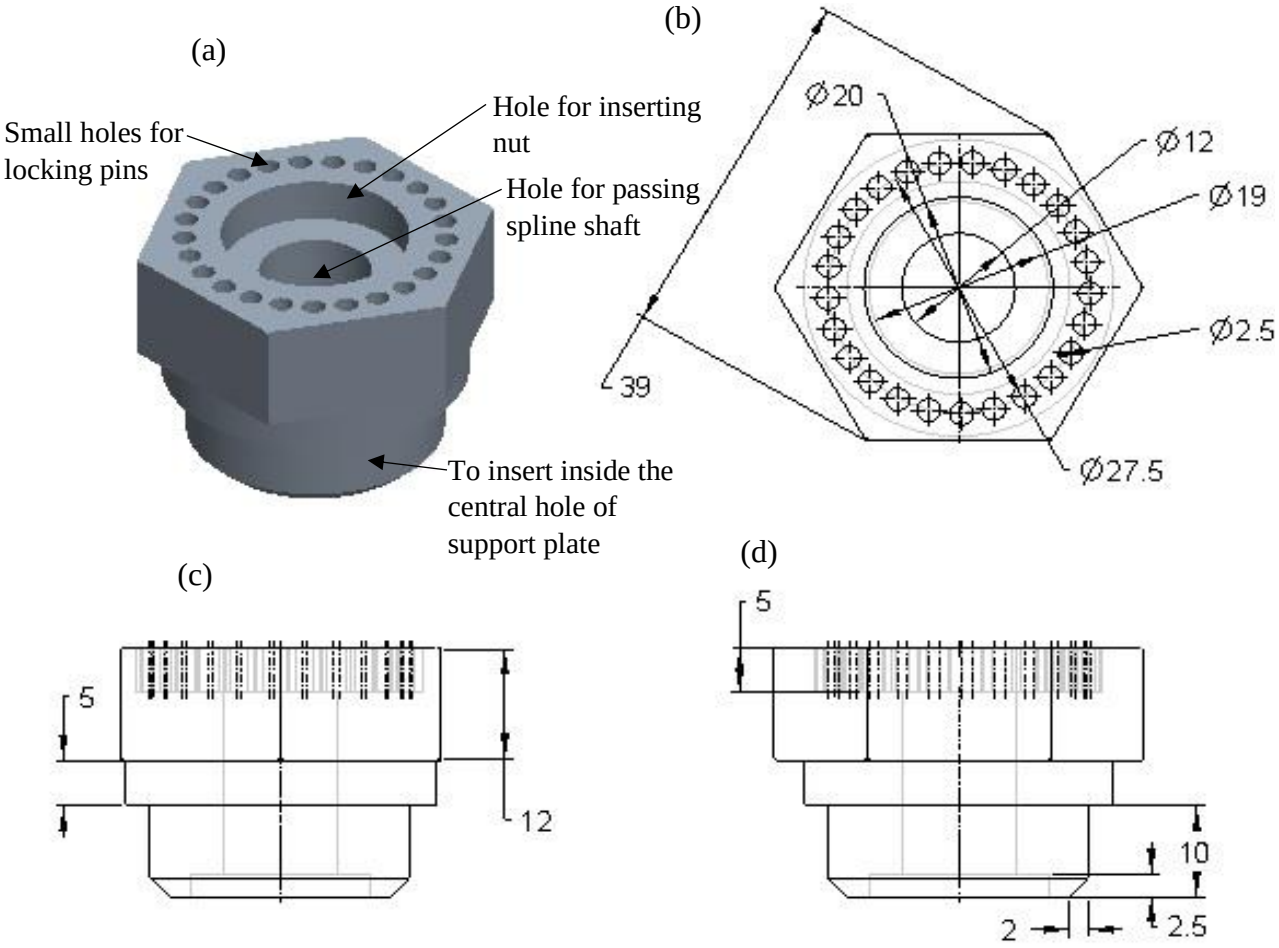

Fig. 4.23 (a) 3-D view, (b) top view, (c) side view, and (d) front view of the 3-D CAD model of locknut.

4.2.2.6 Nut for translating the racks of the in-situ honing tool

The nut of the in-situ MRH tool is used for translating the racks of the tool by rotating the spline attached with it. The 3-D CAD model of this component is made to easily understand its shape which is as shown in Fig. 4.24(a). This nut is a feature with extruded cylindrical feature with a hole for inserting spline. The extrusion cylindrical part of this component fits into the locknut. On its longitudinal surface, there are two threaded holes made for fixing the inserted spline shaft with the set screws. Also, on its top face, there are 25 small holes of diameter 2.5 mm are generated. These holes are inserted with pins upto the locknut to restrain further rotational motion of the nut so that racks could be locked at the respective diametric position. Figure 4.24 (a) shows the 3-D CAD model of this lock whereas Figs. 4.24 (b), and (c) show the top view, and projected front view of the CAD model of nut respectively.

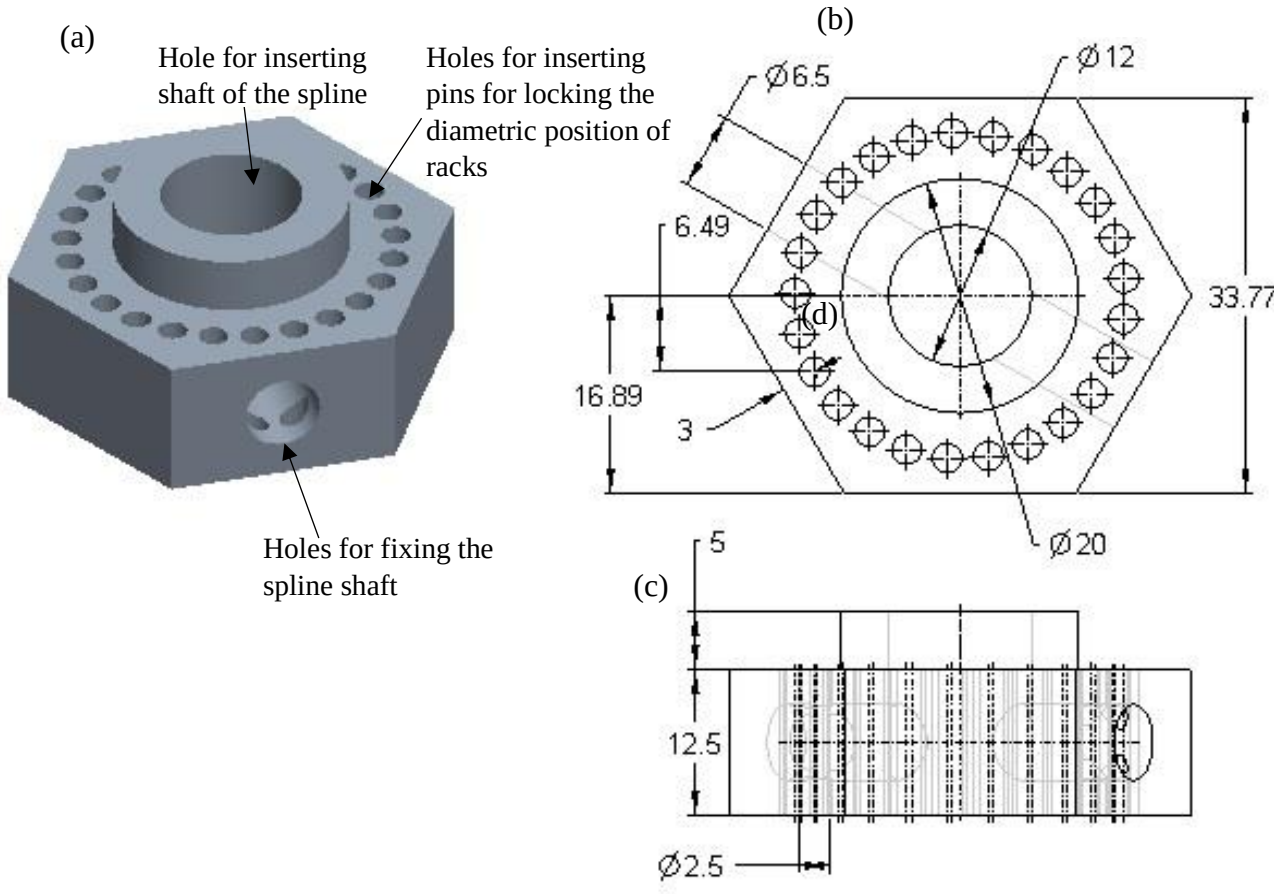

Fig. 4.24 (a) 3-D view, (b) top view, (c) projected front view of the CAD model of nut for rotating the spline in the in-situ MRH tool.

4.2.2.7 Tool holder for holding the tool with the finishing setup

Tool holder is used to hold the in-situ MRH tool with the rotational magnetorheological honing setup for performing the finishing operation. The 3-D CAD model of this components is shown

by the Fig. 4.25 (a). This tool holder is also provided two threaded holes beside the holding shaft. Through this hole, the axial motion of the nut is made restrained using set screws. Therefore, the nut's rotational and axial motions are made restrained for locking the racks. Figures 4.25 (b), (c), and (d) depict the top view, side view, and front view respectively of the CAD model made for this component in Fig. 4.25(a). The detailed dimensional specifications of this component are given in these orthographic views. Using the information provided in Fig. 4.25, the tool holder is fabricated.

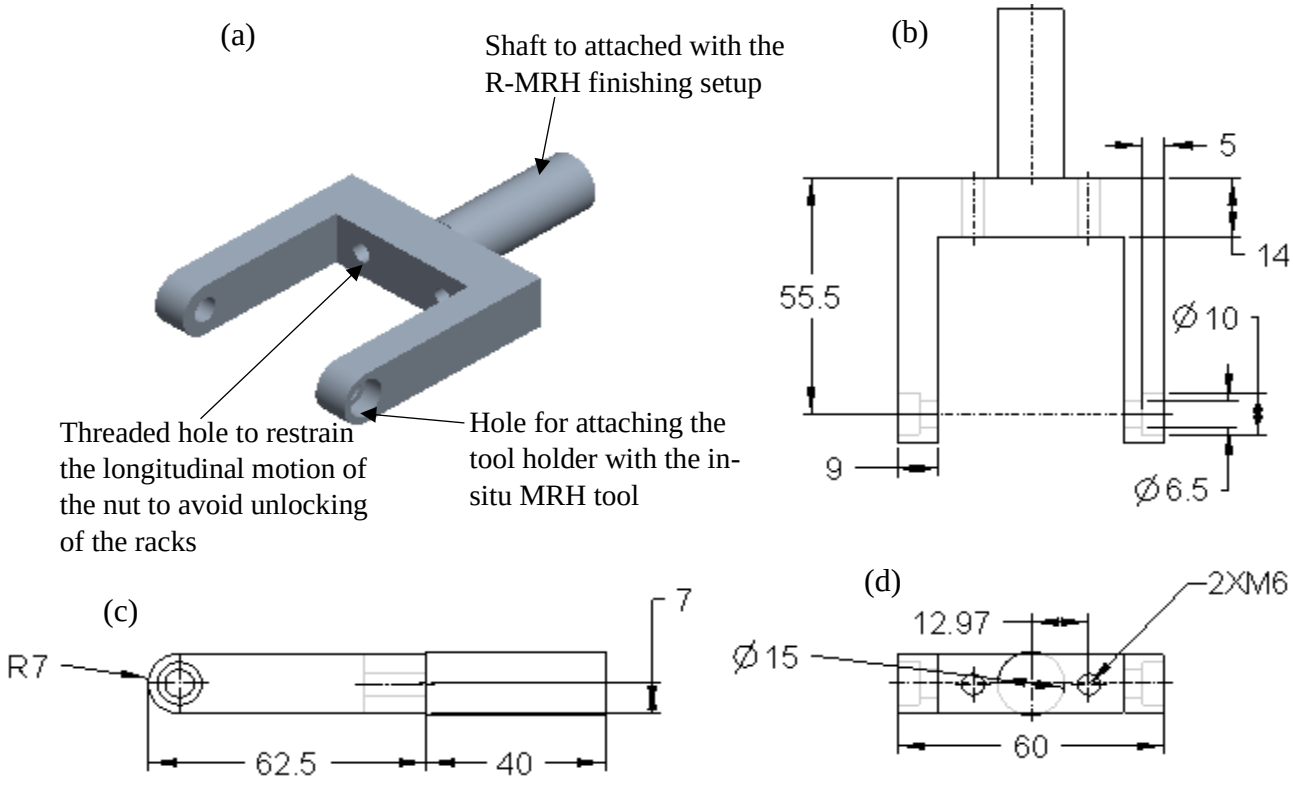

Fig. 4.25 (a) 3-D view, (b) top view, (c) side view, and (d) front view of the CAD model of tool holder.

4.2.2.8 Permanent magnet of the in-situ honing tool

Permanent magnet is the most important component used in the in-situ magnetorheological honing (MRH) tool for performing the magnetorheological honing using this tool. Since the in-situ MRH tool uses a spline rolling rack mechanism to change the diametric location of the magnets and honing stones with a broad range of variable diameters. Owing to the roller rack mechanism, the magnets of this tool is adjusted to a radially offset position. Therefore, in order to maintain a uniform gap between the permanent magnets of the tool and the internal surface of the tubular workpiece for achieving uniform finishing, the shape of the magnets of the

present in-situ MRH tool is designed as a combination of the trapezoidal and the curved magnets (irregular) as shown in Fig. 4.26 (a). To investigate the capability of the in-situ honing tool with the magnets of such shape to induce sufficient magnetic field for performing the magnetorheological honing process, it has been already successfully demonstrated with the magnetostatic finite element analysis results (Figs. 4.13 - 4.16). The CAD model and dimensional specification of the finalized permanent magnet are shown in Fig. 4.26. The shape of the permanent magnet is visualized with the 3-D CAD model as shown in Fig. 4.26 (a). Whereas, the dimensional detail of the magnet is provided through the top view, side view and front view of the CAD model as shown in Fig. 4.26 (b), (c), and (d) respectively. The permanent magnet is fabricated of NdFeB magnet.

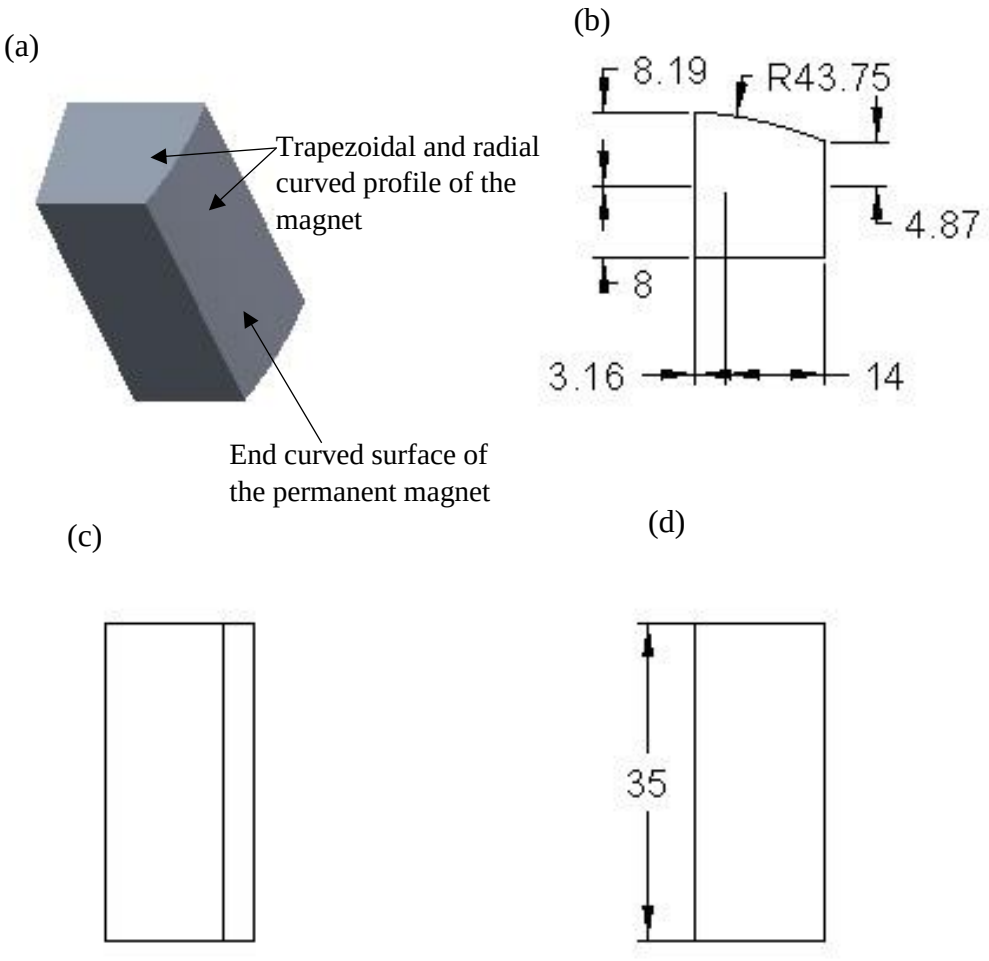

Fig. 4.26 (a) 3-D view, (b) top view, (c) side view, and (d) front view of the CAD model of the trapezoidal permanent magnet.

Using the CAD model of the commercially available components like honing stones, set screws

etc., and the CAD model of the components to be fabricated (Figs. 4.18 - 4.26), the in-situ honing tool is assembled in the form of complete tool. While designing, each component of the tool is designed to show the complete picture of the in-situ honing tool. Hence, the exploded view of the assembled in-situ honing tool is shown in Fig. 4.27. The bill of material of these components is also represented in this figure (Fig. 4.27) using serial number.

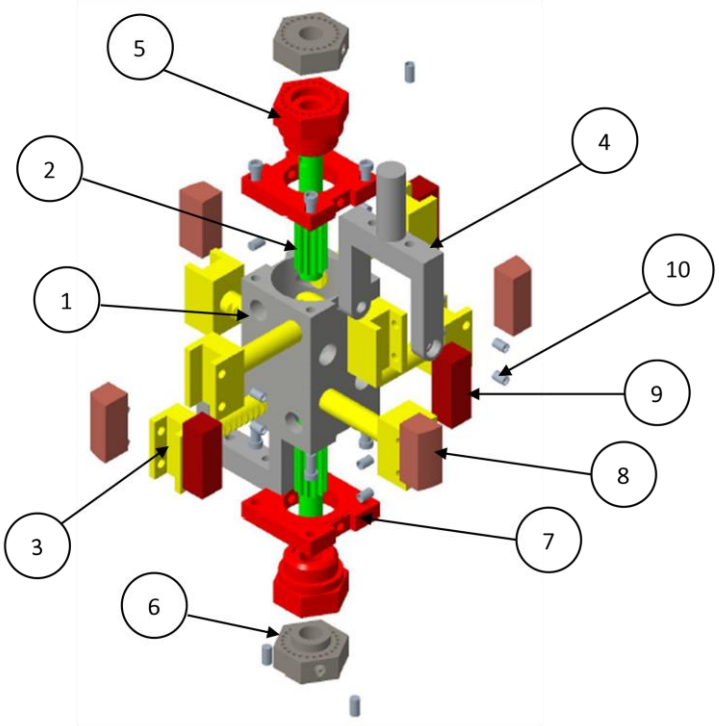

Bill of materials		
Sl. No.	Part name	Quantity
1	Mandrel	1
2	Spline shaft	2
3	Rack	8
4	Tool holder	2
5	Locknut	2
6	Nut	2
7	Locknut supporting plate	2
8	Permanent magnet	4
9	Honing stone	4
10	Set screws (M6)	40

Fig. 4.27 Exploded 3-D CAD model of the in-situ honing tool along with the bill of materials.

4.2.3 Fabrication of the in-situ magnetorheological honing tool

Based on the variation in magnetic field distribution at different positions and analysis of magnetic lines as discussed in Figs. 4.13 - 4.16, the design of the present in-situ honing tool has been finalized for fabrication. Then, for the finalized design of the in-situ honing tool, the detailed dimensions through the CAD model of each component (Figs. 4.18 - 4.26) are drawn. Further, with the help of these drawings, the present in-situ honing tool has been fabricated as shown in Fig. 4.28. For precisely fabricating the finalized tool design, the relevant machining processes are utilized with computer numerical control (CNC) machines. The present developed in-situ honing tool is also intended for performing the traditional honing. Therefore, to make this tool more robust to bear a high pressure without wearing the spline shaft and teeth of the racks, the proposed tool's assembling parts other than the magnets are made of non-magnetic stainless-steel material. Also, the use of the stainless-steel material makes it easier

for handling while assembling and dismantling the high magnetized NdFeB permanent magnets used in this tool. Therefore, selecting stainless-steel for a tool assembly other than the magnets in the present in-situ MRH tool is found beneficial for the effectiveness of this tool.

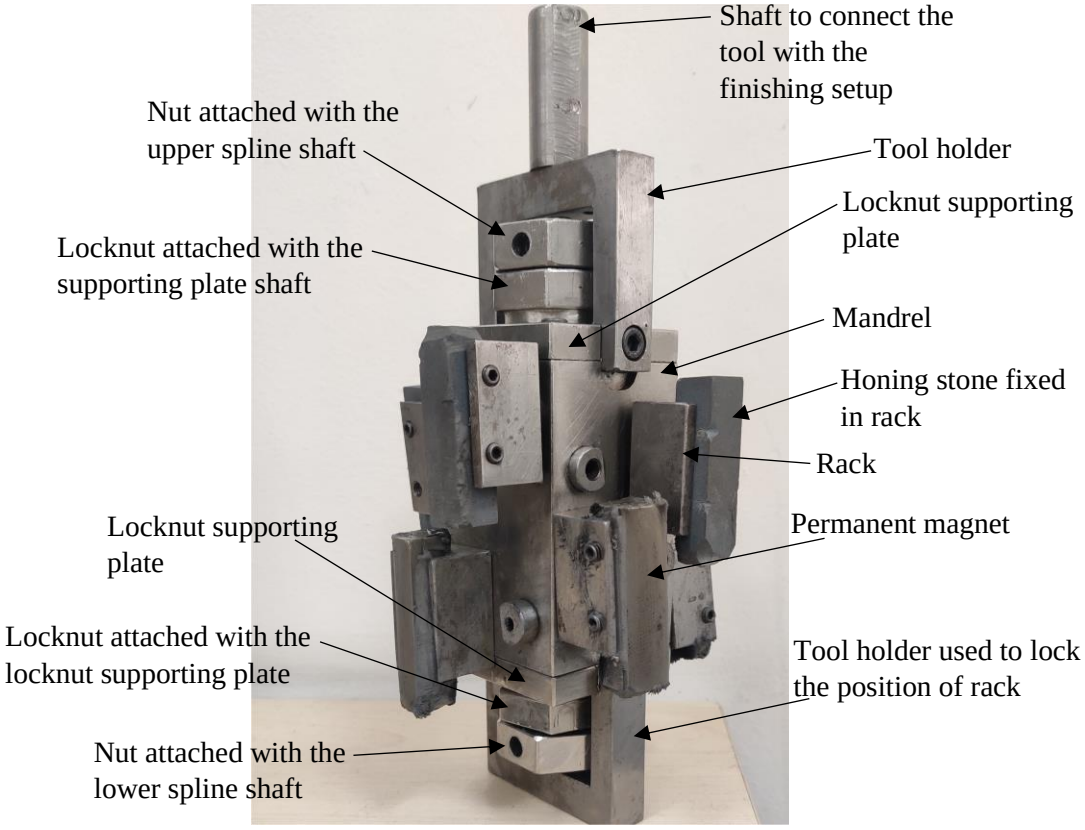

Fig. 4.28 Photograph of the fabricated in-situ magnetorheological (MR) honing tool.

The established experimental-setup with the novel developed in-situ magnetorheological honing (MRH) tool for finishing the interior surface of cylindrical workpieces is demonstrated in Fig. 4.29. This experimental setup is used for conducting the experimentation on the internal surface of the cylindrical workpieces to achieve good dimensional-accuracy, minimized tolerance, high surface finish quality i.e., surface roughness and waviness. This results in an improvement in functional performance with high productivity. The fabricated in-situ MRH tool is attached to a C-shaped bracket through the Z-axis horizontal-slide of the experimental setup. The rotating and reciprocating motions of the tool are governed by servo motors through servo-drives with the help of a programmable logic controller (PLC). The workpiece cylinder is attached with an aluminium-cylindrical fixture which is fixed with a coupling. The coupling is fixed on the height-adjusting fixture as seen in Fig. 4.29. The machine controls the different motions using the PLC program fed through the computer interface. For performing the traditional honing, four fine-grits silicon carbide (SiC) abrasive bonded honing stones are

employed in the in-situ MRH tool. However, for the MRH, this tool uses four trapezoidal curved shape permanent NdFeB magnets.

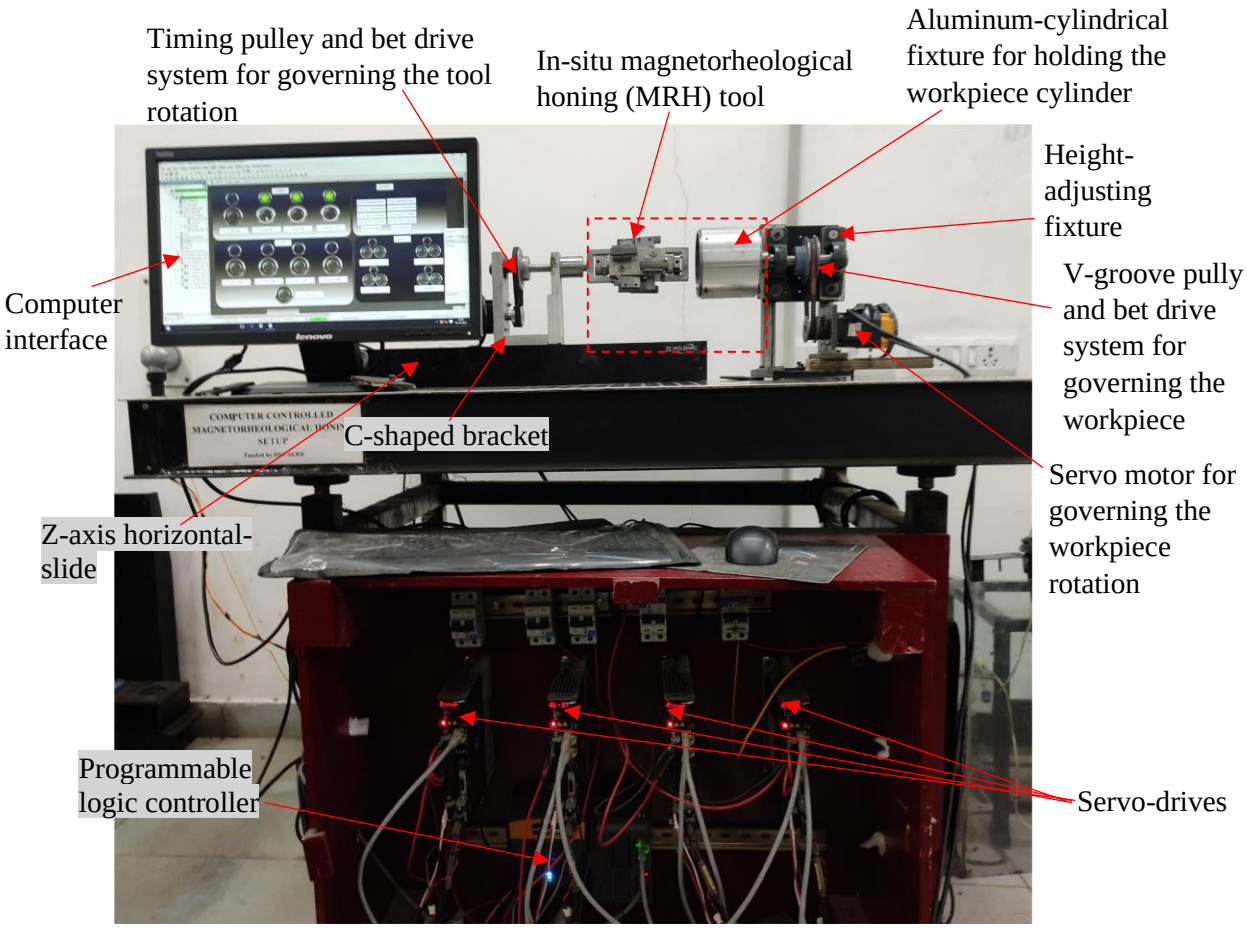

Fig. 4.29 Photograph of the experimental setup used for finishing the internal cylindric surface of the work-parts through the novel designed in-situ magnetorheological (MR) honing tool.

The magnetorheological polishing (MRP) fluid utilized as a finishing mean over the end surface of the four magnets gets stiffened there due to its magnetic behaviour. For the initial surface generation, the in-situ MRH tool is enabled to rotate and reciprocate within the oppositely rotating workpiece cylinder by making honing stones in firm contact with the workpiece's finishing surface. Similarly, after initial surface generation through traditional honing, the same tool performs MRH process at the same setup over the initial honed surface for achieving their fine finished surface. Thus, the presently designed single in-situ MRH tool is found beneficial to achieve fine finishing from the machined cylindrical surface using the traditional honing and MRH process at a single setup. This results in wide usefulness of the present designed in-situ MRH tool along the R-MRH with a higher productivity as compared to the different tools and setups.

During the MR honing process, the permanent magnets are used as a source of the magnetic field and the working gap plays an important role to control the intensity of the magnetic field which further controls the rigidity of MRP fluid and finishing performance. Therefore, in the present work, the working gap is adjusted through a spline rolling rack mechanism of the in-situ MRH tool where the spline shaft of the tool gets rotated with the rotation of the connecting nut. This results in the translational motion of magnets along with the translation motion of the racks (Fig. 4.11). Thus, the working gap in this work is maintained through the translational distance of the rack (D_t) and angular distance of the nut connected to the spline shaft (θ_s) which is given in Eq. (4.1).

$$D_t = \left(\frac{\pi D_s}{360}\right) \times \theta_s \tag{4.1}$$

Where, D_s is the major diameter of the spline shaft. Therefore, for maintaining a particular gap between the magnets and inside surface of the tubular workpiece, first of all, the racks of the magnets are translated outward up to contacting the inner surface of the tubular workpiece by rotating the spline shaft through the connecting nut. Then, using the relation in Eq. (4.1), corresponding to the value of the working gap, the angular distance is calculated. Carefully angle is marked on the locknut and then the nut is rotated precisely to achieve accurate angular distance corresponding to the given working gap so that racks translated in an inward direction. After achieving the exact marked angular position on the locknut, the nut is locked with locknut inserting the lock pin in the matching holes of the nut and locknut. Thus, a particular working gap gets maintained with the translational motion of magnets along with racks while rotating the spline shaft through the connecting nut for a particular angle in the in-situ MR finishing process.

4.2.4 Advantages of the in-situ MR honing tool

With the development of the in-situ honing tool, the following advantages have been achieved while finishing the internal surface of the ferromagnetic or non-ferromagnetic cylindrical workpieces.

- The in-situ honing tool can perform fine finishing from the initial machined surface using the conventional honing to final magnetorheological (MR) finished using the magnetorheological honing process on a single finishing setup.
- The finishing capability of this tool from the initial machined surface to finely MR honed surface enables this tool to be applicable on a wide range of industrial

applications to finish their inner cylindric surface with a high finishing performance.

- The permanent magnet used in this tool with the capability to produce a high magnetic field which results in high finishing capability.
- This tool is found advantageous for finishing the machined surface to achieve the fine-finishing at a single in-situ RMRH setup in terms of less time consumption, less power consumptions, etc., by avoiding multiple setups from initial surface generation to final fine finished surface.
- This tool has enough flexibility to be used independently either for the traditional honing or R-MRH process on initially generated surface.
- The working mechanism of this tool makes it easy for maintaining the proper gap between the end surface of the permanent magnet and the inner surface of the workpiece cylinder.
- Due to the spline rolling rack mechanism utilized in this tool, it is found useful for a great diametric range i.e., 90 mm to 140 mm to finish the inside cylindrical surfaces.
- The diametric range of applicability of this tool allows it to be commercially useful for finishing high diametric ranged components such as outer bearing raceways used in heavy machineries, spindle housings, oil pipes, sanitary pipes in food industries, cylindrical molds, etc.

4.2.5 Material removal mechanism in internal surface finishing using in-situ honing tool

As the present developed in-situ MRH tool is a novel magnetorheological (MR) finishing tool, therefore, understanding the material removal mechanism while performing the finishing operation with this tool becomes an important task. Therefore, in this section, the material removal mechanism is studied for the initial surface generation through the traditional honing and fine finishing with the present developed in-situ MRH tool.

4.2.5.1 Mechanism of initial surface generation through the traditional honing using the in-situ magnetorheological (MR) honing tool

In this work, the initial surface of the cylindric workpiece is generated by performing the traditional honing using the in-situ honing tool. The honing stones used in this tool for performing the traditional honing are made up of fine grits silicon carbide (SiC). To understand the role of the motions of the in-situ MRH tool and the cylindrical workpiece on the abrasion of the material with traditional honing, the analysis of the finishing mechanism is performed

as shown in Fig. 4.30. For generating the initial internal surface of the cylindrical workpiece, the in-situ MRH tool is rotated and reciprocated simultaneously inside the workpiece cylinder as shown in Fig. 4.30(a). The abrasive grits of the honing stones firmly contacting the finishing inside surface of the cylindrical workpiece undergo two-body abrasion (Rabinowicz *et* al., 1961). Due to the direct interaction of the rigidly fixed abrasive grits with the finishing surface of the workpiece, these grits transmit finishing forces directly to the workpiece's finishing surface. The firm contact of the honing stones with the finishing surface results in an application of a normal force (F_{tr_n}) on it through the honing stones. Owing to this F_{tr_n}, the grits of the honing stones get inserted into the gap between the asperities over the finishing surface as depicted in Fig. 4.30(b). When the rotational motions of the in-situ MRH tool and the cylindrical workpiece, and the to-and-fro motion of the tool are performed, the interacted abrasive grits apply shear forces in the form of tangential force (F_{tr_tn}) and axial force (F_{tr_ax}) as shown in Figs. 4.30(c) and (d). The simultaneously rotational and reciprocation motion of the honing stones cause the acting of total cutting shear force (F_{tr_cut}). The total cutting force is related to the tangential and axial shear force as given in Eq. (4.2).

$$F_{tr\_cut} = \sqrt{{F_{tr\_tn}}^2 + {F_{tr\_ax}}^2} \tag{4.2}$$

As the abrasive grits inserted in between the roughness peaks caused by normal force (F_{tr_n}) and apply the F_{tr_cut} shear force, the ploughing action may take place on finishing surface. Due to which the material abrasion during the traditional honing takes place with a higher material removal rate. Also, the new roughness peaks are generated due to the material of the side of the ploughed region. When the in-situ MRH tool performs axial motion (in-stroke) during traditional honing, an abrasive grit of the honing stone interacting with a roughness peak tends to deform it along its translational motion direction as shown in Fig. 4.30(c). However, during its returning stroke (out-stroke), the same roughness peak experiences deformation in the counter-direction due to the axial shear force from the interacting abrasive grit of the honing stone as shown in Fig. 4.30(d). Therefore, the continuous change in a direction tending to deform the roughness peaks from in-stroke to out-stroke direction by the abrasive grits of the honing stone and the concurrent rotational motion of the in-situ MRH tool and cylindrical workpiece, cause the roughness peaks to get abraded from the workpiece surface. This results in the generation of the initial surface over the inner surface of the cylindrical workpieces for further MRH process using the same in-situ MRH tool on the same setup.

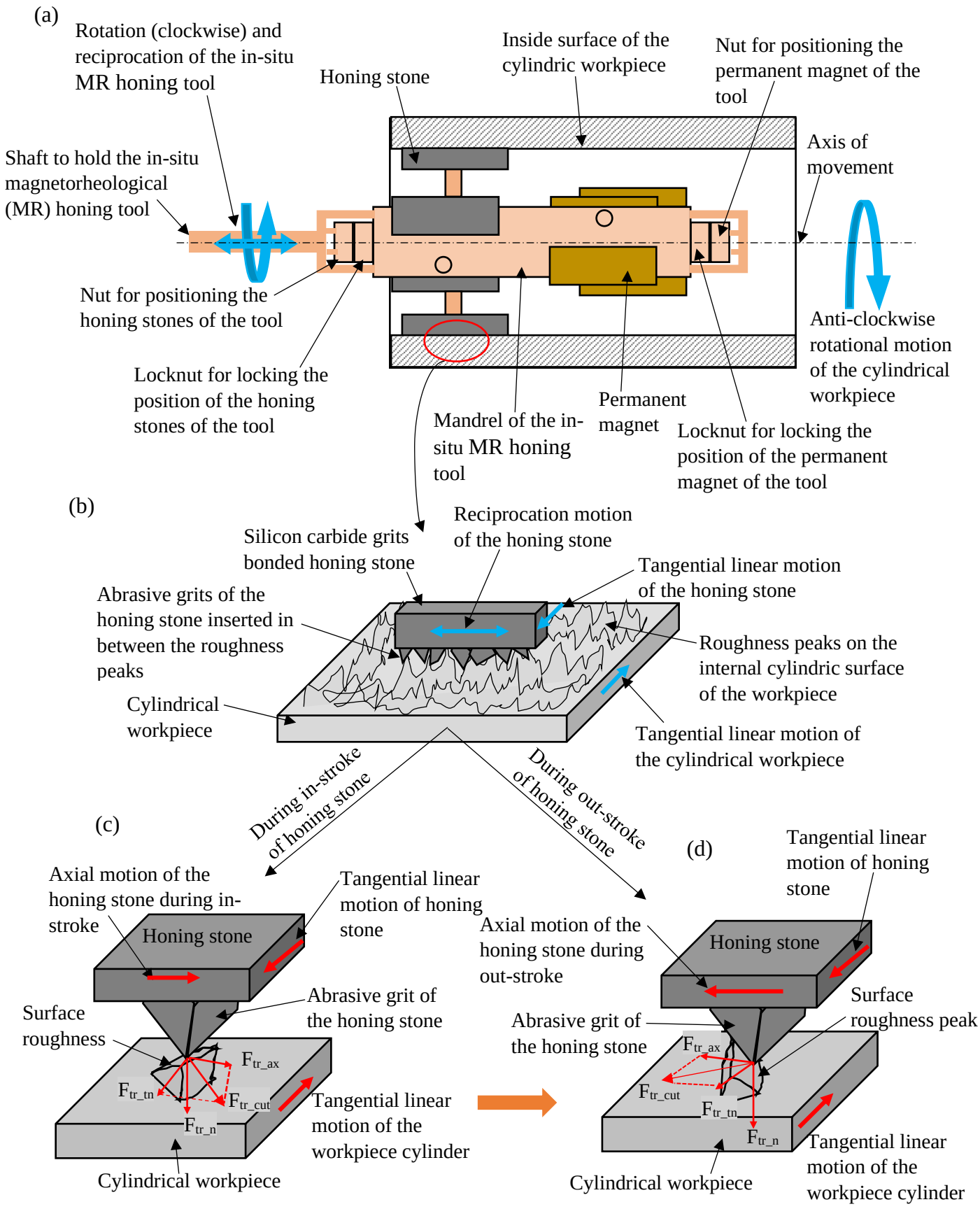

Fig. 4.30 (a) Schematic image of initial surface generation in traditional honing on the inner surface the cylindric workpiece using in-situ honing tool, (b) magnified view of contact between the honing stone and workpiece surface roughness during material abrasion mechanism (c) while in-stroke of the tool, and (d) out-stroke of the tool.

4.2.5.2 Mechanism of material abrasion in magnetorheological honing process using the in-situ magnetorheological (MR) honing tool

The motions involved in the magnetorheological (MR) honing process in this work are also the same as the motions performed while conducting the traditional honing as displayed in Fig. 4.31(a). Therefore, material abrasion which causes the finishing action on the internal surface of the cylindrical workpieces also takes place during MRH using the in-situ MRH tool. In this work, magnetorheological (MR) honing is used for further fine-finishing the interior cylindrical workpieces surface. The freely suspended non-magnetic SiC abrasives in the MRP fluid perform finishing operation under their stiffness caused by magnetic particles of the fluid due to the induced magnetic field of the permanent magnet of the in-situ MRH tool. Therefore, the abrasion of the materials from the workpiece finishing surface takes place through the three-body abrasion mechanism (Rabinowicz *et* al., 1961). As the magnitude of the wear rate of materials in the case of three-body abrasion is lower than the wear rate of material in two-body abrasion (Rabinowicz *et* al., 1961) therefore, the finishing rate of the traditional honing is larger than the finishing rate of MRH. Although, the finishing quality in the MRH is found much better than the finishing in the traditional honing. In three-body abrasion, the freely suspended micron-sized abrasive particles of the MRP fluid abrade the materials with a lower rate but produces a higher level of surface texture. This happens because the stiffened abrasive particles abrade the roughness peaks in the micro-chip form in an incremental step with consistent abrasion. Also, since in this case, the normal force is governed by the magnetic field produced by the NdFeB permanent magnets utilized in the in-situ MRH tool, this force abrades the materials in a deterministic manner without creating the new roughness peaks resulting in a fine with a higher level of surface texture. The constricted working-space between the curved end surface of permanent magnet the present tool and the interior cylindric surface of the workpiece occupied with the MRP fluid causes the stiffly stuck active abrasive particles (AAPs) in the magnetic EIPs columnar chains to act the normal magnetic force (F_{mr_n}) on the finishing surface of the workpiece. The non-magnetic AAPs are pushed away toward the workpiece finishing surface from the tool's magnetic curved surface by magnetized EIPs which are attracted toward magnetic surface of the tool. The pushed away AAPs from the magnetic surface of the tool apply a normal magnetic force (F_{mr_n}) over the interior surface of the cylindrical workpiece as shown in Figs. 4.31(b) and (c). This F_{mr_n} is accountable for the penetration of the AAPs over the finishing surface of the workpiece. Due to relative motion of the AAPs of MRP fluid along with the in-situ MRH tool's motion, the shear force is applied on the finishing surface as seen in Figs. 4.31(b) and (c).

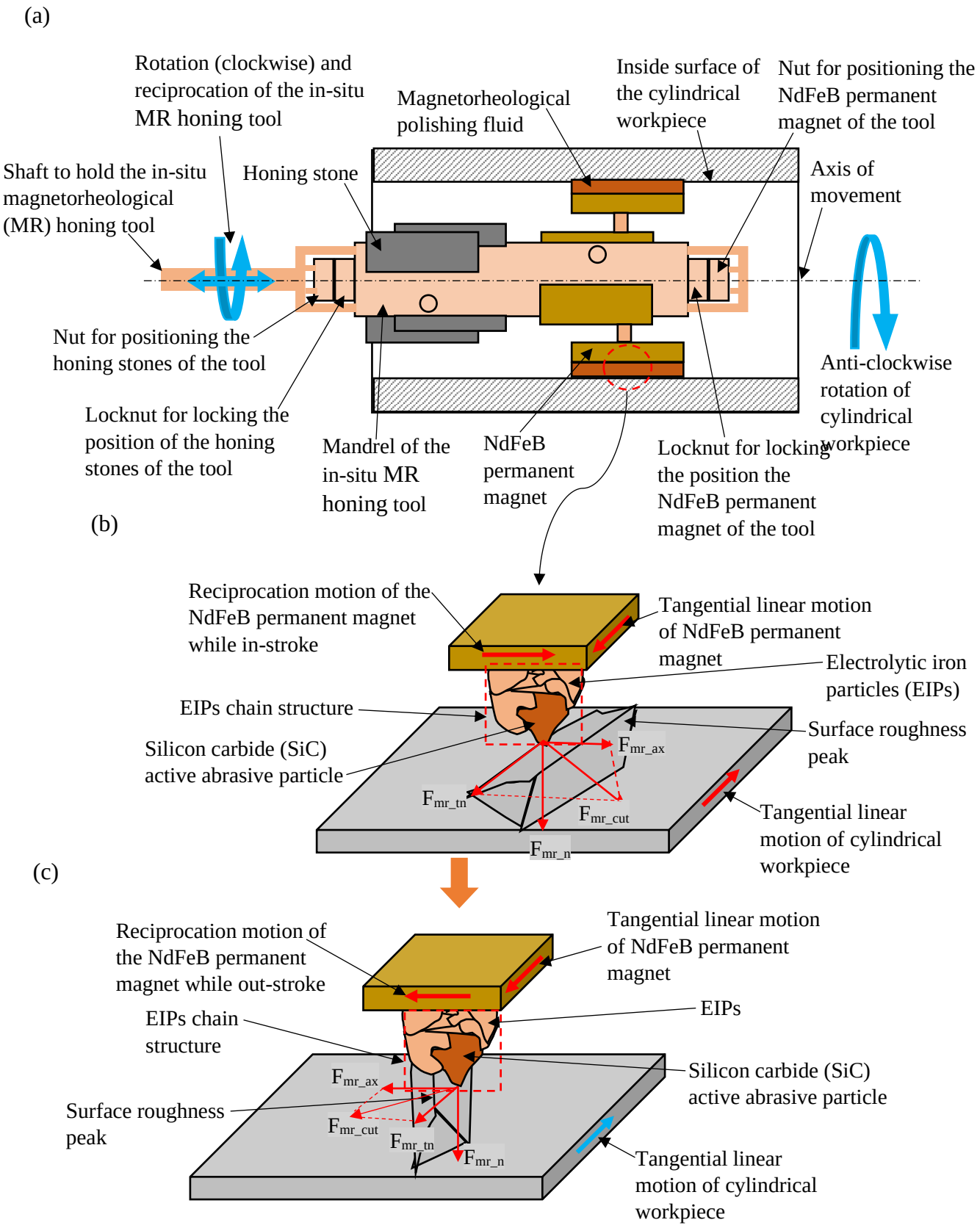

Fig. 4.31 (a) Rotational magnetorheological honing (RMRH) performed on the internal cylindrical workpiece surface using the in-situ magnetorheological honing tool (b) action of finishing forces while in-stroke of the in-situ MRH tool into the cylindrical workpiece, and (c) action of finishing forces while out-stroke of the in-situ MRH tool from the cylindrical workpiece.

In this work, as the cylindrical workpiece is also given rotational motion opposite to the in-situ MRH tool rotation, the rotating speed of the AAPs w.r.t. finishing surface is enhanced. The tangential shear force applied by an AAP is directly dependent on its relative rotational speed. Therefore, the total tangential shear force applied by an AAP on the interior surface of the cylindrical workpiece (F_{mr_tn}) is depicted as in Figs. 4.31(b) and (c). The axial shear force (F_{mr_ax}) is prompted by the translational motion of the in-situ MRH tool. The resultant of both shear forces acting on the interior surface of the cylindrical workpiece is known as the total cutting shear force (F_{mr_cut}). The total cutting shear force (F_{mr_cut}) is related to the tangential shear force (F_{mr_tn}) and the axial shear force (F_{mr_ax}) as in Eq. (4.3).

$$F_{mr\_cut} = \sqrt{F_{mr\_tn}^2 + F_{mr\_ax}^2} \tag{4.3}$$

Hence, the F_{mr_cut} as obtained in Eq. (4.2) is responsible for the material removal. Figs. 4.31(a) and (b) represent the detailed mechanism of the material abrasion from the finishing surface of the cylindrical workpiece. When the rotating in-situ MRH tool is inserted (in-stroke) into the oppositely rotating workpiece cylinder, the AAP which contacts the roughness peak tends to deform it along the resultant direction of the axial and tangential motion of the AAP as Fig. 4.31(a). Further, in the returning out-stroke of the in-situ MRH tool, the contacting roughness peak with the AAP gets deformed in the opposite direction to the deformation direction of the in-stroke. Thus, the continuous change in the direction of the deformation of the roughness peaks with the interactive AAPs prompts the abrasion action on the roughness peaks. In this way, the detachment of the surface roughness peaks from the inner surface of the cylindrical workpiece results in fine finishing.

4.3 Conclusions

From the development of rotational magnetorheological honing (R-MRH) process for finishing the internal cylindrical surface of the workpieces as well as design and fabrication of an in-situ honing tool performed in this chapter for performing traditional as well as magnetorheological honing at a single setup using the single tool, the following conclusions have been drawn.

- The fixture with two ball bearings to hold the cylindrical workpiece can give precisely accurate rotational motion to the cylindrical workpiece resulting in a more uniform finishing action.

- The improved fixture with the auto-centered three-jaw chuck of the developed R-MRH finishing setup can finish the internal surface of the cylindrical workpieces with variable diameters.
- The extent of improvement in finishing productivity and performance obtained from this developed R-MRH process makes this process useful for internal fine finishing the surface of a variety of industrial products such as hydraulic cylinders, molds, circular dies, hydraulic rack cylinder and cylindrical barrel for injection molding machine, sanitary pipes in food industries etc.
- The uniform distribution and the magnitude of the magnetic field induced by the permanent magnet of the tool on the workpiece finishing surface obtained in the magnetostatic simulation and experimental measurement conducted in the present study revealed that the present developed in-situ MRH tool is in good agreement for the performing the R-MRH process.
- The capability of the present developed in-situ MRH tool to finish both traditional honing as well as magnetorheological honing makes this tool to be useful in a great variety of industrial products which requires micro-finishing to fine finishing without changing the tool and finishing setup.

CHAPTER 5

EXPERIMENTATIONAL VALIDATION OF A DEVELOPED ROTATIONAL MAGNETORHEOLOGICAL HONING PROCESS

In this chapter, the internal surface finishing performance and productivity of the present developed rotational magnetorheological honing (R-MRH) process are experimentally analyzed with the existing magnetorheological honing process (Grover and Singh, 2018a). Furthermore, the optimum process parameters of the present process are predicted using response surface methodology (RSM) technique (Dabnun, *et* al., 2005) and their effect on finishing performance is studied for fine finishing the EN-31 steel cylindrical workpiece. Also, the preliminary experimentations are performed to validate the feasibility of the novel designed and fabricated in-situ honing tool.

5.1 Preliminary experimentations with the developed rotational magnetorheological honing setup

The experimentations were performed to confirm the improvement in performance of the R-MRH process as achieved in the theoretical investigation performed in chapter 3 of this study on the experimental setup as shown in Fig. 5.1. The improvement in finishing performance was analyzed by performing two types of experimentations like when the workpiece cylinder was kept stationary (existing MRH process) and when the same workpiece cylinder was kept rotating (present R-MRH process). All the process variable are kept same except workpiece's rotational motion as shown in the Fig. 5.1. During the experimentation on the interior surface of the ferromagnetic (mild steel) workpiece cylinder, the magnetorheological polishing (MRP) fluid was utilized as a finishing agent. The MRP fluid was synthesized based on the literature (Grover and Singh, 2018a) and reported as in Table 5.1. The components of the MRP fluid were measured with a weight measuring instrument (electronic compact scale SF-400C). The measured components were mixed adequately into the DC controller mixing chamber. The synthesized MRP fluid was applied over the magnetic end surface of the present tool which got stiffened due to the magnetic behavior of EIPs. The abrasives stuck in between the magnetized EIPs chain structure and executed the finishing operation by their predetermined movements on the inside surface of the workpiece cylinder. The curved radial permanent magnet based magnetorheological honing (MRH) tool was made rotating and reciprocating simultaneously inside the stationary cylindrical workpiece fixed in the two ball bearings of the fixture as shown in Fig. 5.1(a). Whereas, the MRH tool was made rotating and reciprocating inside the oppositely rotating ferromagnetic cylindrical workpiece as demonstrated in Fig. 5.1(b).

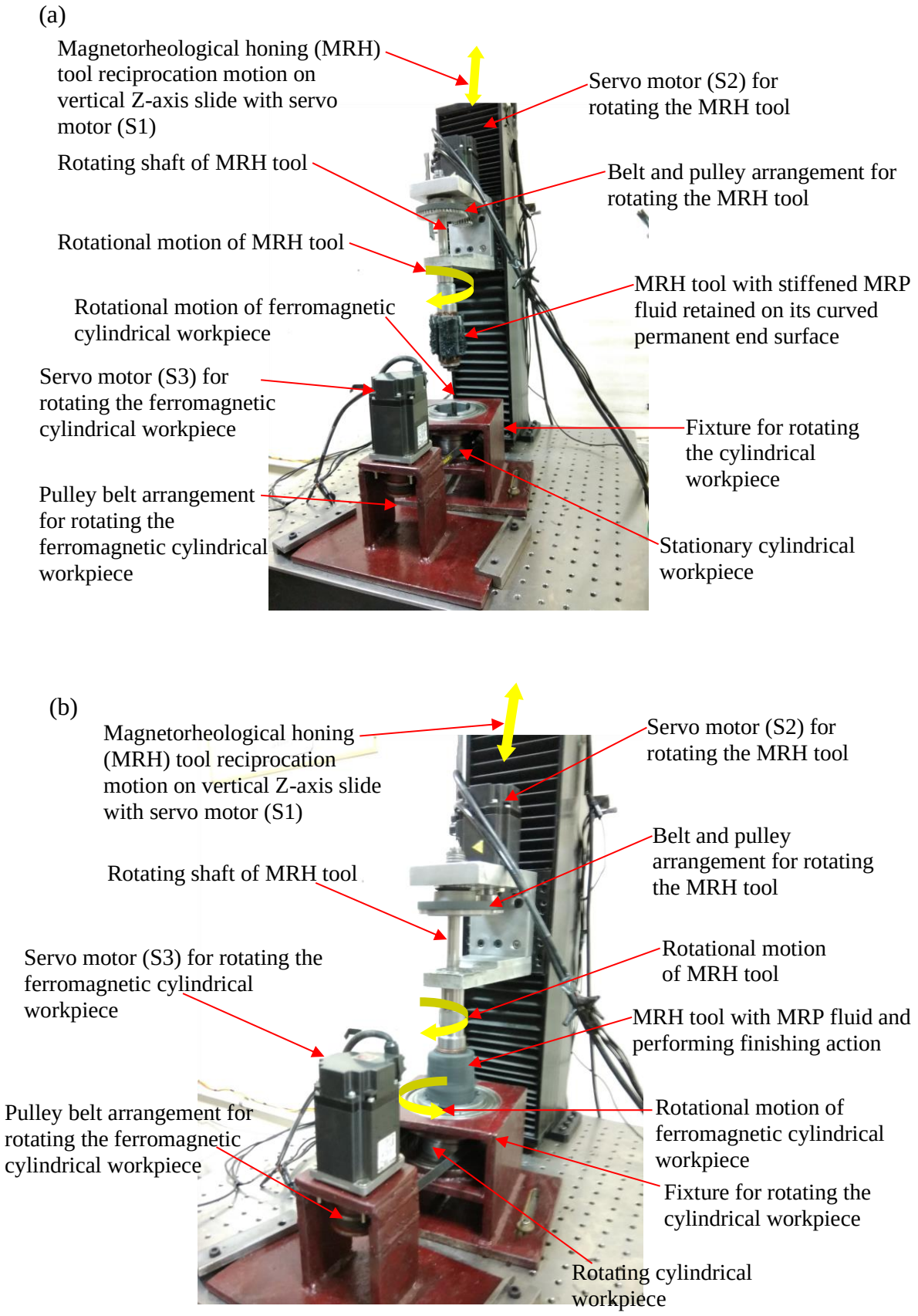

Fig. 5.1 Photograph of rotational magnetorheological honing (R-MRH) process setup during (a) when the ferromagnetic cylindrical workpiece is kept stationary and (b) when the ferromagnetic cylindrical workpiece is kept rotating.

The programmable logic controller (PLC) used in the finishing setup provided very precise control on the motions of the tool and workpiece cylinder. As three kinds of motions were required for performing the R-MRH process, therefore, three servo motors were used in the finishing setup. The cylindrical workpiece is fixed between two bearings tightly attached in the fixture as shown in Fig. 5.1.

Table 5.1 Experimental processes parameters and conditions

Parameters	Magnetorheological honing process used for finishing the inner surface of a stationary mild steel cylindrical workpiece	Rotational magnetorheological honing process used for finishing the inner surface of a rotating mild steel cylindrical workpiece
MRH tool's rotational speed, (rpm) (clockwise)	400	400
MRH tool's reciprocation speed, (cm/min)	70	70
Ferromagnetic cylindrical workpiece's rotational speed, (rpm) (anticlockwise)	0	20
Working gap, (mm)	2	2
Each finishing cycle time (min)	20	20
Total finishing time (min)	60	40
Finishing length of the inner surface of the cylindrical workpiece (mm)	50	50
Finishing internal diameter of the cylindrical workpiece (mm)	60	60
Magnetorheological polishing (MRP)	20 % by vol. electrolytic iron particles (mesh number 500), 20 % by vol. SiC abrasive particles (mesh number 800) and 60 % by volume base fluid (20 % by weight grease AP3 and 80 % by weight paraffin oil)	

On the other side of the fixture, a servo motor is mounted which transmits the power for rotating the workpiece cylinder through v-groove pully and v-belt drive. Based on the trial experiments, the value of process parameters involved in R-MRH process i.e., MRH tool's rotational and reciprocation speed, rotational speed of cylindrical workpiece and working gap are considered while experimentation. The working gap was filled with the indigenously made magnetorheological (MR) polishing fluid. The MRP fluid is applied manually with a spoon on the magnetic end surface of the MRH-tool before starts of each set of the finishing trial. The MR-polishing fluid changes after the completion of each 20 min of the finishing period to obtain the fresh edges of the abrasive particles in every set of finishing the trial. The experimental parameters and their condition based on the preliminary trial experiments are given in the Table 5.1. In this study, the surface roughness of initial surface and after each finishing action was measured with the Mitutoyo Surf tester SJ-400. While measuring the

surface roughness, the cut-off length, and number of sampling length considered in the surface measuring instrument were 0.25 mm and 5 respectively. For visual analysis of the improvement achieved from the experimentation for both type of experimental work (stationary and rotating cylindrical workpiece), the scanning electron microscopy (SEM) tests have been performed at Zeiss scanning electron microscope (model No. JEOL JSM 6510 LV) on initial and final finished surfaces in this study.

5.1.1 Results and discussion

The improvement in surface finishing performance and productivity obtained in the rotational magnetorheological honing (R-MRH) process in comparison with the MRH process (when workpiece is kept stationary) is analyzed through the experimental results. There are three repetitive trials have been conducted using the finishing parameters as reported in Table 5.1 to finish the interior surface of the rotational and stationary cylindrical workpieces. The average of the final finished results in three trials is considered for the analysis of the finishing improvement achieved with this study and as reported in Table 5.2. The summary of the results achieved from the present preliminary experimental work clearly reveal the improvement achieved in R-MRH process are listed as in Table 5.2. In this table, based on the experimental results of surface finishing, the finishing rate has been calculated and reported to analyze the improvement achieved in the finishing productivity in R-MRH process as compared to the existing MRH process.

The initial value of average surface roughness was measured as 330 nm on the inner ground surface of the three samples of the workpiece cylinders. After 60 min of finishing on the stationary cylindrical workpiece using the finishing parameters as reported in Table 5.1, the final average surface roughness was found as 90 nm. So, the maximum %age change in surface roughness ($\% \Delta Ra$) achieved was 72.72 % with 60 min of finishing time. Whereas, after 40 min of finishing on the rotating cylindrical workpiece (using R-MRH process) with utilizing the process parameters as reported in Table 5.1, the final average surface was found as 50 nm. This results in a maximum $\% \Delta Ra$ of 84.84 % using R-MRH process only in 40 min. Thus, the higher change in surface roughness value with the lesser finishing time when the workpiece cylinder was rotated confirms that the R-MRH process is more efficient to finish the internal surface of the workpiece cylinder as compared to the existing MRH process (when the cylindrical workpiece was kept stationary).

Table 5.2 Summary of experimental results after MR finishing using the experimental parameters and conditions.

Experiment description	Finishing time (min)	Initial surface roughness value (R_a) (nm)	Final surface roughness value (R_a) (nm)	Finishing rate (ΔR_a) (nm/min)	Percentage (%) change in the surface roughness value $\left(\left\lvert\frac{\text{Initial } R_a - \text{Final } R_a}{\text{Initial } R_a}\right\rvert \times 100\right)$
Magnetorheological honing (MRH) process used for finishing the inner surface of a stationary mild steel cylindrical workpiece	60	330	90	4	72.72
Rotational magnetorheological honing (R-MRH) process used for finishing the inner surface of a rotating mild steel cylindrical workpiece	40	330	50	7	84.84

Further, the finishing rate was evaluated as 4 nm/min for the MRH process when the workpiece cylinder was kept stationary as reported in Table 5.2. However, the finishing rate achieved while internal surface finishing of the rotational cylindrical workpiece using the R-MRH process was 7 nm/min as reported in Table 5.2. Therefore, the present developed R- MRH process is found significantly capable to perform better surface finishing with a higher finishing rate. Thus, experimentally it is confirmed that the present developed R-MRH process is more efficient to finish the internal surface of the workpiece cylinders with a higher finishing rate as compared to the stationary cylindrical workpieces.

The results of the finishing action performed in this work are demonstrated through the surface roughness profiles as in Fig. 5.2. Fig. 5.2(a) shows the surface roughness profile of the initial ground interior surface of the workpiece cylinder. After 60 min of MRH finishing on the internal surface of the stationary cylindrical workpiece results in the roughness profile as depicted in Fig. 5.2(b). Further, in Fig. 5.2(c), the roughness profile of the final finished internal surface of the rotating cylindrical workpiece with 40 min of R-MRH finishing is shown. As the rotational motion is given to the workpiece cylinder, the tangential shear force of the active abrasive particles on the finishing surface gets increased as discussed in the theoretical study (Chapter 3).

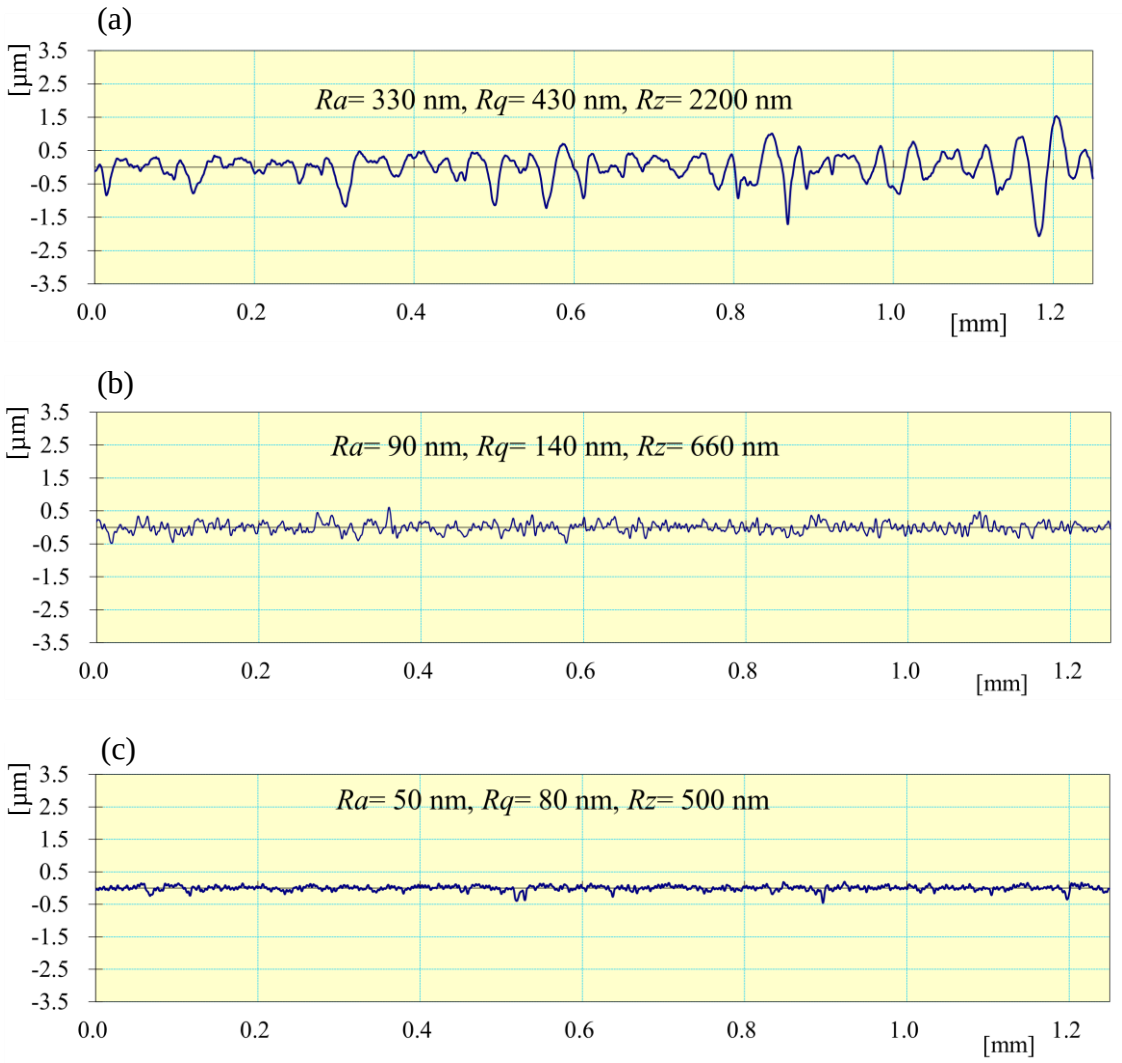

Fig. 5.2 Internal surface roughness profile of ferromagnetic mild steel cylindrical workpiece of (a) initial ground surface, (b) after 60 min of finishing using the existing magnetorheological honing method (when the cylindrical workpiece was kept at stationary), and (c) after 40 min of finishing using the present rotational magnetorheological honing (R-MRH) process (when the cylindrical workpiece was kept rotating).

The increase in shear force caused an enhancement in material removed by cutting the peaks of finishing surface roughness of the cylindrical workpiece from the vicinity of indented abrasive particles. Also, the rotational movement of the workpiece cylinder in the reverse direction to the MRH-tool rotation increases the length of the helical path and decreases the pitch of the helix (chapter 3, Fig. 3.2) which causes more numbers of helical turns on the interior surface of the workpiece. Therefore, more uniform, and a higher rate of material removal is achieved in the R-MRH process. This can be verified with Fig. 5.2(c) which represents the significant improvement in the surface finish (*Ra*=50 nm) in only 40 min of finishing with the present developed R-MRH as compared to the surface finish (*Ra*=90 nm) in 60 min of finishing when the cylindrical workpiece was kept stationary (Fig. 5.2(b)). Hence,

from Fig. 5.2, it is experimentally confirmed that the R-MRH process is more proficient to finish the interior cylindrical surface of the workpieces with a higher finishing performance and productivity as compared to the existing MRH process.

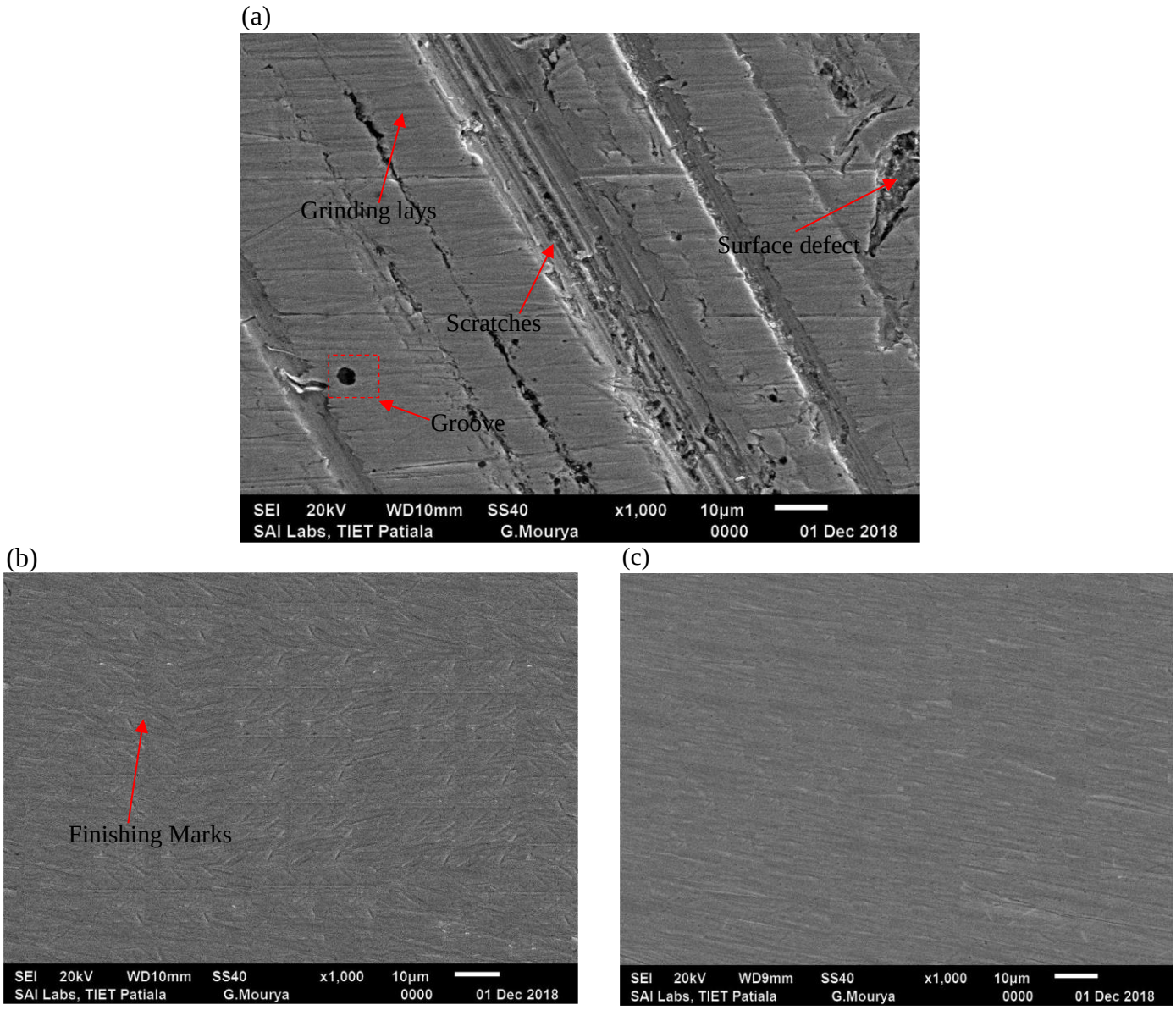

Fig. 5.3 Scanning electron microscopy images at 1000X of inner surface of the ferromagnetic mild steel cylindrical workpiece: (a) initial surface, (b) after 60 min of finishing with the parameters on a stationary cylindrical workpiece, and (c) after 40 min of finishing with the parameters on a rotating cylindrical workpiece using the rotational magnetorheological honing (R-MRH) process.

In this study, the scanning electron microscopy (SEM) has also been conducted for the microscopic analysis of the finished surfaces at 1000X magnification as shown in Fig. 5.3. Using SEM images, the surface characteristics of the finished interior surface of the workpiece cylinder were observed. Figure 5.3(a) represents the SEM image of the initial surface which

has many grinding lays and surface defects due to the rigid abrasive tool and the uncontrollable finishing force applied during initial surface generation through the tradition grinding process. Figure 5.3(b) shows the surface texture of the inner surface after 60 min of finishing action using the existing MRH process when the cylindrical workpiece was kept stationary. In this SEM image of the finished surface, the finishing marks can be seen. The surface characteristics obtained after 40 min of finishing action using the rotation magnetorheological honing (R-MRH) process on the inner surface of the rotating ferromagnetic workpiece cylinder is shown in Fig. 5.3(c). This SEM image shows that the surface characteristic has almost no surface defects and found comparatively better smooth surface. This better-finished surface characteristic was obtained in only 40 min of finishing using the present R-MRH process. Therefore, this SEM image advocates the proficiency of the R-MRH process with a higher finishing rate. Hence, the present developed R-MRH process can be used more efficiently to fulfill the industrial requirement of nano-finishing of the interior surface of different workpiece cylinders. In industries, almost all type of cylindrical components which performs the sliding motion, push fitting in machine assembly, and close tolerances are needed fine-finishing of their internal surface. The overall results showed that with the addition of a further rotational motion of cylindrical workpiece in reverse direction to the MRH-tool rotational direction, a new finishing process named as the R-MRH process is found more efficient in producing the nano-level interior surface finishing of the workpiece cylinders with higher finishing rate as revealed in the experimental results.

5.1.2 Conclusions

In the present work, the developed rotational magnetorheological honing (R-MRH) process has been employed and successfully demonstrated experimentally for better performance due to the rotational motion of the workpiece cylinder compared to the existing MRH process when the cylindrical workpiece was kept stationary during its internal surface finishing. The following conclusions are drawn.

- The maximum percentage change in surface roughness with the R-MRH process gets increased to 84.84 % and the finishing rate is 7 nm/min with tool rotational speed of 400 rpm, tool reciprocation speed of 70 cm/min, and the rotational speed of the mild steel cylindrical workpiece 20 rpm in 40 min of finishing. However, with the stationary cylindrical workpiece, the maximum percentage change in Ra value gets increased to 72.72 % and finishing rate is 4 nm/min in 60 min of finishing which clearly advocates

the higher finishing rate of the present developed R- MRH process.

- The scanning electron microscopy images of the workpiece surfaces reveal that the present developed R-MRH process has the capability to finish the interior cylindrical surface of the workpieces without any surface defects and with a higher finishing rate.

5.2 Experimentation for validating the theoretical analysis of surface roughness in R-MRH process on the improved finishing setup

5.2.1 Experimentation

To validate the theoretical model developed for analysis of the change in surface roughness in the present rotational magnetorheological honing (R-MRH) process, the experimentations have been conducted on the R-MRH process setup as shown in Fig. 5.4. As this improved setup with the automatic centering 3 jaw chuck has been developed to enable the R-MRH process in fine finishing the internal surface of the cylindrical workpieces of the variable diameters, therefore, the experimentations are conducted on this setup. Also, the experimentations conducted in this work, acknowledge the feasibility of the developed setup for MR finishing of the different sizes of cylindrical workpieces. The mild steel material is considered as the workpiece material for the current experimentation. The based on the trial experiments, the finishing parameters are considered and reported in Table 5.3. In this case of experimentation, the process parameters were considered based on the assumed parameters in chapter 3 for the theoretical analysis of the developed surface roughness. Using the parameters as reported in Table 5.3, the experimentations were performed and the surface roughness obtained in the theoretical analysis (Eq. 3.44, chapter 3) is compared with the experimental surface roughness.

Table 5.3 Finishing parameters used for the experimentation.

Process parameters	Numerical values
Rotational speed of magnetorheological honing (MRH) tool	400 rpm
Reciprocation speed of the MRH-tool	70 cm/min
Rotational speed of the mild cylindrical workpiece	40 rpm
Each set of finishing cycle	20 min
Working gap	1.7 mm
Length of the inner surface of the cylindrical workpiece	60 mm
Internal diameter of the cylindrical workpiece	60 mm
Magnetorheological polishing (MRP)	As per the MRP fluid reported in Table 5.1

The synthesized MRP fluid is applied as the finishing medium in the present R-MRH process experimentation. The surface roughness is measured experimentally with the surface tester using Mitutoyo SJ400 model. Using 20 min for each set of finishing duration, the roughness parameters were measured using the Mitutoyo Surftest SJ-400 taking 0.25 mm as a cut-off.

The average variation of the surface roughness after each set of finishing cycle is measured and reported in Table 5.4.

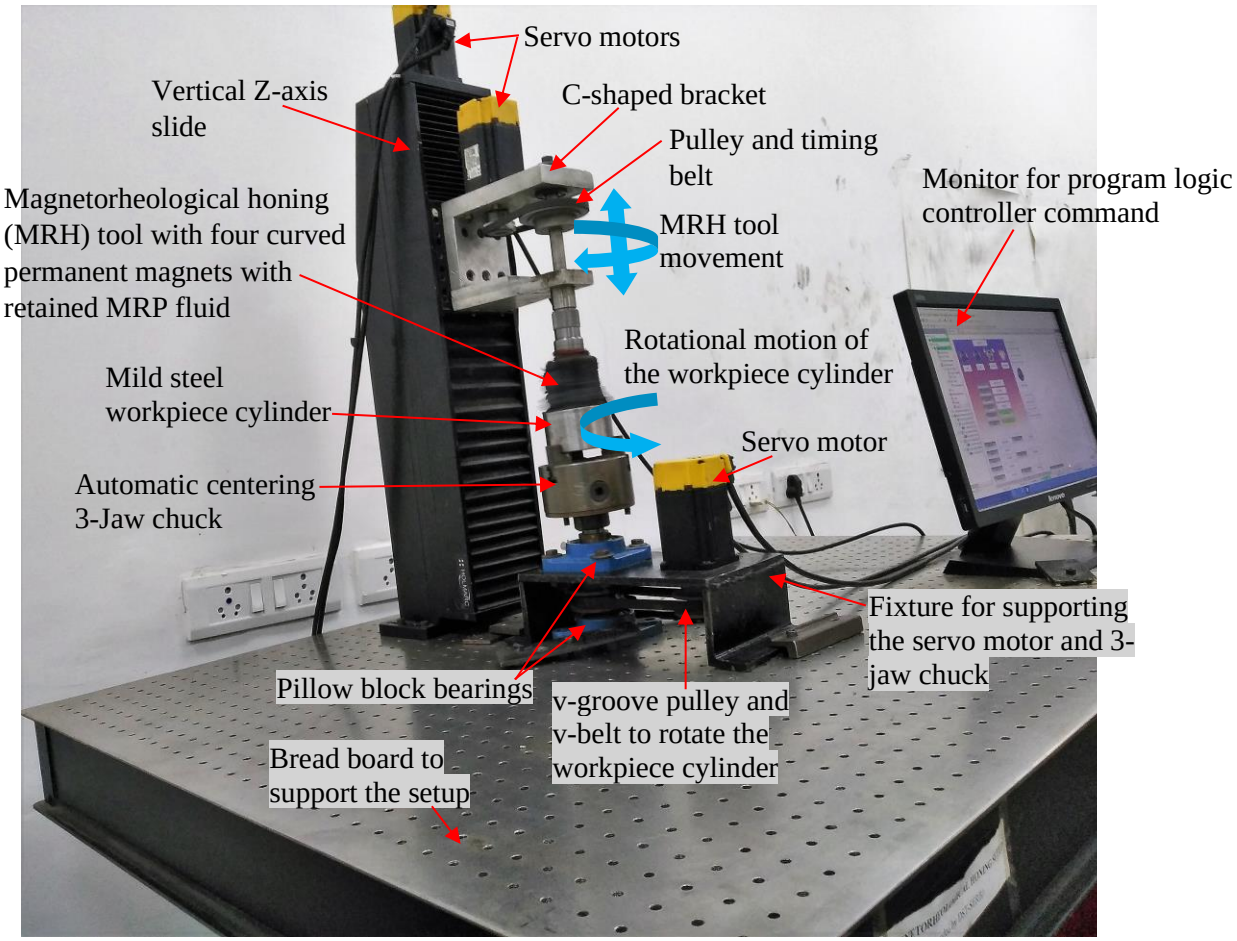

Fig. 5.4 Photograph of the improved rotational magnetorheological honing (R- MRH) setup with the automatic-centering 3-jaw chuck fixture for holding different sizes of the cylindrical workpieces.

For the analysis of the improvement in surface finishing with the rotational magnetorheological honing process on the internal surface, the scanning electron microscopy (SEM) tests have been performed with Zeiss Scanning Electron Microscope. There is a tapered slot has been made in the internal cylindrical surface of the cylindrical workpiece. The workpiece samples are prepared of the same shape, type, and size as that of the slot in the workpiece cylinder. At the end of the experimentation, the SEM test is performed for analyzing the surface texture of the initial surface and final MR finished surface after using the present R-MRH.

5.2.2 Results and discussion

To analyze the effect of rotational motion of the workpiece cylinder in change in the surface roughness with the present rotational magnetorheological honing (R-MRH) process, the

theoretical analysis was performed as in Chapter 3. The surface roughness model was developed (Eq. 3.44) for the R-MRH process. Using Eq. (3.44), the theoretical surface roughness values were calculated and compared with the experimentally obtained surface roughness values as reported in Table 5.4.

Table 5.4 Theoretical and experimental results for change in surface roughness.

No. of finishing cycle (t_c) (Eq. 3.5)	Experimentally measured surface roughness value (nm)	Theoretically calculated surface roughness value (nm) Eq. (3.44)	% Error $= \left\| \frac{\text{Experiemntal} - \text{Theoretical}}{\text{Experiemntal}} \right\| \times 100$
0	330	330	0
116	230	221	3.91
233	135	127	5.92
350	60	62	3.33

The initial ground average surface roughness value over the internal surface of the mild steel cylindrical workpiece was measured as 330 nm which roughness profile is shown in Fig. 5.5(a).

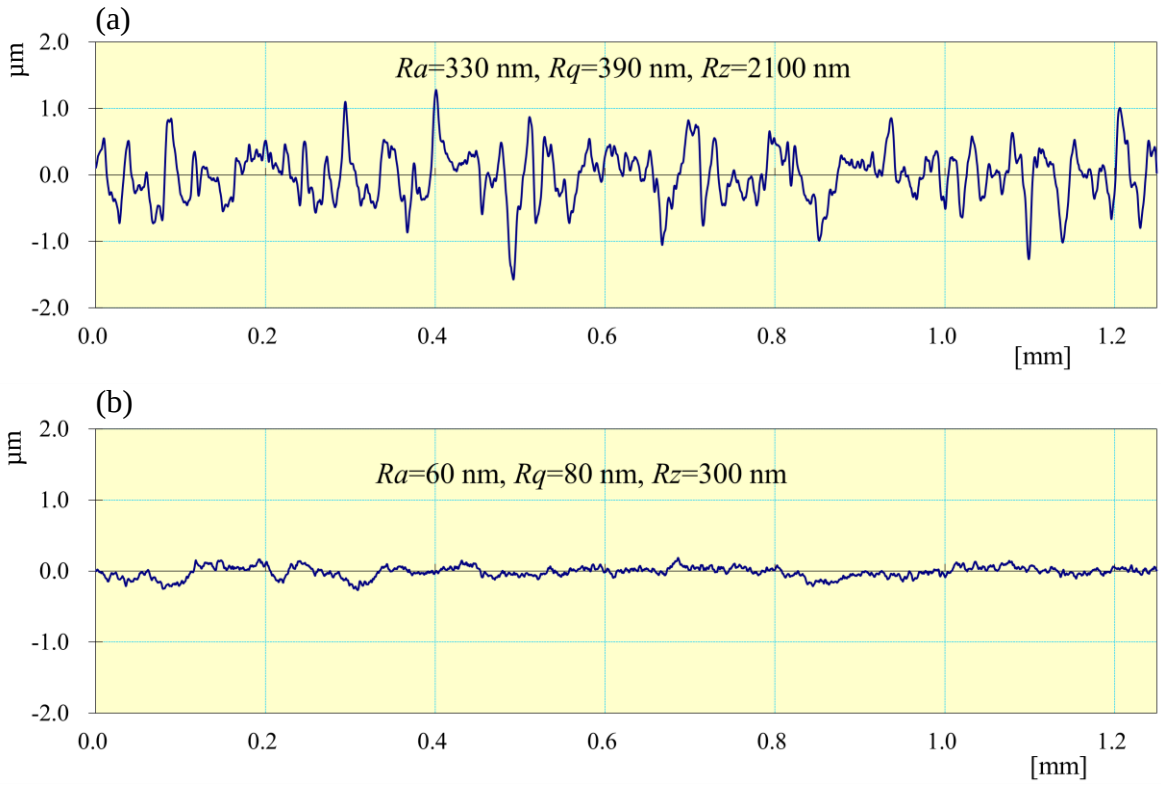

Fig. 5.5 Roughness profile of (a) initial ground surface and (b) final finished mild steel internal cylinder surface with the present R-MRH process after 350 finishing cycles.

The same initial average surface roughness value was taken for the theoretical calculation of change in roughness value. To validate the theoretical model of change in roughness value, the experiments have been performed. After completion of each set of finishing cycles, the values

of the surface roughness were measured and are reported in Table 5.4. After 350 finishing cycles on the internal cylindrical surface with the present R-MRH process, the average surface roughness value gets reduced as 60 nm as shown in Fig. 5.5(b). Whereas from the theoretical surface roughness model (Eq. (3.44)) it reduced to 62 nm. Therefore, the error between the experimental and theoretical surface roughness value after 350 cycles of finishing is found within 5.92 %. The percentage error in the experimental surface roughness value and theoretically calculated surface roughness value after 350 finishing cycle shows a close agreement for validating the roughness model. From the experimental measured results of the surface roughness value after each set of finishing cycle as given in the Table 5.4, it is observed that by rotating the workpiece cylinder in the present R-MRH process, the significant change in surface roughness takes place.

For further analysis of material removal by visualizing surface texture, the scanning electron microscopy (SEM) test was performed at 500X. Figures 5.6 (a) and (b) show the SEM images of the initial ground surface and final MR finished surface (after 350 finishing cycles) of the internal surface of the mild steel workpiece cylinder.

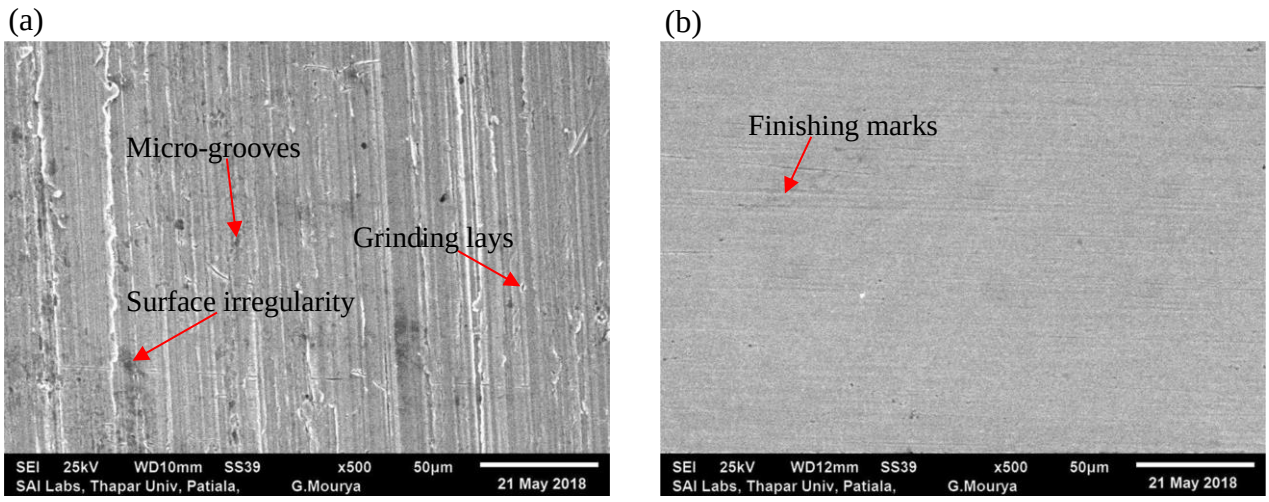

Fig. 5.6 Scanning electron microscopy (SEM) images of (a) initial ground surface and (b) final finished surface with the rotational magnetorheological honing process.

It can be observed that the initial surface of the mild steel cylindrical workpiece (Fig. 5.6 (a)) has various types of surface defects such as micro-grooves, grinding lays, surface irregularity, etc. Whereas after finishing the internal surface with the R-MRH process for 350 numbers of finishing cycles, it resulted in the Fig. 5.6 (b) which has rarely surface defects. The significant improvement in surface texture advocates about the feasibility of developed R-MRH process setup which can be useful for finishing the internal surface of the various sizes of the cylindrical

workpieces with improved finishing performance and productivity of the R-MRH process.

5.2.3 Conclusions

From the experimental analysis performed to confirm the theoretical study in chapter 3, and to test the feasibility of the rotational magnetorheological honing (R-MRH) setup developed which is useful in finishing the internal surface of the cylindrical workpieces of variable diameters, following conclusions have been made.

- The improved R-MRH process with the automatic-centering 3-jaw chuck fixture reveals the flexibility in MR finishing the internal surface of the different sizes of cylindrical workpieces.
- The percentage error in the range of 3.33 % to 5.92 % between the surface roughness evaluated from the developed theoretical roughness model and the experimental measured surface roughness reveals close agreement of the developed model.

5.3 Experimental validation for the in-situ magnetorheological honing (MRH) tool in R-MRH process

5.3.1 Experimentation

To validate the applicability of the novel designed and fabricated in-situ magnetorheological honing (MRH) tool for finishing the inside surface of the cylindrical workpieces, the experimentations have been performed on the experimental-setup as shown in Fig. 5.7. Mild-steel material is considered as the workpiece material because it is a very commonly used material. The experimental parameters and their condition used for the present experimentation are considered as reported in Table 5.5. The condition of the experimental parameters is considered on the basis of preliminary experiments. The change in surface finish is observed after the experimentation to demonstrate the applicability of the present developed novel in-situ honing tool. For generating the initial internal surface of the cylindrical workpiece, the traditional honing is applied on the initial machined interior cylindric surface using the in-situ honing tool. The honing stones are kept in firm contact with the workpiece's finishing surface. With this position of the honing stone, the in-situ honing tool performs traditional honing on the internal surface of the oppositely rotating cylindrical workpiece as per the conditions reported in Table 5.5. The workpiece with the initial machined surface is traditionally honed for 40 min in two sets of finishing cycles of each 20 min. Throughout the complete experimentation in this work, the surface roughness is measured using a Mitutoyo Surftest SJ-

400 after each set of finishing cycle. For surface roughness measurement while traditional honing is performed, the cut-off length of 0.8 mm and the 5 number of sampling lengths are selected in the above-mentioned surface measuring device. Further, for performing the MR honing with the same in-situ honing tool on the traditionally honed surface, the magnets of the tool are adjusted at their diametric position with maintaining 2 mm of working-space.

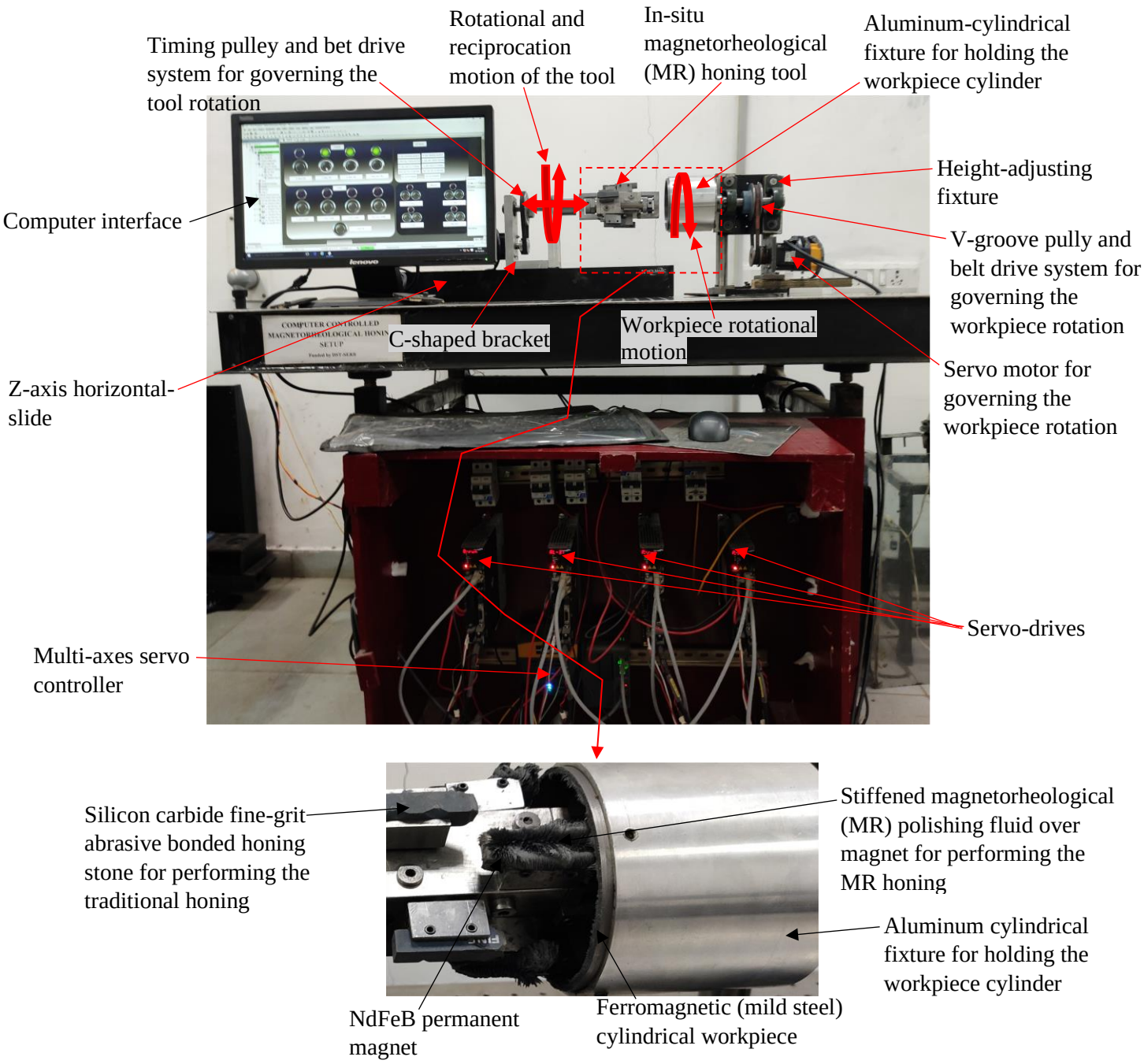

Fig. 5.7 Photograph of the experimental setup used for finishing the internal cylindric surface of the workpiece through the novel designed in-situ magnetorheological honing tool.

In this process, the magnetorheological polishing (MRP) fluid is used as a finishing media over the tool's magnetic end surface instead of honing stones. The composition of the MRP fluid considered in this work in accordance with the previous study conducted for the internal MR finishing of mild steel cylindrical workpiece surface are reported in Table 5.1. Therefore, when the electrolytic iron particles (EIPs) illustrate their magnetic nature under the occurrence of the magnetic field, these particles bear the polishing fluid's rheological properties. The MRP fluid is applied manually to the end-curved surface of the permanent magnet of the in-situ honing tool for fine finishing the inner cylindrical honed surface.

Table 5.5 Experimental parameters and their condition.

Experimental parameters	Condition
Rotating speed of the in-situ magnetorheological (MR) honing tool	350 rpm (clockwise)
Reciprocating speed of the in-situ honing tool	70 cm/min
Rotating speed of the cylindrical workpiece	35 rpm (anti-clockwise)
Working-space	2 mm
Workpiece material	Ferromagnetic (mild steel)
Honing stones for traditional honing	Fine grits silicon carbide bonded
Magnetorheological polishing (MRP) fluid for rotational magnetorheological honing	The composition of the MRP fluid reported in Table 5.1
Each set of finishing cycle	20 min

To determine the improvement in surface finish achieved after implementing the MR honing process on the internal surface of the cylindrical workpiece, the surface roughness is measured while considering the cut-off length of 0.25 mm and 5 number of sampling length in the roughness measuring instrument. To acknowledge the enhancement attained in the straightness of the finished internal cylindrical surface, the surface waviness measurement is conducted on the traditionally honed and the MR finished surface. The surface waviness is also measured using the same Mitutoyo Surftest SJ-400 instrument on which the surface roughness values were measured. In addition, the circularity test is carried out on the initial machined as well as pre- and post-MR honed surface to validate the perfection achieved in the circularity of the finished interior cylindric workpiece surface. With the use of the coordinate measuring machine (CMM), the circularity of the inner cylindric surface is recorded. Furthermore, scanning electron microscopy (SEM) tests are performed on a scanning electron microscope (model No. JEOL JSM 6510 LV) to examine the enhancement in surface morphology with application of the newly developed finishing process.

5.3.2 Results and discussion

The experiments were performed to investigate the applicability of the contemporary developed novel in-situ magnetorheological (MR) honing tool to finish the inner surface of the cylindrical workpieces. The impact of the present finishing process on improvement in surface finish of the internal cylindric workpiece has been studied in this work and detailed results of the study are given as follows.

5.3.2.1 Observation and discussion on the roughness profiles of the finished surfaces

The profiles of machined surface roughness, traditionally honed, and magnetorheological (MR) finished interior surface of the workpiece cylinder are shown in Fig. 5.8. Figure 5.8(a) shows the roughness profile of the workpiece cylinder's initial machined internal surface.

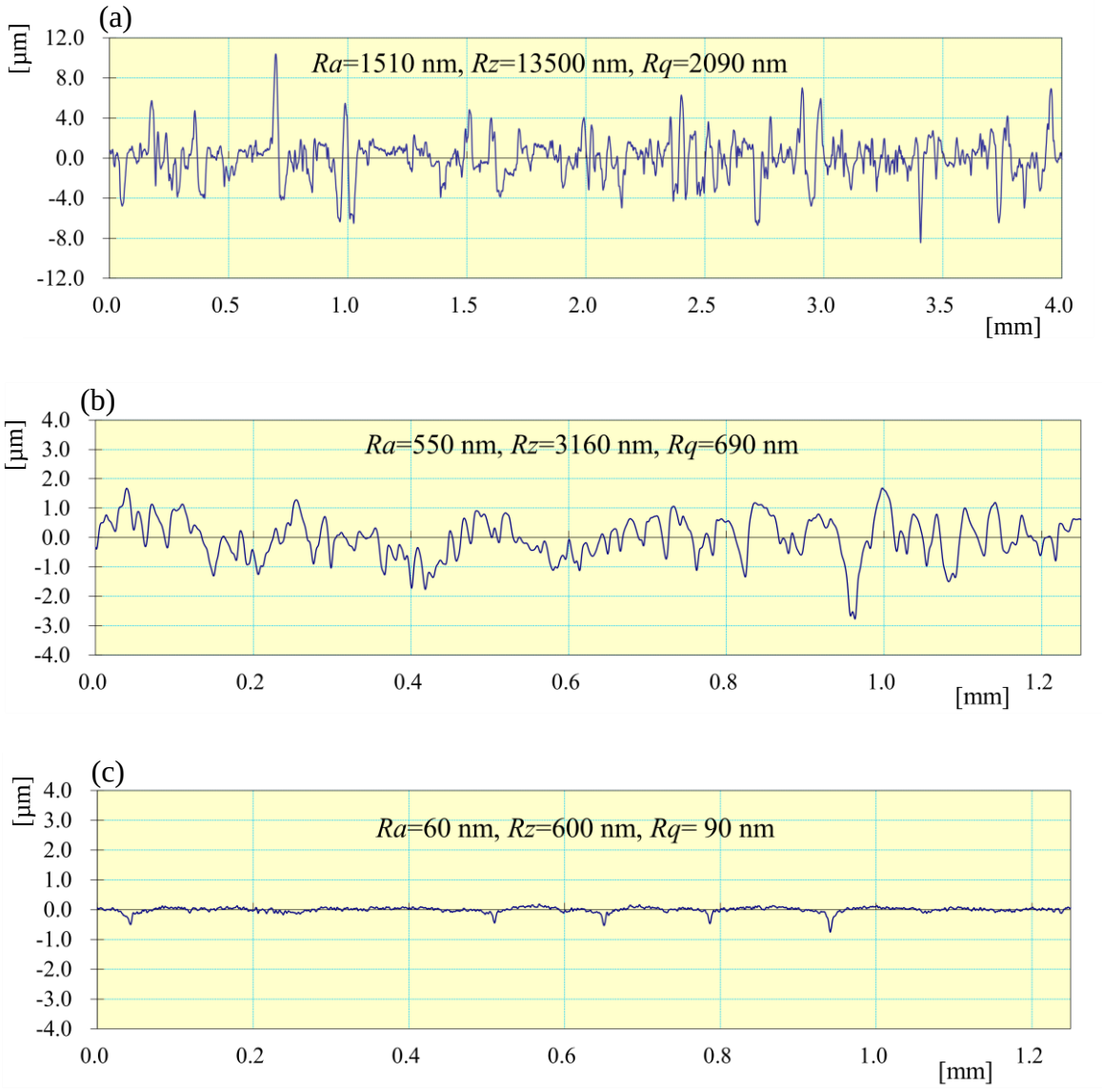

Fig. 5.8 The profile of surface roughness of (a) the machined surface, (b) traditionally honed surface with 40 min of finishing and (c) magnetorheological finished internal cylindric surface with 60 min of MR honing using the in-situ honing tool.

The roughness parameters of the machined internal surface asperity were obtained as *Ra*= 1510 nm, *Rz*= 13500 nm, and *Rq*= 2090 nm. Due to the large value of the asperity parameters of the machined surface of the workpiece, this surface needs to be employed firstly traditional honing and then MR honing method for getting a final fine finished surface. The continuous abrasion during traditional honing causes the reduction in surface roughness. Figure 5.8(b) demonstrates the surface asperity profile of the workpiece's traditionally honed inner cylindric surface after 40 min of finishing using the currently developed in situ MR honing method. The parameter's values of the surface asperity obtained were found as *Ra*=550 nm, *Rz*=3160 nm and *Rq*=690 nm. Therefore, the percentage change (*% Δ*) in the parameters of the surface asperity from the initial machined surface to the traditionally honed interior cylindric surface were found as *%* Δ*Ra*= 63.57, *%* Δ*Rz*=76.59, and *%* Δ*Rq*=66.93. The significant % reduction in the parameters of the surface asperity from the machined surface to the traditionally honed surface advocates that this tool has decent finishing efficacy and performance through traditional honing operation. Hence, the present developed in-situ honing tool is found in good agreement for generating the initial inside surface of the cylindrical workpieces for further MR honing process using the same tool and setup. Further, the initially generated surface from the traditional honing was finished with the same in-situ honing tool through the rotational magnetorheological honing (R-MRH) method. The surface roughness parameters achieved after 60 min of MR honing over the inside traditionally honed workpiece surface were found as *Ra*=60 nm, *Rz*=600 nm, and *Rq*=90 nm as shown in Fig. 5.8(c). So, the % Δ in the parameters of the surface asperity (*%* Δ*Ra*, *%* Δ*Rz*, *%* Δ*Rq*) achieved was *%* Δ*Ra*=89.09, *%* Δ*Rz*=81.01, and *%* Δ*Rq*=86.97. From these values *%Δ* in the parameters of the surface asperity, it can be said that using the MR-finishing process through the presently developed in-situ honing tool, the substantial improvement in the surface finish on the internal cylindrical surface is achieved. Thus, this single in-situ MRH tool can be found useful for finishing the industrial cylindrical products with great range of finishing requirement (micro to nano-level of finishing).

5.3.2.2 Observation and discussion on the surface waviness profile of the finished surfaces

For a perfect cylinder, the straightness is one of the important parameters to judge its dimensional accuracy which is crucial for avoiding the vibration, easy assembly, and disassembly, close fits, tolerances, and avoiding the leakage of fluid during its intended functioning. Therefore, to confirm the applicability of the present developed in-situ honing tool for improving the straightness, the surface waviness measurement was conducted in each finishing process in the present work, and their results were compared. The initial surface

waviness parameters measured on the machined interior cylindrical workpiece surface was found as *Wa*= 1460 nm, *Wz*= 5800 nm, *Wq*= 1720 nm as shown in Fig. 5.9 (a). From the value of the parameters of the surface waviness of the machined surface of the workpiece, it can be correlated that the straightness of the initially machined surface was uneven to a great extent. After 40 min of traditional honing performed on the machined internal surface of the cylindrical workpiece using the in-situ honing tool, the surface waviness parameters were achieved as *Wa*=460 nm, *Wz*=2300 nm, *Wq*=590 nm as shown in Fig. 5.9 (b).

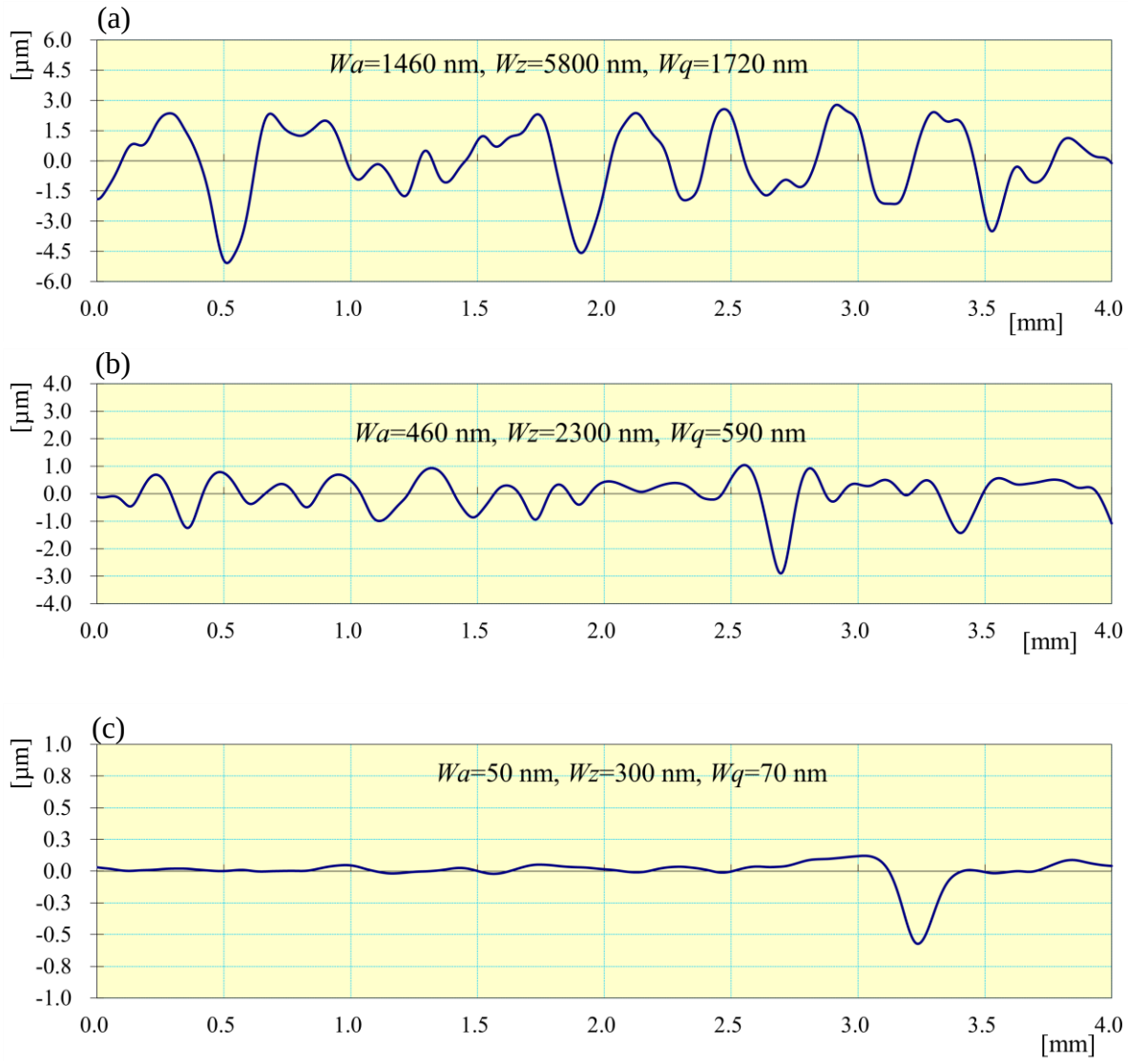

Fig. 5.9 Profile of surface waviness of (a) machined surface, (b) traditionally honed surface with 40 min of honing and (c) magnetorheological finished surface of the ferromagnetic mild-steel cylindric workpiece after 60 min of finishing using the in-situ honing tool.

These values of the surface waviness parameters demonstrate the efficacy of the in-situ honing tool for improving the surface waviness through traditional honing. The improvement in the

parameters of surface waviness with the traditional honing using the present in-situ honing tool was found as *% ΔWa*=68.49, *% ΔWz*=60.34, and *% ΔWq*=65.69. Therefore, based on improvement achieved in *% Δ* in surface waviness parameters in 40 min of honing, it can be said that the method of the initial surface generation for further MR finishing on the same workpiece surface using the same in-situ honing tool is found in good deal.

Further, improvement achieved in the surface waviness through the magnetorheological (MR) honing on the interior honed cylindric surface of the workpiece using the in-situ honing tool was observed as depicted in Fig. 5.9(c). Subsequently 60 min of the MR honing over the interior traditionally honed surface of the cylindrical workpiece, the measured surface waviness parameters were found as *Wa*=50 nm, *Wz*=300 nm, *Wq*=70 nm. These reduced values of the surface waviness parameters show a substantial enhancement in the dimensional accuracy of the MR honed inner surface of the cylindrical workpiece. The %age reduction in the parameters of surface waviness through the MR finishing using the present developed in-situ honing tool from the traditional honed surface was found as *% ΔWa*=89.13, *% ΔWz*=86.95, and *% ΔWq*=88.13. These %age reduction in surface waviness parameters after the MR finishing using the same in-situ honing tool shows its capability to improve the straightness which greatly causes the improvement in the dimensional accuracy of the inside surface of the cylindrical workpieces.

5.3.2.3 Observation and discussion on the circularity of the finished surfaces

Like the surface waviness, the circularity of the cylindrical workpiece is also an important factor through which the extent of dimensional accuracy and level of fits and tolerances can be predicted. This prediction states that the closer the captured points to the true circle of the circular profile, the more accurate the dimension of the circular profile is **(**Singaravel *et* al., 2016**).** Therefore, closer to the true circle results in a lesser value of the circularity which causes minimized heat generation, vibration, and resistance in assembling and disassembling the components during its functioning (Singaravel *et* al., 2016). To acknowledge the improvement in the circularity of the interior cylindric surface after the MR finishing using the presently developed in-situ honing tool, the images of circularity are revealed in Fig. 5.10. Figure 5.10(a) demonstrate the circularity of the initial machined inner cylindric surface of the workpiece. The value of the circularity measured on the machined surface was found as 0.4230. From the circularity image of the machined surface (Fig. 5.10(a)), it can be analyzed that most of the points captured over the interior surface of the cylindrical workpiece are away from the true circle. However, Fig. 5.10(b) shows the circularity image of the interior surface of the

cylindrical workpiece after applying the traditional honing for 40 min over it. From Fig. 5.10(b), it can be easily noticed that a comparatively lesser number of captured points have deviated from the true circle.

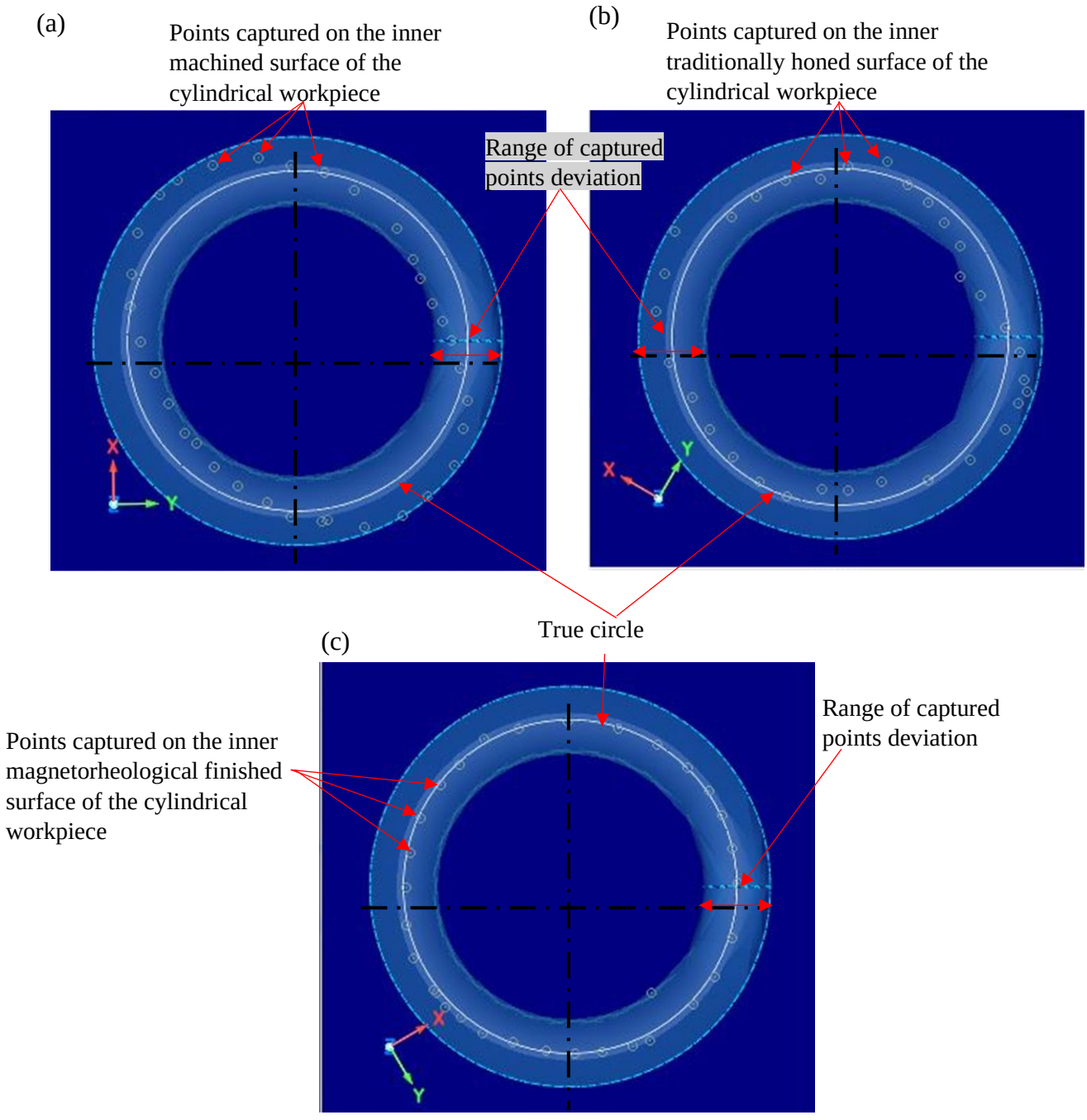

Fig. 5.10 Circularity photograph of (a) initial machined interior surface of the cylindrical workpiece, (b) interior surface of the cylindrical workpiece with 40 min of traditional honing and (c) final finished interior surface of the cylindrical workpiece with 60 min of magnetorheological finishing using the same in-situ honing tool.

Also, the values of the deviated distance of the captured points from the true circle are lesser than the same values of the distance of the captured points on the machined surface (Fig. 5.10(a)). The value of circularity obtained on this surface (traditionally honed) was 0.1179. On comparing the values of the circularity obtained on the machined surface as well as the traditional honed surface, it is clearly observed the improvement in the circularity in honed surface. This improvement in circularity demonstrates that the present developed in-situ honing tool can improve the circularity through the traditional honing which makes it to be used as an initial surface for further MR finishing process.

Figure 5.10(c) shows the circularity image of the final MR finished the interior surface of the cylindrical workpiece with finishing duration of 60 min using the same in-situ honing tool on the same setup. From Fig. 5.10(c), it can be observed that the significant change in the circularity is achieved as most of the captured points are whether on the true circle or quite close to this circle. The value of the circularity of the MR finished internal cylindrical surface was found to be 0.0376. Therefore, the magnitude of circularity obtained in the traditional honing as well as in MR honing state that the contemporary developed in-situ honing tool is capable to improve the circularity of the inside cylindrical surface in both methods of finishing.

The results achieved on the finial MR honed inside surface of the cylindrical workpiece in terms of surface waviness (Fig. 5.9(c)) and circularity (Fig. 5.10(c)) depict that using the presently developed in-situ honing tool and the method of final finishing, high level of dimensional accuracy, minimized vibration, heat generation, and leakage of fluids while operating may attain in industrial products. Also, due to improvement achieved in the circularity and waviness on the interior cylindrical workpiece surface caused in improvement in the cylindricity of this surface and improvement in the cylindricity enables this product for long-lasting and efficacy in its functioning.

5.3.2.4 *Observation and discussion on the scanning electron microscopy (SEM) images of the finished surfaces*

Figure 5.11 demonstrates the SEM images of the initially machined interior surface of the cylindrical workpiece (Fig. 5.11(a)). Also, the SEM image of the finished surface with 40 min of traditional honing on the same machined surface using the in-situ magnetorheological (MR) honing tool (Fig. 5.11(b)). The final magnetorheological (MR) honed surface using the same in-situ honing tool after 60 min of MR honing is depicted in Fig. 5.11(c). From the SEM image of the initial machined inside surface of the cylindrical workpiece as shown in Fig. 5.11(a), the

numerous surface defects like deep grooves, irregularities in the surface texture, scratch marks, and visible cracks can be seen. These surface defects are because of the irregular forces applied by the machining tool while machining action is performed. However, from Fig. 5.11(b), the improvement in the surface texture after applying 40 min of traditional honing with the novel in-situ honing tool can be easily observed.

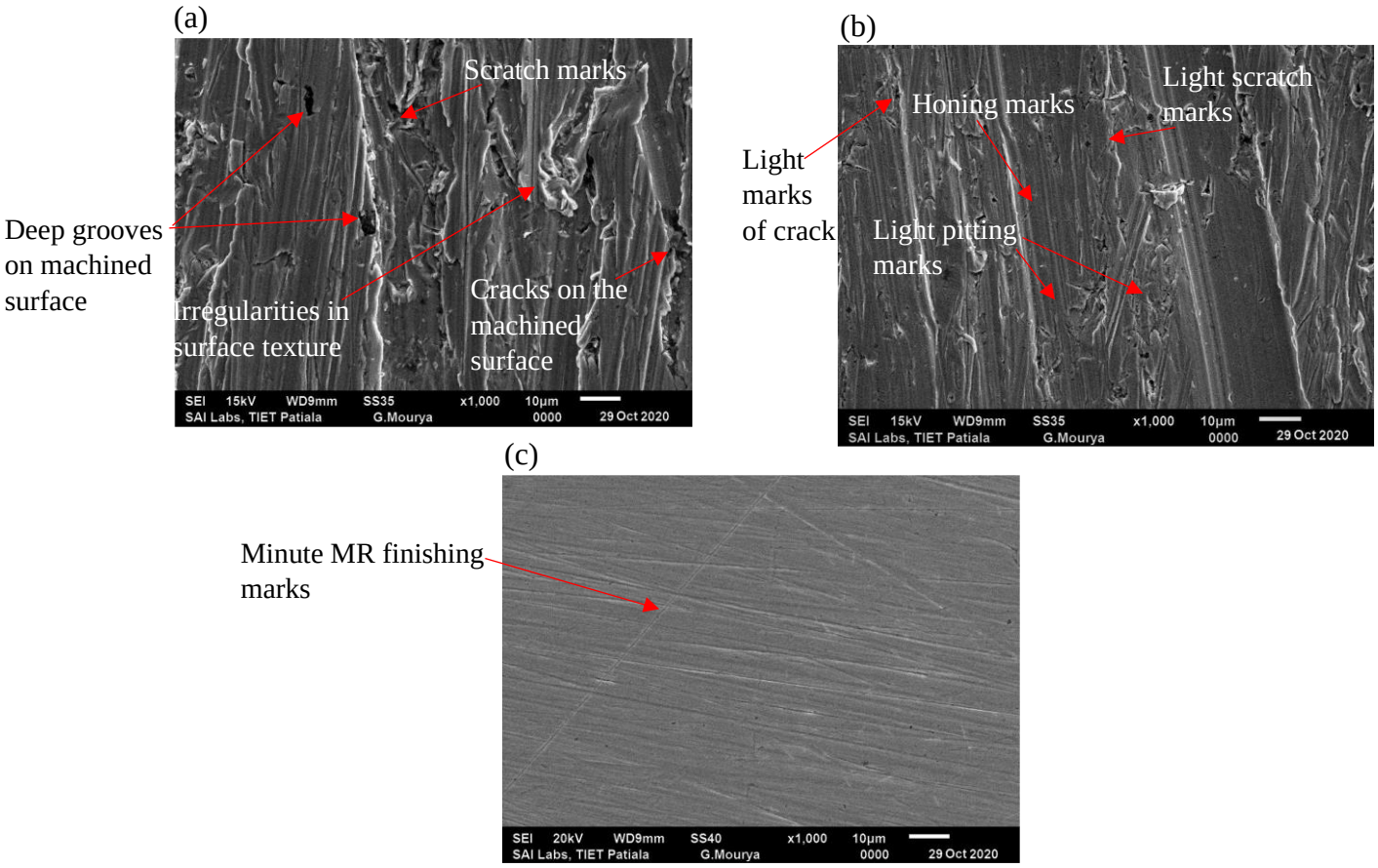

Fig. 5.11 Scanning electron microscopy images of internal surface of the cylindrical workpiece after (a) machining, (b) 40 min of traditional honing using the in-situ magnetorheological honing (MRH) tool, and (c) 60 min of MR finishing using the same in-situ honing tool.

The dull visibility of scratches, pitting, grooves, and crack marks are observed in the SEM image of the traditional honed surface advocates the substantial improvement as compared to the machined surface. This is because of the honing stones which utilized the fine silicon carbide abrasive grits that applies uniform finishing forces as the honing stones were given uniform and precisely controllable motions through the automated in-situ R-MRH process setup (Fig. 5.7). Figure 5.11 (a) depicts the SEM image of the MR finished internal surface of the cylindrical workpiece using the in-situ honing tool in this work. From this figure, it can be clearly seen that there are rarely surface defects observed in it. Few finishing lines are observed

which are the left deep lays from the initial machined surface. Hence, this substantial enhancement in the surface finish quality, dimensional accuracy, and surface textures of the inside surface of the cylindrical workpiece attained from the machined surface to fine finished using a single in-situ honing tool at a single in-situ R-MRH setup advocates about the capability of this tool for a qualitative finishing with a higher finishing productivity. Thus, the contemporary in-situ honing tool can be economically beneficial by using it for internal fine finishing the various industrial application such as oil pipes, cylindrical mould, a cylindrical barrel of the injection moulding machines, valve bodies, bearings, and hydraulic cylinders, etc.

5.3.3 Conclusions

From the experimentation performed with the newly designed and developed in-situ magnetorheological (MR) honing tool, following conclusions have been made.

- The significant improvement obtained in surface finishing using the present in-situ honing tool for traditional honing and MR honing is found as 63.57 % and 89.09 % respectively which revealed the applicability of this single tool in a good order for performing the traditional honing as well as MR honing.
- The present developed novel in-situ honing tool is found in good agreement for finishing the machined surface to achieve the fine-finishing at a single in-situ R-MRH setup which is beneficial in terms of less time consumption, less power consumptions etc. by avoiding multiple setups from initial surface generation to final fine finished surface.
- The capability of the present developed in-situ magnetorheological (MR) honing tool to finish both traditional honing as well as magnetorheological honing makes this tool to be useful in a great variety of industrial products which requires micro-finishing to fine finishing with a single tool at a single setup.

5.4 Parametric analysis of the developed rotational magnetorheological honing (R-MRH) process for fine finishing of the EN-31 cylindrical workpieces

The developed rotational magnetorheological honing (R-MRH) process is an advanced fine-finishing process with improved finishing capability and productivity. So, in this study, for improving the operational efficiency of industrial cylindrical components made up of EN-31 steel material, the internal surface has been finished using the setup of the R-MRH process as shown in Fig. 5.12. The high carbon steel i.e., EN-31 grade steel material is a crucial material which is used in the bearings, gears, bushes, dies, moulds industries etc (Guo *et* al., 2002).

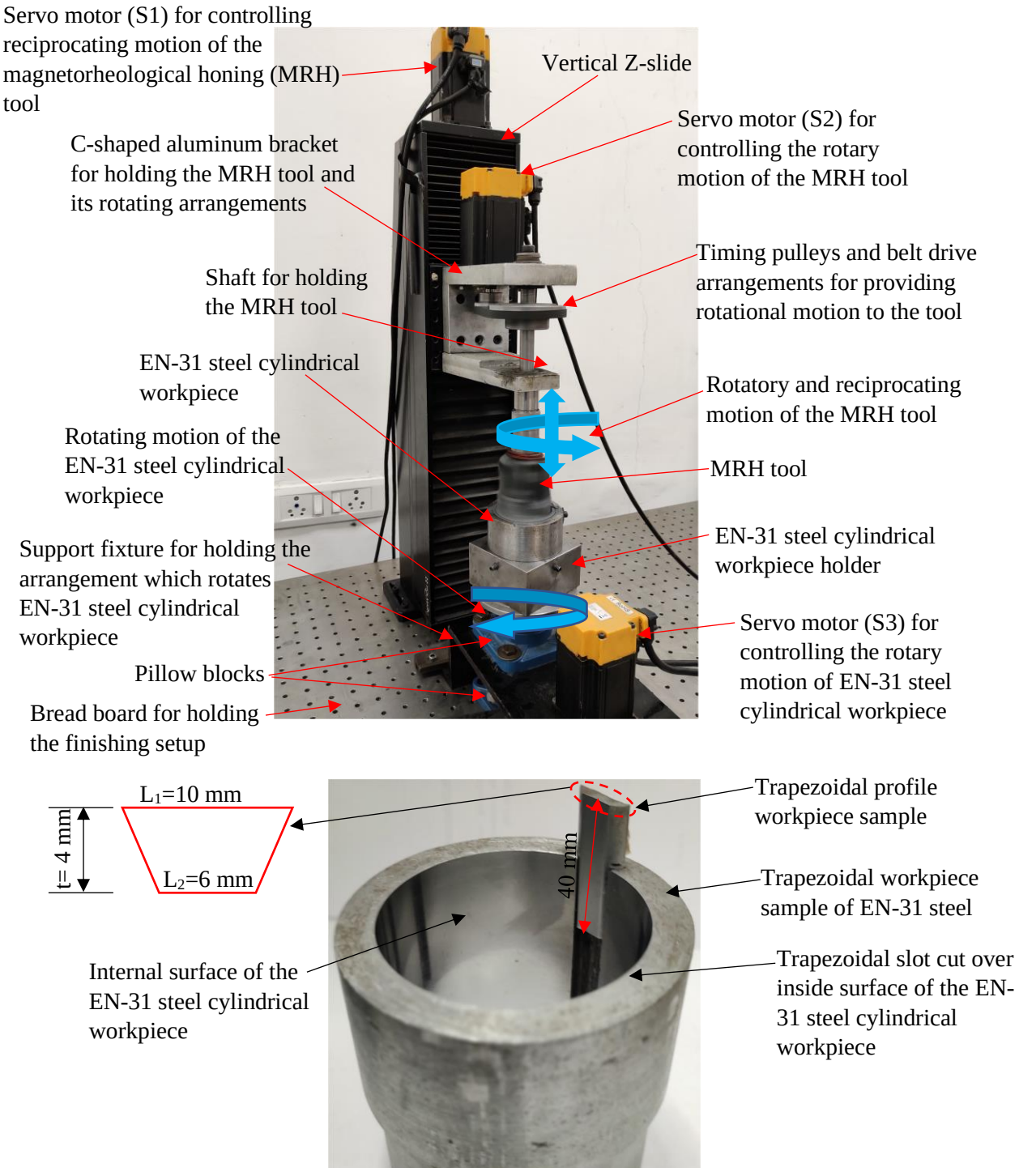

Fig. 5.12 Finishing setup of rotational magnetorheological honing (R-MRH) process for finishing the internal surface of EN-31 steel cylindrical workpiece and its enlarged view.

For analysis of optimum parameters of the R-MRH process to achieve maximum possible finishing on the internal surface of the EN-31 steel cylindrical workpieces, the Response Surface Methodology (RSM) technique has been applied in this work. The RSM is a consolidated technique of graphical, quantitative, and statistical, through which the variables of input and output are established in relation (Yadav et al., 2020). The experiments are done

to achieve the maximum improvement in surface finish, dimensionally excellent surface attributes on the inner surfaces of the EN-31 steel workpiece cylinder with the predicted optimal parameters of the current R-MRH process.

5.4.1 Selection of materials for parametric analysis of the rotational magnetorheological honing (R-MRH) process

The cylindrical workpiece of EN-31 steel materials plays a significant role in the industrial components such as inner outer races of ball bearing (Chen *et* al., 2021; Kanazawa *et* al., 2020). The races of the ball bearing are the important parts as balls of the bearing are inserted within the inner and outer races. As the balls rotated along with the races of the bearing, therefore, fine finishing of the races is a necessary action. This is because if the races are not finely finished, there can be an increase in wear and friction between their surfaces and the balls of the bearing during the functioning of the equipment. Also, due to the increase in wear, the temperature tends to rise which may alter the dimensional accuracy of the bearings. This may tend to reduce the service life of the component. The EN-31 steel has the property to resist the wear, capability to tolerate a high duty load (Trojahn *et* al., 2012). Hence, in the current study, EN-31 steel material is selected as the workpiece cylinder. In this work, firstly a cylindrical workpiece of EN-31 steel material with internal diameter of 61 mm, outer diameter of 80 mm and height of 60 mm is prepared to predict the best variables to apply R-MRH process over this cylinder of EN-31 steel material. The chemical composition of this material is tested on the spectrometer and their %age weight in this material is found as Fe 96.49, C 1.03, S 0.023, P 0.021, Si 0.26, Cr 1.74, Mo 0.08, Ni 0.027, and Cu 0.22. The fabricated cylinder of this material is further featured with a trapezoidal slot cut into its inner surface as demonstrated in Fig. 5.12. This slot is useful for the various tests and characterization of the workpiece samples before and after finishing action is performed on the workpiece's surface. The dimensional description of the trapezoidal slot cut in the cylindrical workpiece of EN-31 steel is kept as 10 mm, 6 mm, and 4 mm ($L_1 \times L_2 \times t$). The L_1 and L_2 are parallel sides of the trapezoidal shape and t is the thickness of the sample. The dimensional feature of the workpiece sample is kept the same as the trapezoidal slot cut made in the inside workpiece cylinder as depicted in Fig. 5.12. As per the number of the designed experiments, the same numbers of the trapezoidal workpiece specimens are prepared. After preparing the workpiece specimens, the initial surface is created by employing the honing which are further being magnetorheological finished. The magnetorheological polishing (MRP) fluid used in the present work consists of the electrolytic iron particles (EIPs), silicon carbide (SiC) polishing abrasives, and base fluid. The volumetric

concentration of each particulate component of the MRP fluid is obtained from the parametric study conducted in this study. The mixture of SiC abrasives, EIPs, and base fluid is further mixed in DC controlled stirring machine. The time taken for stirring the MRP fluid in the mixer varies from 30 to 45 min.

5.4.2 Experimentation

To predict the optimum value of parameters of the rotational magnetorheological honing (R-MRH) process for finishing the internal surface of the cylindrical workpiece of EN-31 steel material this study has been conducted. The prediction of the optimum process parameters is performed through the central composite design in the response surface methodology (RSM) approach. The process parameters used for the present study are inclusively considered based on the works of literature associated with finishing the internal surface of the present material and the finishing process (Grover and Singh, 2019). The selected factors for this study and their levels are reported as in Table 5.6.

Table 5.6 Process parameters and their levels.

Process parameters		Levels				
Symbol	Description	-2	1	0	1	2
S	Volumetric concentration of silicon carbide (SiC) abrasive particles (%)	15	17.5	20	22.5	25
E	Volumetric concentration of electrolytic iron particles (EIPs) (%)	15	17.5	20	22.5	25
T	Rotational speed of the magnetorheological honing tool (rpm)	300	400	500	600	700
A	Reciprocating axial speed of the magnetorheological honing tool (cm/min)	50	60	70	80	90
W	Rotational speed of cylindrical workpiece of EN-31 steel (rpm)	0	10	20	30	40

The considered parameters are the volumetric concentration of the silicon carbide (SiC) abrasive particles (*S*), the volumetric concentration of the electrolytic iron particles (*E*), tool rotation (*T*), tool reciprocating axial speed (*A*), and cylindrical workpiece rotation (*W*). Considering these selected process parameters as the factors and five levels of their values, experiments are designed. Using the factors and their level reported in Table 5.6, fifty experiments are planned through the RSM method in the "Design-Expert 6.0.8 software" which are reported in Table 5.7. To perform the fifty planned experiments, fifty workpiece samples of the EN-31 steel material of the same dimensional specification as discussed earlier in this section are prepared by fabrication and initial surface generation. The initial surface is generated through the traditional honing process. While fabricating the workpiece samples, it

is carefully considered the exactness in the shape and size of these samples with the slot-cut in the workpiece cylinder. This is because it makes it easy for assembling and dissembling the workpiece sample from the slot cut of the workpiece cylinder as presented in Fig. 5.12.

Table 5.7 Designed experiements and the response i.e. improvement in surface finish ($\%\,\Delta Ra$) obtained with 20 min R-MRH finishing on the samples prepared of the EN-31 steel materials.

Sr. No.	Process parameters					Initial average surface roughness (R_{ai}, μm)	Final surface roughness (μm)			Final average surface roughness (μm)	Response ($\%\,\Delta R_a$) (Eq. 5.1)
	S (%)	E (%)	T (rpm)	A (cm/min)	W (rpm)		R_1	R_2	R_3	R_{af}	
1	20	20	500	70	0	0.38	0.20	0.21	0.17	0.19	49
2	20	15	500	70	20	0.37	0.24	0.25	0.20	0.23	38
3	22.5	17.5	600	80	30	0.38	0.33	0.35	0.29	0.32	15
4	20	20	500	70	20	0.36	0.18	0.20	0.14	0.17	52
5	22.5	22.5	600	60	10	0.38	0.24	0.25	0.20	0.23	40
6	22.5	17.5	600	60	30	0.39	0.34	0.34	0.32	0.33	15
7	20	20	500	70	20	0.36	0.18	0.20	0.13	0.17	54
8	20	20	500	70	20	0.37	0.19	0.19	0.16	0.18	52
9	20	20	700	70	20	0.36	0.28	0.29	0.24	0.27	25
10	22.5	17.5	400	80	30	0.37	0.23	0.25	0.19	0.22	40
11	17.5	17.5	600	60	10	0.38	0.28	0.27	0.26	0.27	30
12	22.5	22.5	400	80	30	0.39	0.21	0.22	0.17	0.20	50
13	22.5	22.5	600	80	30	0.36	0.23	0.25	0.19	0.22	38
14	20	20	500	70	20	0.38	0.16	0.15	0.14	0.15	60
15	17.5	22.5	400	60	30	0.37	0.28	0.28	0.24	0.27	28
16	22.5	22.5	400	60	10	0.40	0.29	0.29	0.26	0.28	30
17	20	20	500	70	20	0.39	0.23	0.24	0.19	0.22	44
18	20	20	500	70	20	0.38	0.17	0.20	0.12	0.16	57
19	22.5	17.5	400	60	30	0.36	0.22	0.22	0.19	0.21	42
20	22.5	17.5	600	80	10	0.37	0.27	0.28	0.24	0.26	29
21	20	25	500	70	20	0.36	0.22	0.25	0.16	0.21	43
22	17.5	22.5	400	80	10	0.38	0.28	0.29	0.23	0.27	30
23	17.5	22.5	600	60	10	0.39	0.26	0.28	0.22	0.25	35
24	20	20	500	70	20	0.38	0.19	0.20	0.15	0.18	53
25	20	20	500	70	40	0.37	0.24	0.25	0.20	0.23	38
26	22.5	17.5	400	80	10	0.36	0.18	0.19	0.14	0.17	53
27	17.5	22.5	600	80	30	0.38	0.27	0.28	0.23	0.26	32
28	17.5	17.5	400	60	10	0.39	0.27	0.25	0.26	0.26	33
29	20	20	500	50	20	0.40	0.30	0.32	0.25	0.29	27
30	17.5	17.5	400	80	30	0.40	0.29	0.30	0.25	0.28	30
31	22.5	22.5	600	80	10	0.38	0.19	0.20	0.16	0.18	52

32	17.5	17.5	600	80	30	0.39	0.35	0.34	0.32	0.34	14
33	20	20	300	70	20	0.38	0.30	0.31	0.25	0.29	25
34	22.5	17.5	600	60	10	0.36	0.26	0.27	0.22	0.25	31
35	15	20	500	70	20	0.37	0.27	0.29	0.22	0.26	30
36	17.5	22.5	400	80	30	0.36	0.28	0.26	0.27	0.27	26
37	20	20	500	70	20	0.38	0.19	0.19	0.16	0.18	53
38	17.5	22.5	400	60	10	0.39	0.31	0.32	0.27	0.30	24
39	25	20	500	70	20	0.38	0.21	0.21	0.18	0.20	48
40	22.5	22.5	400	80	10	0.36	0.21	0.22	0.17	0.20	44
41	17.5	17.5	400	60	30	0.38	0.25	0.26	0.21	0.24	37
42	17.5	22.5	600	60	30	0.39	0.28	0.30	0.24	0.27	30
43	20	20	500	90	20	0.38	0.26	0.26	0.22	0.25	35
44	17.5	22.5	600	80	10	0.36	0.23	0.24	0.20	0.22	38
45	17.5	17.5	400	80	10	0.37	0.24	0.26	0.20	0.23	37
46	22.5	17.5	400	60	10	0.39	0.31	0.32	0.27	0.30	24
47	22.5	22.5	600	60	30	0.40	0.26	0.28	0.21	0.25	37
48	22.5	22.5	400	60	30	0.38	0.25	0.25	0.21	0.24	38
49	17.5	17.5	600	80	10	0.39	0.28	0.30	0.24	0.27	30
50	17.5	17.5	600	60	30	0.37	0.28	0.30	0.24	0.27	26

The initial surface roughness over each of the fifty workpiece samples is measured. For conducting the experimentations on these fifty workpiece samples, the experimental parameters and their conditions considered in this work are reported as in Table 5.8. Each experimentation is conducted for 20 min of finishing time on 7665 mm^2 surface area at 40 mm length of the EN-31 steel cylindrical workpiece to be finished. After completion of each planned experiment (Table 5.7) using the present R-MRH process, the surface roughness is measured at three different places (*R1*, *R2*, and *R3*) on the workpiece samples. These measured surface roughness values (*R1, R2, R3*) of each planned experiment are reported in Table 5.7. For calculation of the response in terms of improvement in the surface finish (% ΔRa) in each planned experiment performed for 20 min in this study, the average surface roughness (Ra_f) of measured final surface roughness at three different locations (*R1*, *R2*, and *R3*) is utilized. The response used for further analysis of variance (ANOVA) in the "Design-Expert 6.0.8 software" through the RSM method is calculated from Eq. (5.1).

$$\%\Delta Ra = \frac{(Ra_i - Ra_f)}{Ra_i} \times 100 \tag{5.1}$$

where Ra_i denotes the surface roughness value on the initial traditionally honed surface of the considered work part sample. The RSM method of parameter estimation is centered on mathematics and statistics used in the research and the development of a mathematical formulation for engineering-based problems (Sankar *et* al., 2016). Based on the various

outcomes accomplished from variance analysis (ANOVA), the fit-description, model, diagnostics, and model-graph tabs in this study at a confidence level of less than or equal to 0.05, numerous conclusions have been made.

Table 5.8 Experimental parameters and their condition considered for the experimentations.

Experimental parameters	Condition
Magnetic field induced by each of the four magnets	0.35T
Material of the workpiece cylinder	EN-31 steel
Finishing medium	Magnetorheological polishing (MRP) fluid
Finishing gap	2 mm
Each finishing time	20 min

In the present study, the experimental trials are performed by implementing the samples one after another in the slot of the typical made of the same material as that of workpiece cylinder (Fig. 5.12). The roughness value of the initial honed surface and after 20 min of MR-finished surface is evaluated with the roughness measuring profilometer (Mitutoyo with model number SJ-400). During surface roughness measurement on this instrument, the cut-off length, and number sampling length are kept as 0.25 mm and 5 respectively. Such value of cut-off length (0.25 mm) is considered while measuring the surface roughness because the initial surface is generated from the honing process. Here, the initial surface roughness is found within the limit of 0.36-0.40 μm on each of the fifty EN-31 steel work-part specimens. For experimentations in which the parameters are repeated, the MRP fluid is also replaced after the completion of each experiment.

Further, to observe the perfection in straightness and circularity of the finished surface through the RMRH process, surface waviness measurement and circularity tests are performed on the traditionally honed and the final rotating magnetorheological honed finished interior surface using the best predicted process parameters. The circularity test on the workpiece cylinder is performed on the coordinate measuring machine (CMM). However, the measurement of surface waviness is also performed on the same instrument upon which surface roughness profile is measured. Further to observe the improvement achieved in the surface consistency of the MR-finished surface, the scanning electron microscopy (SEM) (model No. JEOL JSM 6510 LV) experiment is executed on the preliminary and the final finished internal surface of the outer-race of EN-31 steel.

5.4.3 Results and discussion

In the present study, a total of 50 experimentations are conducted to evaluate the outcomes of the selected finishing parameters on the %age improvement in surface finish (*% ΔRa*). The experimental *% ΔRa* (response) is tabulated in Table 5.7. After the experimentation, three Ra values were taken with the assistance of a surface roughness profilometer. To get the final Ra value, the average of three as a final surface roughness (Ra_f) is obtained and reported in Table 5.7. The average final roughness value (Ra_f) is further utilized in Eq. (5.2) to obtain *% ΔRa*. Further, to develop the regression model, an analysis of variance (ANOVA) is utilized. The process parameters with a p-value less than 0.05 are considered as significant parameters and process parameters with a p-value greater than 0.05 are insignificant parameters. The obtained response surface quadratic equation is given in Eq. (5.2).

$$\%\,\Delta R_a = -552.343 + 11.75S + 3.095E + 0.6108T + 6.9724A + 3.712W - 0.514S^2 - 0.454E^2 - 6.7 \times 10^{-4}T^2 - 5.21 \times 10^{-2}A^2 - 2.08 \times 10^{-2}W^2 + 0.37SE - 6.75 \times 10^{-3}ST + 0.0875SA + 0.017ET - 1.56 \times 10^{-3}TA - 2.94 \times 10^{-3}\,TW - \ 0.023AW \quad (5.2)$$

From Eq. (5.2), it can be observed that the significant factors which are taking part in influencing the regression model are found as *S, E, T, A, W, S^2, E^2, T^2, A^2, W^2, SE, ST, SA, ET, TA, TW,* and *AW* as their p-value is less than 0.05. The data corresponding to the ANOVA is reported in Table 5.9. The factors (*S, E, T, A, W*) influence the response (*% ΔRa*) linearly. However, the significant parameters, S^2, E^2, T^2, A^2, and C^2 influence the *% ΔRa* non-linearly. Further, the interaction of *SE, ST, SA, ET, TA, TW,* and *AW* also influence the output response *(% ΔRa*). The p-value of the model after performing ANOVA is found less than 0.05, which shows that the model is significant (Davim, 2001). For lack of fit, the p-value is 0.6372 which is higher than 0.05. This signifies that the lack of fit is not significant. Using Eq. (5.2), the predicted *% ΔRa* is compared with the experimental *% ΔRa* values. It can be validated from the model as the predicted R-square value is 0.77, Adj R-square value is 0.85 and R-square value obtained from the model is 0.90 as reported in Table 5.10. The values of the Adj R-square and predicted R-square signifies that the developed model is enough adequate. Also, the R-squared value is in good agreement to accept this model as this value state that there is a 90 % chance that the predicted surface roughness matches the actual surface roughness.

Table 5.9 Analysis of variance (ANOVA) table for the change in surface roughness (*% ΔRa*) obtained with 20 min of finishing using R-MRH process.

Source	Sum of squares	Degree of freedom	Mean square	F-value	Prob > F		Percentage contribution (%C)
Model	5704.00	17	335.53	17.62	< 0.0001	significant	
S	448.90	1	448.90	23.57	< 0.0001		7.67

E	230.40	1	230.40	12.10	0.0015		3.94
T	136.90	1	136.90	7.19	0.0115		2.34
A	136.90	1	136.90	7.19	0.0115		2.34
W	176.40	1	176.40	9.26	0.0046		3.01
S^2	330.25	1	330.25	17.34	0.0002		5.64
E^2	257.65	1	257.65	13.53	0.0009		4.40
T^2	1441.85	1	1441.85	75.71	< 0.0001		24.63
A^2	869.45	1	869.45	45.66	< 0.0001		14.85
W^2	139.45	1	139.45	7.32	0.0108		2.38
SE	171.13	1	171.13	8.99	0.0052		2.92
ST	91.13	1	91.13	4.79	0.0361		1.56
SA	153.13	1	153.13	8.04	0.0079		2.62
ET	595.13	1	595.13	31.25	< 0.0001		10.17
TA	78.13	1	78.13	4.10	0.0512		1.33
TW	276.13	1	276.13	14.50	0.0006		4.72
AW	171.13	1	171.13	8.99	0.0052		2.92
Residual	609.38	32	19.04				
Lack of fit	460.51	25	18.42	0.87	0.6372	not significant	
Pure error	148.88	7	21.27				2.54
Cor total	6313.38	49					

Further, the influence of each significant parameter and their interaction (linear and non-linear) is determined. The % contribution describes the significance of parameters in the regression analysis of the *% ΔRa*. The weightage of each parameter is calculated by using the ANOVA Table 5.9. The percentage contribution is calculated by using Eq. (5.3).

$$Percentage\ contribution\ = \frac{Sum\ of\ square\ of\ parameter}{Total\ sum\ of\ square\ of\ model} \times 100 \qquad (5.3)$$

Using Eq. (5.3), the percentage contribution of each significant parameter is calculated and reported in Table 5.9. It can be noticed that the SiC abrasives concentration parameters (*S* and S^2) are 10.40 %, tool rotational speed (*T* and T^2) is 14.77 %, and tool reciprocation speed (*A* and A^2) is 10.92 %, the concentration of electrolytic iron particles (*E* and E^2) is 4.08 %, workpiece rotation speed (*W* and W^2) have 2.95 %.

Table 5.10 Other parameters of Analysis of variance (ANOVA).

Parameters	Value
R-Squared	0.90
Adj R-Squared	0.85
Pred R-Squared	0.77
Adeq Precision	14.22

Therefore, the concentration of the SiC abrasive (*S*), tool rotational motion (*T*), and tool

reciprocation motion (*A*) is the majorly contributing process parameters in the *% ΔRa*. The pure error contribution is around 2.30 %. After the regression analysis of the process parameters on the *% ΔRa*, the outcome of the significant parameters has been conferred in this section. The results are observed after the regression analysis of the responses. The effect of percentage concentration of the silicon carbide (SiC) abrasive particles, percentage concentration of electrolytic iron particles, the rotational speed of the MRH tool, the reciprocating speed of the tool, rotational speed of the EN-31 cylindrical workpiece on the percentage reduction in surface roughness (*% ΔRa*) have been observed and evaluated. The effects of these independent controllable variables on the *% ΔRa* value have been discussed as follows.

5.4.3.1 Effect of the volume concentration of silicon carbide (SiC) abrasive particles (S) on percentage change in surface roughness (% ΔRa)

Figure 5.13 depicts the effect of the volume concentration of SiC abrasives on the *% ΔRa*. The % volume concentration of EIPs (*E*), MRH tool rotation (*T*), axial motion of the tool (*A*), and workpiece rotational speed (*W*) are kept constant at 22.5%, 500 rpm, 70 cm/min, and 20 rpm correspondingly. From this figure, it seems that the percentage reduction in surface roughness (*% ΔRa*) rises as S raises to 22.5 %.

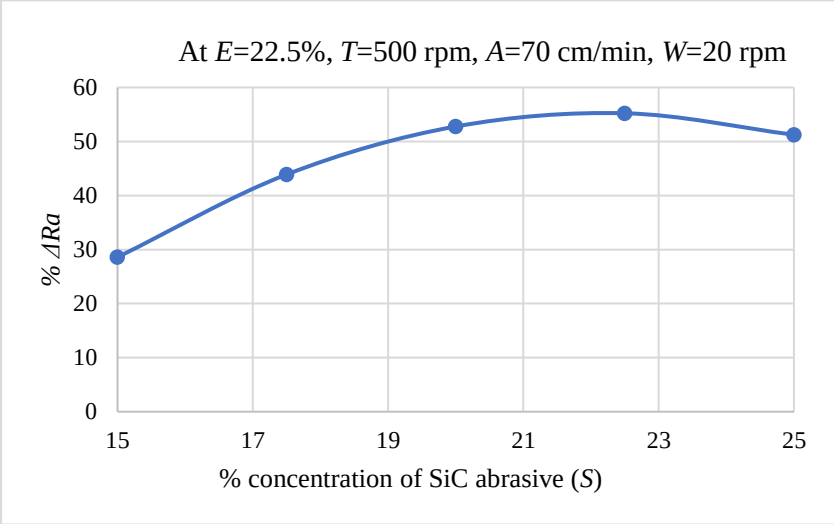

Fig. 5.13 Effect of percentage concentration of SiC abrasive (*S*) on % *ΔRa*.

This is owing as the % *S* increases initially, many active abrasive particles (AAPs) get trapped amid the electrolytic iron particles (EIPs) columnar structure of MRP fluid. Due to this, the large number of abrasive particles cause the enhancement in *% ΔRa*. However, beyond the optimum level of *% S*, the EIPs chain structure gets weaken because large numbers of abrasive

particles are not possibly surrounded by enough EIPs. Due to which it leads to a decrease in the shear strength of the MRP fluid. Further, with the upsurge in the *% S*, the distance between two EIPs (*Y*) increases which reduces the magnetic interaction force as given in Eq. (5.4) (Grover and Singh, 2019). Due to which it leads to a lower material removal rate which decreases the trend line of *% ΔRa*.

$$F_{int} = \frac{\mu_0}{9}\pi\left(\frac{j^4}{W^2}Q^2M^2\right) \tag{5.4}$$

where F_{int} is magnetic interaction force, j is the radius of the electrolytic iron particle (EIP), W is the distance amid the centres of two EIPs, Q is the collect coefficient and M is the magnetization of the magnetic field. The maximum value of the *% ΔRa* was achieved at 22.5 % of the volume concentration of SiC abrasives.

5.4.3.2 Effect of the volume concentration of electrolytic iron particles (EIPs) (E) on percentage change in surface roughness (% ΔRa)

Figure 5.14 depicts the effect of % volume concentration of electrolytic iron particles (*E*) on *% ΔRa*. While evaluating this trend of variation in *% ΔRa* with the change in concentration of EIPs, the tool rotation speed (*T*), axial speed of the tool (*A*), workpiece rotational speed (*W*), and % volume concentration of SiC abrasives (*S*) were kept constant at 500 rpm, 70 cm/min, 20 rpm, and 22.5 % respectively. From this figure, it can be noticed that as the % volume concentration of EIPs (*E*) increases up to the optimum value of 22.5%, the *% ΔRa* trend line increases.

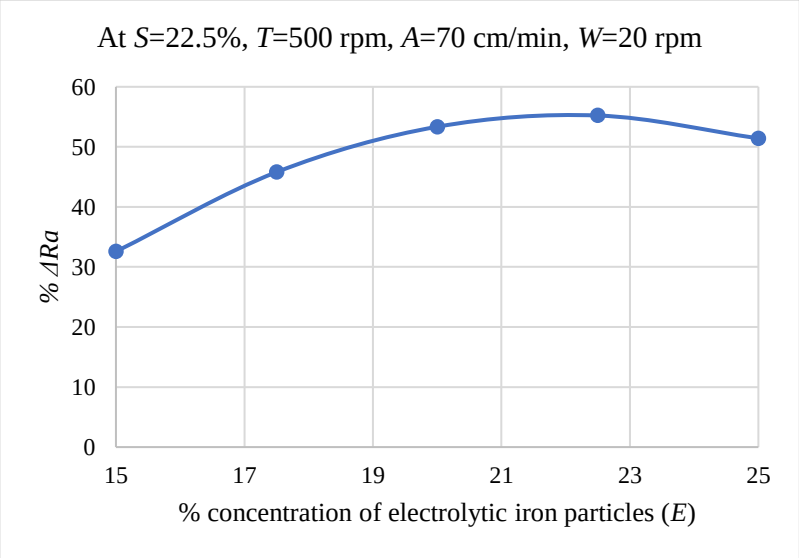

Fig. 5.14 Effects of percentage concentration of EIP particles (*E*) on *% ΔRa*.

This is because, at a lower value of *E*, the distance between the centre of two abrasive (*Y*) increases as in Eq. (5.4) which causes columnar weak structure of EIPs as F_{int} gets decreased. This weak EIPs columnar structure is unable to grip the active abrasive particles (AAPs) rigidly while finishing. But the normal and shear forces increase with the increase in the value of *E*. Furthermore, the magnetic permeability of the MRP fluid increases as the percentage amount of EIPs is increased. This leads to the constant and expansion of the EIPs chains (Khan *et* al., 2018). Moreover, EIPs may form stronger and thicker chains along the magnetic flux lines due to which yield stress of the MRP fluid increases. This leads to the strong gripping of the AAPs in the EIPs chain which performs more cutting the surface asperities during finishing and increases the *% ΔRa*. However, when the value of *E* further increases beyond the optimum value of 22.5%, then the trend of *% ΔRa* decreases. This is because at a higher % volume concentration of the EIPs, adding more EIPs on only aggregates outside the already existing EIPs chain structure leads to a decrease in the number of overall cutting edges of AAPs which are used for the surface finishing (Khan *et* al., 2018). This leads to a decrease in the removal of material from the work part surface. Owing to which there is a decrease in the trend *% ΔRa*. Therefore, the maximum value of the *% ΔRa* was observed at the % volume concentration of EIPs (E) i.e., 22.5.

5.4.3.3 *Effect of the rotation speed of the magnetorheological honing (MRH) tool (T) on percentage change in surface roughness (% ΔRa)*

Figure 5.15 depicts the effect of tool rotation speed (*T*) on *% ΔRa*. Tool axial reciprocation motion (*A*), the workpiece rotation speed (*W*), % volume concentration of electrolytic iron particles, and % volume concentration of SiC abrasives (*S*) were kept constant at 70 cm/min, 20 rpm, 22.5 %, and 22.5 % respectively. It can be observed that as the *T* increases, *% ΔRa* upsurge upto the optimum value of 500 rpm, and then the trend starts decreasing. This is because on increasing *T* initially, the rotational speed of the AAPs that are present in the working space increases. Owing to this, the tangential shear force acting on the AAP upsurges as given in Eq. (3.12) which enhances the shearing of the surface asperities from the work part surface by the tightly gripped AAPs present in the EIPs chain. This increases the material removal rate and surface finishing of the work part, hence, the trend of *% ΔRa* upsurges. However, beyond the optimum value of *T* i.e., 500 rpm, the tangential shear force becomes too high that the AAP tends to loosen the grip in the EIPs chain while finishing. Owing to the loosening of the AAP in the EIP chain, it becomes tough for the AAPs to shear off the surface asperities properly from the work part surface. Hence, the material removal rate decreases due

to which, the trend of the *% ΔRa* decreases at higher tool rotation. So, the decrease in the trend of *% ΔRa* after the optimum value is due to the excess increase of tangential shear force that acts on the AAPs with an upsurge in tool rotation. The maximum value of the *% ΔRa* was attained at the 500 rpm of tool rotation.

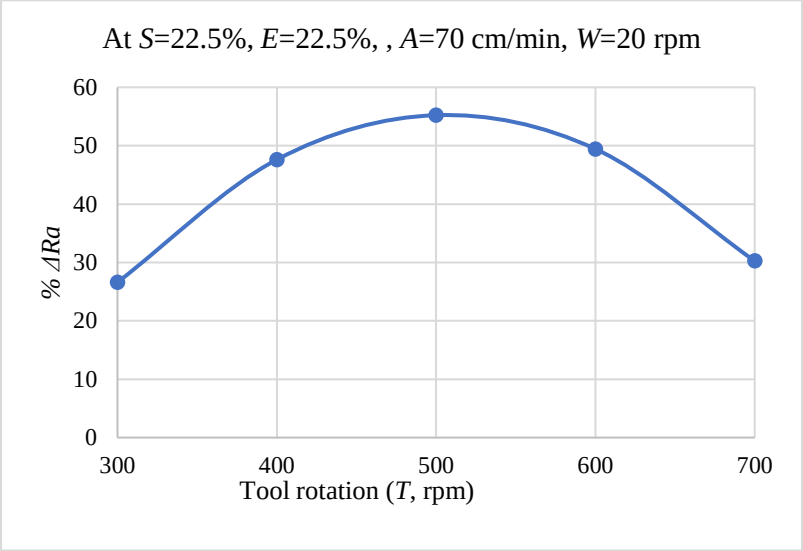

Fig. 5.15 Effects of the rotational speed of magnetorheological honing tool (*T*) on *% ΔRa*.

5.4.3.4 *Effect of the reciprocation speed of magnetorheological honing (MRH) tool (A) on percentage change in surface roughness (% ΔRa)*

Figure 5.16 illustrates the individual effect of the tool axial/reciprocating speed (*A*) on the *% ΔRa*. The rotational speed of tool (*T*), % volume concentration of EIPs (*E*) and % volume concentration of SiC abrasives (*S*), and workpiece rotating speed (*W*) were kept constant at 500 rpm, 22.5 %, 22.5 %, and 20 rpm respectively. From this figure, it is seen that while finishing operation, the speed of axial movement enhances upto optimized value and the trend of *% ΔRa* tends to increase. This is because as the axial speed (*A*) upsurges initially, the relative speed of the AAPs increases along the axial direction. Due to which the axial shear force gets increased as it can be understood with the relation in Eq. (3.14). So, this leads to a higher material abrasion rate causing a fine finishing and a higher *% ΔRa*. However, on further upsurging the axial speed of the MRH tool (*A*) beyond the optimum value, the *% ΔRa* trend tends to decrease. This is because, at a higher value of *A*, the relative speed of the AAPs is enhanced more so that their interaction time with the finishing surface is decreased. The decrease in the interaction time of the AAPs with the finishing surface of the workpiece leads lacking in enhancement in the *% ΔRa*.

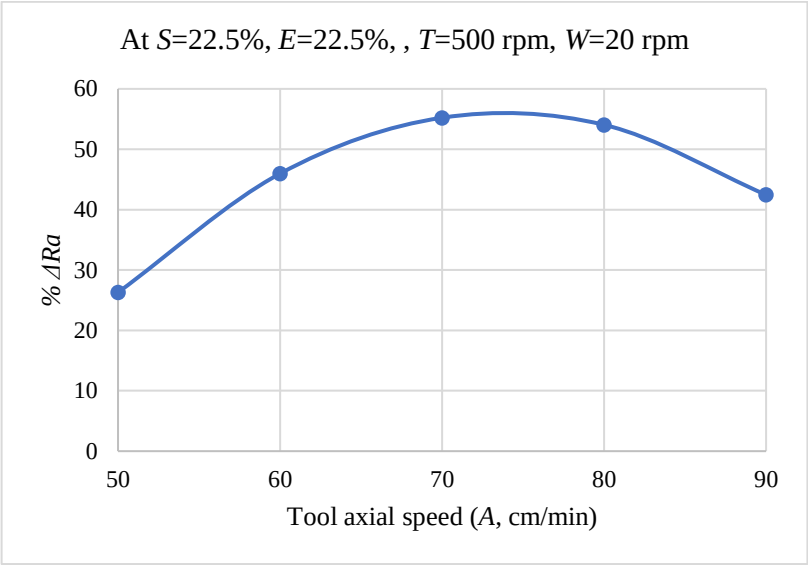

Fig. 5.16 Effect of the reciprocation speed of the magnetorheological honing tool on *% ΔRa*.

5.4.3.5 Effect of the rotational speed of the EN-31 steel workpiece (W) on percentage change in surface roughness (% ΔRa)

Figure 5.17 depicts the effect of workpiece rotational motion (*W*) on *% ΔRa*. The rotational speed of tool (*T*), % volume concentration of EIPs (*E*), and % volume concentration of SiC abrasives (*S*) and the axial speed of the MRH tool (*A*), were kept constant at 500 rpm, 22.5 %, 22.5 %, and 70 cm/min respectively. As the workpiece rotational speed (*W*) increases up to the optimum value of 20 rpm, there is an upsurge in the net tangential shear force as given in Eq. (3.12). Due to this, the shearing of the surface asperities from the work part surface by the AAPs upsurges.

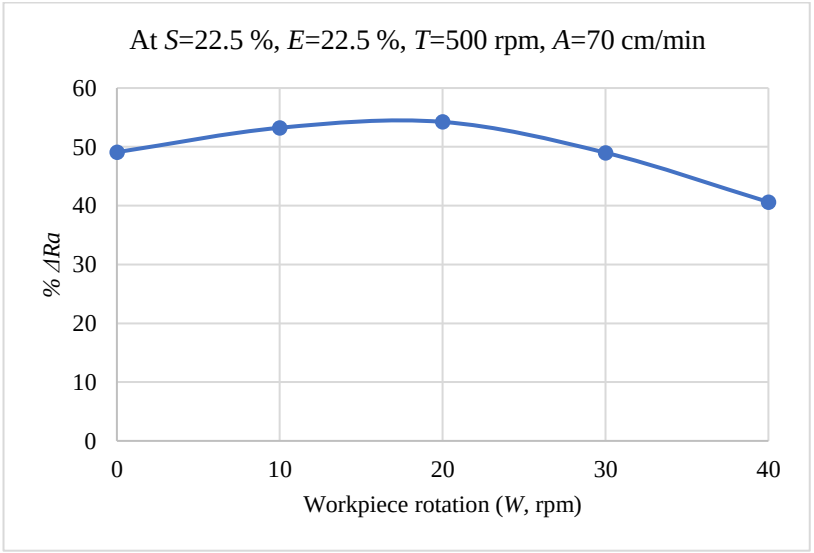

Fig. 5.17 Effect of the rotational speed of EN-31 steel workpiece (*W* rpm) on *% ΔRa*.

This leads to an increase in material abrasion rate which upsurges the trend of *% ΔRa*. However, when the workpiece rotation speed goes beyond the optimum value of workpiece rotation 20 rpm, there is a decrease in the trend of *% ΔRa*. This is because as the *W* speed is increasing, the interaction time during which asperities in the surface and the AAPs collide can decrease. Due to this reduced interaction time, the AAPs are not able to shear off the surface asperities properly in a short moment which leads to a decrease in *% ΔRa*. The maximum value of the *% ΔRa* was achieved at the 20 rpm of workpiece rotation.

5.4.3.6 Interaction effect of the concentration of silicon carbide (SiC) abrasives (S) and electrolytic iron particles (EIPs) (E) on the percentage change in surface roughness (% ΔRa)

Figure 5.18 illustrates the simultaneous effect of the concentration of SiC abrasives and electrolytic iron particles (EIPs) on the *% ΔRa*. While, plotting this graph rest of the parameters i.e., rotational speed of tool (*T*), axial motion of the tool (*A*), and the workpiece rotation (*W*) were kept constant at 500 rpm, 70 cm/min, and 20 rpm correspondingly. In order to achieve substantial surface finish, an adequate concentration of SiC abrasive particles in the MRP fluid relative to the concentration of EIPs must be available.

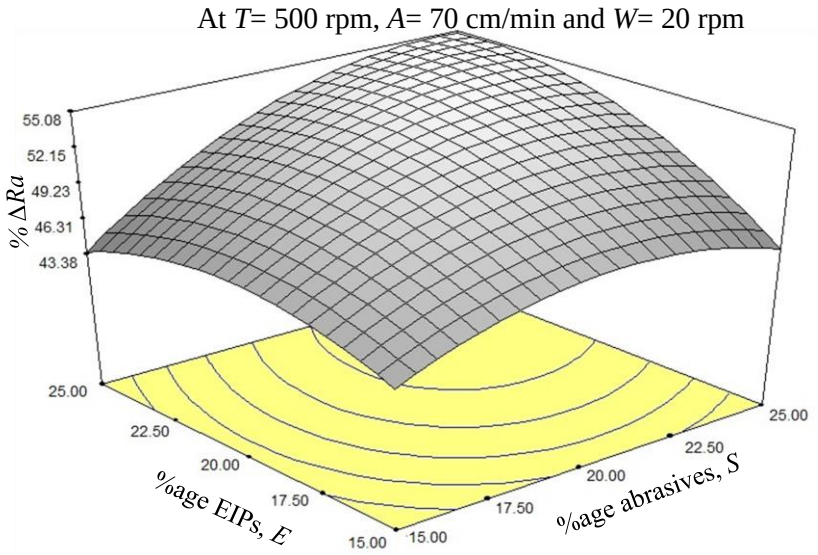

Fig. 5.18 Combined effect of volumetric %age of silicon carbide (SiC) abrasive particles (*S*) and electrolytic iron particles (*E*) on *% ΔRa*.

To grasp the abrasive particles, the EIPs of the MRP fluid produce chains. If the percentage concentration of SiC abrasives is significantly low for a given concentration of EIPs, it may result in less reduction in surface roughness value due to fewer numbers of sharp-edged SiC particles. With low abrasive concentration, the number of active abrasives present over the

surface of the workpiece stays lower to perform sufficient finishing. Also, even though the %age concentration of SiC abrasives is too high for the same quantity of EIPs in the fluid, it may consequence to less improvement in surface finish. This is owing to a great number of SiC abrasives found least chance to be gripped properly by the same quantity of the EIPs columnar chains. In the MRP fluid, the SiC abrasives stay slack, which adversely affects the finishing of the internal cylindrical surface of the workpiece. Figure 5.18 indicates that the highest *% ΔRa* value is attained using a 22.5 % concentration of the EIPs. Also, this value of EIP's concentration is required to adequately firmly hold the 22.5 % SiC abrasive particles of the MRP fluid when rest of constituents are constant as discussed above. Therefore, with a mixture of 22.5% concentration of EIPs and 22.5% concentration of SiC abrasives in MRP fluid, maximum surface roughness reduction (*% ΔRa*) is accomplished.

5.4.3.7 Interaction effect of rotational speed of the magnetorheological honing (MRH) tool (T) and % volumetric concentration of SiC abrasives (S) on the percentage change in surface roughness (% ΔRa)

Figure 5.19 indicates the combined effect of the different rotating speeds of the MRH tool (*T*) and % volumetric concentration of SiC abrasives (*S*) on *% ΔRa* at a constant value of other parameters such as *A*=70 cm/min, *E*=22.5% and *W*=20 rpm. From this graph, it is observed that the rise in tool rotation speed results in an increase in the percentage change in surface roughness (*% ΔRa*) value for a given concentration of SiC abrasive particles. This happened because as the rotary speed of the MR-honing tool gains, the extent of the total cutting shear force, F_s (Eq. 3.15) acting over the active abrasive upsurges. However, with a given concentration of SiC abrasives (22.5 %), the increase in the *% ΔRa* limits the rotating speed of the tool to a specific value of 500 rpm. The *% ΔRa* begins decreasing after achieving 500 rpm tool rotation speed and *S* is 22.5 %. This is because the MRP fluid's binding force does not remain high sufficient to firmly grip the abrasives and removes the material from the interior of workpiece's finishing surface beyond the MRH tool's rotational speed (500 rpm). The centrifugal force applied on the EIPs due to the rotation of the tool weakens the normal magnetic force acting after 500 rpm of tool rotation in between magnetic iron particles. In the present analysis, the more rise in the concentration of SiC abrasives exceeding 22.5 % makes it hard for EIP chains to tightly grip them.

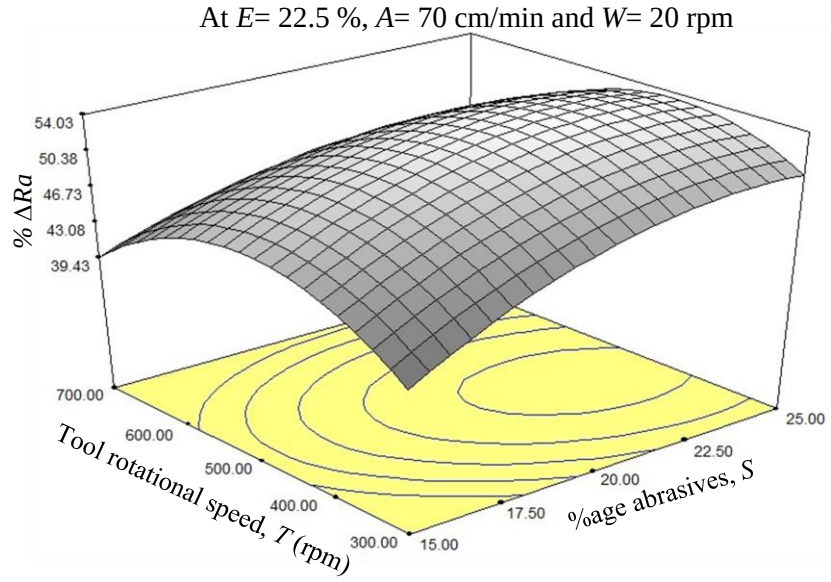

Fig. 5.19 Combined effect of volumetric %age of silicon carbide (SiC) abrasive particles (*S*) and rotational speed of the MRH tool (*T*) on *% ΔRa*.

Therefore, with the greater %age concentration of SiC abrasives, i.e., after 22.5 % to 25 %, the *% ΔRa* reduces. The highest *% ΔRa* is achieved with an optimal combination of 22.5 % of the concentration of SiC abrasives with a 500 rpm rotating MRH tool.

5.4.3.8 Interaction effect of % volumetric concentration of SiC abrasives (S) and reciprocating speed of the MRH tool (A) on the percentage change in surface roughness (% ΔRa)

In Fig. 5.20, the cumulative effect of SiC abrasive concentrations and the axial speed of the MRH tool on *% ΔRa* with 22.5 % of EIP concentration, 500 rpm of the MRH tool's rotating speed, and 20 rpm of the workpiece rotation is found. As the axial speed of the MRH tool increases, the axial shear force acting on the abrasives increases (Eq. 3.14). So, they abrade more material that contributes to an improved *% ΔRa*. The *% ΔRa* value upsurges with the upsurge in the %age concentration of abrasive particles up to 22.5 % for a specific axial speed of the MRH tool, as it is seen in Fig. 5.20. This is because of the enhancement in %age concentration of the SiC abrasives which further upsurges the number of the sharp-cutting-edged abrasives. However, further, an increase in %age accumulation of the SiC abrasives beyond the 22.5 % causes the reduction in *% ΔRa* in the current analysis. The explanation behind it is the concentration on the inner surface of the cylindrical workpiece of a larger number of abrasive particles that could not be effectively retained by the iron particles' chains.

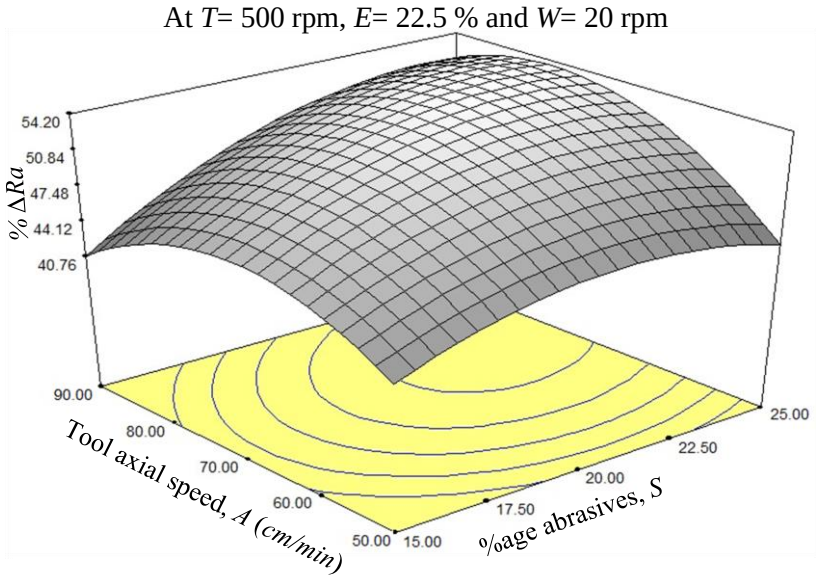

Fig. 5.20 Combined effect of % volumetric concentration of SiC abrasive particles (*S*) and reciprocating speed of the MRH tool on *% ΔRa*.

Easily scattered abrasives travel along the inner side of the cylindrical surface and are incapable of finishing. With the axial speed of the MRH tool, the percentage important in the surface finish (*% ΔRa*) upsurges but restricts it to a speed of 70 cm/min. With further addition in the axial speed of the magnetic MRH tool, the duration of the interaction of the AAP with the interior workpiece's finishing surface decreases which consequences to decreased finishing effectiveness. A mixture of 22.5 % SiC abrasives concentration in the MRP fluid with 70 cm/min axial speed of the MRH tool obtains the highest *% ΔRa*.

5.4.3.9 Interaction effect of % concentration of the electrolytic iron particles (EIPs) (E) and the rotational speed of the MRH tool (T) on the percentage change in surface roughness (% ΔRa)

Figure 5.21 presents the combined effects of the %age concentration of the electrolytic iron particles (EIPs) and the rotational speed of the MRH tool on the %age improvement in the surface finish (*% ΔRa*) when S= 22.5%, *A*=70 cm/min, and *W*=20 rpm. This figure displays that that with an initial enhancement in %age concentration of the EIPs and the tool rotation the *% ΔRa* increases. This happens because the large number of EIPs can strongly grip the SiC abrasive particles which act like material removing tool. The stiffly griped SiC abrasive may cause conveniently abrasion of materials. However, the initial increasing tool rotation causes the AAPs to apply the enhanced tangential shear force due to their enhanced relative speed as it can be well understood with Eq. (3.12). But this increasing trend of the *% ΔRa* continues till

T=500 rpm and *E*=22.5 % by achieving maximum improvement in surface finish. Beyond these values of *T* and *E*, the *% ΔRa* starts decreasing.

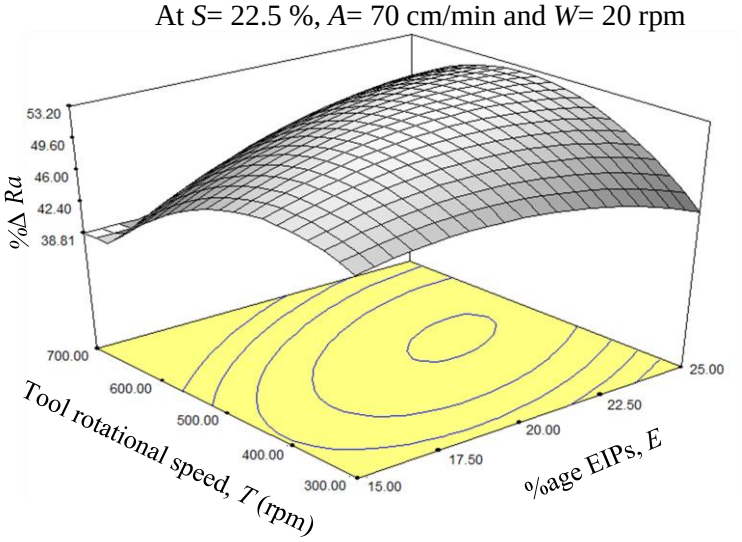

Fig. 5.21 Combined effect of % concentration of the electrolytic iron particles (EIPs) (*E*) and the rotational speed of the MRH tool (*T*) on *% ΔRa*.

This happens because excess of the EIPs cause less exposure of fresh edges of the SiC abrasive particles due to surrounded by the magnetized iron particles. However, further increasing of the tool rotation causes the dominance of the centrifugal force over the magnetic force on the EIPs chains. Due to this the EIPs chains become instable which results in decrement in the finishing performance by reduction in *% ΔRa*.

5.4.3.10 Interaction effect of the reciprocation speed (A) and the rotational speed of the magnetorheological honing (MRH) tool (T) on the percentage change in surface roughness (% ΔRa)

Figure 5.22 shows the combined effect of the magnetorheological honing (MRH) tool rotation and reciprocation motion (*T* and *A* respectively) on the %age change in surface roughness (*% ΔRa*) when other parameters are kept constant as *S*= 22.5 %, *E*=22.5 %, and *W*=20 rpm. From this figure, it can be observed that with simultaneous initial enhancement in *T* and *A*, the *% ΔRa* increases. This is because with increasing in *T* and *A*, cause the enhancement in the tangential and axial force applied by the active abrasive particles (AAPs) as it can be well understood with Eqs. (3.12 and 3.14). Such trend of increasing *% ΔRa* continues upto *T*=500 rpm and *A*=70 cm/min. Beyond this value of *T* and *A*, the *% ΔRa* starts decreasing. This is because with excess increase in *T* causes instability of the EIPs chain structure. However, the interaction time of the AAPs gets decreased due to increasing beyond the limit in *T* and *A*.

Therefore, the instability in chain structures and less interaction time of the AAPs results in decrement in *% ΔRa*.

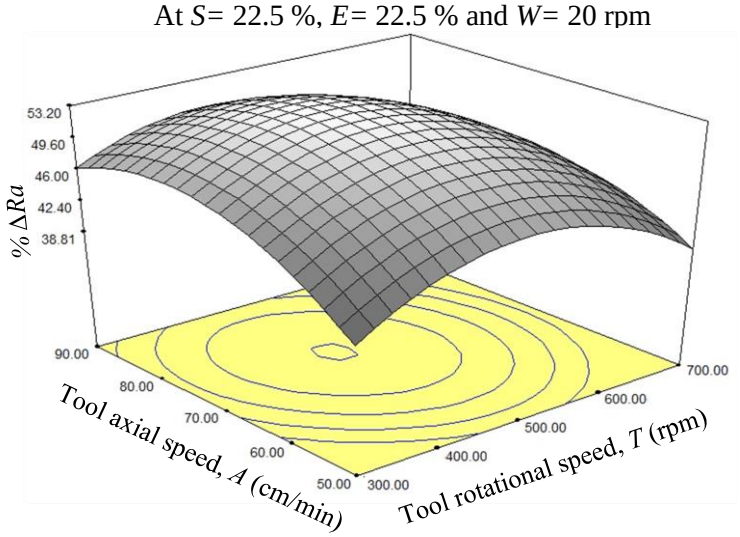

Fig. 5.22 Combined effect of the reciprocation speed (*A*) and the rotational speed of the magnetorheological honing (MRH) tool (*T*) on *% ΔRa*.

5.4.3.11 Interaction effect of the MRH tool rotation (T) and workpiece rotation (W) on the percentage change in surface roughness (% ΔRa)

Figure 5.23 shows the combined effect of the magnetorheological honing (MRH) tool rotation (*T*) and workpiece rotation (*W*) on the %age change in surface roughness or improvement in surface finish (*% ΔRa*) when concentrations of SiC abrasives (*S*) and EIPs (*E*), and axial speed of tool (*A*) are maintained at constant values of the parameters such as 22.5 %, 22.5 % and 70 cm/min correspondingly. This figure displays that with initial increase in *T* and *W*, the *% ΔRa* increases. This is because by increasing these parameters, the shear force applied by the AAP on the finishing surface of the workpiece increases as in Eq. (3.12). But, this trend in *% ΔRa* starts decreasing after achieving *T*=500 rpm and *W*=20 rpm. This happens because further increasing in their values, the EIPs chain get instable because of dominance of centrifugal force over magnetic force exerted by the EIPs chain structure. Also, the increment in *T* and *W* beyond the optimum value causes the significant reduction in interaction time of the AAPs due to their more enhanced relative motion. Therefore, the reduced interaction time of the AAPs with the finishing surface of the workpiece results in lesser finishing performance by reduced *% ΔRa*.

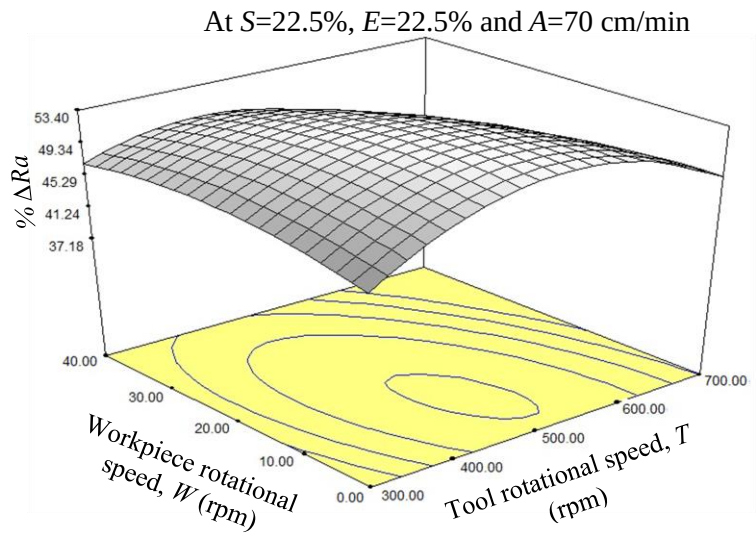

Fig. 5.23 Combined effect of the MRH tool rotation (*T*) and workpiece rotation (*W*) on *% ΔRa*.

5.4.3.12 Interaction effect of the speed of reciprocation speed of the MRH tool (A) and the speed of workpiece rotary motion (W) on the percentage change in surface roughness (% ΔRa)

Figure 5.24 depicts the combined effect of the speed of axial movement of the tool (*A*) and speed of workpiece rotary motion (*W*) on the %age improvement in surface finish (*% ΔRa*) when concentrations of SiC abrasives and EIPs (*S* and *E* respectively) and tool rotation (*T*) are kept constant at 22.5%, 22.5% and 500 rpm respectively. From this figure, it can be observed that with increase in *A* and *W*, the *% ΔRa* increases.

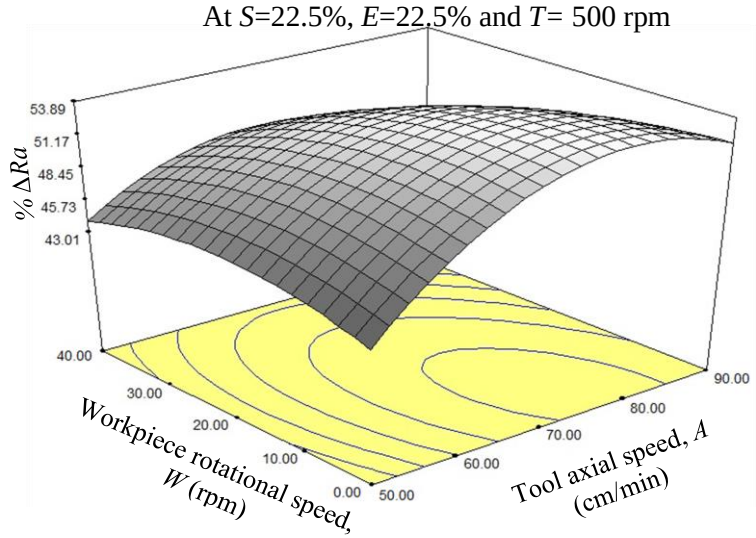

Fig. 5.24 Combined effect of the speed of reciprocation speed of the MRH tool (*A*) and the speed of workpiece rotary motion (*W*) on *% ΔRa*.

The increasing of these parameters reasons the improvement in the relative speed of the AAPs along the tangential and axial direction both. Therefore, due to this increment in the relative speed of the AAPs, the overall cutting shear force increases which can be well understood by the Eq. (3.15). The increasing trend of the $\%\,\Delta Ra$ continues up to A=70 cm/min and W=20 rpm and after that it starts decreasing. This decrement in the $\%\,\Delta Ra$ is caused by reduced interaction time of the AAPs which is because of the upsurge in the additional relative speed of the abrasive particles along with the tool rotation. Therefore, beyond the optimum value of the A and W the $\%\,\Delta Ra$ decreases as displayed in Fig. 5.24.

5.4.4 Confirmatory experiments

Therefore, from the complete analysis of the RSM study, the optimum process parameters are obtained as E= 22.5 %, S=22.5 %, T=500 rpm, A=70 cm/min, and W=20 rpm for effectively finishing the EN-31 steel cylindrical workpiece's internal surface. To ensure the repeatability of the regression model obtained in this study through the implementation of the response methodology (RSM) technique, further five experimentations were performed. The finishing time of the experiments were taken as 20 min as equal to the finishing time of the designed experiments. Also, the values of the parameters were kept within the range of the designed experiments (Table 5.7). The parameters considered for these five random experimentations are reported as in Table 5.11. For these five experiments initial and final surface roughness were measured while experimentations. With the help of the experimental measured surface roughness values, the %age change in surface roughness ($\%\,\Delta Ra$) was calculated using Eq. (5.1). The substituting the values of the process parameters in the regression model (Eq. 5.2), the predicted $\%\,\Delta Ra$ is calculated and reported as in Table 5.11. Therefore, from this table, the predicted and experimental $\%\,\Delta Ra$ were compared using % error. The % error is calculated using Eq. (5.5).

$$\%\,error = \frac{(Experimental\,\%\,\Delta Ra - Predicted\,\%\,\Delta Ra)\times 100}{Experimental\,\%\,\Delta Ra} \tag{5.5}$$

Therefore, to get the finishing ability of this R-MRH process for interior surface finishing of the workpiece cylinder of the EN-31 steel, further finishing operation is performed on the cylindrical workpiece EN-31 steel material using the optimum process parameters obtained in this study. In this work, the finishing action on the interior surface of the workpiece cylinder of the EN-31 steel is conducted until the extensive enhancement in surface finish is not noticed. The finishing time of each set of finishing were taken as 20 min. The finishing operation was

carried out on a 40 mm length of EN-31 cylindrical workpiece which finished approximately 7665 mm^2 of surface area.

Table 5.11 Confirmation experiments for validating the regression model.

Sr. No	Process parameters					Initial average surface roughness, Ra_i (nm)	Final average surface roughness, Ra_f (nm)	Experimental % ΔRa (Eq. 5.1)	Theoretical % ΔRa (Eq. 5.2)	% Error (Eq. 5.5)
	S (%)	*E* (%)	*T* (rpm)	*A* (cm/min)	*W* (rpm)					
1	20	20	300	70	20	410	290	29.00	29.84	-2.88
2	22.5	17.5	600	60	10	400	290	27.00	24.35	9.82
3	15	20	500	70	20	380	250	32.00	33.66	-5.19
4	17.5	22.5	400	80	30	370	270	26.00	25.35	2.52
5	20	20	500	70	20	390	200	48.72	53.21	-9.22

Therefore, to track the improvement in the surface finish after each set of finishing action the surface roughness was measured. The surface roughness reduced from 390 nm to 60 nm in 40 min of finishing cycle time. The roughness values after every 20 min reduced as 180 nm and 60 nm respectively. After 40 min of finishing cycle no much significant improvement was observed. The total % ΔRa improvement after 40 min of finishing cycle over 7665 mm^2 was observed as 84.61 %.

5.4.5 Analysis of the performance of the R-MRH process with the optimized parameters

To acknowlegdge the finishing performance of the present R-MRH procee on the EN-31 steel workpiece, the surface roughness profiles of the initial and final finished surface was measured and compared. Figures 5.25(a) and (b) demonstrate the surface roughness profiles of initial honed surface and final MR finished internal surface of EN-31 steel. Figure 5.25(a) reflects the before MR finishing surface roughness profile parameters that are recorded and achieved as *Ra*= 390 nm, *Rz*= 2500 nm, *Rq*= 500 nm. However, Fig. 5.25(b) exihibits the profile of surface asperity of the interior surface of the currently MR-finished EN-31 cylindrical workpiece after 40 min of finishing with optimised parameters. The final finished surface roughness parameters on the inside surface of workpiece cylinder are observed as *Ra*= 60 nm, *Rz*= 600 nm, *Rq*= 90 nm with the R-MRH finishing process. The %age reduction in the roughness variables of the arithmetic mean of roughness (Ra), the highest peak value of roughness (Rz) and the root mean square of roughness (Rq) is thus attained after 40 min of the R-MRH method, using the best parameters on the surface of the typical EN-31 cylindrical workpiece as 84.61 %, 76 % and 82 % respectively.

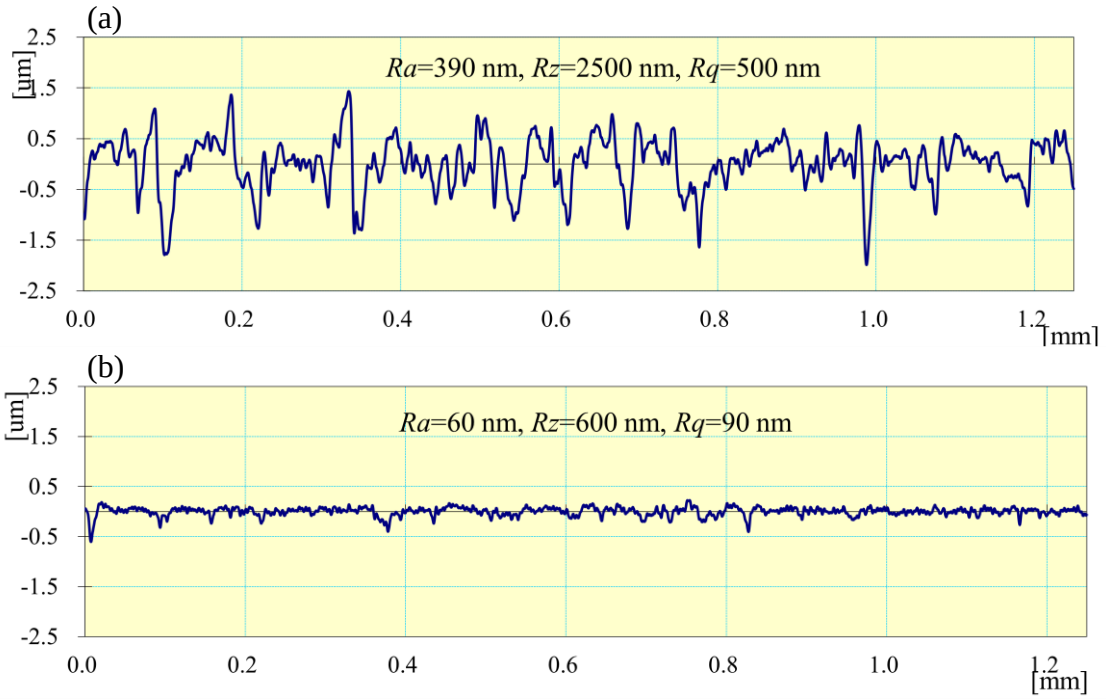

Fig. 5.25 Surface roughness profile of (a) initial honed surface (b) after 40 min of final finished surface area 7665 mm^2 through R-MRH process with optimized finishing parameters.

Consequently, the finishing rate is obtained as 8.25 nm/min. Whereas, in the permanent magnet based magnetorheological honing (MRH) process when workpiece rotation was kept stationary (Grover and Singh, 2019), the minimum surface roughess was reduced to *Ra*=95 nm from *Ra*=476 nm of initial surface roughness in 120 minutes. The finishing rate obtained from this study was found as 3.175 nm/min. This degree of variation in surface roughness profile parameters from the before MR-finished to the after MR-finished surface confirms the substantial increase in surface finish. Therefore, the use of the current R-MRH method to finish the inside surface of the EN-31 cylindrical workpiece is a good deal for improving the finishing productvity and quality of surface finish significantly to increase its operational performance.

The surface waviness parameters were determined using the same surface roughness profilometer to validate the improvement in surface waviness obtained on the inside surface of the EN-31 cylindrical workpiece through the current R-MRH process. These waviness parameters were measured on the surface before and after performing the R-MRH operation. The waviness parameters were reported as *Wa*= 380 nm, *Wz*= 1700 nm, *Wq*= 410 nm on the prior R-MRH finished surface of the present workpiece surface as depicted in Fig. 5.26(a). The final waviness parameters were attained to *Wa*= 80 nm, *Wz*= 400 nm, *Wq*= 100 nm by finishing this surface with R-MRH process for 2 sets (each 20 min) of finishing time (40 min). The

surface waviness profiles on the final finished surface is illustrated in Fig. 5.26(b). Therefore, the %age change in arithmetic mean of surface waviness (*Wa*), root means surface waviness square (*Wq*), and the highest surface waviness peak value (*Wz*) were observed as 78.94 %, 76.47 %, and 75.60 % with 40 min of present finishing operation on the inner of the EN-31 cylindrical workpiece. These %age change in waviness parameters also demonstrate the capacity of the R-MRH process to significantly increase the straightness, increasing the dimensional precision as well as the fits and tolerances of the EN-31 steel cylindrical workpiece.

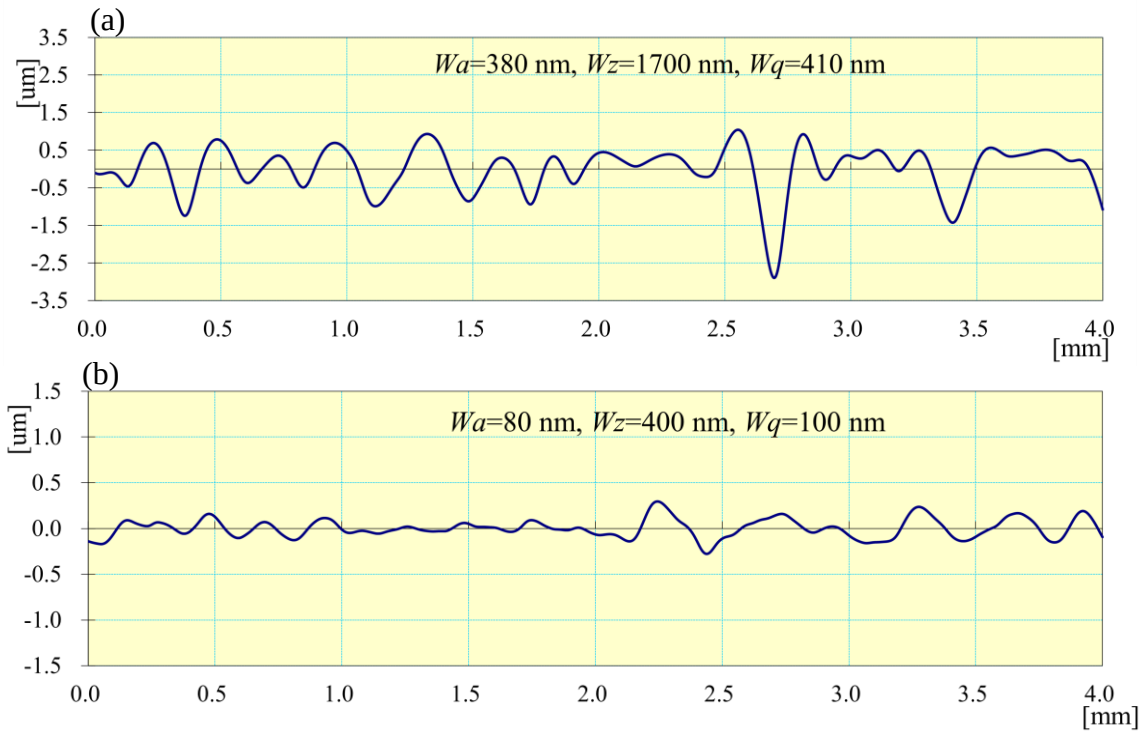

Fig. 5.26 Surface waviness profile of (a) initial honed surface, and (b) after 40 min of final finished surface area 7665 mm^2 through R-MRH process with optimized finishing parameters.

Therefore, it can be said that the use of R-MRH process for improving the dimensional exactness, straightness, fits and tolerances on an industrial cylindrical product of EN-31 steel material may be a better alternative for the manufacturing industries. To assure the improved performance in improving the circularity of the interior surface of the cylindrical workpiece of EN-31 steel as achieved with 40 min of rotating magnetorheological honed at optimised process variables, the circularity inspection was done on the initial honed surface and final rotating magnetorheological honed surface using the coordinate measuring machine. The circularity of a cylinder indicates that how well the circle of the cylinder is similar to its true circle. Thus, the circularity gives the part's dimensional precision (Arab and Dixit, 2020).

Dimensional precision is needed to limit vibration and rise in temperature in the cylindrical products while it is performing its functional activity (Tan *et* al., 2019*)*. Therefore, to affirm the improvement in the circularity achieved on the inside surface of the cylindrical workpiece of EN-31 steel by finishing this surface with present R-MRH process, circularity of the initial honed as well as final MR finished surface has been measured. Fig. 5.27(a) displays a description of the circularity of the initial honed interior surface of the cylindrical workpiece of EN-31 steel.

The circularity was accessed as 0.1904 on this surface. It can be noted from the circularity image of the initial honed surface (Fig. 5.27(a)) that most of the points reported on that surface have differed from the circularity graph's true circle. Whereas, Fig. 5.27(b) demonstrates the image of the circularity of the final finished inner surface surface of the cylindrical workpiece of EN-31 steel with R-MRH process. As most of the observed points either are on or very close to the true circle, the large increase in the circularity can be easily noticed. The circularity value was found as 0.0275. Figures 5.27(a) and (b) indicate that after R-MRH process over the inside surface of the cylindrical workpiece of EN-31 steel at the optimum finishing parameters, most of the points captured in the circularity image are located closer to the true circle. As the snapped points are nearest to the true circle, the degree of circularity is claimed to be higher. Consequently, Fig. 5.27(b) means that the present R-MRH method is considered to be useful for improving the internal surface circularity of the cylindrical workpiece of EN-31 steel. Therefore, based on the degree of improvement in the circularity attained by finishing it with the R-MRH process on the inside surface of the cylindrical workpiece of EN-31 steel, it can be said that other important industrial components of EN-31 materials can also be finished to enhance their functional performance similar to the present component. Figures 5.28(a) and (b) are showing the images of scanning electron microscopy (SEM) performed on before R-MRH finished and after R-MRH finished inner surface of the cylindrical workpiece of EN-31 steel after 40 min at optimized parameters. Figure 8.28(a) demonstrate various kinds of surface faults like honing lays, surface irregularities, shallow grooves, cracks, etc. These defects in surface are as a result of the solid-solid contact of the honing stone with the interior surface of the cylindrical workpiece of EN-31 steel while generating the initial surface.

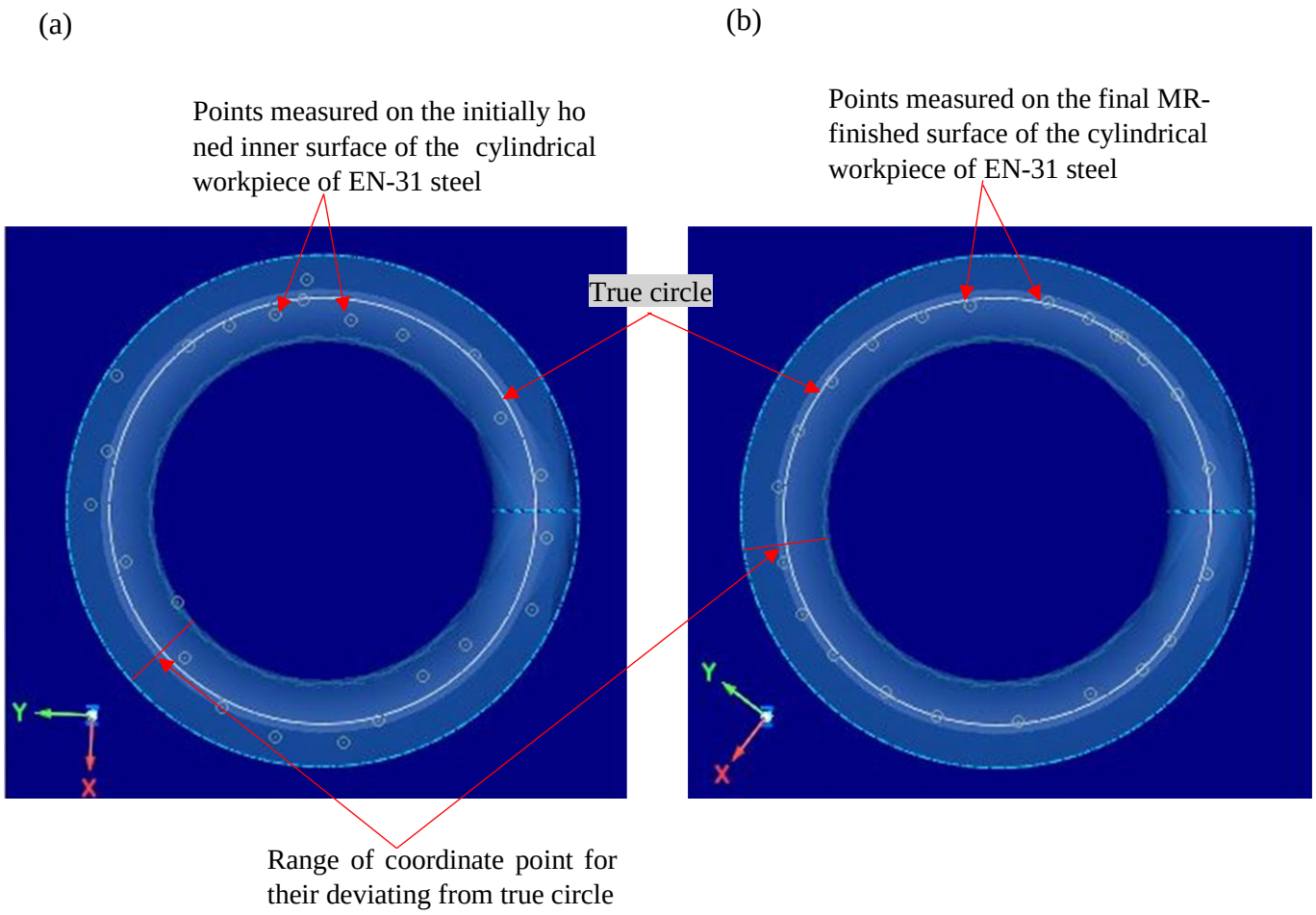

Fig. 5.27 Circularity images of (a) the initial internal honed surface, and (b) the final MR-finished surface using its optimised parameters with a 40 min of R-MRH operation on 7665 mm^2 of surface area of cylindrical workpiece.

The visible size of the abrasives rigidly bonded in the honing stone results in such a various types flaws on surface are revealed in Fig. 5.28(a). However, with the use of the R-MRH process on the initial traditionally honed inner side of present work-part, the micro-sized SiC particles of the MRP fluid abrade the material in the form of micro-chip. The material abrasion action performed by these micron-sized loose abrasives of the MRP fluid results in the fine-finished and defect-free inner surface of the cylindrical workpiece of EN-31 steel as depicted in Fig. 5.28(b). Therefore, on comparing Figs. 5.28(a) and (b), it can be easily observed that using the R-MRH process, the surface texture of the various types of industrial components of EN-31 steel like outer race of ball bearing can significantly be improved. Therefore, the major improvement in the MR finished surface texture, circularity, and waviness on the interior surface cylindrical workpiece of EN-31 steel indicates that the R-MRH process can be a great deal to upgrade its practical utility.

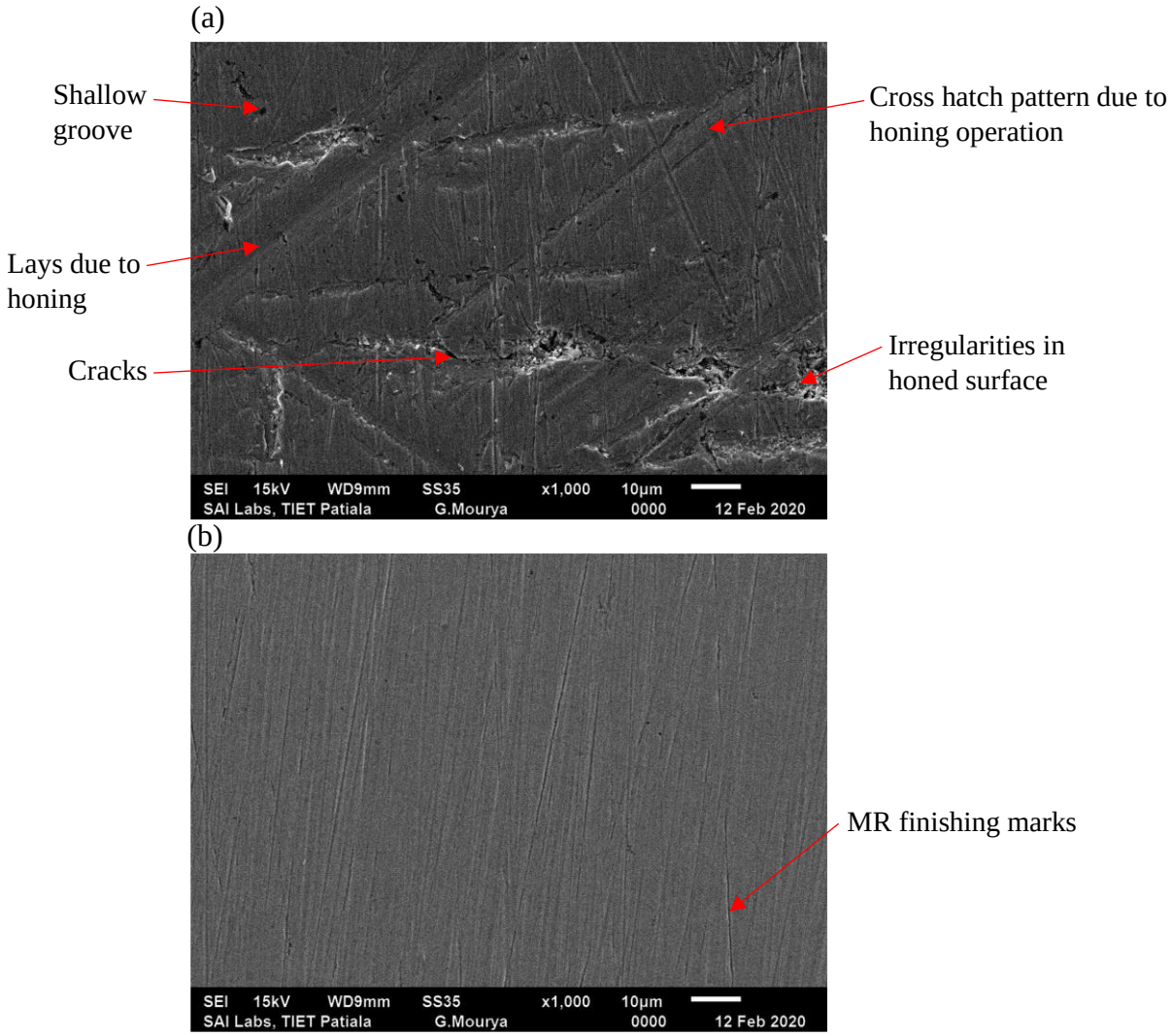

Fig. 5.28 Scanning electron microscopy images on (a) the initial honed surface, and (b) the final MR finished surface of the cylindrical workpiece of EN-31 steel using R-MRH process for 40 min of finishing with the optimized parameters on the 7665 mm^2 of the internal surface area of the cylindrical workpiece of EN-31 steel.

5.5 Conclusions

The fine finishing of the inner surface of a cylindrical workpiece of EN-31 steel using the rotating magnetorheological honing (R-MRH) process was accomplished successfully. From this work, the following conclusions have been made.

- The optimum parameters of the R-MRH process predicted in this study % concentration of SiC abrasive particles of 22.5, % concentration of the electrolytic iron particles of 22.5 in MRP fluid, tool rotating speed of 500 rpm, axial speed of the tool 70 cm/min, workpiece rotating speed of 20 rpm are found in good order for enhancing the surface finish.

- The error obtained between the experimental and the predicted % ΔRa in the present work is found within – 8.22 to 9.82% which concludes that the developed regression model is decently accurate, therefore, the predicted optimized process parameters for finishing the internal surface of the cylindrical workpiece of EN-31 steel of EN-31 steel is found in good order.
- The extent of improvement achieved in the final finished internal surface of the cylindrical workpiece of EN-31 steel in terms of average surface roughness as 84.61 %, average surface waviness as 79.94 %, in circularity as 85.55% and in the surface texture from SEM image of the cylindrical workpiece of EN-31 steel with 40 min of R-MRH finishing over 40 mm height of the workpiece cylinder with internal diameter of 61 mm using the optimized process parameters reveal the efficacy of the present finishing process for improving the surface finish, surface characteristics, and geometric accuracy of the MR finished surface which improving its functionality. This may result in saving the power consumption of the system, less wear and tear of the component of the system causing economic benefits for the industries or individual.
- The finishing performance of the R-MRH process on the internal surface of the cylindrical workpiece of the EN-31 steel also reveals that this process may be applicable for fine finishing the various other industrial cylindrical products of the EN-31 steel such as in roller bearing, dies, cylindrical molds, etc.

CHAPTER 6

FINISHING OF INTERNAL SURFACE OF VARIOUS INDUSTRIAL CYLINDRICAL WORKPIECES USING THE ROTATIONAL MAGNETORHEOLOGICAL HONING PROCESS

In this chapter, various industrial cylindrical workpieces are finely finished using the present developed rotational magnetorheological honing (R-MRH) process. Some of the finished industrial cylindrical workpieces are real-time industrial components whereas some of them are typical components. The real-time industrial cylindrical workpieces finished in this work are cylindrical barrel of hydraulic cylinder (CBHC), a cylindrical mold of plastic bottle cap, housing cylinder of power steering. Whereas, the typical industrial cylindrical workpieces finished in this work is cast-iron cylindrical mold. Also, in this work, a cylindrical work part of EN-31 steel is finished which revealed the applicability of this process for various industrial workpiece of EN-31 steel. The fine finishing of the internal surface of these cylindrical components improves the operative performance for their respective application in industries.

6.1 Internal surface finishing of cylindrical barrel of a hydraulic cylinder for improving its functional performance using rotational magnetorheological honing process

A hydraulic cylinder is one of the crucial mechanical components which is used in different types of industrial machines such as bulldozers, trenchers, excavators, crop harvesters, tractors and loaders, hydroelectric stations, aeroplanes, automated supply lines, transportation equipment, etc. (Zhang *et* al., 2012; Quan *et* al., 2014). The common feature among these machines is a need for high power to accomplish the desired work, like moving, pressing, lifting the heavy-weight materials. The smoothness in the functioning of these types of machinery is directly linked with the quality of surface finish and the selection of material (Younglee, 2020). The importance of the hydraulic system in a machine can be understood with the fact that in a very common construction hydraulic excavator machine, only 30 % of the consumed energy is used for moving the load. Whereas more than 60 % of energy is consumed in power losses and for driving the hydraulic system (Zimmerman *et* al., 2007). Therefore, even a small improvement in the hydraulic system may give a substantial impact on the total energy consumption and its efficiency. The poor internal surface finish of the cylindrical barrel of hydraulic cylinder (CBHC) induces high friction between the piston and the internal surface of the cylinder barrel. This high friction results in high power consumption in hydraulic power transmission, high wear and tear rate of this surface, high heat generation during operation, leakage of hydraulic oil, and short life cycle of this component (Raju *et* al.,

2005; Zhao *et* al., 2015; Zhang *et* al., 2016). In industry the internal surface of the CBHC is finished with the honing (Younglee, 2020). With application of the honing for finishing the inside surface of the CBHC, the surface can be finished upto a certain limit. Further finishing of that limit may improve the functionality of the hydraulic cylinder. Also, the finished surface with traditional honing induces various types of surface defects such as deep groove, cavity, scratch, heat affected zone, stress concentration, irregularities in surface etc. These defects are induced due to the direct contact of the tool with the finishing surface and action of uncontrollable finishing forces (Bedi and Singh, 2018a). Therefore, to deal with limitations involved in traditional honing while finishing the inside surface of the cylindrical barrel of the hydraulic cylinder (CBHC), the present developed rotational magnetorheological honing (R-MRH) process is utilized.

In this work, a real-time cylindrical barrel of the hydraulic cylinder (CBHC) of an electro-hydraulic system has been considered for improving its functionality by finishing with the R-MRH process. As R-MRH process is a recently developed MRP fluid-based internal cylindrical finishing process, so, deciding the best process parameters for finishing this component is a challenging task. Therefore, in this work, a study has been conducted to predict the best process parameters, and then using those parameters, the internal surface of the CBHC is finished for improving its functional performance. The smooth functioning of the hydraulic cylinder with minimized power may be achieved by reducing the friction and wear of the internal CBHC surface which is obtained by fine-finishing the respective surface.

6.1.1 Materials and Methods

6.1.1.1 Selection of the material and workpiece preparation

The real-time cylindrical barrel of the hydraulic cylinder (CBHC) of an electro-hydraulic system is taken for conducting MR finishing on its internal surface. However, a honing process is mainly utilized to finish the inner surface of the CBHC in industries (Younglee, 2020). The material composition of this component used in the current study is obtained from the spectroscopy test as tabulated in Table 6.1.

Table 6.1 Chemical composition of the cylindrical barrel of the hydraulic cylinder (CBHC)

Compositional element	Fe	C	Si	Mn	P	S	Cr	Mo
%age composition of element	98.27	0.10	0.27	0.75	0.04	0.012	0.13	0.02
Compositional element	Ni	Co	Cu	W	Pb	Sn	As	
%age composition of element	0.08	0.02	0.24	0.018	0.03	0.013	0.014	

Using this test, it is found that the material of the considered real-time CBHC workpiece is a carbon-steel alloy with grade St52, 1.0421. This material offers many important properties which make it very crucial for the wide range of industrial applications. A few of the properties of this material (carbon-steel alloy with grade St52, 1.0421) are high corrosion-resistant and wear-resistant, etc. For the present study, the carbon-steel alloy material as a real-time CBHC is finished using the R-MRH process. The dimensional specification of the present work-part (real-time CBHC) is found as the internal diameter of 64 mm, an outer diameter of 76 mm and its overall length is 164 mm. For preliminary experimentations and further study to predict the optimized finishing parameters, the CBHC component is cut in the form of a ring of height 15 mm each. The internal surface roughness of the CBHC workpieces which was procured by its manufacturing industry is considered as the initial surface roughness for the present study. In this work, the magnetorheological polishing (MRP) fluid is utilized as a finishing agent. It is comprised of the magnetisable electrolytic iron particles (EIPs) powder, silicon carbide (SiC) abrasive particles, paraffin oil and AP3 grease. The concentration of each MRP fluid components is considered as volumetric. The concentrations of each components of the MRP fluid used in this work is considered as per the composition reported in Table 5.1 in chapter 5. All the components are measured carefully and are mixed thoroughly in the AC motor-controlled mixer for 25 to 35 minutes.

6.1.1.2 Experimentation

The experimentation on finishing the inner surface of the cylindrical barrel of the hydraulic cylinder (CBHC) using the rotational magnetorheological honing (R-MRH) process is depicted in Fig 6.1. The for performing the experimentation the servo motor S1, S2 and S3 govern the reciprocation motion the tool, rotation motion of the tool and workpiece rotation respectively. The programmable logic controller (PLC) governs all the motions performed by the servo motors through the drives in the (R-MRH) process as shown in Fig. 6.1. The height adjusting fixture is made with an adjustable platform with numerous of threaded holes over its surface. Here, two pillar plates each with two slots are used for adjusting the height of the CHBC workpiece. As the centre of the MRH tool is to align with the centre of the rotating cylinder workpiece, the adjustable platform is locked in place with a nut and bolt mechanism to rigidly fix its position. Further, two pillow blocks are attached on the adjustable platform of the height adjusting fixture. With these pillow blocks, a coupling shaft is connected. Further, a workpiece holder is coupled with the coupling shaft. Also, to provide rotation to the CBHC workpiece, a

v-shaped pulley is attached to the coupling shaft in between the two pillow blocks as shown in Fig. 6.1.

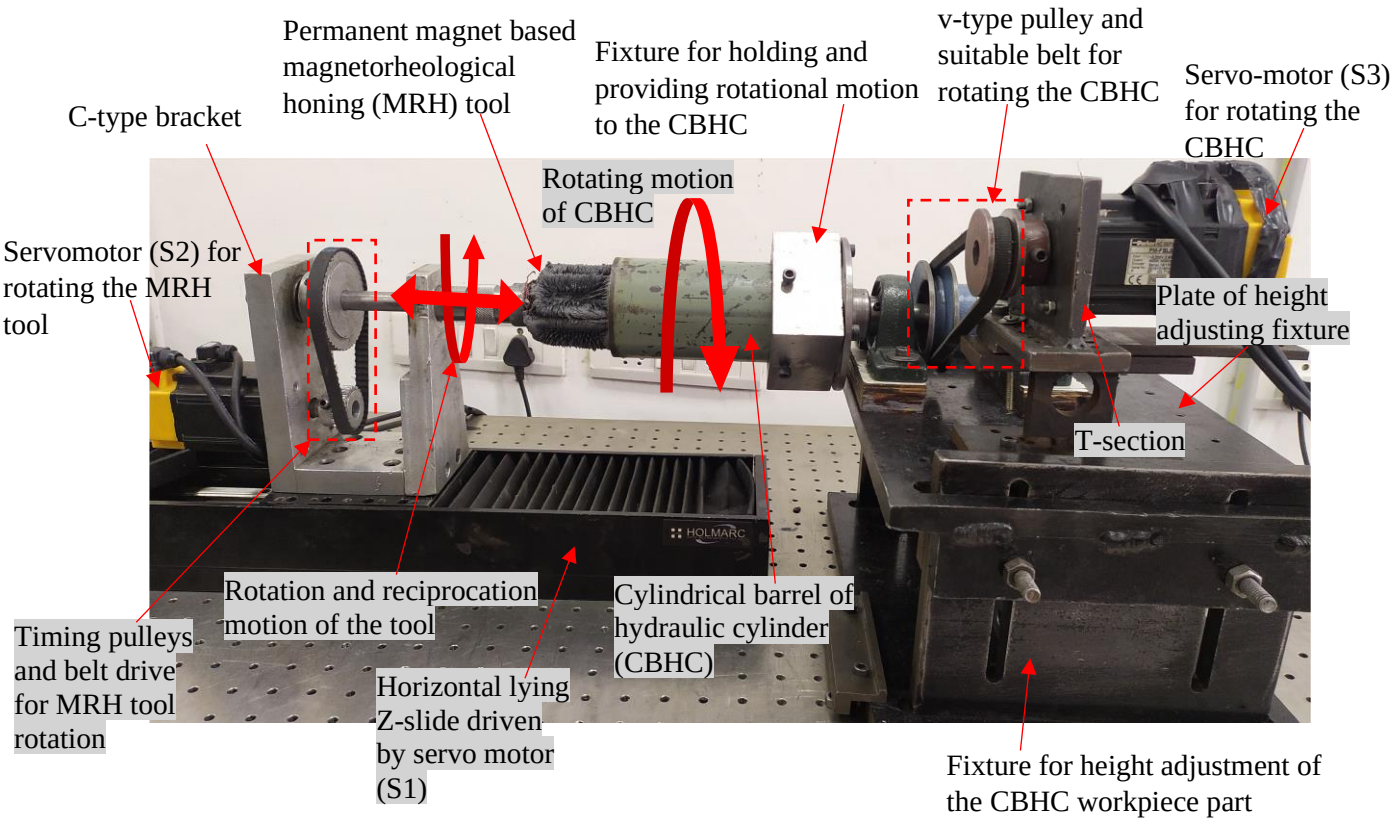

Fig. 6.1 Experimentation on finishing the inside surface of the cylindrical barrel of hydraulic cylinder (CBHC) using the rotational magnetorheological honing (R-MRH) finishing process.

Thus, experimentation is performed over the inner surface of the CBHC component using the rotational MRH process as shown in Fig. 6.1. Further, to find the optimum finishing parameters, the central composite design (CCD) in response surface methodology (RSM) technique is utilized with 4 parameters and 5 levels as reported in Table 6.2. Preliminary experiments are done on the internal surface of the cylindrical barrel of the hydraulic cylinder (CBHC) using the experimental setup as shown in Fig. 6.1 to determine the variable finishing process parameters range. Cylindrical honing is performed for initial surface generation over the CBHC workpiece part and the initial average roughness value (Ra) of the part are measured in the range of 290-390 nm. The SJ-400 Mitutoyo surface roughness profilometer with a cut off length of 0.25 mm is used to measure the surface asperity of the CBHC workpiece parts. The preliminary experiments are performed for 20 min over the 3015.93 mm^2 internal surface area of the CBHC workpiece parts as shown in Fig 6.2(a). After the preliminary experimentation, the range of the finishing process parameters re selected as reported in Table 6.2.

Table 6.2 Finishing parameters and their levels required for the finishing of the cylindrical barrel of hydraulic cylinder (CBHC) using the rotational magnetorheological honing (R-MRH) process.

Finishing parameters	Unit	Levels				
		-2	-1	0	1	2
Rotational speed of the MRH tool (*T*)	rpm	300	350	400	450	500
Reciprocation speed of the MRH tool (*A*)	cm/min	30	50	70	90	110
Rotational speed of the CBHC (*W*)	rpm	0	15	30	45	60
Working gap (*G*)	mm	1	1.5	2	2.5	3

Based on this range of parameters, the CCD is utilized. Thus, a total of 30 experiments are planned and performed over the CBHC workpiece parts as reported in Table 6.3. During experimentation, each experiment is carried out on the CBHC workpiece part (internal diameter of 64 mm and length of 15 mm) for 20 min of the finishing period. The CBHC workpiece parts are held in the workpiece holder using screws as shown in Fig. 6.2(a). As the experimentation is performed, the rotating and reciprocating MRH-tool enters the CBHC work part. Under the action of magnetic field owing to the permanent magnet, the MRP fluid is stiffened over the magnetic surface of the MRH-tool surface (Singh *et* al., 2015). This MRP fluid helps in finishing the inside surface of the CBHC workpiece part.

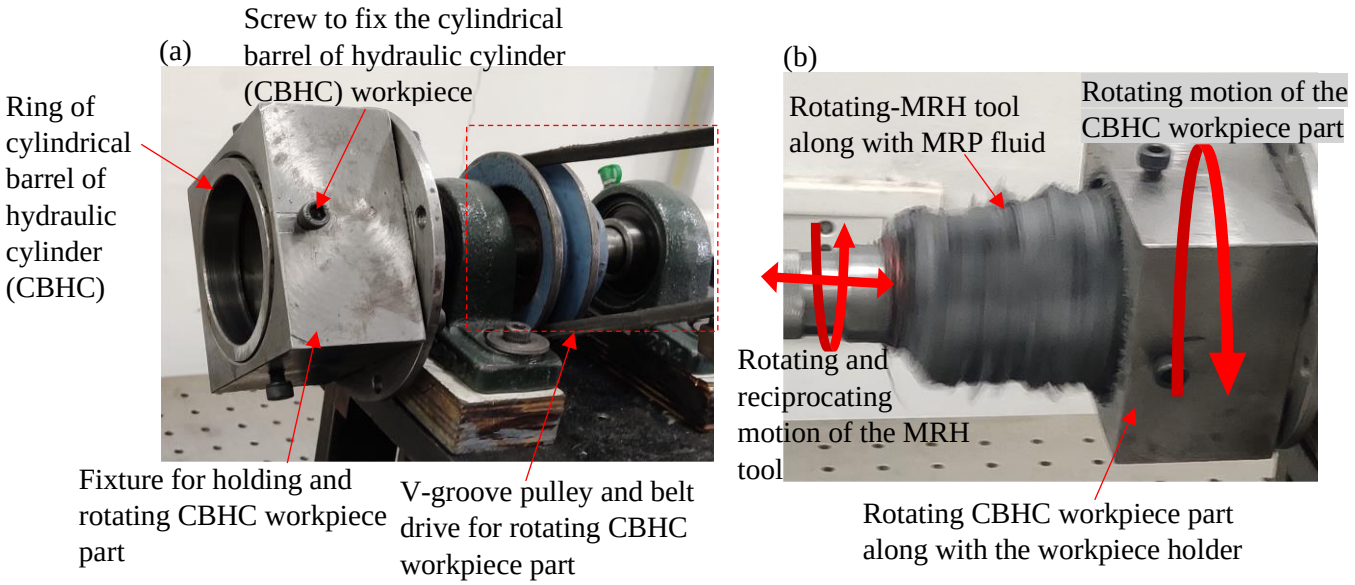

Fig. 6.2 (a) Fixture holding and rotating the cylindrical barrel of hydraulic cylinder (CBHC) and (b) finishing operation of the ring of real-time CBHC for preliminary and planned experimentations.

The response as the percentage reduction in surface roughness value (*% ΔRa*) for each experiment which is calculated from Eq. (6.1) and reported in Table 6.3

$$\%\Delta Ra = \frac{(Ra_i - Ra_f)}{Ra_i} \times 100 \quad (6.1)$$

where Ra_i is the initial average surface roughness and Ra_f is the average of final surface roughness measured at three different points (*R1*, *R2*, and *R3*) after 20 min of finishing. Thus, the experiments are performed over the inner surface of the CBHC workpiece parts utilizing the MRH tool with the corresponding parametric conditions are reported in Table 6.3. In addition, with the help of scanning electron microscopy, the study of the surface characteristics of the CBHC workpiece has been observed. Further, the dimensional accuracy is analyzed using the co-ordinate measuring machine.

Table 6.3 Plan of experiment and their response *% ΔRa* after finishing with the rotational magnetorheological honing (R-MRH) process over the inner surface of the cylindrical barrel of hydraulic cylinder (CBHC) workpieces.

S. No.	*T* (rpm)	*A* (cm/min)	*W* (rpm)	*G* (mm)	Ra_i (nm)	*R1* (nm)	*R2* (nm)	*Ra* (nm)	Avg. Ra_f (nm)	*% ΔRa* (Eq. 6.1)
1	450	90	45	2.5	320	172	178	178	176	45
2	350	90	15	1.5	310	110	116	100	109	65
3	450	90	15	2.5	300	160	170	147	159	47
4	450	50	15	1.5	310	182	196	180	186	40
5	400	30	30	2	290	187	201	185	191	34
6	450	50	45	2.5	320	162	176	160	166	48
7	350	90	45	1.5	330	98	112	96	102	69
8	400	70	60	2	290	92	106	90	96	67
9	450	50	15	2.5	300	176	190	174	180	40
10	450	90	45	1.5	320	118	132	116	122	62
11	350	50	15	1.5	310	142	156	140	146	53
12	500	70	30	2	290	199	213	197	203	30
13	350	50	45	1.5	320	156	170	154	160	50
14	400	70	0	2	290	156	170	154	160	45
15	400	70	30	1	300	122	136	120	126	58
16	400	110	30	2	320	130	144	128	134	58
17	350	90	15	2.5	320	130	144	128	134	58
18	400	70	30	2	310	77	91	75	81	74
19	350	90	45	2.5	300	131	145	129	135	55
20	400	70	30	2	390	101	115	99	105	73
21	350	50	15	2.5	300	176	190	174	180	40
22	400	70	30	2	310	83	97	81	87	72
23	400	70	30	2	320	124	138	122	128	60
24	450	90	15	1.5	330	178	192	176	182	45
25	450	50	45	1.5	300	110	124	108	114	62
26	350	50	45	2.5	320	214	228	212	218	32
27	300	70	30	2	310	126	140	124	130	58
28	400	70	30	2	300	74	88	72	78	74
29	400	70	30	3	290	156	170	154	160	45
30	400	70	30	2	310	80	94	78	84	73

6.1.2 Results and discussion

The analysis of variance (ANOVA) was performed with the obtained experimental data obtained. The data of ANOVA after finishing the inside surface of the cylindrical barrel of the hydraulic cylinder (CBHC) using the rotational magnetorheological honing (R-MRH) process are reported in Table 6.4.

Table 6.4 Analysis of variance (ANOVA) for the percentage reduction in surface roughness (%ΔRa).

Source	Sum of square	Degree of freedom	Mean squares	F-value	Prob > F (P-value)	Remarks	% contribution of the involving factors
Model	4568.26	11	415.30	15.23	< 0.0001	significant	
T	330.04	1	330.04	12.10	0.0027		5.92
A	693.38	1	693.38	25.42	< 0.0001		12.43
W	260.04	1	260.04	9.53	0.0063		4.66
G	477.04	1	477.04	17.49	0.0006		8.55
T^2	1170.03	1	1170.03	42.90	< 0.0001		20.98
A^2	997.74	1	997.74	36.58	< 0.0001		17.89
W^2	342.03	1	342.03	12.54	0.0023		6.13
G^2	594.67	1	594.67	21.80	0.0002		10.66
TA	248.06	1	248.06	9.10	0.0074		4.45
TW	189.06	1	189.06	6.93	0.0169		3.39
WG	126.56	1	126.56	4.64	0.0450		2.27
Residual	490.94	18	27.27				
Lack of fit	342.94	13	26.38	0.89	0.6039	not significant	
Pure error	148.00	5	29.60				2.65
Total	5059.20	29					

From ANOVA performed in this study, the p-value of the model is found less than 0.0001 which is obviously less than 0.05. So, the p-value of the regression model is significant. Also, the p-value for the lack of fit is 0.6039 which is greater than 0.05 making it non-significant. Therefore, based on the P-value of the regression model and lack of fit, it is found that the developed regression model is acceptable. Further, to analyze the contribution of the factors involved in the developed regression model a P-values is analyzed. So, the factors which contributed significantly to the regression model are with the P-value less than 0.05 and are reported in Table 6.4. The regression model derived from the ANOVA performed on the experimental study is expresses as in Eq. (6.2).

$$\%\Delta Ra = -565.154 + 2.154T + 3.955A + 0.078W + 76.833G - 0.003T^2 - 0.015A^2 - 0.016W^2 - 18.625G^2 - 0.004TA + 0.005TW - 0.375WG \quad (6.2)$$

Therefore, from the developed regression model and ANOVA table it is observed that T, A, W, G, T^2, A^2, W^2, G^2, TA, TW, *and* WG are significantly impacting factors to the regression model. The percentage contribution of various process parameters on the percentage reduction

in surface roughness ($\%\,\Delta Ra$) on MR finishing the surface of the hydraulic cylinder workpiece parts is reported in Table 6.4. It is calculated from the ANOVA data in Table 6.4. The percentage contribution (%age cont.) of the finishing parameters is calculated using Eq. (6.3) (Das *et* al., 2012).

$$\%age\ cont. = \frac{Sum\ of\ square}{Total\ sum\ of\ square} \times 100 \tag{6.3}$$

The major contributing factor is the reciprocating speed of the R-MRH tool (R_t+R_t^2) as its %age contribution (%age cont.) is found as a 30.32. The reciprocating speed is contributing highest in the regression model. The abrasion mechanism takes place by a continuous change in direction of rubbing action performed by the active abrasive particles (AAPs) on the roughness peaks. Due to which the roughness peaks get sheared and finishing takes place. Therefore, in this process, reciprocating motion plays a major role in finishing action. However, the rotational speed of the R-MRH tool (T and T^2) is the second-highest contributing parameters with %age cont. value is 26.90. From this study, it is found that the rotation speed of the hydraulic cylinder (W and W^2) is the least contributing parameter as its %age cont. value is 10.79. But still, it is a significant value that improves the adequacy of the regression model for the prediction of response. Also, this significance of the %age cont. of the rotating motion of the CBHC acknowledges the importance of this motion in finishing performance.

To analyze the adequacy of the developed regression model, the other parameters of the ANOVA are also reported in Table 6.5.

Table 6.5 Other parameters of analysis of variance (ANOVA)

R-squared	0.903	Pred R-squared	0.635
Adj R-squared	0.844	Adeq precision	10.559

The correlation coefficient (R^2) is found as 0.903 which indicates that the model is sufficient for the prediction of the surface finish with arbitrary value of the process parameters from the range of process parameters (Table 6.1). The value of adjusted R^2 and predicted R^2 are found 0.844 and 0. 635. This significance of the difference between both the adjusted R^2 and the predicted R^2 (0.209) revealed a moderate correlation on the developed regression model that is desirable for the suitability of the model (Sirwal *et* al., 2020). Adequate precision is found to be 10.559 which is greater than 4 which is expected for the model to help access the design space.

6.1.2.1 Effect of significant individual parameters on the process performance

Figure 6.3(a) depicts the effect of tool rotation speed (T) on *% ΔRa*. The workpiece rotation (W), tool reciprocation (A) and working gap (G) were kept constant at 30 rpm, 70 cm/min, and 2 mm, respectively. It can be observed that with the increase in T upto 400 rpm, there is an upsurge in the trend of the *% ΔRa*, and then the trend starts decreasing. This is owing to the increase in the value of T it influences the increase in the rotational speed of the active abrasive particles (AAPs) that rotates and collide with the surface asperities of rotating work part surface. It results in increment in the centrifugal force and tangential force as discussed in theoretical study performed in chapter 3. Thus, this results in an upsurge in the shearing of the asperities from the inner surface of the hydraulic cylinder. This is achieved by firmed gripping the AAPs in the EIPs chains. Hence, an increment in the trend of *% ΔRa* is obtained. Further, on increasing the tool rotational speed beyond 400 rpm, there is an excessive increment in centrifugal force (F_{cen}) owing to which the EIPs chains tend to loosen their grip over the AAPs during finishing (Sirwal *et* al., 2020). Owing to this, AAPs lose their capability to shear off the surface asperities properly from inside surface of the cylindrical barrel of hydraulic cylinder (CBHC) workpiece. Thus, a decrement in the trend of the *% ΔRa* is observed at higher tool rotation. Hence, due to this decrement in the trend of *% ΔRa* beyond tool rotational speed of 400 rpm there is an excess increase in centrifugal force (F_{cen}) that acts on the AAPs. The maximum value of the *% ΔRa* was attained at the 400 rpm of tool rotation.

Figure 6.3(b) depicts the effect of workpiece rotation (W) on *% ΔRa*. The tool rotation (T), tool reciprocation (A) and working gap (G) were kept constant at 400 rpm, 70 cm/min, and 2 mm, respectively. It can be observed that as the workpiece rotation increases upto 30 rpm, there is an increment in *% ΔRa*. The increment in W_r results in increased net relative speed of the AAPs w.r.t. the finishing internal surface of CBHC. Owing to this, there is an increase in the tangential shear force applied by the AAPs on the roughness peaks of CBHC. This enhanced tangential shear force leads to an increment in the trend of *% ΔRa*. On further increasing the workpiece rotation beyond 30 rpm, there is a decrement in the trend of *% ΔRa*. Also, the increase in workpiece rotation allows the contact time between the work part surface asperities and AAPs during finishing to be decreased. Due to the reduced interaction time in such a short interaction time, the AAPs may be found unable to properly shear off the asperities from the workpiece surface, leading to a decrease in the trend of *% ΔRa*. At 30 rpm of workpiece rotation, the maximum value of the *% ΔRa* was reached.

Figure 6.3(c) shows the effect of the tool reciprocation (A) at tool rotation (T) of 400 rpm, workpiece rotation (W) of 30 rpm and 2 mm of the working gap (G). As the A increase upto 70 cm/min, the trend of the $\% \Delta Ra$ upsurges. With an initial increase in A, the number of finishing cycles per minute and axial shear force (F_{axs}) applied by AAPs get increases as it has been discussed in chapter 3 (Eq. 3.14).

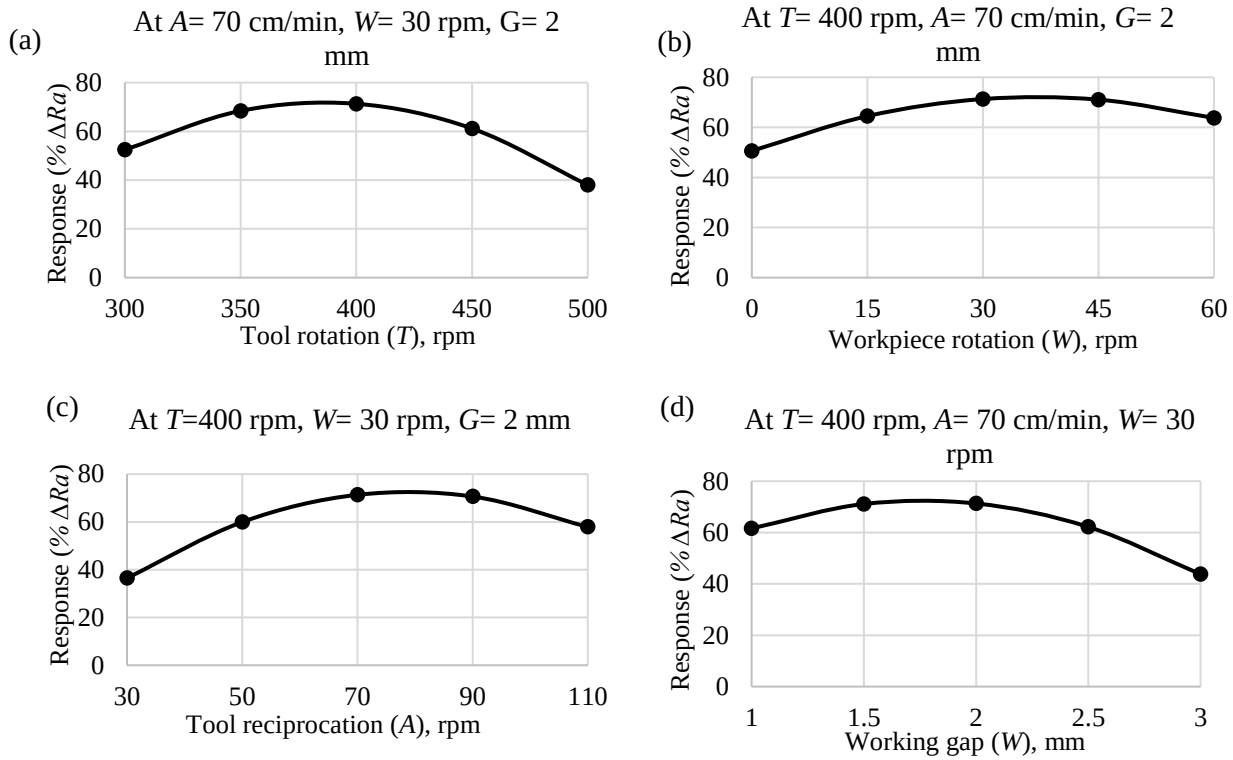

Fig. 6.3 Effect of (a) tool rotation (T), (b) workpiece rotation (W), (c) tool reciprocation (A) and (d) working gap (G), on percentage reduction in the surface roughness ($\%\Delta Ra$).

This results in an enhanced number of collisions with an increased magnitude of the axial force between AAPs and asperities of the inner surface of the CBHC workpiece part. Due to which, the improvement in surface finish enhances. Beyond 70 cm/min of A, the contact time between the AAPs and the internal finishing surface of the workpiece decreases. Also, at the excessively enhanced axial speed of AAPs, the chain structure of the EIPs gets unstable (Sirwal *et* al., 2020). Therefore, this induces a decrease in $\% \Delta Ra$. At 70 cm/min of tool reciprocation, the maximum value of the $\% \Delta Ra$ was achieved.

Figure 6.3(d) shows the effect of the working gap (G) at tool rotation (T) of 400 rpm, workpiece rotation (W) of 30 rpm and working gap of 2 mm. The $\% \Delta Ra$ in the surface finish is less at the lower gap. At less G, the magnitude of magnetic field at the end surface of the tool and

workpiece part's inside surface remains same. Due to such values of the magnetic field at finishing surface as compared to the magnetic surface of the tool resists the relative motion of the AAPs. Also, the less MRP fluid is occupied in the gap for performing the finishing action. Therefore, with initial increment in G, the $\% \Delta Ra$ increases. But beyond 2 mm of the G, the intensity of the magnetic field gets lowered which causes the loosening of the EIPs chain structure. Therefore, the loose grip of the EIPs chain structure results in decreased $\% \Delta Ra$. The maximum $\% \Delta Ra$ is achieved at 2 mm of the working gap.

6.1.2.2 Combined effect of significant interacting parameters on the process performance

Figure 6.4(a) demonstrates the simultaneous effect of the tool rotation (*T*) and reciprocating speed of the tool (*A*) on the percentage reduction in surface roughness ($\% \Delta Ra$) when the cylindrical workpiece rotation (*W*) and working gap (*G*) are kept constant at 30 rpm and 2 mm. From this figure it is observed that with initial increase in *T* and *A* simultaneously, the $\% \Delta Ra$ increases. This increment in $\% \Delta Ra$ occurs till *A* = 70 cm/min, and *T* = 400 rpm. Further increment in *A* and *T*, it starts decreasing. Such trend in $\% \Delta Ra$ is observed due to the variation in *A* and *T* because with initial increase in these parameters the relative speed of the active abrasive particles (AAPs) increases along the helical path direction. This increased relative speed causes enhancement in resultant cutting shear force (F_s) (chapter 3, Eq. 3.15) due to which the improvement in surface finish takes place. But beyond *A*= 70 cm/min, and *T* = 400 rpm, the $\% \Delta Ra$ starts decreasing because of the reduced interaction time due to excessive increase in the relative speed of the AAPs over the finishing surface. Also, the excessive increase in *T* results in instable electrolytic iron particles (EIPs) chain structure resulting in the loose grip over the AAPs in this structure (Sirwal *et* al., 2020). Further, the loose grip over AAP by EIPs chain structure consequently provides poor finishing action.

Figure 6.4(b) demonstrates the concurrent effect of the tool rotation (*T*) and workpiece rotation (*W*) on the $\% \Delta Ra$ when the tool reciprocation speed (*A*) and working gap (*G*) are kept constant at 70 cm/min and 2 mm. From this figure it can be observed that with initial increase in *T* and *W* causes the increment in $\% \Delta Ra$. It happens owing to the initial increment of *T* and *W*, upsurges the relative speed of AAPs which results in rise in the tangential shear force applied by AAPs on the asperities of the workpiece surface. Further, the increase in *T* and *W* causes favorable alteration in the parameters of the helical path formed by an active abrasive particle over the finishing surface of the workpiece (Singh *et* al., 2015) which results in improved

finishing performance. Also, the workpiece rotation triggers the shuffling of AAPs in the MRP fluid while finishing as discussed in the early section of this manuscript.

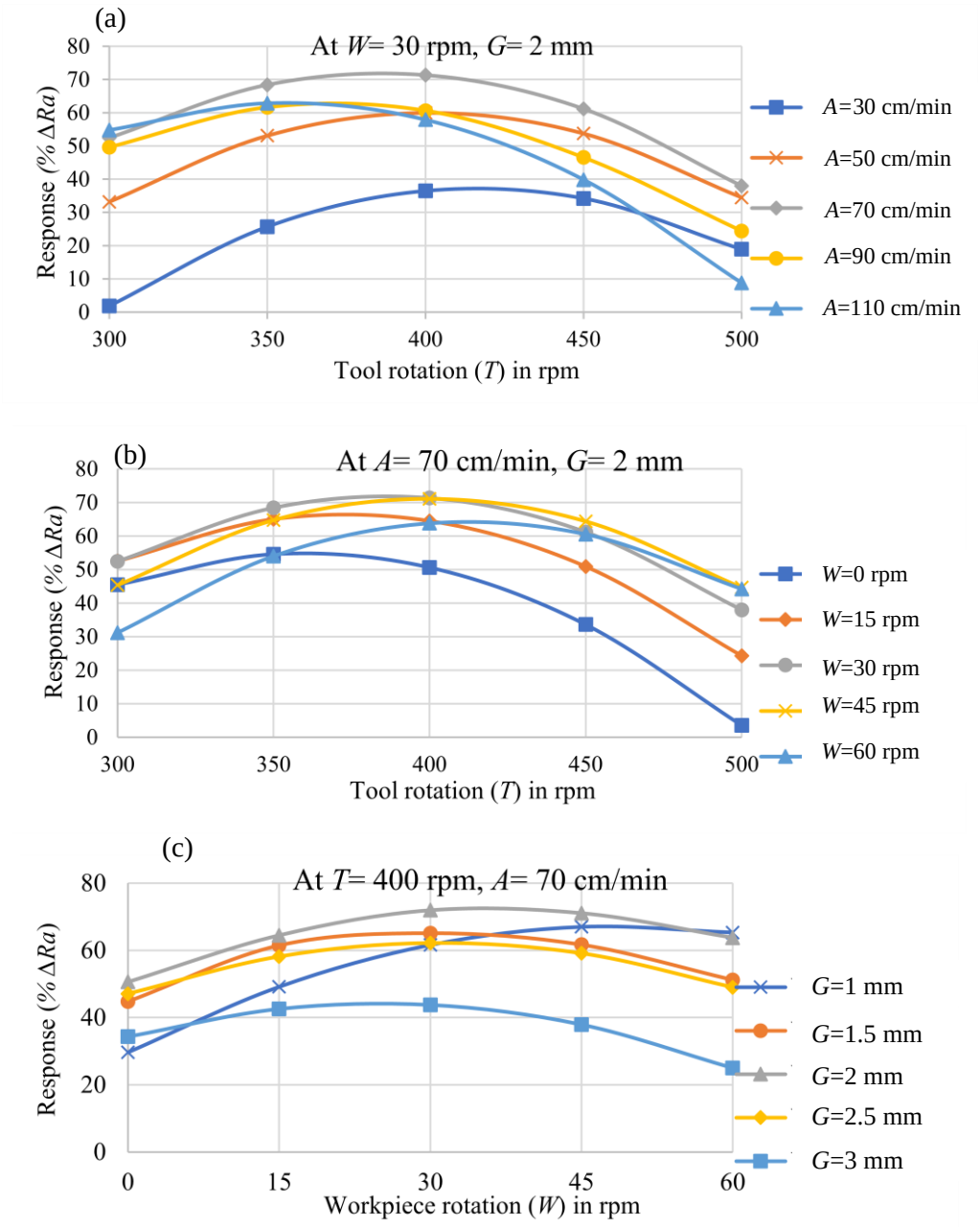

Fig. 6.4 Combined effect of (a) tool rotation (*T*) and tool reciprocation (*A*) on percentage change in surface roughness (*% ΔRa*) keeping workpiece rotation (*W*) and working gap (*G*) as constant at 30 rpm and 2 mm respectively (b) *T* and *W*, on *% ΔRa* when *A* and *G* are kept constant at 70 cm/min and 2 mm respectively (c) *W* and *G*, on *% ΔRa* when *T* and *A* are kept constant at 400 rpm and 70 cm/min respectively.

The shuffling of the AAPs results in a consistently large number of sharp-edged AAPs present on the finishing surface. Therefore, the enhanced tangential shear force and shuffling of AAPs result in increasing *% ΔRa*. Such trend is kept continue till *T*= 400 rpm and *W* = 30 rpm. Beyond

these values of *T*and *W*, the *% ΔRa* starts decreasing because of access increment in *T* and *W* result in less time for AAPs to get into interaction with roughness peaks of the finishing surface of the workpiece (Martorelli1 *et* al., 2016). Also, the enhanced speed of T_r on oppositely rotating workpiece with excessively enhanced *W* makes the EIPs to instable due to the dominating of centrifugal force (F_{cen}) on the indenting magnetic force (Sirwal *et* al., 2020). Due to which the loosely gripped AAPs perform poor finishing action. Therefore, the *% ΔRa* trend is observed decreasing beyond the *T* =400 rpm and *W*= 30 rpm.

Figure 6.4(c) depicts the simultaneous effect of the workpiece rotation (*W*) and working gap (*W*) on the percentage reduction in surface roughness (*% ΔRa*) when tool rotation (*T*) and tool reciprocation (*A*) are kept constant at 400 rpm and 70 cm/min respectively. From this figure, it is noticed that with initial increase in *W* and *G* the *% ΔRa* upsurges and it continues increasing till *W* = 30 rpm, and *G* = 2 mm. This happens because initially increasing the *W* and working gap causes more shuffling of the AAPs and increase in the values of negative slope of magnetic field in the working gap resulting in a greater number of AAPs could perform relative speed over the finishing surface. But beyond these values of the *W* and *G*, the *% ΔRa* starts decreasing owing to an increase in working gap cause the lower intensity of magnetic field at inside surface of the cylindrical barrel of hydraulic cylinder (CBHC) workpiece part. Due to which the chain structures of magnetic EIPs grips the AAPs loosely. The loosely gripped AAPs in the EIPs become more inefficient when their interaction time is also gets reduced due to enhanced *W*. Therefore, with further increase in *W* and *G* beyond 30 rpm and 2 mm respectively when *T* and *A* are kept constant at 400 rpm and 70 cm/min respectively, the finishing performance decreases and results in reduced *% ΔRa*.

6.1.2.3 Process parameters optimization and validation

Optimization of parameters were predicted after regression analysis, to find the best combination of process parameters that enhance the surface finish by the maximum percentage. The optimized quadratic mathematical model is obtained from experimental data using Eq. (6.2) which would maximize the percentage reduction in surface roughness (*% ΔRa*). Maximize *% ΔRa* subjected to

300 rpm ≤ T ≤ 500 rpm

30 cm/min ≤ A ≤ 110 cm/min

0 rpm ≤ W ≤ 60 rpm

1 mm ≤ G ≤ 3 mm

The optimum parameters were predicted based on the percentage reduction in surface roughness value. The regression model (Eq. 6.2) is used to achieve the maximum $\%\,\Delta Ra$. From the model, the optimized parameters obtained were as tool rotation speed is 400 rpm, hydraulic cylinder workpiece rotation is 30 rpm, tool reciprocation speed is 70 cm/min and working gap is 2 mm for obtaining maximum $\%\,\Delta Ra$. The confirmatory tests were carried out to verify the accuracy of the model. The values of the process parameters were considered randomly from their minimum to maximum range as reported in Table 6.6. Also, the finishing time considered for this confirmatory test is 20 min over the CBHC workpiece part with internal diameter as 64 mm and length as 15 mm. The range of the initial honed surface roughness on the workpiece parts which are used for confirmation experiments is lying between 290 to 390 nm. The predicted %age reduction in surface roughness ($\%\,\Delta Ra$) is compared with the experimental % ΔRa through the % error between them. Therefore, % error between predicted $\%\,\Delta Ra$ and experimental $\%\,\Delta Ra$ is calculated using Eq. (6.4).

$$Percentage\ error\ (\%\ error\ ) = \frac{|Experimental\ \%\Delta Ra - Predicted\ \%\Delta Ra|}{Experimental\ \%\Delta Ra} \times 100 \qquad (6.4)$$

From the confirmatory experiments, the percentage error between the experimental and predicted $\%\,\Delta Ra$ varies from 6.06 to 9.41.

Table 6.6 Confirmation experiments to verify the accuracy of the developed regression model.

Sr. No.	Finishing parameters				Initial *Ra*i (nm)	Final *Raf* (nm)	Experimental $\%\,\Delta Ra$ (Eq.6.1)	Predicted $\%\,\Delta Ra$ (Eq.6.2)	% Error (Eq. 6.4)
	T (rpm)	*A* (cm/min)	*W* (rpm)	*G* (mm)					
1	330	75	40	1	370	143	61.35	57.4	6.44
2	410	60	15	2	380	172	54.74	59.04	7.86
3	480	70	30	1.5	340	164	51.76	48.63	6.06
4	370	110	25	2.5	360	150	58.33	53.46	8.35
5	450	60	55	3	390	289	25.90	23.46	9.41

Therefore, from magnitude of the % error it can be said that the developed regression model is in strong agreement for predicting the surface roughness within the current range of the process parameters. Based on the analysis of variance study through the response surface methodology techniques performed in this work, the optimum process parameters have been obtained. The confirmation study of the regression model through the experimental study is the proof of the accuracy and repeatability of the model. The obtained optimum parameters using the developed

regression model of MR finishing over the inner surface of cylindrical barrel of hydraulic cylinder (CBHC) workpiece parts are the rotational speed of tool of 400 rpm, reciprocation speed of 70 cm/min, workpiece rotational speed as 30 rpm and working gap as 2 mm. By using these optimum process parameters, the MR finishing was performed with the present rotational-MRH process to examine the process performance on CBHC workpieces. The experimentations were performed for 60 min on the entire internal surface area of 32974 mm^2 with internal diameter of 64 mm and length 164 mm of CBHC component (Fig. 6.1) which had an initial honed surface roughness of 380 nm. After each 20 minutes the MRP fluid was changed for restoring the finishing capability of the SiC abrasive particles present in it.

6.1.2.4 Study of the finished surface with optimal process parameters

By using optimized parameters (T=400 rpm, A=70 cm/min, W=30 rpm, and G=2 mm), the performance of the R-MRH process to finish interior surface of the cylindrical hydraulic cylinder barrel (CBHC) has been achieved. The finishing operation on the interior surface of the CBHC was carried out until a substantial improvement in the surface finish was noticed. Post finishing the inside surface of the CBHC for 60 min, a significant improvement in the surface finish was achieved. Each set of finishing time is considered to be 20 min of finishing time during the experiment. After each 20 min of R-MRH process on interior surface of CBHC, the the surface finish was assessed. The finishing is performed till 60 min which provides the substantial improvement in surface finish. Enhancement in surface quality has been reported by the analysis surface roughness profiles, surface waviness assessment, circularity assessment, and scanning electron microscopy (SEM) images as follows.

The surface asperity of the initial honed surface and the final finished interior surface of the CBHC with the R-MRH process was measured using the roughness profileometer as mentioned in the experimental section. The surface asperity profiles are demostrated in the Fig. 6.5. Figure. 6.5(a) depicts the asperities of the initial internal surface of the real-time CBHC workpiece part. The parameters of the roughness profile of the initial internal surface of the CBHC workpiece was found as *Ra*= 380 nm, *Rz*= 2300 nm, and *Rq*= 490 nm. However, Fig. 6.5(b) represents the asperities of the final finished internal surface of the CBHC workpiece using the rotational magnetorheological honing (R-MRH) process for 60 min of finishing. The parameters of the roughness profile of the final finished internal surface of CBHC workpiece part in the current work are obtained as *Ra*= 40 nm, *Rz*= 300 nm, and *Rq*= 50 nm. From the roughness parameters of the initial honed and final MR-finished internal surface of the CBHC workpiece, the substantial improvement in surface finish was accomplished.

Fig. 6.5 Surface roughness profiles of the (a) initial honing surface (b) final finished surface using MR-finishing on the internal surface of the entire real-time cylindrical barrel of hydraulic cylinder (internal diameter of 64 mm and length of 164 mm) with 60 min of finishing.

Thus, the %age reduction in the roughness parameters of the interior surface of the CBHC workpiece was determined as % ΔRa = 89.47, % ΔRz = 86.95 and % ΔRq = 89.79. These improvements in surface asperity parameters from initial honed to the MR-finished surface authorize the substantial improvement in the surface finish. In order to validate the improvement in straightness achived along the length of the internal surface of the CBHC by employing the R-MRH process for finishing it, the surface waviness was measured on the initial honed and final finished surface of the CBHC as shown in Fig. 6.6. Figure 6.6(a) demonstrates the waviness parameters of the initial internal honed surface of the CBHC workpiece part that are *Wa*=200 nm, *Wz*=1100 nm, and *Wq*=260 nm. Whereas, with 60 min of finishing with the R-MRH process on the interior surface area of the 32974 mm^2 CBHC work-part using the optimised process parameters, the waviness parameters were obtained as *Wa* = 50 nm, *Wz* = 200 nm, *Wq* = 60 nm as presented in Fig. 6.6(b).

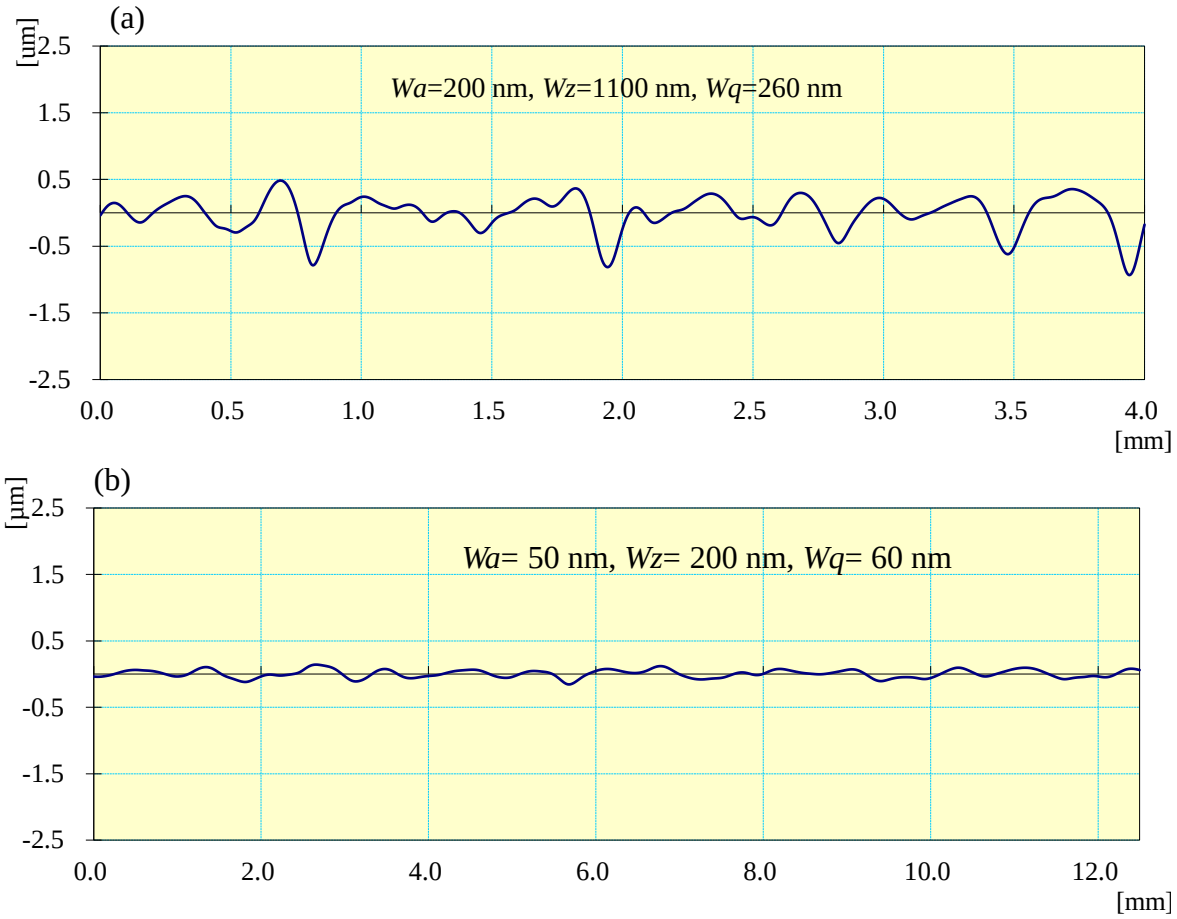

Fig. 6.6 Surface waviness profiles of the (a) initial honing surface (b) final finished surface using MR-finishing on the internal surface of cylindrical barrel of hydraulic cylinder with 60 min of finishing.

Hence, the % reduction in waviness parameters of the final MR-finished inside surface the CBHC workpiece from the surface waviness of initial honing surface are found as $\% \Delta Wa$= 75.47, $\% \Delta Wz$ = 81.81, and $\% \Delta Wq$ = 76.92. These values of reduction in surface waviness parameters demonstrate that finishing the internal surface of the CBHC component using the R-MRH process is in good agreement for improving its straightness. The improved straightness in the inside surface of the CBHC workpiece part further enhances its dimensional accuracy that results in its smooth functioning and least chances of the fluid (oil) leakage from the hydraulic cylinder.

Functional performance of the hydralic cylinder is based on how precisely piston performs in-stroke and out-stroke motion without fluid leakage and minimum resistance offered by internal surface of the cylindrical barrel of the hydraulic cylinder (CBHC). The improvement in circularity of the cylindrical barrel may cause to offer minumum resistances as well as avoids the fluid leakage from one side of piston to other side. Therefore, in this study, improvement

in the circularity is analyzed. In order to validate the improvement in the circularity on the inside surface of the CBHC achieved in this work, the circularity assessment was carried out on the initial honed and final surface of the MR-finishing using the coordinate measuring machine (CMM). The circularity test is used to determine how well the circle is closer to the actual circle of the cylinder, that offers the dimensional stability of the part (Martorelli1 *et* al., 2016). Therefore, the improvement in circularity value in this work is demonstarted in Fig. 6.7.

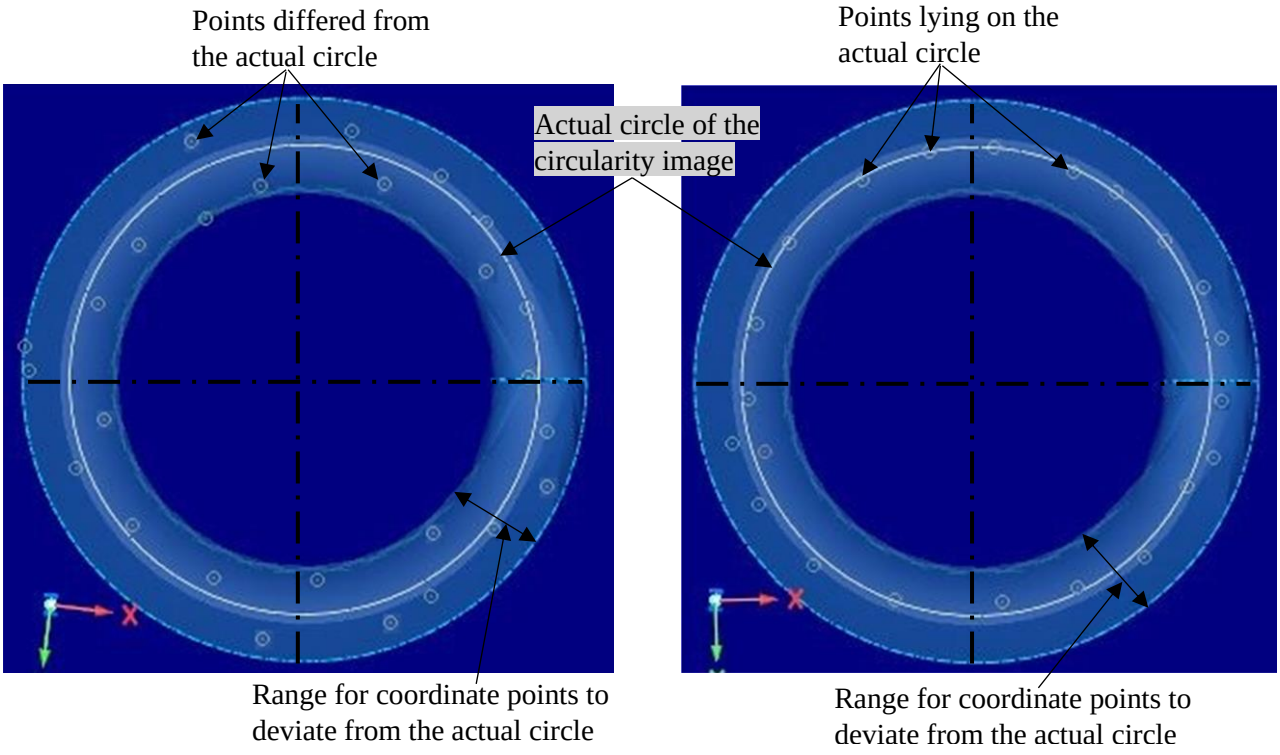

Fig. 6.7 Circularity images of (a) initial interior surface of cylindrical barrel of the hydraulic cylinder and (b) final finished surface of the entire real-time CBHC (internal diameter of 64 mm and length of 164 mm) with 60 min of R-MRH finishing using the optimal parameters.

Figure 6.7(a) depicts the circularity photograph of the initial internal honed surface of the real-time CBHC workpiece part and its values was measured as 0.1903. From this figure, it can be seen that most of the points marked on the initial honed surface have differed from the actual circle of the circularity diagram. Whereas, Fig. 6.7(b) depicts the circularity image of the internal finished surface of the CBHC workpice using R-MRH process. Major improvement in circularity can be clearly verified as most of the points reported either lie on the actual circle or are very nearly to it. The circularity value was reduced to 0.0389 with 60 min on 32974 mm^2 surface area of MR finished inside surface of the CBHC workpiece from its initial circularity value of 0.1903 on the honed surface. Figs 6.7(a) and (b) reveal that after R-MRH finishes over the interior surface of the CBHC workpiece, almost all of the points reported in the circularity

test are found closer to the true circle. The level of circularity is said to be better as the points recorded are closer to the actual circle. That's why, Fig. 6.7(b) means that the R-MRH process is considered to be useful for improving the circularity of the inner surface of the CBHC workpiece.

Figure 6.8(a) and (b) depict the scanning electron micrographs of the initial internal honed and the finally MR-finished inner surface area 32974 mm^2 of the CBHC with 60 min of finishing with the optimal parameters.

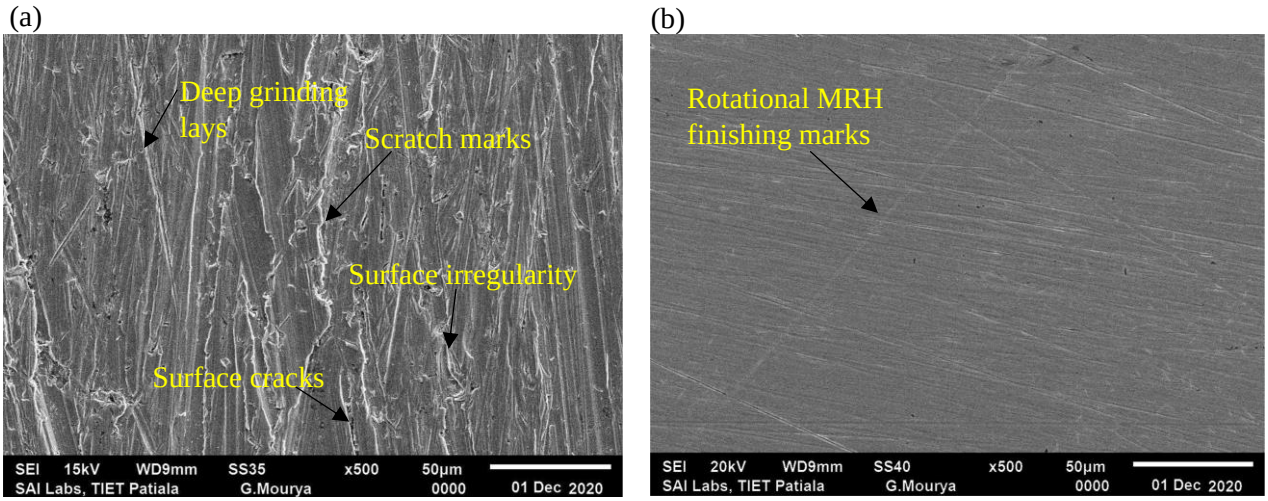

Fig. 6.8 The scanning electron micrograph of (a) initial honed surface, and (b) final R-MRH finished interior surface of the entire real-time cylindrical barrel of hydraulic cylinder (internal diameter of 64 mm and length of 164 mm) with 60 min of finishing time using optimum process parameters.

As the real-time cylindrical barrel is used for this study, the finishing performed by the manufacturing industry had utilized the honing process. Therefore, it can be seen in Fig. 6.8(a) that various kinds of surface defects such as deep honing lays, surface irregularities, scratches, scratching marks, etc. are present. Such surface defects are identified as a result of the direct interaction of the honing with the inside surface of the CBHC during the honing process. However, using the R-MRH process on the initial honed surface of CBHC, the micron-sized abrasive particles abrades the roughness peaks by rubbing action performed by them under magnetic application indentation force (F_{in}) (chapter 3, Fig. 3.1) and resultant cutting shear force (F_s) in microchip form (chapter 3, Eq. 3.15). This results in an improvement in the surface texture of the inside surface of the CBHC as shown in Fig. 6.8(b). This figure represents few finishing marks left on the MR-finished surface as compared to the initial honed surface in Fig. 6.8(a).

Figure, 6.9(a) shows the present real-time CBHC component of the electro-hydraulic system which has been finished with the present R-MRH process in this work.

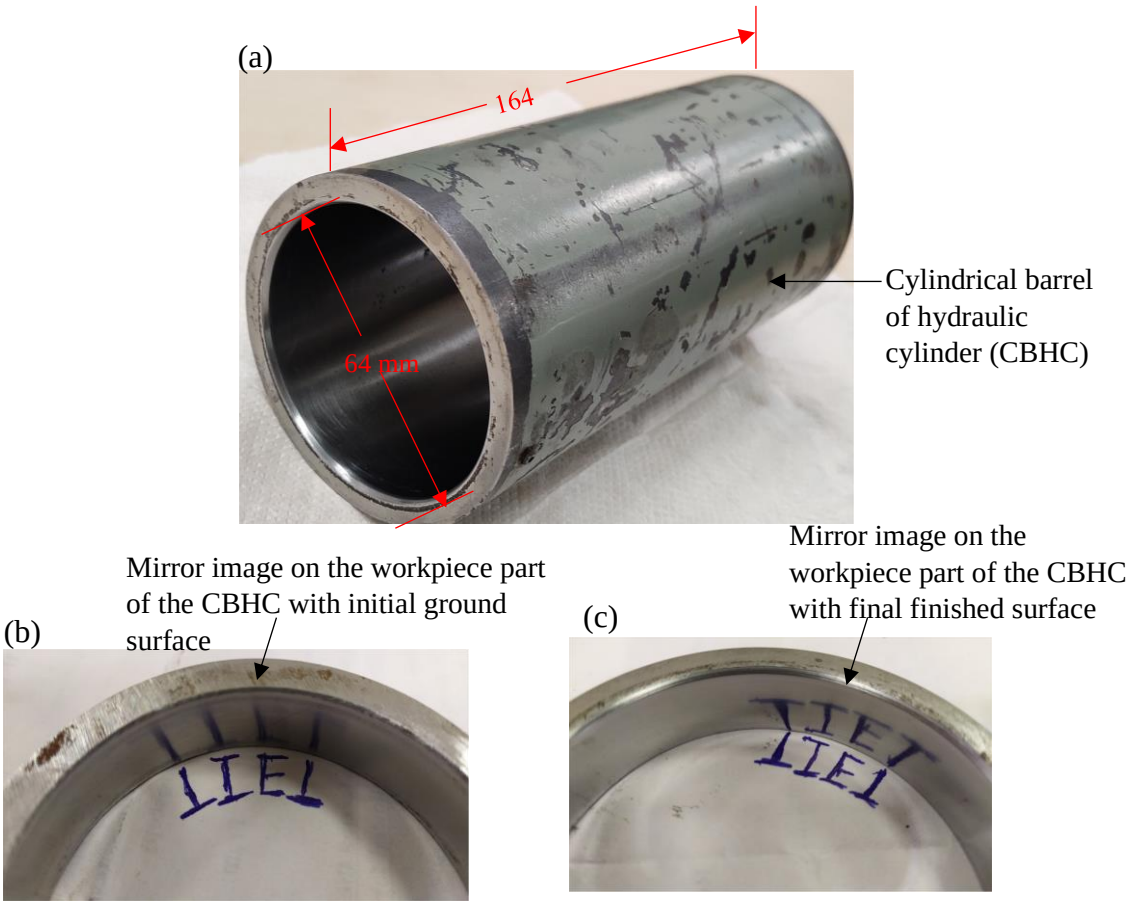

Fig. 6.9 (a) real-time cylindrical barrel of hydraulic cylinder (CBHC), (b) mirror image of the initial internal honing surface of the CBHC work-part, and (c) mirror image of the MR finished inside surface of the CBHC work-part with 60 min of R-MRH process.

To acknowledge the improvement in surface finish, the mirror images of the initial and final R-MRH finished surface have been depicted in Figs. 6.9(b) and (c) respectively. Therefore, from the mirror image, it can be said that with 60 min of R-MRH finishing on the complete inside CBHC workpiece surface area of 32974 mm^2 results in mirror like finishing. Thus, the substantial enhancement in surface finish, surface waviness, circularity, surface characteristics and mirror like visual signify that finishing the interior surface of the cylindrical barrel of the hydraulic cylinder (CBHC) through the R-MRH process with the predicted optimal parameters is found in good deal for improving its functional performances.

6.1.2.5 Improvement in functional applicability of the cylindrical barrel of hydraulic cylinder

The friction force and power loss are the most important key for consideration of the hydraulic cylinder's design (Johannesson, 1980). As the friction force and power loss are the dependent

outcomes of the internal surface roughness of the cylindrical barrel of the hydraulic cylinder, therefore, in this section, the reduction in power loss caused by friction force is analyzed. The static friction coefficient (μ_{sf}) is controlled by the parameters such as normal load, contact area, surface roughness, and the material properties. The static friction coefficient (μ_{sf}) is expressed as in Eq. (6.5) (Li *et* al., 2020).

$$\mu_{sf} = (1-\delta)\mu_l + \mu_m\delta + \mu_n \tag{6.5}$$

where μ_l, μ_m, μ_n represent frictional interaction parameters of roughness peaks, valley and wear part respectively and δ is considered as 0.5 for the elastic deformation otherwise it is 1. Further, the values of μ_l, μ_m and μ_n are dependent on the root mean square value of the surface roughness (Li *et* al., 2020). So, lower value of the roughness parameters results, the lower values of μ_l, μ_m and μ_n. Hence, the lower the value of the frictional interaction parameters results in a lower values of the static frictional force. Therefore, using the static frictional coefficiet (μ_{sf})), the frictional force (F_{fr}) is calculated using Eq. (6.6).

$$F_{fr} = \mu_{sf} P_n \tag{6.6}$$

where P_n is the normal load acting on the internal surface of the cylindrical barrel of the hydraulic cylinder (CBHC). So, it can be clearly correlated that as the value of the μ_{sf} is reduced due to decreased surface roughness as shown in Fig. 6.5(b), the frictional force (F_{fr}) is reduced which results in less power loss. Hence, the fine finished interior surface of the CBHC may found beneficial for reducing the power loss and smooth functioning of the hydraulic cylinder for its intended functions.

6.1.3 Conclusions

A rotational magnetorheological honing (R-MRH) process is used to finish the internal surface of the hydraulic cylinder. The response surface methodology technique with the central composite design is used to analyze the influence of finishing process parameters on the percentage reduction in surface roughness value. This forecasts the optimum process parameters for finishing the internal surface of the cylindrical barrel of hydraulic cylinder (CBHC) effectively with the present R-MRH process. The following conclusions demonstrate the effectiveness of the MR finished surface of the CBHC in improving the effectiveness in its widespread applications.

- The average surface roughness value was decreased to 40 nm from the initial honed surface roughness value of 380 nm after 60 min of MR finishing over the surface area of 32974 mm^2 with the R-MRH process while utilizing the optimum parameters. The results signify that the present R-MRH process is capable to fine finish the surface of the CBHC.
- The reduction in surface waviness and circularity of internal surface of CBHC was found to 50 nm and 0.0389 from the initial values of honed surface 200 nm and 0.1903 respectively with 60 min of MR finishing using the R-MRH process. These results indicate that present R-MRH process is potent to improve the dimensional as well as geometric accuracy on the inside surface of the CBHC. The improvement in the circularity test over the internal surface of the CBHC workpiece reveals the enhancement in dimensional accuracy.
- Scanning electron microscope photographs and mirror images reveal enhancement in surface characteristics with the R-MRH tool over the internal surface of the CBHC.
- The fine finished surface may reduce friction between piston and its internal surface of the cylindrical barrel, power consumption while transferring the motion, wear, and tear rate of the CBHC internal surface, and generation of heat during operation, leakage of hydraulic oil and thus increasing the life cycle of CBHC.

6.2 Fine finishing of a real-time plastic bottle cap mould using the present rotational magnetorheological honing process

A lot of cylindrical components in the industries related to automobile, medical, food, defense etc., are manufactured using casting and injection mounding processes (Otitoju *et* al., 2020). In the casting process, a solid material is dissolved, heated to suitable temperature (generally treated to change its chemical structure), and is then added into a mold or cavity, which keeps it in a proper form during solidification. The casting process for manufacturing cylindrical products have few benefits such as dimensional accuracy, inexpensive production, easy production of complicated geometric products, and utilization of maximum materials (McGeough *et* al., 2001). In injection molding process, injecting molten material is injected into a mold which then cools and ejects a plastic part from the machine (Aggarwal and Singh, 2020). Super-finish surface of molds with good surface integrity has various benefits over the finished products such as good tolerance and fits, increased product quality, and high load bearing capability. Since, the surface characteristics of the industrial components majorly decide their reliability and long life of industrial, there it is essential to have mold with high grade of finish. Further, it is also essential for mold to high dimensional accuracy. This is

because inaccuracy in dimension of mold may lead to inaccurate component. This can further lead to wear and friction owing to which there are chances of intermixing of colors in the plastic products (Grover and Singh, 2018).

For finishing of the mold various traditional processes are used such as internal surface grinding (Grover and Singh, 2018a), and hand-held grinding (Menning and Stoeckhert, 2013). However, in these traditional processes, the finishing force are uncontrollable which may lead to the various surface defects and effects the dimensional accuracy of the product.

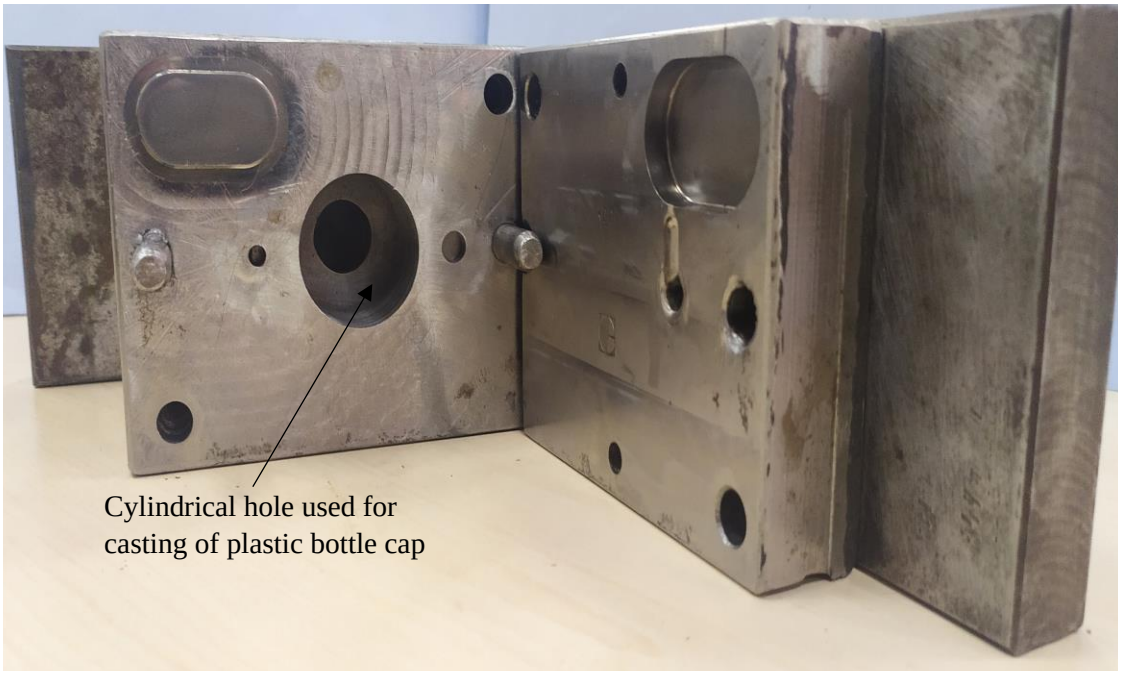

Fig. 6.10 Photograph of the plastic bottle cap mold.

Therefore, in the present work, a real time cylindrical mould which is used in the industry for casting the plastic bottle cap is finely finished using the present rotational magnetorheological honing (R-MRH) process. The photograph of this component is as shown in Fig. 6.10. Fine finishing the products of the plastic material using the traditional finishing method is a challenging task. Therefore, to get highly finished casted products (plastic bottle cap), its mold (Fig. 6.10) is finished using the rotational magnetorheological honing (R-MRH) process. The mold is made of EN-8 steel alloy. The properties such as lower shrinkage capacity, excellent machinability, higher damping capability, higher wear and abrasion resistance while casting the products has increase the importance of EN-8 in the mold industries (Campbell and Flake, 2011). The outline of present work is divided into two parts. Initially, the optimum process parameters of the present R-MRH process are predicted for fine finishing of the plastic bottle cap mold. The experimentation for this study is conducted as shown in Fig. 6.11. For this, the

response surface methodology is used. Under this technique, the central composite design is considered for optimization. Secondly, to analyze the capability of present process (R-MRH process) for fine finishing of the internal surface of the bottle cap mould, the surface roughness reduction, improvement in surface texture, circularity, and reduction in surface waviness are investigated after final finishing on its internal surface. The present R-MRH process tends to enhance the service life of EN-8 molds by providing fine finishing with minimal friction, wear, and improved functional efficacy.

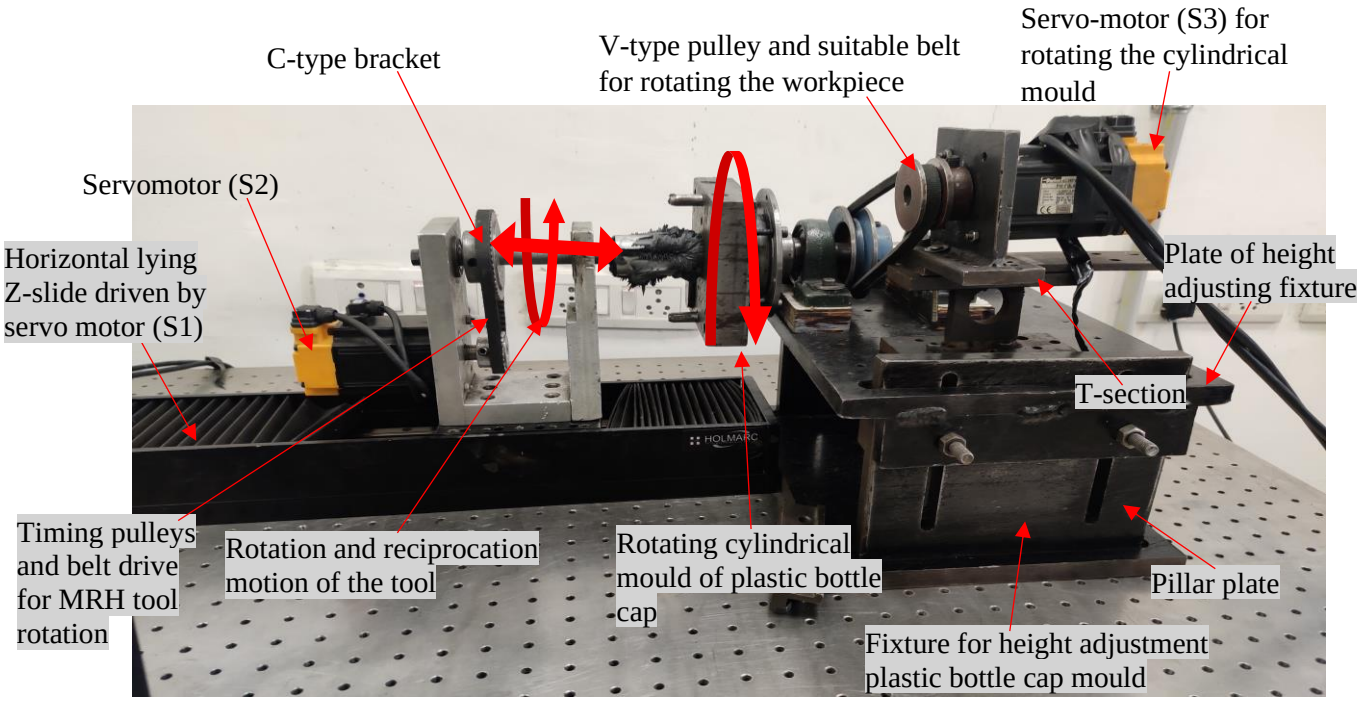

Fig. 6.11 Experimentation for internal surface finishing of the bottle cap mould using rotational magnetorheological honing process.

6.2.1 Material and methods

In the present work, cylindrical mold of EN-8 alloy steel used for manufacturing the bottle cap with a 38 mm diameter and 30 mm length is used for analysing applicability of the present R-MRH process for enhancing the operative features of this component. The image of the traditionally finished mold is depicted in Fig. 6.10. The chemical composition of the bottle cap mold material is obtained by spectroscopy test performed on the spectrometer and the value in terms of weight percentage are reported in Table 6.7. From this test it is found that the material is EN-8 steel alloy. This material may be selected by the manufacturer for making the plastic bottle cap mould under consideration as it is needed for the functional mold. Initially, traditional grinding is done on workpiece samples to eliminate the uneven marks from the cylindrical inner mold surface. After that workpieces are cleaned using the acetone and maintained properly before the magnetorheological (MR) fluid-based finishing. For conducting

the present study on this component, the magnetorheological polishing (MRP) fluid is used as finishing agent.

Table 6.7 Chemical composition of the material of the bottle cap mould.

Element	% composition
Iron (Fe)	98.5
Carbon (C)	0.330
Silicon (Si)	0.214
Manganese (Mn)	0.474
Phosphorous (P)	0.044
Sulphur (S)	0.040
Chromium (Cr)	0.121
Molybdenum (Mo)	0.025
Nickel (Ni)	0.046
Aluminum (Al)	0.013
Cobalt (Co)	0.007
Copper (Cu)	0.104
Niobium (Nb)	0.031
Tin (Ti)	0.002
Vanadium (V)	0.002
Tungsten (W)	0.345

So, based on the preliminary experimentations the composition of the MRP fluid has been selected. The composition of MRP fluid used was 20 % by volume of electrolytic iron particles (EIPs) (500 mesh size), 20 % by volume of SiC abrasive (800 mesh size) and 60 % by volume of carrier fluid. In addition, the carrier fluid is made with 80 % by wt. of paraffin oil and 20 % by wt. AP3 grease.

6.2.1.1 Experimentation

The present experimentation on the plastic bottle cap mould is performed using the rotational magnetorheological honing (R-MRH) process as shown in Fig. 6.11. As the centre of the MRH tool is to align with the centre of the rotating cylinder workpiece, the adjustable platform is locked in place with a nut and bolt mechanism to rigidly fix its position. With these pillow blocks, a coupling shaft is connected. Further, a rectangular block workpiece holder is coupled with the coupling shaft. Also, to provide rotation to the mould workpiece, a v-shaped pulley is attached to the coupling shaft in between the two pillow blocks as shown in Fig. 6.11. Thus, finishing can be performed over the mould component using the rotational MRH process. The use of two blocks makes the fixture enough rigid for zero eccentricity while the rotating motion of EN-8 cylindrical mold workpiece. The MRP fluid is employed over the external bulged magnetic tool surface. The EIPs of the MRP fluid get magnetized and attracted to the external bulged surface of the present tool. Thus, the rotating motion and the axial motion of the MRH tool over the inner side surface of the oppositely rotating EN-8 steel cylindrical mold cause the

finishing action.

6.2.1.2 Design of experiments

Using the newly developed rotational magnetorheological honing (R-MRH) process, the detailed study for the effective finishing of the internal cylindrical surface of the plastic bottle cap mould of EN-8 steel alloy has been performed. In the present work, three parameters namely MRH tool rotational speed (*T*), MRH tool reciprocation speed (*A*) and workpiece rotational speed (*W*) are selected. Each of these parameters have their own influence in the present R-MRH process. The simultaneous rotational motion of MRH tool and workpiece, governs the net tangential shear force acting on the active abrasive particles (AAPs) which shear off the surface asperities from the work part in tangential direction. Similarly, the reciprocation of the tool governs the axial force of the AAPs which shear off the surface asperities from the work part axially. The output of the process is taken as % change in surface roughness ($\% \Delta Ra$).

Further, to determine the range of the various process parameters, the preliminary experimentation was performed over the internal surface of the cylindrical mold. The initial average surface roughness (Ra) value is measured between 390-430 nm. For measuring the surface roughness, the SJ-400 Mitutoyo surface roughness profilometer with the cut off length of 0.25 mm is used. The results obtained from the preliminary experimentations are further utilized for the selection of the process parameters which are reported in Table 6.8. In the present work, for analyzing the effect of the various parameters on the internal surface of the EN-8 mold, design of experiments (DOE) is used. For analyzing the individual and combined effect of the process parameters, response surface methodology (RSM) is used.

Table 6.8 Process parameters and their range

Finishing parameters	symbol	Levels				
		-2	-1	0	1	2
Rotational speed of the MRH tool (rpm)	*T*	250	350	450	550	650
Reciprocation speed of the MRH tool (cm/min)	*A*	35	55	75	95	115
Rotational speed of the cap mould (rpm)	*W*	5	15	25	35	45

The foremost objective of the regression model is to provide the analysis of the reduction in the process variability in $\% \Delta Ra$ and to enhance the efficiency of the present R-MRH process. In the present model, the relation amid the output ($\% \Delta Ra$) and the input independent parameters is given by Eq. (6.7).

$$\% \Delta Ra = f(T, A, W) \quad (6.7)$$

where f is the response function, *T* is MRH tool rotational speed in rpm, *A* is the reciprocation speed of tool in cm/min and *W* is the workpiece rotation in rpm.

In present study, three parameters and five levels design are utilized to study the experimentations with the help of the central composite design (CCD). In total of 20 experiments are designed by the CCD as reported in Table 6.9. Each experimentation is performed for 20 min and after each experimentation, the MR polishing fluid is changed over the MRH tool surface. This is done so that the abrasive cutting edges remain fresh during the surface finishing of the internal cylindric surface of the EN-8 mold. Further, to verify the efficiency of the present model, the confidence level of the regression model is kept as 95 %. Next, to strengthen the relationship between the output response (*% ΔRa*) and the process parameters, the F-level test from analysis of variance (ANOVA) is performed. The % change in the average surface roughness (*% ΔRa*) is calculated using Eq. (6.1). Further, to demonstrate the efficacy of the present R-MRH process for the fine finishing of the internal surface of the EN-8 mold surface, the hardness, circularity, waviness, and the surface characteristics are analyzed with the micro hardness tester Mitutoyo HM-210 model, coordinate measuring machine (CMM), and scanning electron microscopy.

Table 6.9 Plan of experiment and their response *% ΔRa* after 20 min of rotational magnetorheological honing (R-MRH) process over plastic bottle cap mould.

Sr. No.	MRH tool rotation, *T* (rpm)	Tool reciprocation, *A* (rpm)	Workpiece rotation, *W* (rpm)	Initial surface roughness Rai value (nm)	*R1* (nm)	*R2* (nm)	*R3* (nm)	Final average *Raf* (nm)	Response (*% ΔRa*) (Eq. 6.1)
1	450	25	75	390	130	120	110	120	70
2	450	25	115	410	180	170	160	170	59
3	450	25	75	400	110	120	130	120	70
4	450	25	75	390	120	120	120	120	69
5	550	35	55	400	150	140	130	140	65
6	350	15	95	390	160	150	140	150	61
7	250	25	75	420	250	260	270	260	38
8	650	25	75	400	160	170	180	170	57
9	350	15	55	410	190	200	210	200	50
10	450	45	75	420	160	150	140	150	64
11	450	25	75	430	170	160	150	160	63
12	550	15	95	410	160	170	180	170	59
13	450	25	35	390	220	230	240	230	41
14	550	35	95	400	130	140	150	140	65
15	350	35	55	420	210	220	230	220	48
16	450	25	75	390	110	100	90	100	74

17	450	25	75	410	140	120	100	120	71
18	550	15	55	420	250	240	230	240	43
19	350	35	95	430	200	220	240	220	49
20	450	5	75	410	260	240	220	240	42

6.2.2 ***Results and discussion***

In the present study, total 20 experiments are performed to analyze the effect of the process parameters on the outcome response (*% ΔRa*). The experimentation data after performing finishing is reported on the Table 6.9. Further, the roughness value is taken at three different points (*R1*, *R2* and *R3*) over the internal cylindric surface after MR finishing and reported in Table 6.9. Further the final roughness value is obtained by taking the average of three surface roughness value which is further utilized in Eq. (6.1) for obtaining the *% ΔRa*. Next, for developing the statistical model, analysis of variance (ANOVA) is used as reported in Table 6.10. From the ANOVA model, it was found that the predicted model's p-value (PV) is found smaller than 0.05. This reveals that the present model is significant. Further, the P value of the lack of fit is higher than 0.05 (0.48) which confirms the non-significancy of the lack of fit. Similarly, the parameters with PV lesser than 0.05 are significant parameters and parameters having P-value higher than 0.05 are non-significant parameters.

Table 6.10 Final ANOVA table for the percentage change in surface roughness (*% ΔRa*).

Source	Sum of squares	Degree of freedom	Mean squares	F-value	Prob>F		% contribution (Eq. 6.3)
Model	2311.43	8	288.93	17.29	< 0.0001	Significant	
T	240.25	1	240.25	14.38	0.0030		8.17
W	196.00	1	196.00	11.73	0.0057		6.67
A	240.25	1	240.25	14.38	0.0030		8.17
T^2	789.12	1	789.12	47.23	< 0.0001		26.84
W^2	449.30	1	449.30	26.89	0.0003		15.28
A^2	591.98	1	591.98	35.43	< 0.0001		20.13
TW	242.00	1	242.00	14.49	0.0029		8.23
WA	98.00	1	98.00	5.87	0.0339		3.33
Residual	183.77	11	16.71				
Lack of fit	90.44	6	15.07	0.81	0.6047	not significant	
Pure error	93.33	5	18.67				3.17
Cor total	2495.20	19					

In the mathematical regression model, the non-significant parameters are not included and the significant parameters are namely *T, A W,* T^2, A^2, W^2, *TW* and *AW*. The ANOVA analysis of the effect of the significant parameters on the output response (*% ΔRa*) is reported in Table. From the ANOVA, F-value of the present predicted quadratic model is 17.29 (Table 6.10)

which confirms the significance of the present model. The second order mathematical regression model equation which is utilized for analyzing the effect of the process parameter on *% ΔRa* is obtained and given by Eq. (6.8).

$$\%\,\Delta R_a = -141.51 + 0.417T + 0.494W + 2.50A - 5.73 \times 10^{-4}T^2 - 2.86 \times 10^{-2}W^2 - 1.24 \times 10^{-2}A^2 + 5.50 \times 10^{-3}TW - 1.75 \times 10^{-2}WA \quad (6.8)$$

where *T* is the MRH tool rotation (rpm), *A* is the MRH tool reciprocation (cm/min) and *W* is the workpiece rotation (rpm). The *% ΔRa* predicted is calculated for each experimentation trial using Eq. (6.1), and is further compared with the experimental values. The closeness amid the predicted and experimental values can also be authenticated from model as the R-squared value is 93.52 % and Adj R-squared is 88.81 % value showing the accuracy of model. Further the effect of each significant parameter on the output response (*% ΔRa*) in the terms of the percentage contribution (%age cont.) has been analyzed using Eq. (6.3) and reported in Table 6.10. From the values of %age contribution (Table 6.10), it can be seen that the %age cont. of MRH tool rotation ($T+T^2$) contributes majorly as 35.01 %, followed by reciprocation speed of MRH tool ($A+A^2$) as 28.30% and then least of three parameters but significantly contributing parameter workpiece rotation ($W+W^2$) as 21.95 %. Further, after the regression analysis, the outcomes of the various significant parameters have been discussed in this section.

6.2.2.1 Individual effects of the process parameters on %age change in surface roughness

Figure 6.12 depicts the effect of magnetorheological honing (MRH) tool rotation speed (*T*) on %age change in surface roughness (*% ΔRa*) when the reciprocating motion of the tool and the rotating speed of the cylindrical cup mould are kept constant at 75 cm/min and 35 rpm respectively. From this figure, as the speed of tool rotation (*T*) increases, *% ΔRa* enhances. It keeps continue upto 550 rpm and then *% ΔRa* starts decreasing. This happens because with initial increase in *T*, the rotating speed of the active abrasive particles (AAPs) increases which perform motion alongwith the MRH tool. This increased rotational speed of the AAPs caused them to apply enhanced tangential shear force as discussed in chapter 3 using Eq. (chapter 3, 3.15). Due to which the enhanced shearing action of the surface asperities from the workpiece surface takes place. The repetitive action of shear with enhanced speed causes the increased rate of material removal from the finishing surface of work part. Therefore, the trend of *% ΔRa* upsurges. However, after achieving the maximum value of *% ΔRa* at *T*= 550 rpm, the further increase in the value of *T* causes the decrement in *% ΔRa*. This happens because on further

increasing the tool rotation speed the AAPs particles experiences excessive centrifugal forces in the opposite direction of the magnetic forces.

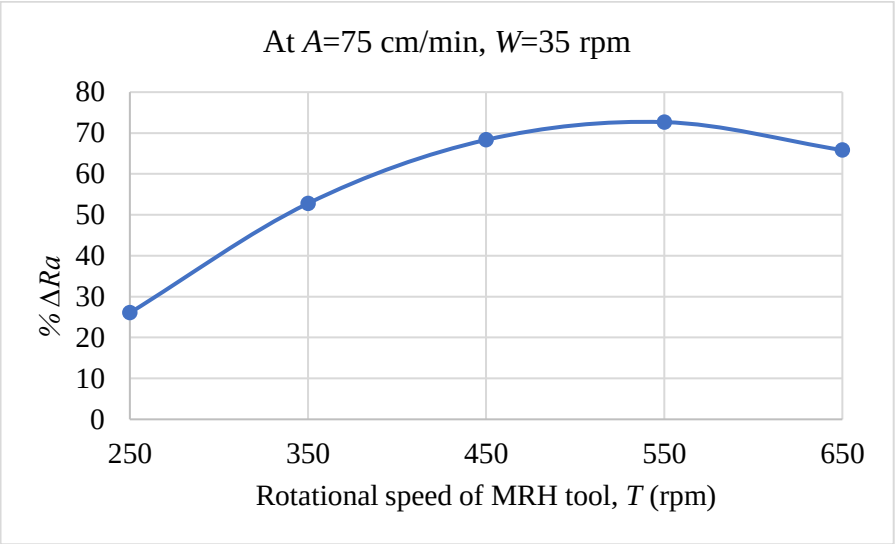

Fig. 6.12 Effect of rotational speed of MRH tool (*T*) on %age change in surface roughness *(% ΔRa*).

Due to the magnetic forces, the AAPs remain stiffly stuck in the electrolytic iron particles (EIPs) chain structure. Hence, at high speed of AAPs which is caused by high speed of tool rotation, the centrifugal forces start countering the effects of the magnetic forces for gripping the AAPs through EIPs chain structure. Hence, at higher speed the loosening of the AAPs in the EIP chain takes place due to which it becomes difficult to shear off the surface asperities properly from work part surface by the AAPs. Hence, the material removal rate decreases and further due to which the trend of the *% ΔRa* decreases. The maximum value of the *% ΔRa* was attained at the 550 rpm of the MRH tool rotation.

Figure 6.13 demonstrate the effect of the reciprocating speed of the magnetorheological honing (MRH) tool (*A*) on the improvement in surface finish (*% ΔRa*) when the tool rotation and the rotational speed of the cap mould are kept constant at 550 rpm and 35 rpm respectively. From this figure, as the reciprocation speed of the tool enhances upto 75 cm/min, the *% ΔRa* continues to increasing. But, beyond the 75 cm/min value of tool reciprocation the *% ΔRa* starts decreasing. This is because as the reciprocating speed (*A*) enhances initially, the relative speed of the AAPs increases over the longitudinal internal surface of the cylindrical cap mold. Due to which the axial shear force gets increased as it can be understood with the relation in Eq. (3.14, chapter 3). So, this leads to a higher material abrasion rate causing a fine finishing and a higher *% ΔRa*. However, beyond *A*=75 cm/min, the *% ΔRa* trend decrease because at a higher

value of *A*, the relative speed of the AAPs is enhanced in such an extent that their interaction time with finishing surface is decreased.

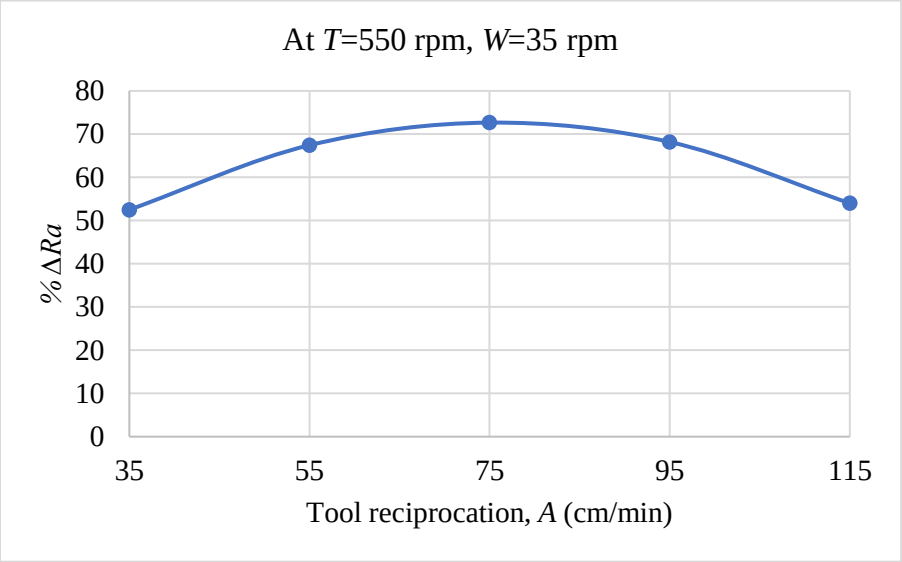

Fig. 6.13 Effect of reciprocating speed of MRH tool (*A*) on %age change in surface roughness (*% ΔRa*).

The decrease in the interaction time of the AAPs with the finishing surface of the workpiece leads to lacking in enhancement in the *% ΔRa*. So, it is found that 75 cm/min is the optimum value of the reciprocation speed at which maximum improvement is surface finish can be achieved.

Figure 6.14 demonstrate the effect of workpiece rotational motion (*W*) on *% ΔRa* when the tool's rotational speed (*T*) and reciprocation speed (*A*) are kept constant at 550 rpm and 75 cm/min respectively. From this figure, as the workpiece rotational speed (*W*) increases upto the 35 rpm, the improvement in surface finish (*% ΔRa*) takes place, but after *W*=35 rpm it starts decreasing. This happens because with initial increase in workpiece rotation the enhancement in tangential shear forces applied by the AAPs takes place (Chapter 3, Eq. (3.12)). Due which the rate of shearing-off of the surface asperities from the workpiece surface by the AAPs enhances. This leads to increase in material abrasion rate which enhances the trend of *% ΔRa*. However, when the workpiece rotation speed goes beyond 35 rpm, there is a decrease in *% ΔRa*. This is because as the W speed enhances, the interaction time during which asperities in the surface and the AAPs collide can decrease. Due to the reduced time of interaction, the AAPs are not able to shear off the surface asperities properly in the short moment of the time

which leads to a decrease in *% ΔRa*. The maximum value of the *% ΔRa* was achieved at the 35 rpm of workpiece rotation.

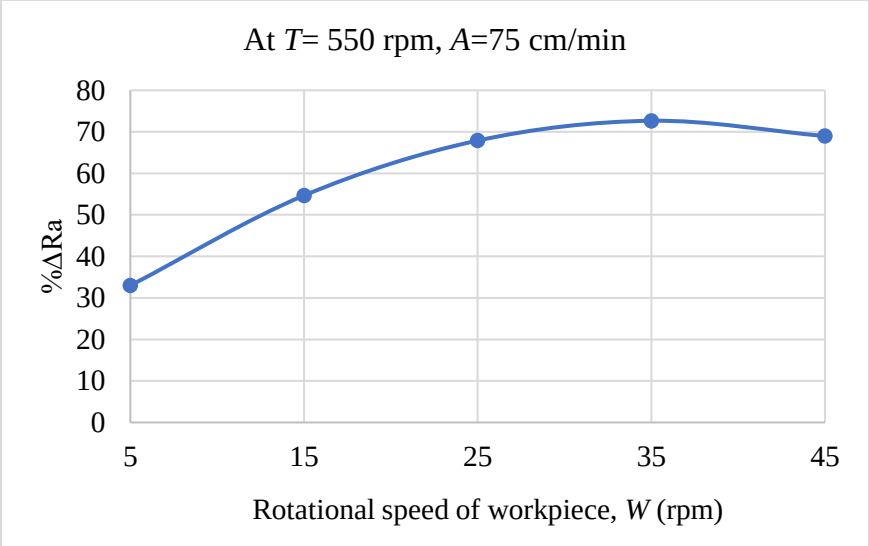

Fig. 6.14 Effect of rotational speed of the plastic bottle cap mould component (*W*) on %age change in surface roughness (*% ΔRa*).

6.2.2.2 Combined effects of the interacting process parameters on %age change in surface roughness

Figure 6.15 shows the interaction effect of tool rotation (*T*) and workpiece rotation (*W*) on the improvement in surface (*% ΔRa*) when the reciprocating speed of the tool (*A*) is kept constant. From this figure, it is seen that with initial increase in tool rotation and workpiece rotation the simultaneously the improvement in surface increases. This happens upto *T*=550 rpm and *W*= 35 rpm. But, beyond these values of *T* and *W* (550 rpm and 35 rpm respectively), the *% ΔRa* starts decreasing. The reason for such variation in *% ΔRa* increase in *T* and *W* has been stated in the explaination corresponding to the Figs. 6.13 and 6.14 respectively. Beyond those explaination increase in *% ΔRa* is also caused due to enhancement in shuffling of the the AAPs due to workpiece rotation. A higher shuffling of the AAPs causes a higher number of sharp-edged AAPs to consistently available at the finishing surface of the workpiece. Beyond the optimum value of *T* and *W*, the interaction time reduces and the centrifugal forces acting on AAPs gets enhanced in such extent that the grip of EIPs chain structure gets loose. Hence, finishing performance gets decreases. From this figure, the optimum values of *T* and *W* are found as 550 rpm and 35 rpm respectively.

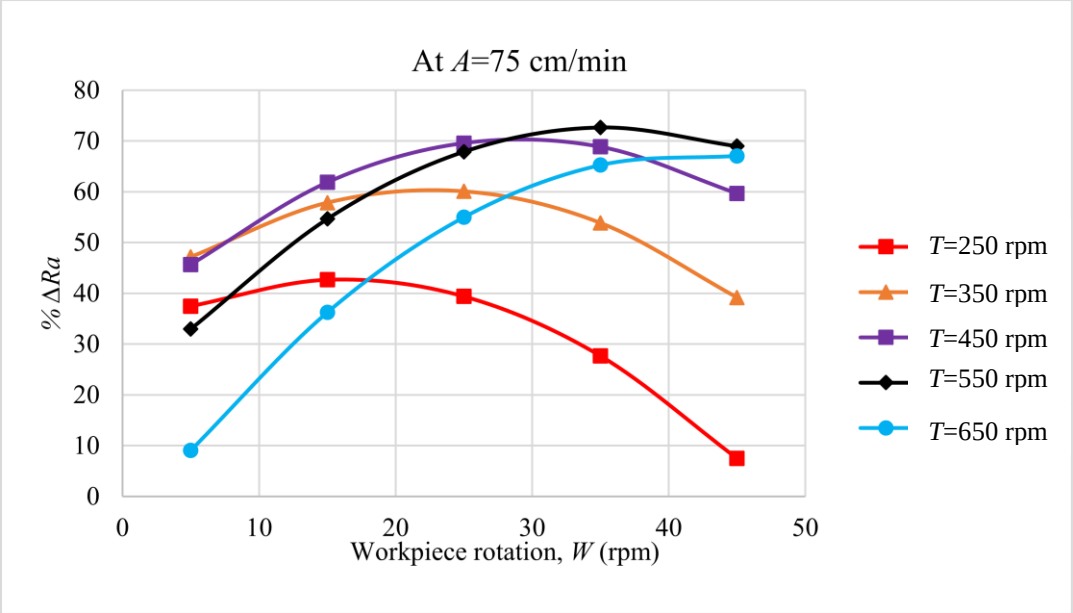

Fig. 6.15 Combined effect of the MRH tool's rotational speed (*T*) and the rotational speed of the plastic bottle cap mould component (*W*) on %age change in surface roughness (*% ΔRa*).

Figure 6.16 shows the interaction effect of the workpiece rotation speed (*W*) and reciprocation speed of the MRH tool (*A*) on the improvement in surface finish (*% ΔRa*) when the tool rotational speed (*T*) is kept constant at 550 rpm. From this figure, it is found that with initial increase in the values of W and *A* simultaneously the *% ΔRa* increases.

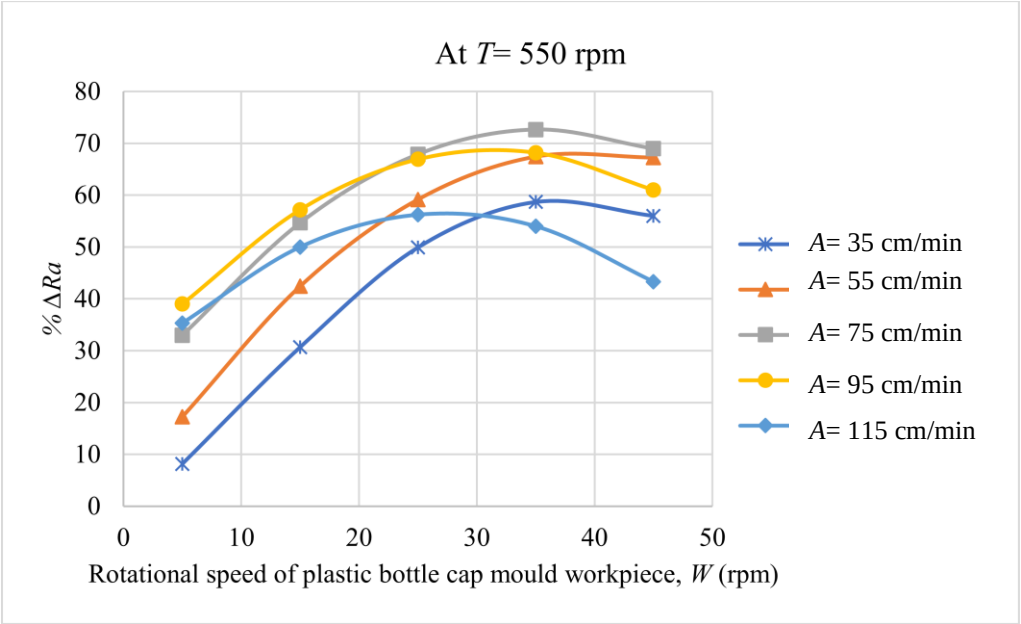

Fig. 6.16 Combined effect of the MRH tool's reciprocation speed (*A*) and the rotational speed of the plastic bottle cap mould component (*W*) on %age change in surface roughness (*% ΔRa*).

This is because the initial increase of *W* and *A* causes the increase in overall cutting shear force by increasing in tangential and axial shear forces as the relative speed of AAPs increases along rotating as well as reciprocating direction. But after achieving maximum *% ΔRa* at *W*= 35 rpm and *A*= 75 cm/min, the *% ΔRa* starts decreasing. This is due to with excess increase in these values causes to reduction in interaction time of the AAPs with the surface asperity. Due to which the AAPs moves from the asperity without abrading it. Therefore, the optimum value of *A* and *W* are found as 75 cm/min and 35 rpm respectively over which maximum surface finish is achieved.

6.2.2.3 Analysis of the finished internal surface of the plastic bottle cap mould with optimal process parameters

By using optimized parameters (*T*=550 rpm, *A*=75 cm/min, and *W*=35 rpm), the performance of the R-MRH process to finish interior surface of the EN-8 steel alloy mould has been achieved. The finishing operation on the interior surface of the EN-8 steel alloy bottle cap mould was carried out until a substantial improvement in the surface finish was observed. After 40 min finishing the inside surface of the workpiece mould, a significant improvement in the surface finish was achieved. Each set of finishing time is considered to be 20 min of finishing time during the experiment. After each 20 min of R-MRH process on interior surface of the plastic bottle cap mould, the the surface finish was assessed. The finishing is performed till 40 min of finishing duration which it provides the substantial improvement in surface finish. Enhancement in surface quality was reported by surface roughness analysis, surface waviness assessment, circularity assessment, and scanning electron microscopy (SEM).

The surface asperity of the initial ground surface and the final finished interior surface of the plastic bottale cap mould with the R-MRH process was measured using the roughness profileometer as mentioned in the experimental section. The surface asperity profiles are demostrated in the Fig. 6.17. Figure. 6.17(a) depicts the asperities of the initial internal surface of the real-time plastic bottle cap mould workpiece part. The parameters of the roughness profile of the initial internal surface of the cap mould workpiece was found as *Ra*= 430 nm, *Rz*= 2300 nm, and *Rq*= 520 nm. However, Fig. 6.17(b) represents the asperities of the final finished internal surface of the bottle cap mould workpiece using the rotational magnetorheological honing (R-MRH) process for 40 min of finishing. The parameters of the roughness profile of the final finished internal surface of the bottle cap mold in the current work are obtained as *Ra*= 60 nm, *Rz*= 410 nm, and *Rq*= 80 nm. From the roughness parameters of the initial ground and final MR-finished internal surface of the mould workpiece, the

substantial improvement in surface finish was achieved. Thus, the %age reduction in the roughness parameters of the interior surface of the CBHC workpiece was determined as $\%\,\Delta Ra$ = 86.04, $\%\,\Delta Rz$ = 82.17 and $\%\,\Delta Rq$ = 84.61.

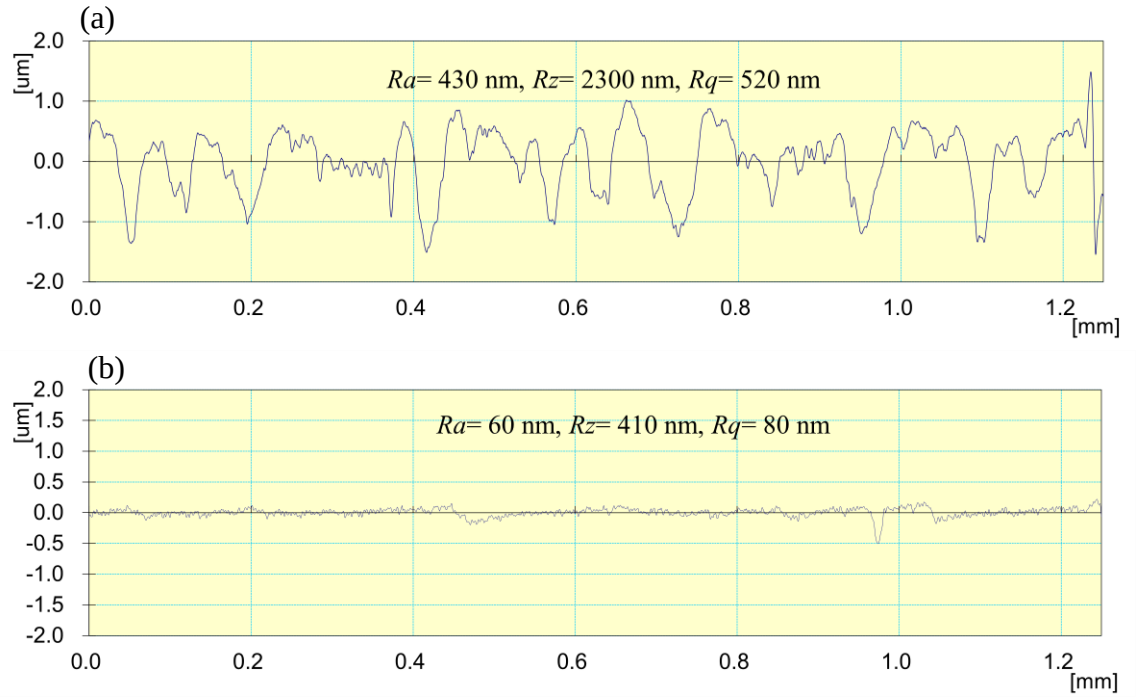

Fig. 6.17 Surface roughness profile of the (a) initial ground surface, and (b) final finished surface using MR-finishing on the internal surface of the entire real-time plastic bottle cap mould (internal diameter of 38 mm and length of 30 mm) with 40 min of finishing.

These improvements in surface asperity parameters from initial honed and the MR-finished surface authorize the substantial improvement in the surface finish. In order to validate the improvement in straightness achieved along the length of the internal surface of the bottle cap mold after employing the R-MRH process for its finishing, the surface waviness was measured on its initial ground and final finished surface as shown in Fig. 6.18. Figure 6.18(a) demonstrates the waviness parameters of the initial internal honed surface of the CBHC workpiece part that are *Wa*= 120 nm, *Wz*= 560 nm, and *Wq*= 150 nm. Whereas, with 40 min of finishing with the R-MRH process on the interior surface area of the 3581.41 mm^2 of bottle cap moukd using the optimised process parameters, the waviness parameters were obtained as *Wa*= 40 nm, *Wz*= 180 nm, and *Wq*= 50 nm as presented in Fig. 6.18(b). Hence, the % reduction in waviness parameters of the final MR-finished inside surface the bottle cap mould workpiece from the surface waviness of initial ground surface are found as $\%\,\Delta Wa$= 66.66, $\%\,\Delta Wz$ = 67.85, and $\%\,\Delta Wq$ = 66.66.

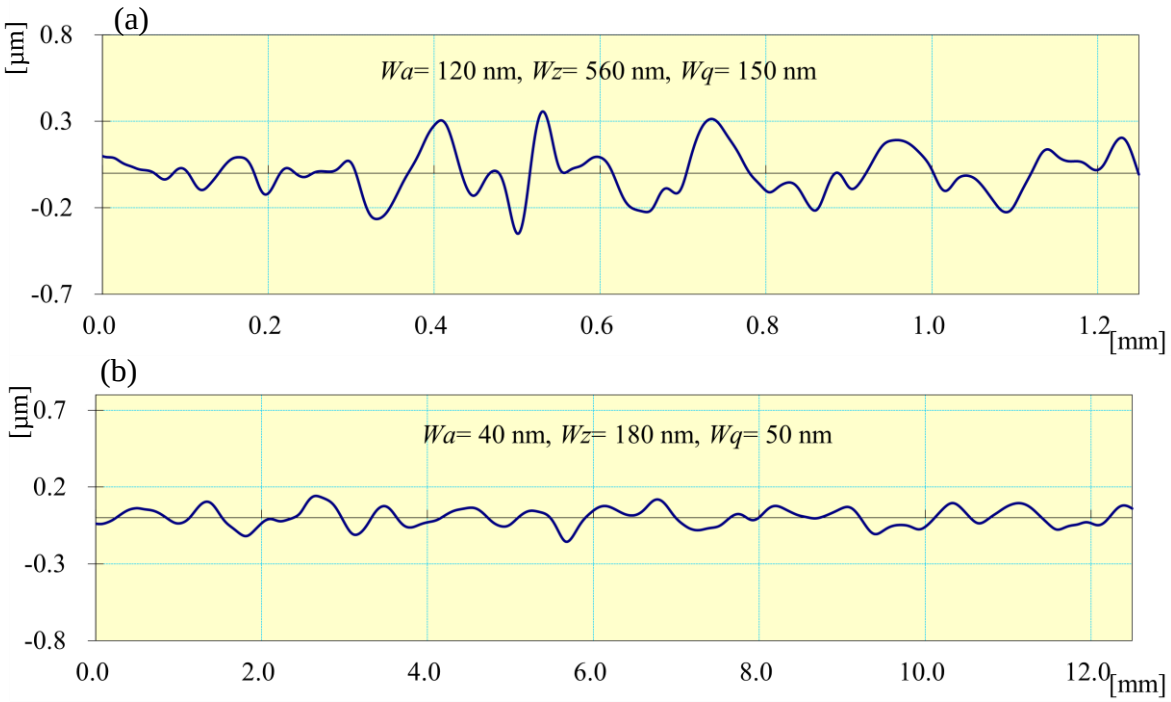

Fig. 6.18 Surface waviness profile of the (a) initial ground surface and (b) final MR-finished surface using R-MRH process on the internal surface of cylindrical the bottle cap mould.

These values of reduction in surface waviness parameters demonstrate that finishing the internal surface of the EN-8 steel alloy mold component (plastic bottle cap mould) using the R-MRH process is in good agreement for improving its straightness.The improved straightness in the inside surface of the bottle cap mould further enhances its dimensional accuracy that results in dimensionally correct end product casted from this mold. Functional performance of this mould is to cast the cap of bottle as much as possble dimensionaly accurate with aesthetically best surface quality. Such requirement of the end product relies on the minimum circularity of the mould. The minimum circularity of the bottle cap mould may cause to offer minumum resistances as well as avoids the prodcut to become distorted shape. Therefore, in this study, reduction in the circularity is analyzed. In order to validate the improvement in the circularity on the inside surface of bottle cap mould achieved in this work, the circularity assessment was carried out on the initial gound and final finished surface using the coordinate measuring machine (CMM). The circularity test is used to determine how well the circle is closer to the actual circle of the cylinder, that offers the dimensional stability of the part (Martorellil *et* al., 2016). Therefore, the improvement in circularity value in this work is demonstarted in Fig. 6.19. Figure 6.19(a) depicts the circularity photograph of the initial internal ground surface of the real-time bottle cap mould workpiece part and its values was measured as 0.2109. From this figure, it can be seen that most of the points marked on the

initial honed surface have differed from the actual circle of the circularity diagram. Whereas, Fig. 6.19(b) depicts the circularity image of the internal finished surface of the bottle cap mould using R-MRH process.

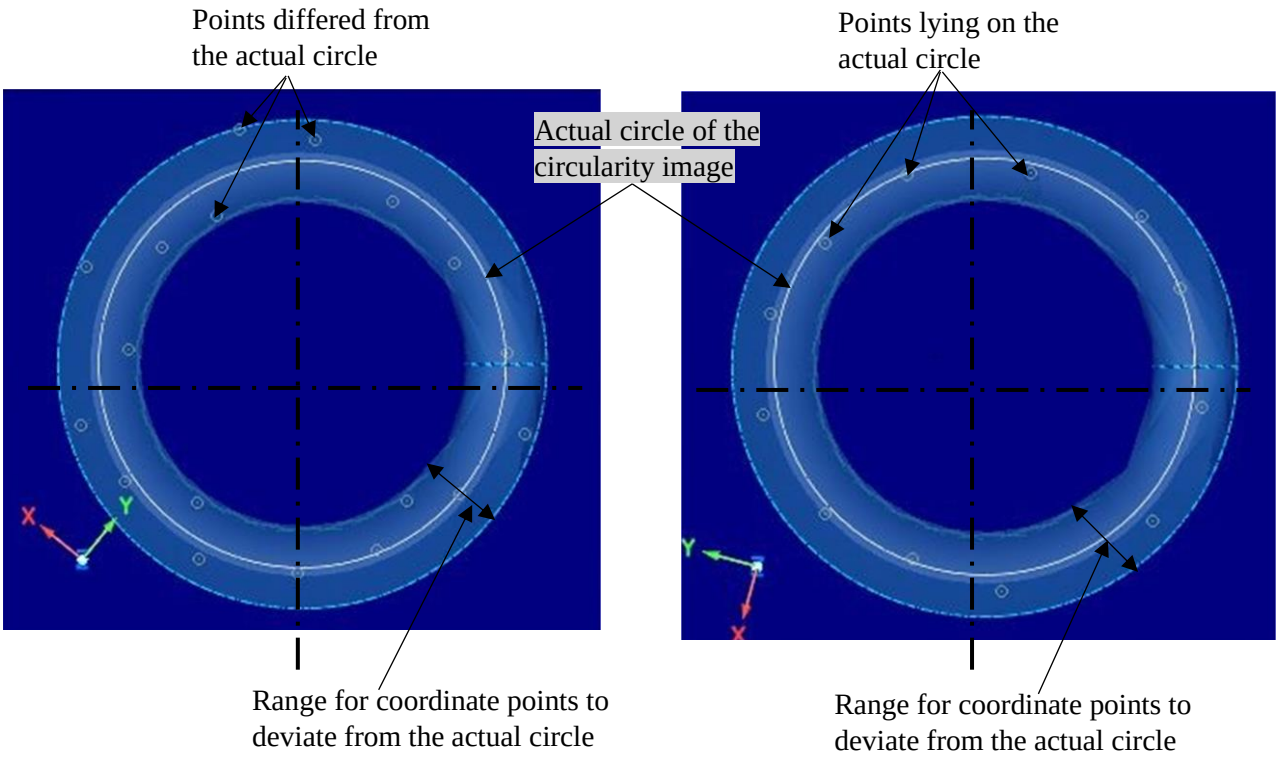

Fig. 6.19 Circularity images of (a) initial interior surface and (b) final MR-finished internal surface of the plastic bottle mold (internal diameter of 38 mm and length of 30 mm) with 40 min of R-MRH finishing using the optimal parameters.

Major improvement in circularity can be clearly verified as most of the points reported either lie on the actual circle or are very nearly to it. The circularity value was reduced to 0.0421 with 40 min on 3581.41 mm^2 surface area of MR finished inside surface of the bottle cap mould workpiece from its initial circularity value of 0.2109 on the gound surface. Figs 6.19(a) and (b) reveal that after R-MRH finishes over the interior surface of the real-time bottle cap mould workpiece, almost all of the points reported in the circularity test are found closer to the true circle. The level of circularity is said to be better as the points recorded are closer to the actual circle. That's why, Fig. 6.19(b) means that the R-MRH process is considered to be useful for improving the circularity of the inner surface of the present considered plstic bottle cap mould.

Figure 6.20(a) and (b) depict the scanning electron micrographs of the initial internal honed and the finally MR-finished inner surface area 3581.41 mm^2 of the plastic bottle cap mould with 40 min of finishing utilizing optimal parameters. As the real-time mould (palstic cap bottle

mould) is used for this study, the finishing was performed by the manufacturing industry using the grinding process. Therefore, it can be seen in Fig. 6.20(a) that various kinds of surface defects such as deep grinding lays, surface irregularities, scratches, scratching marks, etc. are present. Such surface defects are identified as a result of the direct interaction of the grinding tool with the inside surface of the plastic bottle cap mould during the grinding process.

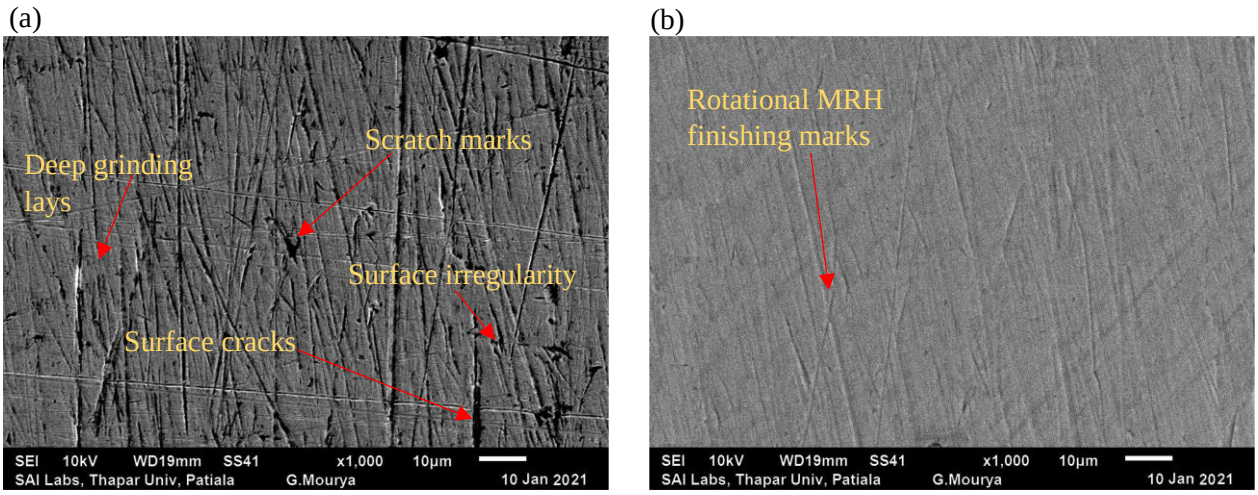

Fig. 6.20 The scanning electron micrograph of (a) initial ground surface, and (b) final R-MRH finished interior surface of the entire real-time cylindrical surface of plastic bottle cap mould (internal diameter of 38 mm and length of 30 mm) with 40 min of finishing time using optimum process parameters.

However, while performing the R-MRH process on the initial ground surface of plastic bottle cap mould, the micron-sized abrasive particles abrades the roughness peaks through the abrasion action. This action is caused by simultaneous rotating and reciprocating motion along with the workpiece rotation under magnetic indentation force which yields the resultant cutting shear force (F_s) in microchip form (chapter 3, Eq. 3.15). Thus it results in an improvement in the surface texture of the inside surface of the plastic bottle cap mold as shown in Fig. 6.20(b). This photograph shows few finishing marks marks left on the MR-finished surface as compared to the initial ground surface in Fig. 6.20(a).

6.2.3 Conclusions

A rotational magnetorheological honing (R-MRH) process is used to finish the internal surface of the plastic bottle cap mould. The response surface methodology technique with the central composite design is used to analyze the influence of finishing process parameters on the percentage reduction in surface roughness value. This forecasts the optimum process parameters for finishing the internal surface of the plastic bottle cap mould efficiently with the present process. The following conclusions demonstrate the effectiveness of the MR finished

surface of the plastic bottle cap mould in improving the effectiveness in its widespread applications.

- The average surface roughness value was decreased to 60 nm from the initial ground surface roughness value of 430 nm after 40 min of MR finishing over the surface area of 3581.41 mm^2 with the R-MRH process after utilizing the optimum parameters. The results signify that the present R-MRH process is capable to fine finish the surface of this mould.
- The reduction in surface waviness and circularity of internal surface of plastic bottle cap mould was found to 40 nm and 0.0421 from the initial values of ground surface waviness 120 nm and 0.2109 respectively with 40 min of finishing using R-MRH process. These results indicate that present R-MRH process is potent to improve the dimensional as well as geometric accuracy on the inside surface of the plastic cap bottle mould. The improvement in the circularity test over the internal surface of the plastic cap bottle mould reveals the enhancement in dimensional accuracy.
- Scanning electron microscope images reveal enhancement in surface characteristics with the R-MRH tool over the internal surface of the plastic cap bottle mould.
- The present developed R-MRH process can successfully finish the various types of the cylindrical mould efficiently for improving their operative functionality.

6.3 Magnetorheological finishing of the internal surface of the cast-iron cylindrical moulds

The cylindrical products such as automotive parts, beverages canes, domestics appliances, glass beaker, epoxy resin rod, polyvinyl chloride pipes, etc. are made of the materials such as glass, plastic, aluminum, fibers, polyvinyl chloride (Razak *et* al., 2011). The requirements of the basic features in the products are sufficient strength and stiffness, functional transparency for glass material products, stable dimensions (straightness and circularity), acceptable surface finish quality (Razak *et* al., 2011; Kryvyi *et* al., 2020; Maan *et* al., 2017), etc. Manufacturing of the cylindrical products of such materials was not found in a good agreement using the fabrication methods other than the casting method (Pawar *et* al., 2015). Therefore, the industrial components of such materials are preferred to manufacture using the casting method. Due to the hot molten metals poured in the cylindrical mold while casting the cylindrical components, the excess rise in temperature may cause in deformation of the mold and degradation of mold material (Mishra *et* al., 2014). Considering these limitations, the cast-iron (CI) is chosen as a material of cylindrical mold for the aforesaid products. Because cast-iron material has a higher

melting temperature than the materials as discussed (glass, plastic, aluminum, fibers, polyvinyl chloride) (Darvell, 2018). Also, the cylindrical mold with a highly finished internal surface ensures the avoidance of intermixing of colors in plastic industrial products (Grover and Singh, 2018a).

Therefore, the surface quality of the such products casted by the mold of cast iron (CI) depends on the finishing quality of the internal surface of the CI cylindrical mold. Because finishing the products of the materials like glass, plastic, aluminum, fibers, polyvinyl chloride using traditional finishing is a tedious task. Therefore, for improving the functional applicability of the cast-iron cylindrical mould by finishing its internal surface using the present developed rotational magnetorheological (R-MRH) process, this study has been performed. For this analysis of improvement achieved in surface finish quality of the internal cylindrical surface of the CI mold, improvement in straightness and circularity are also studied along with surface finishing and surface texture study. This is because the straightness and circularity of a mold are the important features for achieving the dimensional accuracies, tolerances minimization, reducing heat and vibration during the functional operations. Therefore, in this work, the circularity and waviness of the pre- and post-MR-finished cylindrical mold workpiece surface are measured and improvement is tracked. As the R-MRH process is a newly developed internal MR finishing process, the literature regarding the optimum process parameters for fine finishing of the CI cylindrical workpieces lacks. The scarcity of literature causes to perform the study to predict the optimum process parameters of the R-MRH process for inner surface finishing of the CI cylindric mold surface. Tool rotational speed, tool reciprocating speed, workpiece rotating speed, and working-gap are considered as the process parameters for the present work. The parameters for this work are selected based on mechanism of the R-MRH process in which the variable factors are involving. Further, their ranges are selected based on the preliminary experimentations. For predicting the optimum process parameters of the R-MRH process for finishing the inside cylindrical mold's surface of the CI material, the response surface methodology (RSM) method has been utilized. Under this technique, the central composite design is considered for optimization. Then using the predicted optimum process parameters of the R-MRH process for internal finishing of the CI cylindrical workpiece, the finishing capability of this process has been evaluated for the same workpiece cylinder.

6.3.1 Material and methods

6.3.1.1 Selection of material

In this work, a typical cast-iron (CI) cylindrical mould with a 60 mm diameter and 55 mm length is considered for the study of finishing capability of rotational magnetorheological honing (R-MRH) process for finishing its internal surface. The chemical composition of the CI cylindrical mold material by weight percentage is found as Fe 92.79 %, C 3.45 %, Si 2.73 %, Mn 0.55 %, P 0.48 %. Based on its chemical composition, it is found that the material is a gray cast iron (Gumienny and Giętka, 2015). So, this material (gray cast iron) is selected under consideration of cheaper cost, excellent machinability, lower shrinkage capacity, higher melting temperature, higher damping capability, higher wear and abrasion resistance as these properties are needed for the functional mold. There are thirty workpiece samples of the same composition are prepared for conducting the experimentation on the planned experiments (using Design-Expert version 6.0.8.). In this work, magnetorheological polishing (MRP) fluid is used as a finishing medium. The MRP fluid is composed of 20 % electrolytic iron particles (EIPs) of 1000 mesh number, 20 % silicon carbide abrasive particles of 800 mesh number, and 60 % base-fluid. The base-fluid of the MRP fluid is comprised of 20 % grease (AP3) and the rest of 80 % is paraffin oil. The % share of each constituent of the MRP fluid is taken in volume %. The polishing fluid is thoroughly mixed using an AC powered motor fluid mixture.

6.3.1.2 Experimentation

The present experimentation is performed using the rotary magnetorheological honing (R-MRH) process as shown in Fig. 6.21. The concurrent rotary and axial movement of the tool is performed over the inside surface the oppositely rotary movement of the CI cylindric mold. The four set screws in each face of the workpiece holder through which the cast-iron (CI) cylindrical mold is tightly fixed as shown in Fig. 6.21. The rectangular workpiece holder is fixed with the coupling shaft with four screws on each corner of the coupling. The coupling shaft is mounted on both plumber blocks. One plumber block has mounted the fixture. Another plumber block is fixed on the breadboard just below the first one. The use of two plumber blocks makes the fixture enough rigid for zero eccentricity while the rotating motion of cylindrical CI mold workpiece. The magnetorheological polishing (MRP) fluid is employed over the external bulged magnetic tool surface. The electrolytic iron particles (EIPs) of the MRP fluid get magnetized and attracted to the external bulged surface of the present tool. Thus, the rotating motion and the axial motion of the MRH tool over the inner side surface of the oppositely rotating CI cylindric mold cause the finishing action.

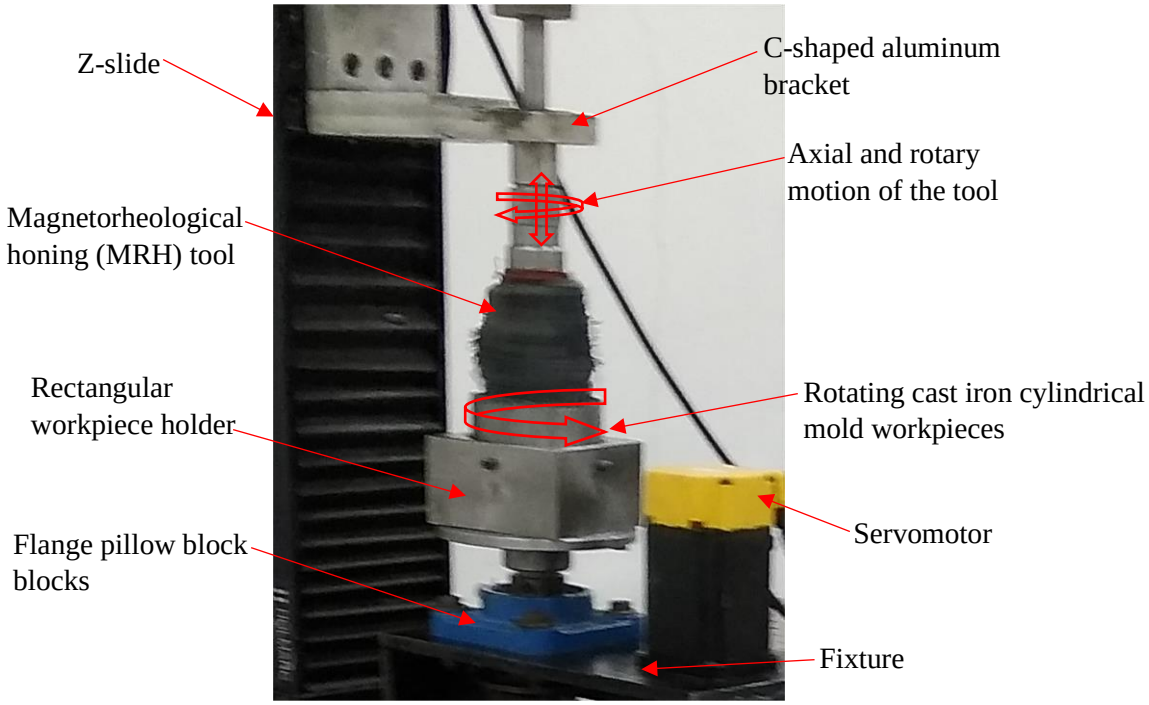

Fig. 6.21 Rotational magnetorheological honing (R-MRH) process for finishing the internal surface of the cast-iron cylindrical mold.

6.3.1.3 Design of experiments

The rotary magnetorheological honing (R-MRH) process is a newly devised MR fluid-based fine finishing operation. The study of process parameters optimization is conducted using the central composite design under RSM-technique. Based on the early experiments performed using the R-MRH process on the mild steel cylindrical workpiece, the four process parameters i.e., tool rotation (T), tool axial speed (A), workpiece rotation (W), and the gap between magnetic tool surface and inner cylindrical workpiece surface (G) are taken as the factors of experimental design. While designing the experiments, there are five levels are considered for the values of the four process parameters (factors) as reported in Table 6.11.

Table 6.11 Process parameters and their ranges.

Process Parameters		Ranges				
Symbol	Description	−2	−1	0	1	2
T	Rotary speed of the magnetorheological honing tool (rpm)	200	300	400	500	600
A	Axial speed of the magnetorheological honing tool (cm/min)	40	60	80	100	120
W	Rotary speed of the cylindrical mold workpiece (rpm)	5	15	25	35	45
G	Gap between the edge surface of the permanent magnet of the magnetorheological honing tool (mm) and the inside surface of the cast iron cylindrical mold workpiece (mm)	1	1.5	2	2.5	3

Using RSM-technique in "Design-Expert 6.0.8 software", thirty experiments are designed which are tabulated in Table 6.12. For conducting the thirty trial experiments, thirty workpiece samples are prepared by the fabrication. Also, the grinding process is applied to their finishing surface for the generation of pre-MR finishing surface.

Table 6.12 Plan of experiments and the responses obtained.

Sr. No.	Process parameters				Initial surface roughness (Rai, nm)	Final average surface roughness (*Raf*, nm)			% ΔRa Eq. (6.1)
	T (rpm)	*A* (cm/min)	*W* (rpm)	*G* (mm)		$R1$	$R2$	$R3$	
1	400	80	25	1	380	180	190	200	50
2	400	120	25	2	390	260	265	270	32
3	400	80	25	3	380	235	228	221	40
4	300	60	15	1.5	400	150	152	148	62
5	400	80	25	2	390	105	105	105	73
6	500	60	35	1.5	380	110	198	186	48
7	400	80	25	2	360	132	122	112	66
8	400	80	25	2	380	117	122	127	68
9	400	80	5	2	420	199	189	209	55
10	400	80	25	2	390	127	117	107	70
11	500	100	35	2.5	400	234	224	214	44
12	500	100	15	1.5	400	274	264	254	34
13	200	80	25	2	390	260	250	240	36
14	300	100	15	1.5	380	230	220	210	42
15	500	100	15	2.5	420	279	269	259	36
16	300	100	35	2.5	410	277	267	257	35
17	400	40	25	2	380	192	182	172	52
18	300	60	15	2.5	390	186	176	166	55
19	300	60	35	2.5	410	215	205	195	50
20	600	80	25	2	400	330	320	310	20
21	400	80	45	2	380	151	141	131	63
22	500	60	35	2.5	380	177	167	157	56
23	300	100	35	1.5	390	193	183	173	53
24	300	100	15	2.5	420	237	227	217	46
25	400	80	25	2	410	137	127	117	69
26	400	80	25	2	400	122	112	102	72
27	500	60	15	2.5	380	246	236	226	38
28	500	60	15	1.5	390	260	250	240	36
29	300	60	35	1.5	420	140	130	120	69
30	500	100	35	1.5	410	248	238	228	42

The surface roughness of each thirty pre-MR-finished ground samples of the workpieces is measured. The experimentations are conducted on the thirty samples using the experimental conditions as reported in Table 6.13. The finishing time of each experiment was taken as 25 min. After 25 min of finishing on each of the thirty samples with the R-MRH process using the parameters as per the designed experiments (Table 6.12), the surface asperity is measured on each sample at three different locations (*R1*, *R2*, and *R3*) as reported in Table 6.12.

Table 6.13 Experimental conditions.

Parameters	Condition
Tool materials	4 NdFeB permanent magnet
Magnetic field	0.35 T
Workpiece materials/shape	Cylindrical cast-iron
Finishing medium	Magnetorheological polishing fluid
Finishing time	25 min

The average value of the surface roughness (*Raf*) of the measured surface asperities (*R1*, *R2*, and *R3*) in each experiment is used to calculate the response ($\% \Delta Ra$) as in Eq. (6.1). RSM method of parameter optimization is based on statistics, and mathematics which is used for analysis, and developing a mathematical model for engineering-based issues (Hazir, *et* al., 2019). Based on the various parameters obtained from the analysis of variance (ANOVA), fit summary, model, diagnostic, and model graph tabs bar of the Design-Expert software while RSM analysis numerous of the conclusions are made in the present study at a confidence level ≤ 0.05. A confidence interval evaluates the probability that a population parameter can lie between two set values.

The experimentation is conducted on the rotary magnetorheological honing (R-MRH) setup (Fig. 6.21). During the experimentation, the MRH tool is made simultaneously rotating and axially reciprocating using the servomotors fixed on the C-type bracket and Z-slide respectively inside the rotating cast-iron (CI) cylindrical mold workpiece as depicted in Fig. 6.21. Also, the CI cylindric workpiece is rotated using the servo-motor attached to the fixture of the R-MRH setup. For characterization of the post-finishing surface of the workpiece, a tapered slot cut is made in it. Matching to the tapered slot cut on the inside of the CI cylindrical mold, all thirty workpiece samples are prepared. For the generation of the initial surface before experimentation, the grinding operation is performed on each work part samples. The initial and final surface roughness is measured on the same reference point in each trial of roughness measurement for getting the exact result of the change in surface roughness on that location. The magnetorheological polishing (MRP) fluid is utilized as the finishing means in this work. The fluid is constituted with the help of literature (Bedi and Singh, 2018a) based on similar workpiece material. While preparing the MRP fluid each component of the fluid is measured carefully on the weight evaluating device “Electronic compact scale model number SF-400”. Firstly, the measured paraffin oil and AP3 grease is poured into the mixing chamber and are mixed uniformly. Side by the measured silicon carbide (SiC) abrasives is mixed thoroughly in the measured electrolytic iron particles (EIPs) powder by spoon manually. Then the mixed SiC and EIPs powder are poured very slowly and intermittently into the mixing chamber in which

AP3 grease and paraffin oil are already mixed. Then all the components are mixed gently for 30 min to get uniformly mixed MRP fluid.

Using the thirty prepared samples of cast-iron (CI) and considering the process parameters as given in Table 6.11, the experimentations are conducted by inserting one by one sample in the slot cut of the CI cylindrical mold. Using the parameters of planned experiments, each experimentation is performed for 25 min of finishing time on the experimental setup as depicted in Fig. 6.21. The initial ground and final MR-finished inside surface roughness of the CI cylindrical mold are measured using the Mitutoyo profilometer (SJ-400) with a 0.25 mm cut-off length at 5 samplings cut-off length. The surface roughness of the initial ground-surface on the thirty CI work part samples is measured and found in the range of 380-420 nm. The polishing fluid used as a finishing agent is applied manually on the permanent magnet's external bulged surface of the tool. The polishing fluid is renewed once in between the 25 min of finishing time so that fresh-edged active abrasives remain available during the entire finishing cycle time of 25 min. The responses obtained after conducting the thirty experiments are further used in predicting the optimum process parameters for finishing the CI cylindrical molds. To validate the response model obtained from this study, further five experiments are performed at random process parameters that are lying within the range of designed experiments.

After confirmation of the theoretical regression model, the finishing ability of the present R-MRH process for nano-finishing of the internal surface of the CI cylindric molds, the further experimentation has been performed using the optimum parameters obtained from the theoretical regression model. Each set of finishing time considered for this experimentation is 20 min. After completion of each set of finishing operation, the surface roughness measurement is performed for predicting the changes in the finishing surface. The finishing is kept continued after each set of finishing operation until the change in surface finish is observed insignificant from its previous set of finishing operation. To confirm the improvement obtained in surface finish and straightness, the measurement of surface roughness and surface waviness is conducted on before and after the MR-finished surface. However, to acknowledge the improvement in the uniformity in circularity and its surface texture, the test for circularity, and scanning electron microscopy tests are performed on before and after the MR-finished internal surface of CI cylindrical mold using the R-MRH process. The circularity of the internal surface of the cylindrical CI mold workpiece is measured on before and after the MR-finished workpiece surface using the coordinate measuring machine (CMM).

6.3.2 Results and discussion

Using the percentage change in surface roughness ($\%\,\Delta Ra$) of each designed experiment as a response, the analysis of variance (ANOVA) is performed. The ANOVA is performed using the central composite design technique under the response surface methodology (RSM) method. The results of the ANOVA are tabulated in Table 6.14.

Table 6.14 Final ANOVA table for the percentage change in surface roughness ($\%\,\Delta Ra$).

Source	Sum of squares	Degree of freedom	Mean square	F-value	P-value	Remarks	% contribution of factors
Model	5530.70	11	502.79	28.96	0.0001	significant	
T	504.17	1	504.17	29.04	0.0001		7.62
A	170.67	1	170.67	9.83	0.00570		2.58
W	620.17	1	620.17	35.72	0.0001		9.37
G	88.17	1	88.17	5.08	0.03690		1.33
T^2	2686.01	1	2686.01	154.71	0.0001		40.58
A^2	1122.01	1	1122.01	64.63	0.0001		16.95
W^2	126.30	1	126.30	7.27	0.01470		1.91
G^2	874.30	1	874.30	50.36	0.0001		13.21
TA	90.25	1	90.25	5.20	0.03500		1.36
TW	121.00	1	121.00	6.97	0.01660		1.83
TG	182.25	1	182.25	10.50	0.00450		2.75
Residual	312.50	18	17.36				
Lack of fit	279.17	13	21.47	3.22	0.10200	not significant	
Pure error	33.33	5	6.67				0.50
Cor total	5843.20	29					

From this table, it is found that *T*, *A*, *W*, *G*, T^2, R^2, W^2, G^2, *TA*, *TW*, *TG* are the significant terms as their P-values are less than 0.05 at 0.95 of the confidence intervals. The significant factors *T*, *A*, *W*, and *G* indicate that these factors influence the response ($\%\,\Delta Ra$) linearly. However, the significant squared factors i.e., T^2, A^2, W^2, and G^2 indicate that these factors influence the $\%\,\Delta Ra$ non-linearly (squared). As the same factor influences the $\%\,\Delta Ra$ linearly as well as non-linearly, therefore, the higher extent of the contribution of the factor (linearly or non-linearly) in influencing the $\%\,\Delta Ra$, enables the visibility of the effects. The interaction effects of the tool rotation (*T*) with tool axial motion (*A*) (i.e., *TA*), tool rotation (*T*) with workpiece rotation (*W*) (i.e., *TW*) and tool rotation (*T*) with working-gap (*G*) (i.e., *TG*) are also observed significant as their P-values are less than 0.05 (Table 6.13). Under the fit summary of the response analysis, lack of fit test, the quadratic source of the consecutive model, the sum of the square, and model summary statics are suggested whereas the cubic sources are aliased. The significant factors are the factors (Table 6.13) which influence the response model

significantly. To know the extent of contribution of the significant factors on the surface response model, the contribution of the source factors is calculated and reported as in Table 6.14. Also, the contribution of the source factors is shown in the bar chart as displayed in Fig. 6.22.

Fig. 6.22 Bar chart of the percentage contribution of the significant factors over the

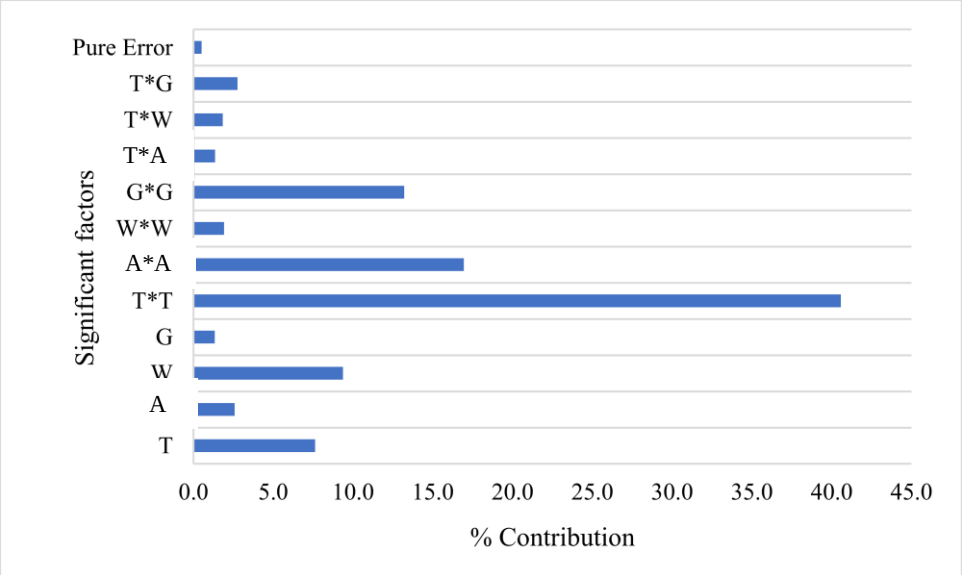

percentage improvement in surface finish.

The contribution values of the response influencing factors show that the factors T, and T^2 have the greatest influence on the response model as their values are summed up to 48.20 %. It means the rotary movement of the tool is the most important parameter in the present rotary magnetorheological honing (R-MRH) operation to finish the inner cylindric surface of the cast-iron (CI) mold workpiece. The second most influencing parameter observed in this work from Table 6.13 is the speed of axial motion of the tool (A). The summed-up value of the contribution of the factors A and A^2 is found as 19.53 %. The third influencing parameter on the response model ($\%\,\Delta Ra$) obtained from the R-MRH process during finishing is the working-gap (G) as the combined value of the contribution of G and G^2 is found as 14.54 %. The total contribution of the rotary speed of the CI workpiece mold cylinder (W) as the contribution of the factors W and W^2 is found as 11.28 %. This value of the % contribution of the CI workpiece mold cylinder's rotation is lesser as compared to the contribution of the other factors (Table 6.14 and Fig. 6.22) however, it is significant in magnitude.

This significant percentage contribution of the workpiece rotary motion in the response model shows its contribution to the enhancement in the finishing ability of the R-MRH process. The

ANOVA table (Table 6.14) shows that the lack of fit was insignificant as it has a P-value of 0.1020. Thus, the insignificant lack of fit was found as good for the generated model. Also, other parameters of the ANOVA analysis are reported in Table 6.15.

Table 6.15 Other parameters of ANOVA.

ANOVA Parameters	Value
R-Squared	0.9465
Adj R-Squared	0.9138
Pred R-Squared	0.8383
Adeq Precision	18.499

The correlation coefficient (R^2) is found as 0.9465 which signifies that the model is found adequate for the predictions. The difference between the adjusted R^2 and predicted R^2 was 0.0755 which was larger than 0.02. The magnitude of the difference between adjusted R^2 and predicted R^2 (0.0755) concluded a reasonable agreement of the pred R^2 with adj R^2 which is desirable for the model's adequacy. The adequate precision was found 18.499 which is far higher than 4 which is required for the model to be useful in navigating the design space. The RSM analysis of the designed experiments resulted in the mathematical relation of the response model ($\%\,\Delta Ra$) with the involving parameters. Theoretically obtained response model ($\%\,\Delta Ra$) from the present study in terms of involving parameters is represented in Eq. (6.9).

$$\%\Delta Ra = -135.578 + 0.447T + 1.829A + 0.239W + 59.5G - 9.895 \times 10^{-4}T^2 - 0.0159A^2 - 0.0215W^2 - 22.583G^2 + 1.187 \times 10^{-3}TA + 2.75 \times 10^{-3}TW + 0.0675TG \quad (6.9)$$

where the terms used in this Equation *T, A, W,* and *G* are the notations of the process parameters as discussed in Table 6.11. With the regression analysis of the *% ΔRa*, the outcomes have been summarised in the graphical representation (Figs. 6.23 and 6.24).

6.3.2.1 Effect of the individual parameters on the percentage change in surface roughness (%ΔRa)

All the significant factors involved in Eq. (6.9) influence the response model developed from the RSM analysis in this work. To evaluate the value of the effect of the significant factors on the response model, the values of process parameters are substituted in Eq. (6.9). The values of effect of the significant parameters are graphically represented in Figs. 6.23 and 6.24. The effects of the factors on the response model are analyzed in two ways. The first one is the analysis of the individual effect of the factors and the second ways of analysis is the analyzing

interaction effects of the factors on the *% ΔRa*. In this section, the individual effect of each factor and the combined effect of the significant interacting factors on the *% ΔRa* are discussed. Fig. 6.23 demonstrates the consequence of the individual factors on *% ΔRa*. Similarly, Fig. 6.24 demonstrates the consequence of the combined factors on *% ΔRa* in the present study.

Figure 6.23(a) is the graphical representation of the impact of the rotary motion of the magnetorheological honing (MRH) tool on the *% ΔRa*. From this figure, it is observed that the tool's rotary speed is varied from *T*=200 rpm to *T*=600 rpm with an interval of *T*=100 rpm, when the remaining parameters are kept constant as *A*=80 cm/min, *W*=35 rpm and *G*=2 mm.

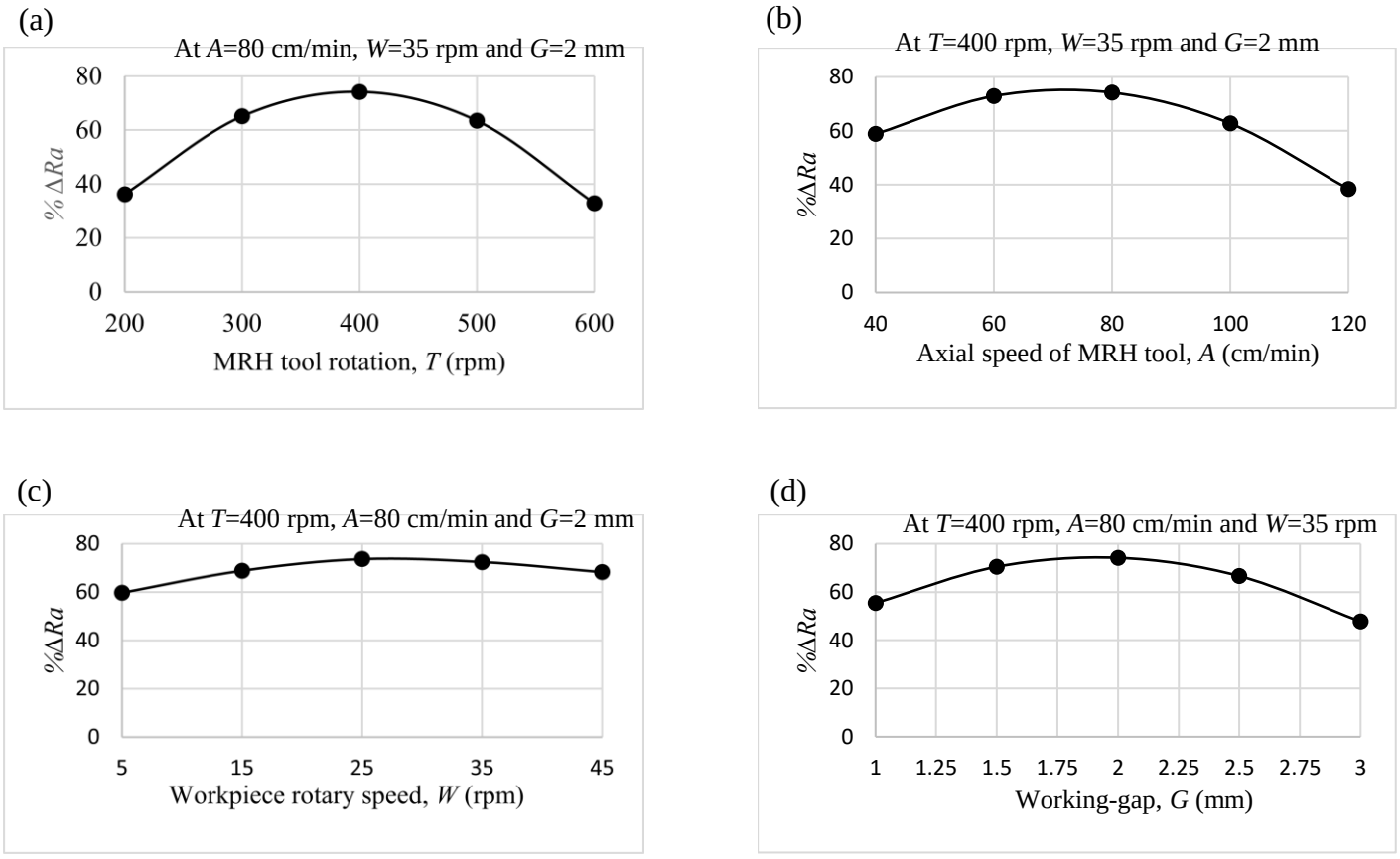

Fig. 6.23 Individual effect of (a) magnetorheological honing (MRH) tool rotary speed (*T*, rpm), (b) MRH tool axial speed (*A*, cm/min), (c) cast iron cylindrical workpiece rotary speed (*W*, rpm) and (d) working-gap (*G*, mm) on the *% ΔRa*.

When the tool rotation is started increasing from *T*=200 rpm, the *% ΔRa* starts increasing and it continues to increase up to *T*=400 rpm. On further increasing the rotary speed of the magnetic tool beyond the optimum value of tool rotation (*T*=400 rpm), the *% ΔRa* starts decreasing. This trend of the effect of the MRH tool's rotary speed on the *% ΔRa* is because of the lesser rotary speed of the tool causes the active SiC particles to make a lower relative rotary motion against the finishing cylindric surface of the cast-iron (CI) mold cylinder. The increasing relative

rotating motion due to the increasing the rotating motion of the tool causes the increase in the tangential shear force (F_{tns}) (Chapter 3, Eq. 3.12) also it causes in increasing the centrifugal force (F_{cen}) as discussed in chapter 3 (Eq. 3.30). Therefore, increasing centrifugal force results in enhanced indentation force which causes the active abrasive particles to indent into the finishing surface. The enhanced tangential shear force acting on the active abrasive particle due to the enhanced rotational speed of the tool which abrades more materials. But at a greater rotary speed than the optimal value of the tool rotary motion (T=400 rpm), a span of the interaction of SiC particle with the cylindric finishing surface of the CI workpiece mold decreases. Also, the centrifugal force (F_{cen}) exerting on the EIP chain structure gets dominating at a higher tool's rotary speed over the inter-particle magnetic force in the stiffer chain structure. Due to which the EIPs the chain structure suffers instability and resulting in poor surface finishing performance. Therefore, at higher rotary speed than the optimum rotary speed (T=400 rpm) of the tool, the adverse effect is noticed on *% ΔRa*.

Figure 6.23(b) describes the trend of the consequence of the axial motion of the present finishing tool on the *% ΔRa*. From this figure, it can be observed that the axial motion (A) is varied from 40 cm/min to 120 cm/min when the remaining parameters are kept constant as T=400 rpm, W=35 rpm, and G=2 mm. From the considered values of A, it is observed that 80 cm/min is the optimum speed of the axial motion of the tool at which the maximum *% ΔRa* can be achieved. Initially, the *% ΔRa* increases with an increase in the speed of the tool's axial motion. The increasing of the *% ΔRa* keeps continue up to the axial speed (A)=80 cm/min. But, on further increasing the axial speed of the tool beyond the optimum axial speed (A=80 cm/min), the *% ΔRa* starts decreasing. This trend of the effect of axial speed on the *% ΔRa* is taken place because the higher axial speed of the finishing tool is asserted on the active SiC particle to perform the higher relative axial motion. The axial shear force (F_{axs}) is related to the axial speed of the tool in direct relation as discussed in chapter 3 (Eq. 3.14). Therefore, with an increase in the relative speed of the axial motion of the tool, the relative axial speed of the active abrasive particles is increased which causes to acting of enhanced F_{axs} over the cast-iron cylindrical mold's finishing surface. The enhanced F_{axs} yields the higher shear off material from the cast-iron cylindrical mold's finishing surface resulting in a higher improvement in the surface finish. But, on further enhancing the axial speed of the tool beyond the optimum axial speed (A=80 cm/min), the improvement in surface finish starts decreasing. This is due to the further increment in the axial relative speed of the abrasive particles result in a reduced span of

contact of the active SiC particle to the finishing mold's surface which results in lesser finishing performance.

Figure 6.23(c) depicts the effect of the rotary speed of the cast-iron (CI) cylindric mold workpiece (*W*) on the *% ΔRa* when the remaining parameters are kept constant as *T*=400 rpm, *A*=80 cm/min, and *G*=2 mm. From this figure, it is observed that with the initial increment in the rotary speed of the CI mold workpiece cylinder, the increment in *% ΔRa* takes place. This increase of the *% ΔRa* takes place up to the workpiece rotary speed (*W)* of 35 rpm which can be said as the optimum rotary speed of the CI workpiece cylinder. But, with further increment in the rotary speed of the CI workpiece cylinder (beyond *W*=35 rpm), the decrement in *% ΔRa* takes place. This trend of *% ΔRa* with the variation in *W* is because initially increase in the *W* causes the elevation in the relative rotary speed of the active SiC particles w.r.t. the finishing workpiece surface. The contribution of workpiece rotation in elevating the relative rotary speed of the active abrasives w.r.t. the finishing surface of the CI workpiece cylinder also contributes to enhancing the tangential force (F_{tns}) while finishing action as discussed in chapter 3 (Eq. 3.12). Therefore, the initial increase in the workpiece rotation upsurges a higher abrasion rate of materials by acting a higher tangential force (F_{tns}) on the roughness peaks. Also, due to the rotary motion of the CI cylindric workpiece mold in the opposite direction of the rotating MRH-tool direction, the non-magnetic abrasive particles tend to perform random motion on the finishing cylindric CI mold's internal surface. The random motion of the non-magnetic abrasive favors the shuffling of the active abrasive particles during finishing action. The shuffling of the active abrasive particles elevates the finishing performance by maintaining a large number of sharp-edged active abrasive particles continuously during the finishing action. But, on further increasing the rotational speed of the CI workpiece cylinder beyond the optimum rotating speed (35 rpm), the relative speed of the active abrasive particles w.r.t. the internal finishing surface of the cylindric CI workpiece gets increasing excessively. Due to the excessive increase in the relative speed of the active abrasive particles, their interaction time with the roughness peaks of the finishing surface starts decreasing and gripped active abrasive particles get disturbed which results in decreasing the finishing performance.

Figure 6.23(d) illustrates the impact of the working-gap (*G*) on the *% ΔRa* while keeping the other parameters constant as *T*=400 rpm, *A*=80 cm/min, and *W*=35 rpm. From this figure, it can be observed that as the working-gap increases up to 2 mm, the finishing performance (*% ΔRa*) increases. This is because initially when the working-gap increases, the volume of the MRP fluid retained in the working-gap increases. Due to which the number of magnetic electrolytic iron particles (EIPs) in the working-gap also increases. The chain structures formed

by a large number of the magnetic iron particles grip the active abrasive particles more stiffly. Therefore, as the working-gap increases, the stiffer EIPs chain structures cause the fine finishing. But on further increasing the working-gap beyond 2 mm, the finishing performance starts decreasing because further increasing the working gap results in a decrease in the intensity of the magnetic field. The decreased intensity of the magnetic field weakens the magnetic force exerted by the magnetized EIPs of the chain structures. The weak magnetic force applied by the EIPs on the active abrasive particles and loosely formed EIPs chain structure cause the inefficient internal surface finishing.

6.3.2.2 Effect of the combined interacting parameters on the percentage change in surface roughness (% ΔRa)

Figure 6.24(a) shows the combined effects of the rotary and the axial speeds of the magnetic honing tool (*T* and *A*) on the *% ΔRa* when the rotating speed of the workpiece (*W*) and the working-gap (*G*) are kept constant at 35 rpm and 2 mm respectively. From this figure, it is observed that as an escalation in simultaneous rotary and axial speed of the MRH tool takes place up to *T*=400 rpm and *A*=80 cm/min respectively, the improvement in surface finishing (*% ΔRa*) increases up to approximately 74% and then starts decreasing. On increasing both factors concurrently, the net relative combined motion of the active SiC particles w.r.t. the workpiece's finishing surface increases. Due to the increased combined relative motion of the active abrasive particles, the total cutting shear force (resultant of axial shear and tangential shear) applied on the finishing surface of the workpiece increases. This causes to increase in surface finishing performance by increasing the abrasion rate of materials. The simultaneous rotary and axial motion of the finishing tool in the present work cause the active SiC particles to traverse along the path forming the helical shape on the finishing CI cylindrical mold surface. As a higher rotary speed is performed by an active SiC particle during finishing operation, a larger helical-shaped track distance is covered by it. Traveling of SiC particle along with the helical-shaped path results in a higher length of the path which results in an enhanced rate of surface finishing. But on further increasing the rotary speed of the finishing tool after achieving the maximum *% ΔRa*, the centrifugal force acting on the chain structure gets dominated over the magnetic force which unstabilizes the chain structure. The unstable chain structure results in a loose grip on the active abrasive particles with the magnetic force generated by the EIPs of the chain structure. Therefore, the increase in the rotary speed of the tool beyond the 400 rpm reduces the finishing performance. A similar trend of variation in *% ΔRa* with the variation in the finishing tool's axial speed is followed. The reason behind such a trend is that with

increasing the axial speed of the finishing magnetic tool, the net relative speed of the SiC particle along with the axial direction increases which result in enhanced finishing performance.

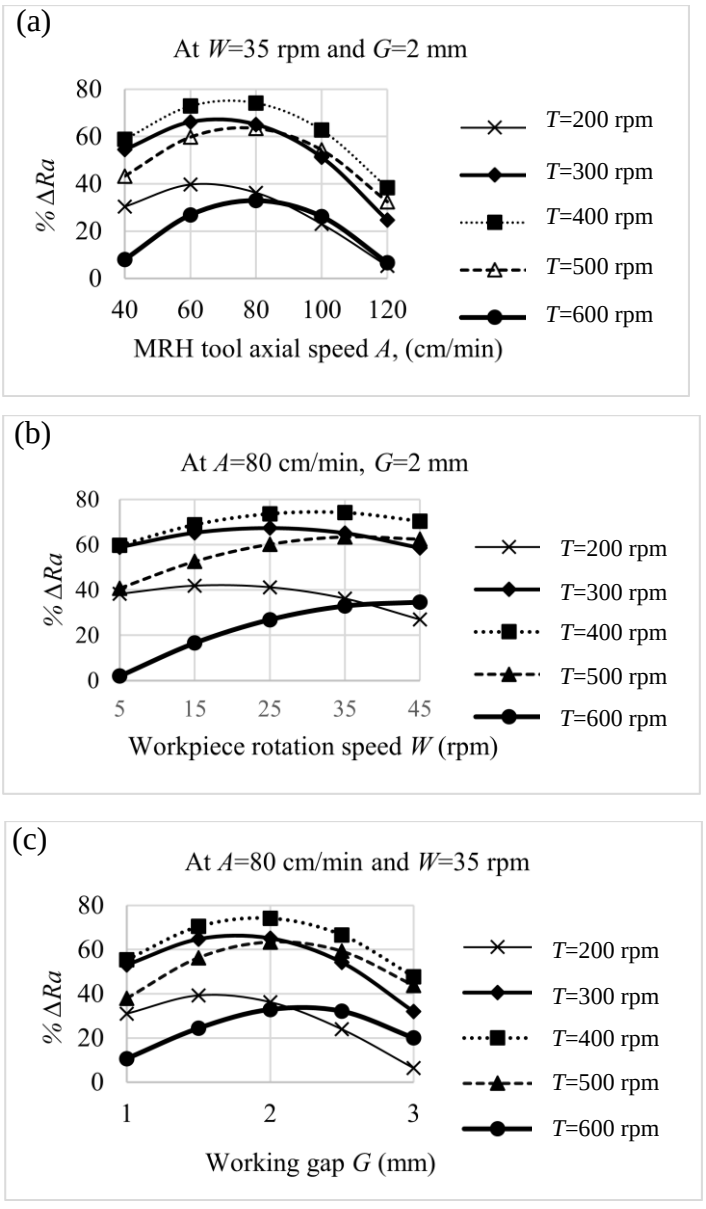

Fig. 6.24 Combined effects on the percentage change in surface roughness (*% ΔRa*) with the (a) tool rotary speed (*T*, rpm) and tool axial speed (*A*, cm/min) and (b) tool rotary speed (*T*, rpm) and workpiece rotary speed (*W*, rpm) and (c) tool rotary speed (*T*, rpm) and working-gap (*G*, mm)

But, on further increasing the axial speed of the finishing magnetic tool (beyond the optimum axial speed *A*=80 cm/min), the axial relative speed of the SiC particle is elevated. With the enhancement in the axial speed of the magnetic tool, the length of a helical-shaped path crossed by an active SiC particle decreases. This causes a reduction in the span of the SiC particle's

interaction with the finishing surface which results in a lower finishing performance. Therefore, the time duration of the SiC particle's interaction with the workpiece's finishing surface acts as a significant role while abrading the materials from the same workpiece mold's surface.

Figure 6.24(b) illustrates the simultaneous impact of the rotary speed of the presently used magnetorheological (MR) finishing tool (*T*) and the speed of rotary motion of cast-iron (CI) cylindric mold (*W*) on the finishing performance (*% ΔRa*) while keeping the axial speed of the tool (*A*), and working gap (*G*) as constant at 80 rpm and 2 mm respectively. It is found that with increasing the tool's rotary speed (*T*), and workpiece rotary speed (*W*) simultaneously up to 400 rpm and 35 rpm respectively, the *% ΔRa* enhances up to 74 %. But, with further increment in the values of *T* and *W* beyond their optimum values at which the maximum *% ΔRa* is achieved, the *% ΔRa* starts decreasing. Increasing both factors (*T* and *W*) concurrently causes enhancement in the net relative rotary speed of the SiC particles against the inner cylindric mold's surface because the rotational direction of both factors is opposite to each other. The enhanced relative rotary speed of the finishing particle increases surface finishing performance. But, beyond the optimum value of the factors (*T=400 rpm* and *W=25 rpm*), the net relative speed of rotary motion of the SiC particle is so increased that its span of interaction with the finishing surface gets decreased. The decreased span of interaction lowers the finishing performance. The abrasion on the finishing surface owing to the net relative rotary speed of the SiC particle initially dominates. But on further increasing the rotary speed of the tool after the maximum *% ΔRa* is achieved, electrolytic iron particles (EIPs) chain structure of the polishing fluid experiences a significant centrifugal force (F_{cen}). The significant F_{cen} may destabilize the chain structure which adversely affects the finishing action. The initial elevation in the speed of the rotary motion of the CI cylindric mold to the oppositely rotating tool direction increases the net relative rotary speed of the active SiC particles against the mold's inner surface. Also, it causes shuffling of the sharp-edged active SiC particles which favor more abrasion causing better finishing action (Das *et* al., 2010). But, on further increasing the workpiece's rotary speed, the duration of contact of the active SiC particles is decreased causing a reduction in the interaction time of the active abrasive particles with the finishing surface of the workpiece. Therefore, beyond the optimum rotary speed of the CI mold workpiece, the improvement in surface finish starts decreasing.

Figure 6.24(c) demonstrates the combined impact of the MRH-tool's rotary speed (*T*) and the working-gap (*G*) on the *% ΔRa* when the reciprocation speed of the tool (*A*) and rotary speed of the CI mold workpiece cylinder are kept constant as 80 cm/min and 35 rpm respectively.

From this figure, it is found that as the working-gap (G) and the tool's rotary speed (T) increase up to 2 mm and 400 rpm respectively, the improvement in the surface finish ($\%\,\Delta Ra$) increases up to 74.18 %. But, on further increasing these factors beyond their optimum value where maximum improvement in the surface finish ($\%\,\Delta Ra=74.18\ \%$) is achieved, $\%\,\Delta Ra$ starts decreasing. Such variation in $\%\,\Delta Ra$ takes place because initially increasing of the T and G caused to enhance the net relative rotary speed of the active SiC particles and increases in the number of SiC particles as space increases for more MRP fluid. This results in an enhancement in $\%\,\Delta Ra$. But, beyond the optimum value of the factors T and G, finishing performance $\%\,\Delta Ra$ starts demoted because the duration of contact of an active SiC particle with the CI mold's finishing surface decreases, the intensity of the magnetic field decreases as the distance increases. The decrease in the magnetic field causes to decrease in magnetic force in the iron particle columnar structure and also the significant centrifugal force (F_{cen}) is caused by the enhanced rotary motion of the finishing tool (T). Therefore, due to the significant F_{cen} and reduced intensity of the magnetic field strength with an increase in the working gap, the weak EIPs chain structures held the active abarsive particles loosely due to which the finishing performance starts decreasing.

6.3.2.3 Confirmatory experimentation for validation of theoretical $\%\,\Delta Ra$

The response model (Eq. 6.9) generated from the implementation of the response methodology (RSM) technique on the designed experiment is confirmed with the five random experiments performed for the same finishing time (25 min). The numerical values of the process parameters were taken such that it must lie within the range in which the theoretical response model is applicable as tabulated in Table 6.16. From the five random experiments using the initial and final measured surface asperity, the experimental $\%\,\Delta Ra$ is obtained.

Table 6.16 Confirmation of the theoretical response model with the experimental results

Sr. No.	Finishing parameters				Initial *Ra* (nm)	Final *Ra* (nm)	Experimental $\%\,\Delta Ra$ (Eq.6.1)	Theoretical $\%\,\Delta Ra$ (Eq.6.9)	% Error (Eq. 6.4)
	T (rpm)	*A* (cm/min)	*W* (rpm)	*G* (mm)					
1	390	80	30	2	410	113	72.43	74.58	2.87
2	420	65	20	2	390	101	74.10	70.27	-5.45
3	470	90	35	1.5	420	190	54.76	59.35	7.73
4	390	100	15	2.5	400	208	48.00	49.77	3.55
5	360	75	35	2.5	420	161	61.66	65.13	5.31

The data obtained from the confirmation experiments are compared with the theoretical change in surface asperity as reported in Table 6.16. Therefore, from this table, it is observed that error

between the experimental *% ΔRa* and *% ΔRa* from the theoretical model lies within the -5.45 % to 7.73 %. This error value approves that the model is suitable for the repeatability of the experimental result.

6.3.2.4 Analysis of surface characterization of the finished surface with the optimum process parameters

Using the optimum process parameters (*T*=400 rpm, *A*=80 cm/min, *W*=35 rpm, and *G*=2 mm), the capability of the R-MRH process for finishing the inside surface of the cast-iron (CI) cylindrical mold workpiece has been obtained. The finishing action on the inside surface of the CI cylindrical mold workpiece was performed until the significant improvement in the surface finish can be observed. After finishing the inside surface of the CI cylindrical workpiece for 40 min, the significant improvement in the surface finish was found. In this experimentation, the first 20 min of MR finishing has been conducted. After 20 min of MR finishing, the improvement in the surface finish was measured, and then further 20 min of MR finishing was conducted after the renewal of MRP fluid over the magnetic tool surface. The improvement in the surface finish is recorded through the surface roughness measurement, surface waviness measurement, circularity measurement, and scanning electron microscopy (SEM) methods of surface characterization. The result of the surface characterizations is described as follows.

The roughness profiles of pre-magnetorheological (MR) finished ground-surface and after MR-finished interior surface of the CI cylindric workpiece was assessed using a roughness profilometer as discussed in the experimentation section. The profiles of surface asperity are depicted in Figs. 6.25 (a) and (b), respectively. Figure 6.25(a) represents the roughness profile parameters of the pre-MR-finished ground-surface which are measured as *Ra*=0.420 µm, *Rz*=2.4 µm, *Rq*= 0.52 µm. Whereas, Fig. 6.25(b) is depicting the surface asperity profile of the presently MR-finished mold's interior surface after 40 min finishing with the optimized parameters. Therefore, with the R-MRH finishing process, the final finished surface roughness parameters are found as *Ra*=0.05 µm, *Rz*=0.4 µm, *Rq*= 0.07 µm. Thus, the % change in roughness parameters of arithmetic mean of roughness (*Ra*), root means square of roughness (*Rq*), and the highest peak value of roughness (*Rz*) is found as 88.09 %, 86.53 % and 83.33 % respectively after 40 min of R-MRH finishing utilizing the optimal parameters on the inner cylindric CI mold's surface. Such extent of the changes in the parameters of the surface roughness profiles from the pre-MR-finished to the after MR-finished surface confirms the significant enhancement in surface finish.

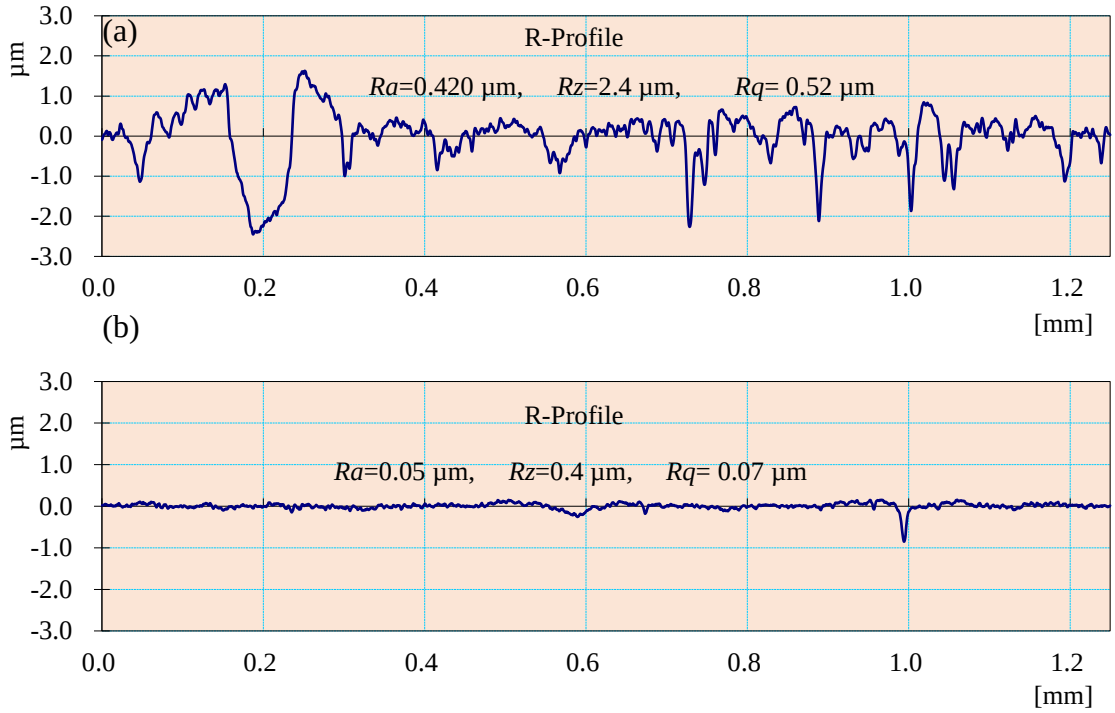

Fig. 6.25 Surface roughness profiles of (a) initial ground inside surface and (b) final MR-finished inside surface of cast-iron cylindrical mold workpiece in 40 min of finishing with the optimized parameters of the R-MRH process.

To check the reduction in the waviness of inside MR-finished surface of the cast-iron (CI) cylindrical mold, the surface waviness parameters of the pre-MR-finished (ground surface) and the after MR-finished surface was assessed using the same surface roughness profilometer. The initial waviness parameters of the pre-MR-finished ground-surface of the CI cylindric mold surface are recorded as *Wa*= 0.17 µm, *Wz*=0.90 µm, *Wq*= 0.22 µm (Fig. 6.26a). After 40 min of the implication of the R-MRH process in finishing the inside cylindrical workpiece surface using the optimum process parameters, the final waviness parameters are attained to *Wa*= 0.04 µm, *Wz*=0.20 µm, *Wq*= 0.06 µm as depicted in Fig. 6.26(b). Thus, the % change in waviness parameters of the arithmetic mean of waviness (*Wa*), root means square of waviness (*Wq*), and the highest peak value of waviness (*Wz*) are found as 76.47 %, 72.72 %, and 77.78 % respectively after 40 min of R-MRH finishing using the optimal parameters on the inner cylindric CI mold's surface. Such values of the % change in the waviness parameters show the capability of the R-MRH process for the great improvement in its straightness which improves the dimensional accuracy as well as fits and tolerances of the product of the cast-iron cylindrical mold. To confirm the improvement in circularity of the inside cylindrical surface of the CI cylindrical mold as obtained after 40 min of finishing with the optimized parameters of the R-MRH process, the circularity test was conducted on the pre-MR finished ground-surface and final MR finished surface using the coordinate measuring machine (CMM). The circularity test

is utilized to predict how the circle is closer to the true circle of the cylindrical part which gives dimensional accuracy of the part (Martorelli *et* al., 2017). To minimize the vibration and heat generation in the cylindrical components during its functional activity, the dimensional accuracy is required (Singaravel *et* al., 2016). The current cylindrical mold which is potent for manufacturing the various cylindrical products with geometric dimensional accuracies, tolerances, straightness, etc. These products need acceptable waviness and circularity values.

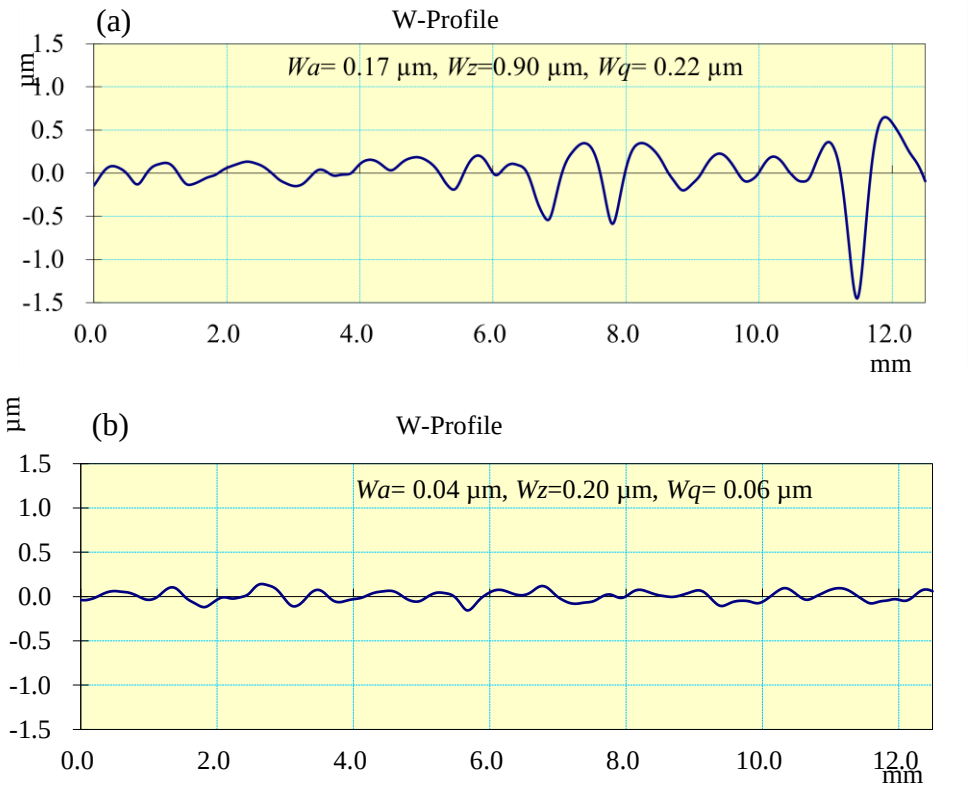

Fig. 6.26 Waviness profiles of the inside surface of (a) initial ground surface and (b) final MR-finished inside surface of cast-iron cylindrical mold workpiece in 40 min of finishing with the optimized parameters of the R-MRH process.

Therefore, the circularity of the finished surface was measured. Figure 6.27 (a) shows the circularity photograph of the pre-MR-finished ground-inner surface of the CI cylindrical mold. The circularity of the pre-MR finished ground-inner surface was measured as 0.1207. From Fig. 6.27 (a), it can be observed that most of the recorded points on the initial ground surface have deviated from the true circle of the circularity graph. However, Fig. 6.27 (b) shows the circularity photograph of the R-MRH finished inner surface of the CI cylindrical mold workpiece. It can be easily observed the significant improvement in the circularity as most of the recorded points are either lying on the true circle or very close to it. Also, the value of the circularity was measured as 0.0437.

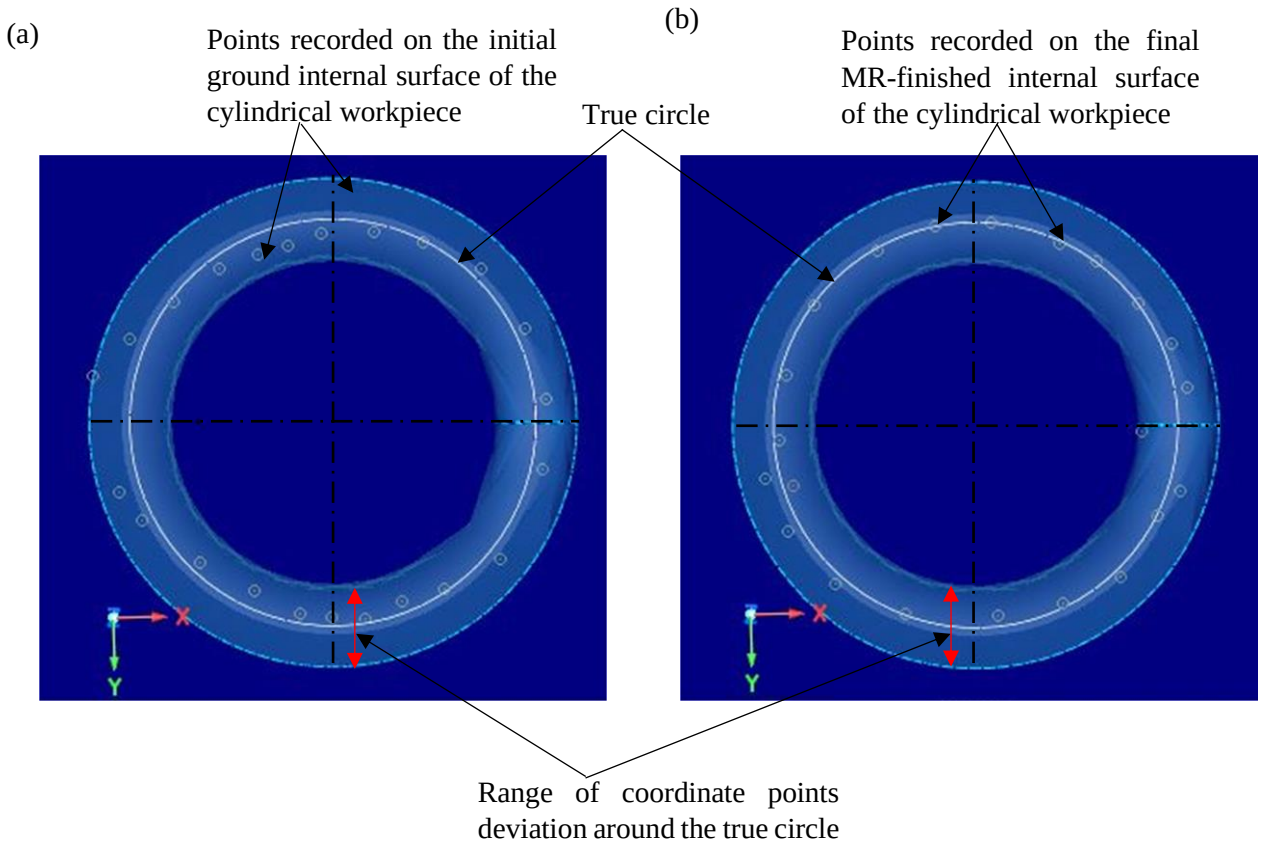

Fig. 6.27 Circularity images of (a) initial ground surface of the inside cast iron cylindrical mold workpiece and (b) final MR-finished surface of cast-iron cylindrical mold workpiece in 40 min of finishing with the optimized parameters of R-MRH process.

From Figs. 6.27 (a) and (b), it is found that after R-MRH finishing over the inside surface of the CI cylindric mold at the optimum process parameters, most of the recorded points in the circularity test are found closer to the true circle. The extent of circularity is said to be better as the recorded points are closer to the true circle. Therefore, Fig. 6.27(b) signifies that the current R-MRH process is found useful for improving the circularity of internal surface of the CI cylinderical molds.

Therefore, the results obtained in the waviness measurement (Fig. 6.26) and circularity (Fig. 6.27), show the improvement in the cylindricity of MR-finished cast-iron cylindrical mold. The improvement in cylindricity obtained in the MR-finished cylindrical mold causes the manufacturing of cylindrical products such as automotive parts, hydraulic and pneumatic parts, beverages canes, domestics appliances, glass beaker, epoxy resin rod, polyvinyl chloride pipes with high precision in dimensional accuracy. These cylindrical products can have close tolerances and excellent fits during assembly. The cylinders with excellent fits and close tolerances are used in pneumatic as well as hydraulic machinery to resist the leakage of air and

oil respectively. High cylindricity makes these components more efficient in functional due to smooth working, uniform pressure acting on such components. Also, improved cylindricity of the components makes them long-lasting and efficient working.

Fig. 6.28 (a) and (b) are showing the images of scanning electron microscopy performed on before MR-finished ground-surface and MR-finished inner surface of the CI mold cylinder after 40 min of finishing with the optimized parameters of the R-MRH process. Fig. 6.28(a), shows a lot of surface defects like grinding marks, surface irregularities, deep grooves, etc. These surface defects are found as a consequence of the direct contact of the cylindrical grinder with the inner surface of the CI cylindrical mold workpiece during the grinding process. The significant size of the abrasives of the cylindrical grinder and high brittleness of the workpiece results in discrete chips formation during the finishing operation (Wu *et* al., 2016). Due to which a lot of surface defects are found as shown in Fig. 6.28 (a). Whereas employing the R-MRH process on the initial ground work-part, micro-sized SiC particles eradicate the material in microchip form which results in nano-finished inside the cylindrical surface of the CI mold as depicted in Fig. 6.28 (b). Thus, the significant improvement in the surface finish texture of the MR-finished, improvement in circularity and waviness on the internal finishing surface of the CI cylindrical mold indicates that the R-MRH process is to be a good deal for enhancing the practical usefulness of the cast iron cylindrical molds.

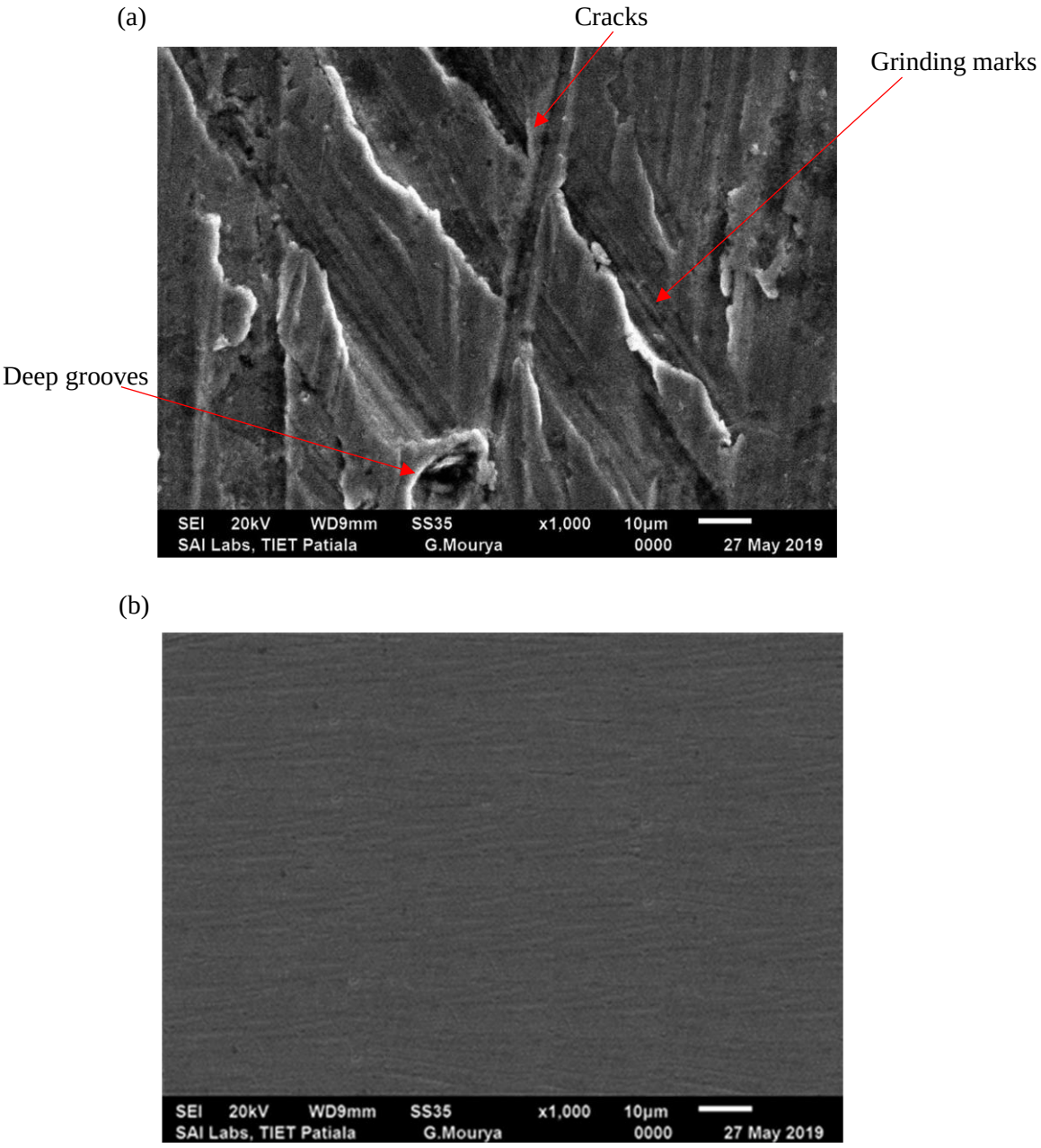

Figure 6.28. The scanning electron microscopy image of the inside surface of the cast-iron cylindrical workpiece mold (a) initial ground surface and (b) final MR-finished surface in 40 min of finishing with the optimized parameters of the R-MRH process.

6.3.3 Conclusions

The fine-finishing of the inner surface of the typical cast-iron (CI) cylindrical molds with the rotary magnetorheological honing (R-MRH) process was successfully performed. The following conclusions have been made from contemporary study.

- The inner surface of the CI cylindrical mold workpiece gets significantly improved after performing R-MRH process with the predicted optimum process parameters as tool rotary speed of 400 rpm, tool axial speed of 80 cm/min, workpiece rotary speed of 35 rpm, and working-gap of 2 mm. This confirms the usefulness of the R-MRH process

with the optimized parameters for improving the long-lasting working performance of the cast-iron cylindrical molds after MR finishing.

- The errors obtained between the experimental and the theoretical % change in roughness values in the present work is found within -5.45% to 7.73% which concludes that there is a good agreement of the present R-MRH method for fine-finishing of the inner cylindrical surface of the CI mold workpieces.
- The 88.09% reduction in *Ra* value on the CI cylindrical inner surface after 40 min of finishing using the contemporary R-MRH method with the optimized process parameters reveal the ability of the present process for super-finishing of the cast-iron practical cylindrical molds after their traditional cylindrical grinding operation.
- The significantly improved roughness profile, waviness profile, circularity, and scanning electron micrograph of the inner cylindrical surface of the CI mold workpiece after the present MR finishing process make sure the functional improvement in CI cylindrical molds for casting the products such as automotive parts, beverages canes, domestics appliances, beakers, and funnels, epoxy resin rod, polyvinyl chloride pipes, etc. Internal surface finishing of a typical outer race of ball bearing of EN-31 steel using rotational magnetorheological honing process.

6.4 Internal surface finishing of a typical outer race of ball bearing of EN-31 steel using rotational magnetorheological honing process

Rolling components of bearings significantly influence the efficiency, running precision, uniformity, and operative life of the equipment in which, these components are used (Xu *et* al., 2019; Wang *et* al., 2020). These components are used in equipment because they support the loads inherent to the machine's function at a low friction level (Cui *et* al., 2016; Zheng et al., 2019). This reduces the power required to drive the equipment, lowering the initial cost of the prime mover and the energy to operate it (Kumar and Singh, 2013). As the bearing primarily consists of the inner race, outer race, and ball in between both races, therefore, the source of the defects can also be within these components of the roller bearing (Adabi *et* al., 2008; Prakash, 2020). The load on the outer race of the bearing causes excessive friction due to which high power is required for operating the equipment (Tandon and Choudhury, 2000). Therefore, to reduce the friction between the inner surface of the outer race and the balls, as much as possible finishing on the internal surface of the outer race is desired (Goepfert, *et* al., 2000). Therefore, the fine-finished internal surface of the outer race of a bearing may reduce friction

by providing smooth motion. These bearings with the fine-finished inner surface of the outer race bear a higher load and simultaneously allow the equipment to perform the smooth rotational motion. The high carbon steel i.e., EN-31 grade steel material is a crucial material that is used in the bearings, gears, bushes, dies, and molds industries (Guo and Liu, 2002). In ball bearing or roller bearing, the outer race is one such part of the bearing which is made of EN-31 steel. This ball bearing is used in various mechanical equipment in the industries such as aerospace industries, automotive industries, defense industries, food industries, and surgical components manufacturing industries, machine tool spindles, axles, or traction motor of railroad vehicles (Chen *et* al., 2020; Kanazawa *et* al., 2020). The smooth operation of numerous equipment in the above-mentioned industries depends on the smooth functioning of the bearings. The functionality of the ball bearings may be improved by reducing the friction between balls and the internal surface of the outer race through the high-quality surface finish. As a higher surface finish is obtained on the internal surface of the outer ball bearing race, a higher improvement in its operational performance may be achieved. Therefore, to improve the operational efficiency of a typical outer race of ball bearing (ORBB) using experimental setup of the R-MRH system, as shown in Fig. 6.29. This technique of finishing the inner cylindrical surface is effectively applicable to both ferromagnetic and non-ferromagnetic working materials with better finishing quality and productivity results. The ORBB's fine-finished internal surface obtained from the R-MRH process may be beneficial for its correct geometric dimensioning, elevated serviceability, consume less power, lowered temperature rises due to minimized friction during operation, etc. As the real-time ORBB is made up of EN-31 steel, the optimized parameters are selected from the parametric analysis performed for this material (EN-31 steel) in chapter 5. Therefore, utilizing the optimized parameters and their condition, the experiments are done to achieve the maximum improvement in surface finish, dimensional accuracy, and surface texture. The finishing potential of this process for inner surface finishing of the cylinder of EN-31 steel is also studied via this analysis. In this research, surface roughness, surface waviness, circularity, and scanning electron microscopy tests were analyzed to determine these improvements achieved on the interior surface of the ORBB. The detailed results obtained from the experimentation performed on the EN-31 cylindrical workpiece (ORBB) at optimum parameters are reported from Figs. 5.25 to 5.28 in chapter 5.

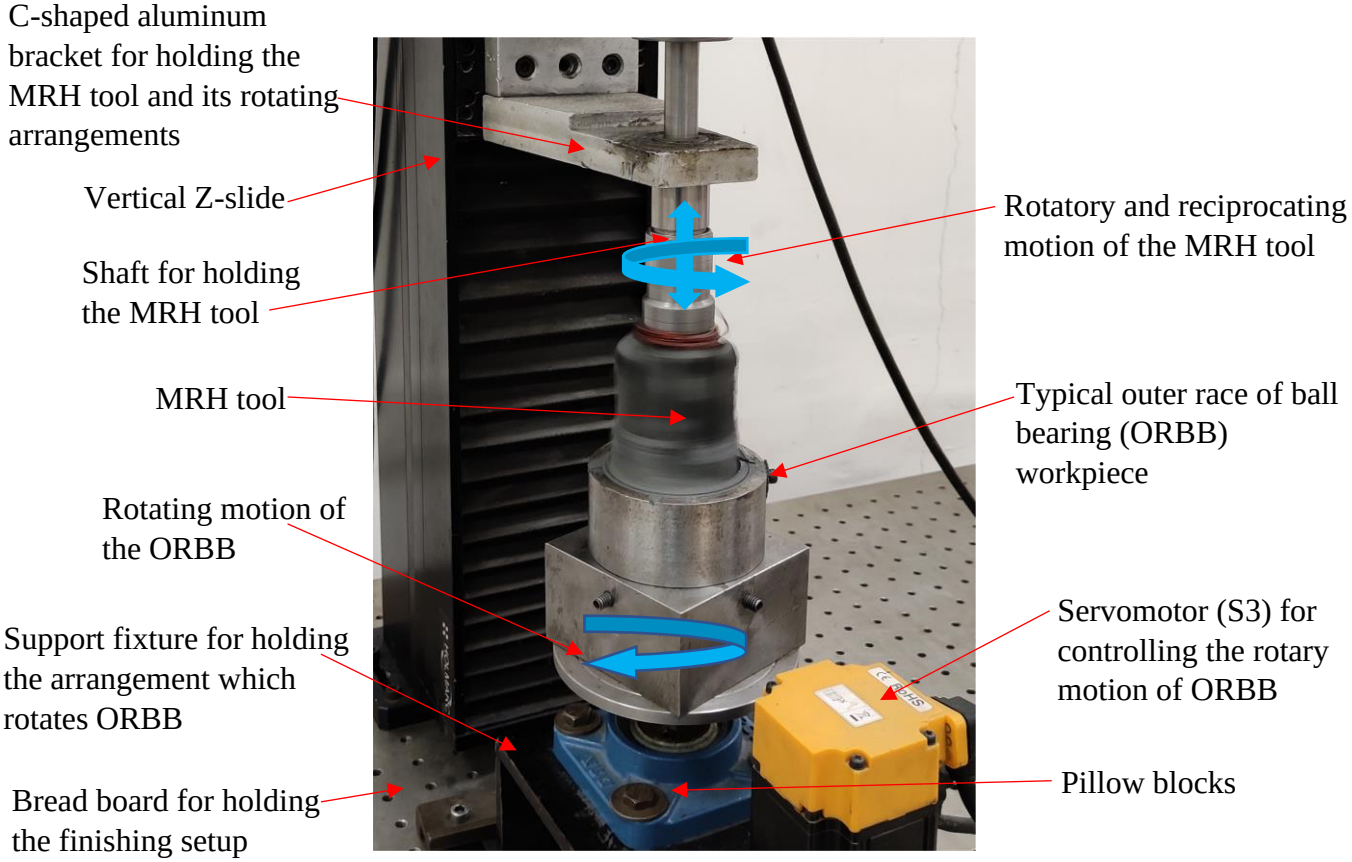

Fig. 6.29 Finishing setup of rotational magnetorheological honing (R-MRH) process for finishing internal surface of the typical outer race of ball bearing (ORBB) and enlarged view of the typical ORBB workpiece.

6.4.1 Conclusions

From the fine finishing of the inner surface of a typical outer race of ball bearing (ORBB) using the rotating magnetorheological honing (R-MRH) process following conclusions have been made.

- The extent of improvement achieved in the final finished internal surface of the ORBB in terms of average surface roughness as 84.61 %, average surface waviness as 79.94 %, in circularity as 85.55 % and in the surface texture from SEM image of the ORBB with 40 min of R-MRH finishing over 40 mm height of the workpiece cylinder with internal diameter of 61 mm using the optimized process parameters reveal the efficacy of the present finishing process for improving the surface finish, surface characteristics, and geometric accuracy of the MR finished surface for improving its functionality. This may result in saving the power consumption of the system, less wear and tear of the

ball bearing component of the system causing economic benefits for the industries or individual.

- The finishing performance of the R-MRH process on the internal cylindrical surface of the ORBB of the EN-31 steel also reveals that this process may be applicable for fine finishing the various other industrial cylindrical products of the EN-31 steel such as in roller bearing, dies, cylindrical molds, etc.

CHAPTER 7

CONCLUSIONS AND SCOPE OF FUTURE

7.1 Conclusions

In the development of the rotational magnetorheological honing (R-MRH), a theoretical study was performed to investigate the effect of the oppositely rotational motion of the cylindrical workpiece on its finishing performance and productivity. In the theoretical study, a surface roughness model was developed for the R-MRH process, and an improvement in finishing performance and productivity was acknowledged as compared to the existing MRH process. To comply the design requirement of the R-MRH process, suitable fixtures were designed and fabricated which could hold and precisely rotate the different size of workpiece cylinders with the same axis as that of the MRH tool rotation. The effectiveness of the developed R-MRH process was also experimentally validated for the improvement in finishing performance and productivity. A significant improvement was achieved with the experimentation of the R-MRH process as compared to the existing MRH process. Further to validate the usefulness of this process for fine finishing the internal surface of the industrial cylindrical workpieces, various industrial components like the cylindrical barrel of hydraulic cylinder, outer race of ball bearing, plastic bottle cap mould, and cast-iron cylindrical mould were successfully finished for improvement in their operational life. Using response surface analysis, the optimum process parameters have been predicted on the EN-31 steel material and industrial components finished in this work. The results achieved from the various experimentations performed were analyzed through surface roughness and waviness measurement, scanning electron microscopy images, and circularity measurement. The analysis of the results obtained in various experimentations revealed that the present developed R-MRH process is found in good agreement for achieving the improved finishing productivity and performance as compared to the existing MRH process. Therefore, on the basis of the study performed in chapters 3-6, the following conclusions have been made.

- The study of the theoretical analysis in the development of the R-MRH process reveals that the inclusion of oppositely rotational motion of the cylindrical workpiece to the existing MRH process causes the enhancement in the relative motion of the active abrasive particles. The enhanced relative speed of the active abrasive particles causes to decrease in pitch length and helix angle and an increase in the length of the helical path followed by an active abrasive particle. Therefore, the decrease in helix angle and

pitch of the helical path enhanced the uniform finishing and the increase in the length of the helical path improves the finishing productivity. Also, the enhancement in the relative speed of active abrasive particles causes enhancement in tangential shear force which improves the finishing rate or productivity of the present developed R-MRH process.

- Theoretical surface roughness results obtained from the surface roughness model in the present study found within 3.33–5.92 % error from the experimental values which shows close agreement.
- The higher reduction in theoretical surface roughness value in less time with the R-MRH process due to the rotational motion of the workpiece cylinder predicts the improvement in surface finishing productivity and performance with the extent of improvement in surface finish and reduction in finishing time as compared to the existing MRH process when the workpiece cylinder was kept stationary during its internal surface finishing.
- Design of the suitable fixtures for holding and rotating the various sizes of workpiece cylinders during the finishing operation fulfills the design requirement in the development of the R-MRH process for effectively and uniformly fine finishing the internal surface of the various industrial cylindrical components such as hydraulic cylinders, circular molds, and dies, hydraulic rack cylinder, cylindrical barrel for injection molding machine, sanitary pipes in food industries, etc.
- The percentage improvement in the surface finish with the R-MRH process is found as 84.84 % and the finishing rate of 7 nm/min when using the tool rotational speed of 400 rpm, tool reciprocation speed of 70 cm/min, and the rotational speed of the mild steel cylindrical workpiece 20 rpm in 40 min of finishing. However, with the stationary cylindrical workpiece, the percentage improvement in the surface finish is found as 72.72 % and the finishing rate of 4 nm/min in 60 min of finishing which clearly advocates the higher finishing rate of the present developed R- MRH process.
- Also, the design of a new in-situ magnetorheological (MR) honing tool reveals the capability in finishing the internal surface of the cylindrical components with the single tool at a single setup for the traditional honing as well as the magnetorheological honing operation which makes this tool to be useful in a great variety of industrial products which requires micro-finishing to fine finishing with a single tool at a single setup. In doing so, it results in beneficial in terms of less time consumption, less power

consumptions, etc. by avoiding multiple setups from initial surface generation to final fine finished surface.

- The significant improvement obtained in surface finishing using the present in-situ honing tool for traditional honing and MR honing is found as 63.57 % and 89.09 % respectively which reveals the applicability of this single tool in good order for finishing the machined surface to achieve the fine-finishing at the same R-MRH setup.
- Regression analysis with response surface methodology reveals the optimized parameters for effective improvement in the surface finish of the EN-31 steel surface. The internal surface roughness on the EN-31 steel cylindrical workpiece (40 mm diameter and 61 mm height i.e., 7665 mm^2 surface area) gets significantly reduced to 60 nm from 390 nm with the R-MRH process in 40 min of finishing time. The surface characteristics of MR finished EN-31 workpiece surface shows a substantial improvement in surface quality as compared to the initial ground surface.
- The finishing performance of the R-MRH process on the internal surface of the cylindrical workpiece of the EN-31 steel also reveals that this process may be applicable for fine finishing the internal surface of the various other industrial cylindrical components of the EN-31 steel such as in roller bearings, the outer race of ball bearings, dies, cylindrical molds, etc.
- The significant improvement in the internal surface roughness of the cylindrical barrel of the hydraulic cylinder (achieved 40 nm from 380 nm of initial surface roughness on 32974 mm^2 of internal cylindrical surface area in 60 min) reveals the R-MRH process can improve the functionality of this cylindrical component by reducing friction between the piston and its internal surface, power consumption while motion transferring, wear and tear rate, heat generation during operation, and further by reducing the leakage of hydraulic oil which may also enhance its service life.
- The substantial improvement in the finishing and surface characteristics achieved on the internal surface of the cylindrical mould (achieved 60 nm from 430 nm of initial surface roughness on 3581.41 mm^2 in 40 min) using the R-MRH process reveals the capability of this process for improving the functional requirement of the component by adding a high-quality surface finish to the end product (plastic bottle cap), avoiding the inter-mixing of color in the casting caps, producing the geometrically and dimensionally correct caps of the bottle.

- The significantly improved roughness profile (change in average surface roughness 88.09 %), waviness profile (change in average surface waviness 74.47 %), circularity value from 0.1207 to 0.0437, and scanning electron micrograph (rarely any marks on the surface) of the inner cylindrical surface of the cast iron mold workpiece after the present MR finishing process reveals that this component can be used for casting the products such as automotive parts, beverages canes, domestics appliances, beakers, and funnels, epoxy resin rod, polyvinyl chloride pipes, etc. without any surface and dimensional defect.
- The extent of improvement achieved in the final MR finished internal surface of the various cylindrical workpieces in terms of reduction in average surface roughness value and average surface waviness, also improvement in circularity and in the surface texture with the R-MRH process using the predicted optimal process parameters reveal the efficacy of the present finishing process for improving the surface finish, surface characteristics, and geometric accuracy of the MR finished surface which may improve their operational functionality. This may result in saving the power consumption of the system, less wear and tear of the component of the system causing economic benefits for the industries or individuals.

7.2 Scope of future work

The present developed rotational magnetorheological honing (R-MRH) tool has successfully shown its capability to fine finish the inner surface of the different ferromagnetic cylindrical workpieces with improved finishing performance and productivity. Some of the scopes of future work by which further efforts can be made to enhance the finishing performance of the present MR honing process are listed as follows.

- The range of the present MRH tool for finishing the internal cylindrical surface is 50 mm to 75 mm, which can be further improved to more variation in its diametric finishing capability from a smaller diameter of the workpiece cylinder to a larger diameter.
- To finish through holes of a pipe of large length, a fixture may be developed which can allow the MR finishing on the internal surface of large length pipes.
- To find out the feasibility of the magnetorheological fluid-based finishing process and to validate the real-time performance of further various industrial applications such as

gun barrel, ball of the flow control valve, air bearings, cylindrical molds, etc. can be used.

- The range of the in-situ honing tool can further be enhanced from smaller to larger for extending its applicability to more variety (diametrically) of the cylindrical workpieces. Also, a more detailed experimental analysis needs to be performed. The in-situ honing tool can further be improved to compact design in a smaller size.

REFERENCES

Adabi, J., Zare, F., Ledwich, G., Ghosh, A., & Lorenz, R. D. (2008, September). Bearing damage analysis by calculation of capacitive coupling between inner and outer races of a ball bearing. In *2008 13th International Power Electronics and Motion Control Conference* (pp. 903-907). IEEE.

Aggarwal, A., & Singh, A. K. (2021). Development of grinding wheel type magnetorheological finishing process for blind hole surfaces. *Materials and Manufacturing Processes*, *36*(4), 457-478.

Alavijeh, M. S., and Amirabadi, H. (2019). Investigation and optimization of the internal cylindrical surface lapping process of 440c steel. *Journal of Mechanical Science and Technology*, *33*(8), 3933–3941. https://doi.org/10.1007/s12206-019-0738-7

Arab, J., & Dixit, P. (2020). Influence of tool electrode feed rate in the electrochemical discharge drilling of a glass substrate. *Materials and Manufacturing Processes*, *35*(15), 1749-1760.

Bedi, T. S., and Singh, A. K. (2016). Magnetorheological methods for nanofinishing – a review. *Particulate Science and Technology*, *34*(4), 412–422. https://doi.org/10.1080/02726351.2015.1081657

Bedi, T. S., and Singh, A. K. (2018a). A new magnetorheological finishing process for ferromagnetic cylindrical honed surfaces. *Materials and Manufacturing Processes*, *33*(11), 1141–1149. https://doi.org/10.1080/10426914.2016.1269925

Bedi, T. S., and Singh, A. K. (2018b). Magnetorheological finishing of ferromagnetic blind-hole type surfaces. *Materials and Manufacturing Processes*, *33*(11), 1169–1176. https://doi.org/10.1080/10426914.2017.1328120

Beyerer, J., & León, F. P. (1997). Detection of defects in groove textures of honed surfaces. *International Journal of Machine Tools and Manufacture*, *37*(3), 371-389.

Cabanettes, F., Dimkovski, Z., and Rosén, B. (2015). Roughness variations in cylinder liners induced by honing tools ' wear. *Precision Engineering*, *41*, 40–46. https://doi.org/10.1016/j.precisioneng.2015.01.004

Campbell Jr, F. C. (2011). Manufacturing technology for aerospace structural materials. Elsevier.

Chen, M., Liu, H., Su, Y., Yu, B., and Fang, Z. (2016). Design and fabrication of a novel magnetorheological finishing process for small concave surfaces using small ball-end

permanent-magnet polishing head. *International Journal of Advanced Manufacturing Technology*, *83*(5–8), 823–834. https://doi.org/10.1007/s00170-015-7573-5

Chen, S., Chen, X., Li, Q., & Gu, J. (2021). Experimental Study on Cage Dynamic Characteristics of Angular Contact Ball Bearing in Acceleration and Deceleration Process. *Tribology Transactions*, *64*(1), 42-52.

Cui, L., Zhang, Y., Zhang, F., Zhang, J., & Lee, S. (2016). Vibration response mechanism of faulty outer race rolling element bearings for quantitative analysis. *Journal of Sound and Vibration*, *364*, 67-76.

Dabnun, M. A., Hashmi, M. S. J., & El-Baradie, M. A. (2005). Surface roughness prediction model by design of experiments for turning machinable glass–ceramic (Macor). Journal of Materials Processing Technology, 164, 1289-1293.

Daneshi, A., Jandaghi, N., and Tawakoli, T. (2014). Effect of dressing on internal cylindrical grinding. *Procedia CIRP*, *14*, 37–41. https://doi.org/10.1016/j.procir.2014.03.064

Darvell, B. W. (2018). Materials science for dentistry. *Woodhead publishing*.

Das, M., Jain, V. K., & Ghoshdastidar, P. S. (2009, January). Parametric study of process parameters and characterization of surface texture using rotational-magnetorheological abrasive flow finishing (R-MRAFF) process. In *International Manufacturing Science and Engineering Conference* (Vol. 43628, pp. 251-260).

Das, M., Jain, V. K., and Ghoshdastidar, P. S. (2010). Nano-finishing of stainless-steel tubes using rotational magnetorheological abrasive flow finishing process. *Machining Science and Technology*, *14*(3), 365–389. https://doi.org/10.1080/10910344.2010.511865

Das, M., Jain, V. K., and Ghoshdastidar, P. S. (2011). The out-of-roundness of the internal surfaces of stainless steel tubes finished by the rotational-magnetorheological abrasive flow finishing process. *Materials and Manufacturing Processes*, *26*(8), 1073–1084. https://doi.org/10.1080/10426914.2010.537141

Das, M., Jain, V. K., and Ghoshdastidar, P. S. (2012). Nanofinishing of flat workpieces using rotational-magnetorheological abrasive flow finishing (R-MRAFF) process. *International Journal of Advanced Manufacturing Technology*, *62*(1–4), 405–420. https://doi.org/10.1007/s00170-011-3808-2

Davim, J. P. (2001). A note on the determination of optimal cutting conditions for surface finish obtained in turning using design of experiments. *Journal of materials processing*

technology, *116*(2-3), 305-308.

Dimkovski, Z., Anderberg, C., Rosén, B., Ohlsson, R., and Thomas, T. R. (2009). Quantification of the cold worked material inside the deep honing grooves on cylinder liner surfaces and its effect on wear. *Wear*, *267*, 2235–2242. https://doi.org/10.1016/j.wear.2009.06.008

Danobat (2020). Machning solutions for all industries. https://www.danobatgrinding.com/en/machining-solutions

Fei, C., Zuzhi, T., & Xiangfan, W. (2015). Novel process to prepare high-performance magnetorheological fluid based on surfactants compounding. *Materials and Manufacturing Processes*, *30*(2), 210-215.

Genc, S.; Phule, P.P. (2002) Rheological properties of magnetorheological fluids. Smart Materials and Structures 11:140–146.

Goepfert, O., Ampuero, J., Pahud, P., & Boving, H. J. (2000). Surface roughness evolution of ball bearing components. *Tribology transactions*, *43*(2), 275-280.

Gorana, V. K., Jain, V. K., & Lal, G. K. (2004). Experimental investigation into cutting forces and active grain density during abrasive flow machining. International Journal of Machine Tools and Manufacture, 44(2-3), 201-211.

Gorana, V. K., Jain, V. K., & Lal, G. K. (2006). Forces prediction during material deformation in abrasive flow machining. *Wear*, *260*(1-2), 128-139.

Grabon, W., Pawlus, P., and Sep, J. (2010). Tribological characteristics of one-process and two-process cylinder liner honed surfaces under reciprocating sliding conditions. *Tribology International*, *43*(10), 1882–1892. https://doi.org/10.1016/j.triboint.2010.02.003

Grover, V., and Singh, A. K. (2018a). Improved magnetorheological honing process for nanofinishing of variable cylindrical internal surfaces. *Materials and Manufacturing Processes*, *33*(11), 1177–1187. https://doi.org/10.1080/10426914.2017.1339322

Grover, V., & Singh, A. K. (2018b). Modelling of surface roughness in a new magnetorheological honing process for internal finishing of cylindrical workpieces. *International Journal of Mechanical Sciences*, *144*, 679-695.

Grover, V., & Singh, A. K. (2019). Parametric optimization of a newly developed magnetorheological honing process for internal finishing of EN-31 cylindrical workpieces. *Engineering Research Express*, *1*(2), 025036.

Gumienny, G., & Giętka, T. (2015). Continuous Cooling Transformation (CCT) Diagrams Of

Carbidic Nodular Cast Iron. *Archives of Metallurgy and Materials*, *60*.

Guo, Y. B., & Liu, C. R. (2002). Mechanical properties of hardened AISI 52100 steel in hard machining processes. *J. Manuf. Sci. Eng.*, *124*(1), 1-9.

Gupte, P. S., Wang, Y., Miller, W., Barber, G. C., Yao, C., Zhou, B., & Zou, Q. (2008). A study of torn and folded metal (TFM) on honed cylinder bore surfaces. *Tribology transactions*, *51*(6), 784-789.

Hashimoto, F., Yamaguchi, H., Krajnik, P., Wegener, K., Chaudhari, R., Hoffmeister, H. W., and Kuster, F. (2016). Abrasive fine-finishing technology. *CIRP Annals - Manufacturing Technology*, *65*(2), 597–620. https://doi.org/10.1016/j.cirp.2016.06.003

Hazir, E., & Ozcan, T. (2019). Response surface methodology integrated with desirability function and genetic algorithm approach for the optimization of CNC machining parameters. *Arabian Journal for Science and Engineering*, *44*(3), 2795-2809.

Heng, L., Kim, Y. J., and Mun, S. D. (2017). Review of Superfinishing by the Magnetic Abrasive Finishing Process. *High Speed Machining*, *3*(1), 42–55. https://doi.org/10.1515/hsm-2017-0004

Hung, L. X., Lien, V. T., Pi, V. N., & Long, B. T. (2019). A study on coolant parameters in internal grinding of 9CrSi steel. In *Materials Science Forum* (Vol. 950, pp. 24-31). Trans Tech Publications Ltd.

Ibrahim, A. F., K.Shather, D. S., and Hamdan, D. W. K. (2014). Studying Abrasive Flow Machining Conditions by Using Taguchi Method. *Eng. and Tech. Journal*, *32*(4).

Jain, R. K., Jain, V. K., & Dixit, P. M. (1999). Modeling of material removal and surface roughness in abrasive flow machining process. *International Journal of Machine Tools and Manufacture*, *39*(12), 1903-1923.

Jain, V. K., Jayswal, S. C., and Dixit, P. M. (2007). Modeling and simulation of surface roughness in magnetic abrasive finishing using non-uniform surface profiles. *Materials and Manufacturing Processes*, *22*(2), 256–270. https://doi.org/10.1080/10426910601134096

Jain, V. K. (2008). Abrasive-based nano-finishing techniques : an overview. *Machining Science and Technology*, *12*(3), 257–294. https://doi.org/10.1080/10910340802278133

Jain, V. K. (2009). Magnetic field assisted abrasive based micro-/nano-finishing. *Journal of Materials Processing Technology*, *209*(20), 6022–6038. https://doi.org/10.1016/j.jmatprotec.2009.08.015

Jeevanantham, S., Robinson, S, D. S., Sivaram, N. M., Nallusamy, S., and Prabhu, N. M. . (2017). Effect of machining parameters on MRR and surface roughness in internal grinding using EN8, EN31 steel. *International Journal of Applied Engineering Research*, *12*(11), 2963–2968.

Jha, S., and Jain, V. . K. (2004). Design and development of the magnetorheological abrasive flow finishing (MRAFF) process. *International Journal of Machine Tools and Manufacture*, *44*, 1019–1029. https://doi.org/10.1016/j.ijmachtools.2004.03.007

Jha, S., and Jain, V. K. (2006a). Nanofinishing Techniques. In *Micromanufacturing and Nanotechnology* (pp. 171–195). Springer. https://doi.org/https://doi.org/10.1007/3-540-29339-6_8

Jha, S., and Jain, V. K. (2006b). Modeling and simulation of surface roughness in magnetorheological abrasive flow finishing (MRAFF) process. *Wear*, *261*, 856–866. https://doi.org/10.1016/j.wear.2006.01.043

Johannesson, H. (1980). *On the optimization of hydraulic cylinder seals* (Doctoral dissertation, Luleå tekniska universitet).

Kamble, V. G., and Kolekar, S. (2014). Analysis of Rheological Properties of Mr Fluid Based on Variation in Concentration of Iron Particles. *American Journal of Nanotechnology*, *516*(52), 12–16. https://doi.org/10.3844/ajntsp

Kanazawa, Y., De Laurentis, N., & Kadiric, A. (2020). Studies of friction in grease-lubricated rolling bearings using ball-on-disc and full bearing tests. Tribology Transactions, 63(1), 77-89.

Kathiresan, S., & Mohan, B. (2018). Experimental analysis of magneto rheological abrasive flow finishing process on AISI stainless steel 316L. *Materials and Manufacturing Processes*, *33*(4), 422-432.

Kemet. (2021). Cylindrical Lapping Using Helilaps. *Kemet International Ltd.* https://www.kemet.co.uk/blog/toolroom/cylindrical-lapping-using-helilaps-technical-article#:~:text=Cylindrical Lapping is a two,several Tenths of a millimetre.

Khan, D. A., & Jha, S. (2018). Synthesis of polishing fluid and novel approach for nanofinishing of copper using ball-end magnetorheological finishing process. *Materials and Manufacturing Processes*, *33*(11), 1150-1159.

Khatri, N., Manoj, J. X., Mishra, V., Garg, H., & Karar, V. (2018). Experimental and simulation

study of nanometric surface roughness generated during magnetorheological finishing of silicon. *Materials Today: Proceedings*, *5*(2), 6391-6400.

Killop, J. T. (1976). *U.S. Patent No. 3,982,415*. Washington, DC: U.S. Patent and Trademark Office.

Krolczyk, G., Raos, P., & Legutko, S. (2014). Experimental analysis of surface roughness and surface texture of machined and fused deposition modelled parts. Tehnički vjesnik, 21(1), 217-221.

Kryvyi, P., Dzyura, V., Maruschak, P., Panin, S., Lyashuk, O., & Vlasov, I. (2020). Influence of curvature and cross-sectional shape of cylindrical surface formed by turning on its roughness. *Arabian Journal for Science and Engineering*, *45*(7), 5615-5622.

Kumar, A., Ghosh, S., & Aravindan, S. (2017). Grinding performance improvement of silicon nitride ceramics by utilizing nanofluids. *Ceramics International*, *43*(16), 13411-13421.

Kumar, R., & Singh, M. (2013). Outer race defect width measurement in taper roller bearing using discrete wavelet transform of vibration signal. *Measurement*, *46*(1), 537-545.

Kumar, S. S., and Hiremath, S. S. (2016). A Review on Abrasive Flow Machining (AFM). *Procedia Technology*, *25*(Raerest), 1297–1304. https://doi.org/10.1016/j.protcy.2016.08.224

Lee, J., & Malkin, S. (1993). Experimental investigation of the bore honing process.

Li, X., Dong, M., Jiang, D., Li, S., & Shang, Y. (2020). The effect of surface roughness on normal restitution coefficient, adhesion force and friction coefficient of the particle-wall collision. *Powder Technology*, *362*, 17-25.

Loveless, T. R., Williams, R. E., and Rajurkar, K. P. (1994). A study of the effects of abrasive-flow finishing on various machined surfaces. *Journal of Materials Processing Tech.*, *47*(1–2), 133–151. https://doi.org/10.1016/0924-0136(94)90091-4

Maan, S., Singh, G., & Singh, A. K. (2017). Nano-surface-finishing of permanent mold punch using magnetorheological fluid-based finishing processes. *Materials and Manufacturing Processes*, *32*(9), 1004-1010.

Martínez-Mateo, I., Carrión-Vilches, F. J., Sanes, J., and Bermúdez, M. D. (2011). Surface damage of mold steel and its influence on surface roughness of injection molded plastic parts. *Wear*, *271*(9–10), 2512–2516. https://doi.org/10.1016/j.wear.2010.11.054

Martorelli, M., Gerbino, S., Lanzotti, A., Patalano, S., & Vitolo, F. (2017). Flatness, circularity and cylindricity errors in 3D printed models associated to size and position on the working

plane. In *Advances on Mechanics, Design Engineering and Manufacturing* (pp. 201-212). Springer, Cham.

McGeough, J. A. (1988). Advanced methods of machining. *Springer Science & Business Media*.

McGeough, J. A., Leu, M. C., Rajurkar, K. P., De Silva, A. K. M., & Liu, Q. (2001). Electroforming process and application to micro/macro manufacturing. *CIRP Annals*, *50*(2), 499-514.

Mehra, D., Mahapatra, M. M., & Harsha, S. P. (2018). Effect of wear parameters on dry abrasive wear of RZ5-TiC in situ composite. *Industrial Lubrication and Tribology*.

Mennig, G., & Stoeckhert, K. (Eds.). (2013). Mold-making handbook. *Carl Hanser Verlag GmbH Co KG*.

Mishra, V., Goel, H., Mulik, R. S., & Pandey, P. M. (2014). Determining work-brush interface temperature in magnetic abrasive finishing process. *Journal of Manufacturing Processes*, *16*(2), 248-256.

Mulik, R. S., & Pandey, P. M. (2013, November). Experimental investigations into the finishing force and torque in magnetic abrasive finishing process. *In ASME 2013 International Mechanical Engineering Congress and Exposition.* American Society of Mechanical Engineers Digital Collection.

Niranjan, M. S., and Jha, S. (2014). Flow Behaviour of Bidisperse MR Polishing Fluid and Ball End MR Finishing. *Procedia Materials Science*, *6*(Icmpc), 798–804. https://doi.org/10.1016/j.mspro.2014.07.096

Otitoju, T. A., Okoye, P. U., Chen, G., Li, Y., Okoye, M. O., & Li, S. (2020). Advanced ceramic components: Materials, fabrication, and applications. *Journal of Industrial and Engineering Chemistry*, *85*, 34-65.

Pan, Z., Feng, Y., and Liang, S. Y. (2017). Material microstructure affected machining: a review. Manufacturing Review, *4*, 5. doi:10.1051/mfreview/2017004

Paswan, S. K., Bedi, T. S., & Singh, A. K. (2017). Modeling and simulation of surface roughness in magnetorheological fluid based honing process. *Wear*, *376*, 1207-1221.

Pawar, P., Ballav, R., & Kumar, A. (2015). A review on machining process of glass materials. In *IEEE Conference on Emerging Trends in Engineering, Business and Disaster Management"[ICBDM 2015]: Noorul Islam University, Kumaracoil, Tamilnadu, India, Print ISSN* (pp. 0976-2558).

Pinchuk, S., Vnukov, A., & Cheranev, R. (2019). Peculiarities of producing an electrolytic iron powder from rolling manufacture waste. *Chemistry & Chemical Technology, 1 (13), 2019*, (1), 121-128.

Prakash, G. (2020). A Bayesian approach to degradation modeling and reliability assessment of rolling element bearing. *Communications in Statistics-Theory and Methods*, 1-22.

Qin, P.-P., Yang, C.-L., Huang, W., Xu, G.-W., and Liu, C.-J. (2016). Honing Process of Hydraulic Cylinder Bore for Remanufacturing. *4th International Conference on Sensors, Measurement and Intelligent Materials (ICSMIM 2015), Icsmim 2015*, 64–68. https://doi.org/10.2991/icsmim-15.2016.14

Quan, Z., Quan, L., and Zhang, J. (2014). Review of energy efficient direct pump controlled cylinder electro-hydraulic technology. *Renewable and Sustainable Energy Reviews*, *35*, 336–346. https://doi.org/10.1016/j.rser.2014.04.036

Rabinowicz, E., Dunn, L. A., & Russell, P. G. (1961). A study of abrasive wear under three-body conditions. *Wear*, *4*(5), 345-355.

Raju, H. P., Narayanasamy, K., Srinivasa, Y. G., & Krishnamurthy, R. (2005). Characteristics of extrude honed SG iron internal primitives. *Journal of Materials Processing Technology*, *166*(3), 455-464.

Ravaud, R., Lemarquand, G., Lemarquand, V., & Depollier, C. (2008). The three exact components of the magnetic field created by a radially magnetized tile permanent magnet. *Progress In Electromagnetics Research*, *88*, 307-319.

Razak, A. A. A., Hameed, A. M., & Sultan, S. R. (2011). Modeling of the cure of Epoxy based composite heated at constant temperature in cylindrical mould. *Diyala Journal of Engineering Sciences*, *4*(01), 1-11.

Rhoades, L. (1991). Abrasive flow machining : a case study. *Journal of Materials Processing Technology*, *28*, 107–116.

Rodewald, W., Wall, B., Katter, M., & Uestuener, K. (2002). Top Nd-Fe-B magnets with greater than 56 MGOe energy density and 9.8 kOe coercivity. *IEEE Transactions on magnetics*, *38*(5), 2955-2957.

Sabri, L., & El Mansori, M. (2009). Process variability in honing of cylinder liner with vitrified bonded diamond tools. *Surface and Coatings Technology*, *204*(6-7), 1046-1050.

Sabri, L., Mezghani, S., and Mansori, M. El. (2010). A study on the influence of bond material on

honing engine cylinder bores with coated diamond stones. *Surface and Coatings Technology*, *205*(5), 1515–1519. https://doi.org/10.1016/j.surfcoat.2010.10.016

Sabri, L., Mezghani, S., El Mansori, M., and Zahouani, H. (2011). Multiscale study of finish-honing process in mass production of cylinder liner. *Wear*, *271*(3–4), 509–513. https://doi.org/10.1016/j.wear.2010.03.026

Sadizade, B., Araee, A., Oliaei, S. N. B., & Farshi, V. R. (2020). Plateau honing of a diesel engine cylinder with special topography and reasonable machining time. *Tribology International*, *146*, 106204.

Sankar, M. R., Jain, V. K., and Ramkumar, J. (2009). Experimental investigations into rotating workpiece abrasive flow finishing. *Wear*, *267*(1–4), 43–51. https://doi.org/10.1016/j.wear.2008.11.007

Sankar, M. R., Jain, V. K., & Ramkumar, J. (2010). Rotational abrasive flow finishing (R-AFF) process and its effects on finished surface topography. *International journal of machine tools and manufacture*, *50*(7), 637-650.

Sankar, M. R., Jain, V. K., and Ramkumar, J. (2016). Nano-finishing of cylindrical hard steel tubes using rotational abrasive flow finishing (R-AFF) process. *International Journal of Advanced Manufacturing Technology*, *85*(9–12), 2179–2187. https://doi.org/10.1007/s00170-015-8189-5

Sankar, M. R., Jain, V. K., Ramkumar, J., Sareen, S. K., & Singh, S. (2019). Medium rheological characterization and performance study during rotational abrasive flow finishing (R-AFF) of Al alloy and Al alloy/SiC MMCs. *The International Journal of Advanced Manufacturing Technology*, *100*(5), 1149-1163.

Saraswathamma, K., Jha, S., and Rao, P. V. (2015). Rheological characterization of MR polishing fluid used for silicon polishing in BEMRF process. *Materials and Manufacturing Processes*, *30*(5), 661–668. https://doi.org/10.1080/10426914.2014.994767

Shukla, V. C., Pandey, P. M., Dixit, U. S., Roy, A., & Silberschmidt, V. (2017). Modeling of normal force and finishing torque considering shearing and ploughing effects in ultrasonic assisted magnetic abrasive finishing process with sintered magnetic abrasive powder. *Wear*, *390*, 11-22.

Sidpara, A., Das, M., and Jain, V. K. (2009). Rheological characterization of magnetorheological finishing fluid. *Materials and Manufacturing Processes*, *24*(12), 1467–1478.

https://doi.org/10.1080/10426910903367410

Sidpara, A., and Jain, V. K. (2012). Nano–level finishing of single crystal silicon blank using magnetorheological finishing process. *Tribology International*, 47, 159–166. doi:10.1016/j.triboint.2011.10.008

Sidpara, A., & Jain, V. K. (2013). Analysis of forces on the freeform surface in magnetorheological fluid based finishing process. *International Journal of Machine Tools and Manufacture*, *69*, 1-10.

Singaravel, B., Marulaswami, C., & Selvaraj, T. (2016). Analysis of the effect of process parameters for circularity and cylindricity errors in turning process. In *Applied Mechanics and Materials* (Vol. 852, pp. 255-259). Trans Tech Publications Ltd.

Singh, A. K., Jha, S., & Pandey, P. M. (2013). Mechanism of material removal in ball end magnetorheological finishing process. *Wear*, *302*(1-2), 1180-1191.

Singh, A. K., Jha, S., & Pandey, P. M. (2015). Performance analysis of ball end magnetorheological finishing process with MR polishing fluid. *Materials and Manufacturing Processes*, *30*(12), 1482-1489.

Singh, G., Kumar, H., Kansal, H. K., & Srivastava, A. (2020). Effects of Chemically assisted Magnetic Abrasive Finishing Process Parameters on Material Removal of Inconel 625 tubes. *Procedia Manufacturing*, *48*, 466-473.

Singh, S., Shan, H. S., & Kumar, P. (2002). Wear behavior of materials in magnetically assisted abrasive flow machining. *Journal of Materials Processing Technology*, *128*(1-3), 155-161.

Singh, M., & Singh, A. K. (2019). Performance investigation of magnetorheological finishing of rolls surface in cold rolling process. *Journal of Manufacturing Processes*, *41*, 315-329.

Sirwal, S. A., Singh, A. K., & Paswan, S. K. (2020). Experimental analysis of magnetorheological finishing of blind hole surfaces using permanent magnet designed tools. *Journal of the Brazilian Society of Mechanical Sciences and Engineering*, *42*(3), 1-23.

Sudheesh, P. K., and Govindan, P. (2013). Experimental investigations and optimization of jig grinding process. *IMPACT: International Journal of Research in Engineering and Technology (IMPACT: IJRET)*, *1*(3), 65–76.

Sooraj, V. S., & Radhakrishnan, V. (2014). Fine finishing of internal surfaces using elastic abrasives. *International Journal of machine tools and manufacture*, *78*, 30-40.

Tan, R., Zhao, X., Zhang, S., Zou, X., Guo, S., Hu, Z., & Sun, T. (2019). Study on ultra-precision

processing of Ti-6Al-4V with different ultrasonic vibration-assisted cutting modes. *Materials and Manufacturing Processes*, *34*(12), 1380-1388.

Tandon, N., & Choudhury, A. (2000). A theoretical model to predict the vibration response of rolling bearings in a rotor bearing system to distributed defects under radial load. *J. Trib.*, *122*(3), 609-615.

Tawakoli, T. Ã., Rasifard, A., and Rabiey, M. (2007). High-efficiency internal cylindrical grinding with a new kinematic. *International Journal of Machine Tools and Manufacture*, *47*, 729–733. https://doi.org/10.1016/j.ijmachtools.2006.09.020

Tilger, M., Siebrecht, T., and Biermann, D. (2017). Fundamental Investigations of Honing Processes Related to the Material Removal Mechanisms. *WGP Annual Congress Aachen, 5.-6. October 2017*, 121–127. https://d-nb.info/1155019458/34#page=131

Torrance, A. A. (2002). The effect of grit size and asperity blunting on abrasive wear. *Wear*, *253*, 813–819. https://doi.org/https://doi.org/10.1016/S0043-1648(02)00103-5

Trojahn, W., & Valentin, P. (2012). Bearing steel quality and bearing performance. *Materials Science and Technology*, *28*(1), 55-57.

Wang, D., Shinmura, T., and Yamaguchi, H. (2004). Study of magnetic field assisted mechanochemical polishing process for inner surface of Si3N4 ceramic components finishing characteristics under wet finishing using distilled water. *International Journal of Machine Tools and Manufacture*, *44*(14), 1547–1553. https://doi.org/10.1016/j.ijmachtools.2004.04.024

Wang, Y., and Hu, D. (2005). Study on the inner surface finishing of tubing by magnetic abrasive finishing. *International Journal of Machine Tools and Manufacture*, *45*(1), 43–49. https://doi.org/10.1016/j.ijmachtools.2004.06.014

Wang, Z., Ma, H., Chen, H., Yan, B., & Chu, X. (2020). Performance degradation assessment of rolling bearing based on convolutional neural network and deep long-short term memory network. *International Journal of Production Research*, *58*(13), 3931-3943.

Xu, C., Wu, T., Huo, Y., & Yang, H. (2019). In-situ characterization of three dimensional worn surface under sliding-rolling contact. *Wear*, *426*, 1781-1787.

Yadav, R. D., & Singh, A. K. (2019). A novel magnetorheological gear profile finishing with high shape accuracy. *International Journal of Machine Tools and Manufacture*, *139*, 75-92.

Yamaguchi, H., and Shinmura, T. (1999). Study of the surface modification resulting from an

internal magnetic abrasive finishing process. *Wear*, *225–229*, 246–255.

Yadav, R. D., Singh, A. K., & Arora, K. (2020). Parametric analysis of magnetorheological finishing process for improved performance of gear profile. *Journal of Manufacturing Processes*, *57*, 254-267.

Yamaguchi, H., & Shinmura, T. (2000). Study of an internal magnetic abrasive finishing using a pole rotation system: Discussion of the characteristic abrasive behavior. *Precision Engineering*, *24*(3), 237-244.

Yamaguchi, H., & Shinmura, T. (2004). Internal finishing process for alumina ceramic components by a magnetic field assisted finishing process. *Precision Engineering*, *28*(2), 135-142.

Yamaguchi, H., Shinmura, T., and Ikeda, R. (2007). Study of internal finishing of austenitic stainless steel capillary tubes by magnetic abrasive finishing. *Journal of Manufacturing Science and Engineering, Transactions of the ASME*, *129*(5), 885–892. https://doi.org/10.1115/1.2738957

Youngleee (2020) Honed tubes|SRB tubes|hydraulic cylinder tubes precision. Available at: http://www.sino-alloy.com/steel-tubes/honed-tube.html.

Yoon, S., Tu, J. F., Lee, J. H., Yang, G. E., and Mun, S. D. (2014). Effect of the magnetic pole arrangement on the surface roughness of STS 304 by magnetic abrasive machining. *International Journal of Precision Engineering and Manufacturing*, *15*(7), 1275–1281. https://doi.org/10.1007/s12541-014-0467-x

Zhang, D., Li, W., Lin, Y., & Bao, J. (2012). An overview of hydraulic systems in wave energy application in China. *Renewable and Sustainable Energy Reviews*, *16*(7), 4522-4526.

Zhang, J., Shang, J., Pramanik, N., Rao, P. N., & Li, B. (2016). Development of low-cost air-based hydraulic leakage detection system through real-time pressure decay data acquisition technology. *The International Journal of Advanced Manufacturing Technology*, *87*(9), 3473-3483.

Zhao, X., Zhang, S., Zhou, C., Hu, Z., Li, R., & Jiang, J. (2015). Experimental study of hydraulic cylinder leakage and fault feature extraction based on wavelet packet analysis. *Computers & Fluids*, *106*, 33-40.

Zheng, X., Zhang, Y., & Du, S. (2020). The state-of-art of microstructural evolution of bearing materials under Rolling Contact Fatigue. *Materials Science and Technology*, *36*(2), 131-149.

Zimmerman, J. D., Pelosi, M., Williamson, C. A., & Ivantysynova, M. (2007, January). Energy consumption of an LS excavator hydraulic system. In *ASME International Mechanical Engineering Congress and Exposition* (Vol. 42983, pp. 117-126).

LIST OF PUBLICATION

SCI Journals:

1. **Paswan S.K.**, Singh A.K. Analysis of surface finishing mechanism in a newly developed rotational magnetorheological honing process for its productivity improvement. *Wear* 2019; 426-427: 68–82.
   Status: ***Online Published***
   Publisher: Elsevier
   Impact factor: 3.892.
2. **Paswan S.K.**, Singh A.K. Theoretical and experimental investigations on nano-finishing of internal cylindrical surfaces with a newly developed rotational magnetorheological honing process. *Proceedings of the Institution of Mechanical Engineers, Part C: Journal of Mechanical Engineering Science* 2020; 234(2): 363-383.
   Status: ***Online Published***
   Publisher: Sage
   Impact factor: 1.762
3. **Paswan S.K.**, Singh A.K. Investigation of optimized parameters for magnetorheological finishing the internal surface of the cast-iron cylindrical molds. *Arabian Journal for Science and Engineering* 2021; **46:** 2147–2164.
   Status: ***Online Published***
   Publisher: Springer
   Impact factor: 2.334
4. **Paswan S.K.**, Singh A.K. Theoretical analysis of a novel in-Situ magnetorheological honing process for finishing the internal surface of tubular workpieces. *Wear* 2021; 203698
   Status: ***Online Published***
   Publisher: Elsevier
   Impact factor: 3.892
5. **Paswan S.K.**, Singh A.K. Analysis of finishing performance in rotating magnetorheological honing process with the effect of particles motion. *Proceedings of the Institution of Mechanical Engineers, Part E: Journal of Process Mechanical Engineering* 2011; 0954408921990132.
   Status: ***Online Published***

Publisher: Sage

Impact factor: 1.620

6. **Paswan S.K.**, Singh A.K. Internal magnetorheological finishing of a typical outer race of ball bearing. *Materials and Manufacturing Processes.*

   Status: ***Under revision***

   Publisher: Taylor and Francis

   Impact factor: 4.616

7. **Paswan S.K.**, Aggarwal A.K., Singh A.K. Magnetorheological finishing on cylindrical barrel of hydraulic cylinder for improving its performance. *Proceedings of the Institution of Mechanical Engineers, Part E: Journal of Process Mechanical Engineering.*

   Status: ***Under revision***

   Publisher: Sage

   Impact factor: 1.620

International Conference:

Sunil Kumar Paswan, Anant Kumar Singh, A rotational magnetorheological honing(R-MRH) process for improving operational function of cylindrical mold, 40th*MATADOR International Conference on Advanced Manufacturing and Design* July 8-10, 2019, Hangzhou, China.

Book Chapter:

Paswan S.K., Singh A.K. (2019) Nano-finishing of internal surface of power steering housing cylinder using rotational magnetorheological honing process. In: Shunmugam M., Kanthababu M. (eds) Advances in Micro and Nano Manufacturing and Surface Engineering. Lecture Notes on Multidisciplinary Industrial Engineering. Springer, Singapore. https://doi.org/10.1007/978-981-32-9425-7_26.